Pulsar Timing

Royal Netherlands Academy of Arts and Sciences
P.O. Box 19121, 1000 GC Amsterdam, the Netherlands

Proceedings of the colloquium,
Amsterdam, 24-27 September 1996

ISBN 90-6984-247-5

Koninklijke Nederlandse Akademie van Wetenschappen
Verhandelingen, Afd. Natuurkunde, Eerste Reeks, deel 50

Pulsar Timing, General Relativity and the Internal Structure of Neutron Stars

Edited by Z. Arzoumanian, F. van der Hooft and E.P.J. van den Heuvel

Amsterdam, 1999

Contents

Part V: Neutron Star Interiors and Glitch Models

Part VI: Evolution and Modeling

Part VII: Timing and Evolution of X-ray Binaries

Part VIII: Pulsar Velocities and Merger Rates

Part IX: Observations Giant Pulses

Preface

Pulsar timing is one of the most precise branches of physics. It has led to verification of a most important prediction of general relativity: the existence of gravitational radiation (Taylor & Weisberg 1989; Taylor 1995). The rate of decay of the orbital period of the binary pulsar PSR 1913+16 which provided this proof, at the same time ruled out a number of rival theories of Einstein's version of general relativity (Taylor & Weisberg, 1989), a very fundamental result.

Timing of millisecond pulsars has allowed some of the most precise tests of general and special relativity in the solar system, showing for example that the moon and planets influence the rate of atomic clocks on Earth; it also helped to test the long-term precision of terrestrial atomic time standards (Taylor 1987, 1991). Furthermore it has led to the discovery of the first planetary system around another star - the only other planetary system so far known to have terrestrial planets (Wolszczan, this volume). Pulsar timing also provided us with the sole way - so far - to probe the internal structure of neutron stars, by studying pulsar glitches and post-glitch behaviour. This has provided very strong evidence for the presence of a superfluid in the neutron star core and allows one to study the interactions between this core and the solid crust of the star. Pulsars in addition are powerful probes for studying the interstellar medium: the dispersion of the arrival times of the pulses at different frequencies yields information about the total number of free electrons along the line of sight and thus on the distance of the pulsar. Fluctuations in brightness and arrival times provide information on the density fluctuations in the interstellar medium and on the transverse velocity of the pulsar. Timing studies of X-ray pulsars also reveal important information on neutron stars: like for binary radio pulsars, doppler-timing of the orbital motion yields information on neutron star masses and companion masses; X-ray timing studies promise even to allow tests of strong-field general relativity (Van der Klis, this volume). It is wonderful that something as simple as measuring the arrival times of pulses can give such a wealth of information.

The first international meeting devoted solely to timing was the NATO Advanced Study Institute 'Timing Neutron Stars' held in Çesme in the spring of 1988 (Ögelman & van den Heuvel 1989). Since then many new discoveries have been made, particularly in the field of binary and millisecond pulsars and on fast X-ray variability of accreting neutron stars. The 75th anniversary of the Astronomical Institute 'Anton Pannekoek' of the University of Amsterdam coinciding with the 10th anniversary of the Amsterdam-Utrecht Center for High Energy Astrophysics provided a nice occasion for a new meeting on this subject. Funding for the meeting was provided by the Royal Netherlands Academy of Arts and Sciences through the programme of Royal Academy Colloquia. Additional support was provided by the Netherlands Science Foundation NWO, through a Spinoza grant to one of us (van den Heuvel).

We were very happy to have gathered at this Colloquium almost all of the major workers in this field worldwide, observers as well as theoreticians. We very much enjoyed their lively presentations and contributions to the discussions which are reproduced here in written form. Time, of course, always is scarse and a few review speakers have not been able to send in their manuscripts before our final deadline (in late 1997). For their presentations we refer to papers or reviews published elsewhere: Alpar (1995); Bildsten et al. (1997); Lamb (1991); Sauls (1989); Spruit & Phinney (1998) and Srinivasan (1997). For the field of physics of neutron star interiors we have taken the freedom to invite an additional contribution from N. Glendenning which seems very relevant for the subject of this meeting. It predicts an observable effect from a phase transition in the neutron star interior.

We would like to thank all participants to the colloquium for their contributions which made this for us a wonderful meeting, and this book one with which we are very happy. We thank Mrs. Manita Kooy of the Royal Academy for her invaluable help in organizing this Colloquium.

Zaven Arzoumanian
Frank van der Hooft
Edward P.J. van den Heuvel

References

Alpar, M.A. 1995, in The Lives of the Neutron Stars, ed. M. Alpar, Ü. Kiziloğlu & J. van Paradijs (Dordrecht: Kluwer), 185

Bildsten, L. et al. 1997, ApJS, 113, 367

Lamb, F.K. 1991, in Neutron Stars: Theory and Observation, ed. J. Ventura & D. Pines, (Dordrecht: Kluwer), 445

Ögelman, H. & van den Heuvel, E.P.J. (eds) 1989, Timing Neutron Stars, (Dordrecht: Kluwer), 774

Sauls, J. 1989, in Timing Neutron Stars, ed. H. Ögelman & E.P.J. van den Heuvel, (Dordrecht: Kluwer), 457

Spruit, H. & Phinney E.S. 1998, Nature, 393, 139

Srinivasan, G. 1997, in: Stellar Remnants (SaasFee Course 25), S.D. Kawaler, I. Novikov & G. Srinivasan, Heidelberg: Springer), 97

Taylor, J.H. 1987, in Proc. 13th Texas Symposium on Relativistic Astrophysics, ed. M.P. Ulmer, Singapore: World Scientific, Singapore), 467

Taylor, J.H. 1991, in Proc. IEEE, 79, 1054

Taylor, J.H. 1995, in Pulsars - proceedings of the Diamond Jubilee Symposium of the Indian Acad. Sci., ed. G. Srinivasan), Journal of Astrophysics and Astronomy, 16, 307

Taylor, J.H. & Weisberg, J.M. 1989, ApJ, 345, 434

Mysteries in Relativistic Astrophysics

Parallel to the Royal Academy Colloquium there was a one-day symposium for the general public on 'Mysteries in Relativistic Astrophysics', organized by graduate students and staff of the Astronomical Institute, to celebrate the 75th anniversary of the Institute. Speakers at this symposium on 26 September 1996, which was held in conference center 'de Rode Hoed' in Amsterdan and attended by some 300 participants, were professors P. Charles (Oxford University), R. Ellis (Cambridge University), M. Schmidt (California Institute of Technology), J.H. Taylor (Princeton University) and C. Wheeler (University of Texas at Austin).

List of participants:

Achterberg, A.	a.achterberg@astro.uu.nl
Alberts, F.	hammi@astro.uva.nl
Alpar, A.	alpar@newton.physics.metu.edu.tr
Arzoumanian, Z.	arzouman@spacenet.tn.cornell.edu
Backer, D.C.	dbacker@astro.berkeley.edu
Bailes, M.	mbailes@physics.unimelb.edu.au
Bell, J.	jb@jb.man.ac.uk
Belloni, T.	tmb@astro.uva.nl
Berger, M.	michielb@astro.uva.nl
Bhattacharya, D.	dipankar@rri.ernet.in
Bisscheroux, B.	bartb@astro.uva.nl
Blaauw, A.	blaauw@astro.rug.nl
Blandford, R.D.	rdb@tapir.caltech.edu
Brown, G.E.	gbrown@insti.physics.sunysb.edu
Butcher, H.R.	butcher@nfra.nl
Camilo, F.	fernando@jb.man.ac.uk
D'Amico, N.	damico@astbo1.bo.cnr.it
Datta, B.	datta@iiap.ernet.in
de Bruyn, A.G.	ger@nfra.nl
Ergma, E.	ene@physics.ut.ee
Esposito-Farèse, G.	gef@binah.cc.brandeis.edu
Fruchter, A.	fruchter@stsci.edu
Galama, T.J.	titus@astro.uva.nl
Graham Smith, F.	fgs@jb.man.ac.u
Groot, P.J.	paulgr@astro.uva.nl
Hartman, J.W. †	
Henrichs, H.	huib@astro.uva.nl
Hermsen, W.	w.hermsen@sron.nl
Iping, R.	riping@uog.edu
Itoh, N.	n_itoh@hoffman.cc.sophia.ac.jp
Johnston, S.	simonj@physics.usyd.edu.au
Kaspi, V.M.	vicky@ipac.caltech.edu
Kouveliotou, C.	kouveliotou@eagles.msfc.nasa.gov
Kouwenhoven, M.	m.l.a.kouwenhoven@astro.uu.nl
Kramer, M.	p671mik@mpifr-bonn.mpg.de
Kuijpers, J.	j.kuijpers@astro.uu.nl
Kulkarni, S.R.	srk@astro.caltech.edu
Kuulkers, E.	e.kuulkers@sron.nl
Lamb, F.	flamb@astro.uiuc.edu
Lestrada, J.-F.	lestrada@obspm.fr
Li, X.	lixd@astro.uva.nl

Link, B.	blink@dante.physics.montana.edu
Lorimer, D.	dunc@mpifr-bonn.mpg.de
Lyne, A.G.	agl@jb.man.ac.uk
Manchester, R.N.	rmanches@atnf.csiro.au
Muslimov, A.	muslimov@lhea1.gsfc.nasa.gov
Nelemans, G.	gijsn@astro.uva.nl
Nice, D.J.	dnice@nrao.edu
Pethick, C.J.	pethick@nordita.dk
Petit, G.	gpetit@bipm.fr
Phinney, E.S.	esp@tapir.caltech.edu
Pines, D.	d-pines@uiuc.edu
Pols, O.	onno@ll.iac.es
Portegies Zwart, S.	spz@grape.c.u-tokyo.ac.jp
Prince, T.	prince@srl.caltech.edu
Radhakrishnan, V.	rad@rri.ernet.in
Ruderman, M.	
Sandhu, J.	jss@astro.caltech.edu
Sarna, G.M.	sarna@camk.edu.pl
Sauls, J.	sauls@snowmass.phys.nwu.edu
Savonije, G.J.	gertjan@astro.uva.nl
Siemsen, R.H.	
Smit, J.M.	m.smit@sron.nl
Srinivasan, G.	srini@rri.ernet.in
Strom, R.G.	strom@nfra.nl
Takens, R.J. †	
Tanaka, Y.	tanaka@astro.isas.ac.jp
Tauris, T.M.	tauris@astro.uva.nl
Taylor, J.H.	joe@pulsar.princeton.edu
Thorsett, S.E.	stece@pulsar.princeton.edu
Toscano, M.	mtoscano@physics.unimelb.edu.au
van den Heuvel, E.P.J.	edvdh@astro.uva.nl
van der Klis, M.	michiel@astro.uva.nl
van der Hooft, F.	vdhooft@astro.uva.nl
van den Horn, L.J.	vdhorn@phys.uva.nl
van Paradijs, J.	jvp@astro.uva.nl
Verbunt, F.	f.w.m.verbunt@astro.uu.nl
Voute, L.	lodie@astro.uva.nl
Wex, N.	nwex@physics.usyd.edu.au
Whyborn, N.	
Wijers, R.A.M.J.	ramjw@ast.cam.ac.uk
Wijnands, R.A.D.	rudy@astro.uva.nl
Wolszczan, A.	alex@astro.psu.edu

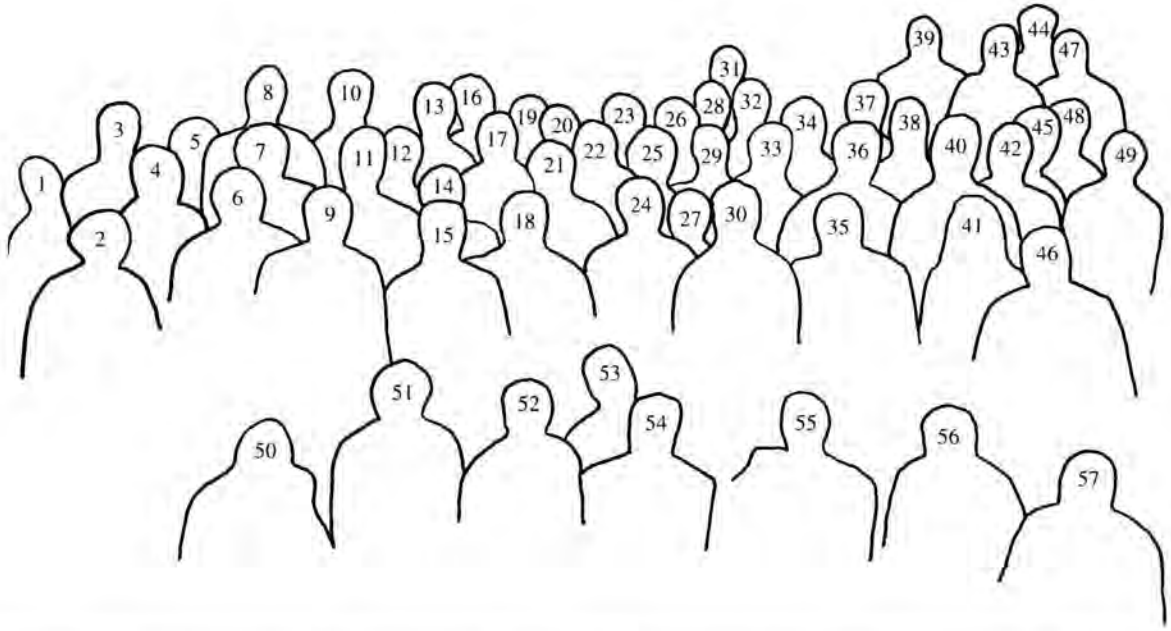

1	J.-F. Lestrada	18	S. Kulkarni	35	E. Ergma	52	E.S. Phinney		H. Henrichs
2	V. Radhakrishnan	19	N. Whyborn	36	B. Bisscheroux	53	A. Muslimov		W. Hermsen
3	R. Wijers	20	S. Thorsett	37	N. Wex	54	N. Itoh		V. Kaspi
4	L. Voute	21	A.G. Lyne	38	T. Tauris	55	Z. Arzoumanian		C. Kouveliotou
5	D. Bhattacharya	22	B. Link	39	M. Ruderman	56	C. Pethick		M. Kramer
6	G.M. Sarna	23	A. Wolszczan	40	O. Pols	57	E. Kuulkers		J. Kuijpers
7	R.J. Takens †	24	X. Li	41	R. Iping				G. Nelemans
8	G. de Bruyn	25	T. Prince	42	J.W. Hartman †		**Not on picture:**		G. Petit
9	R.N. Manchester	26	M. Toscano	43	F. Lamb		A. Achterberg		S. Portegies Zwart
10	T. Galama	27	B. Datta	44	F. Graham Smith		F. Alberts		G.J. Savonije
11	J.H. Taylor	28	R. Wijnands	45	G. Esposito-Farèse		T. Belloni		R.H. Siemsen
12	A. Blaauw	29	J. Bell	46	D. Pines		M. Berger		M. Smit
13	M. Kouwenhoven	30	M. Bailes	47	A. Fruchter		R.D. Blandford		R. Strom
14	F. Verbunt	31	D. Backer	48	A. Alpar		G. Brown		Y. Tanaka
15	D. Nice	32	S. Johnston	49	G. Srinivasan		H. Butcher		M. van der Klis
16	F. Camilo	33	J. Sandhu	50	E.P.J. van den Heuvel		N. D'Amico		F. van der Hooft
17	L.J. van den Horn	34	D. Lorimer	51	J. Sauls		P. Groot		J. van Paradijs

Part I:

Pulsar Timing — General and Fundamental aspects

G. Petit

The Stability of Atomic Time Scales versus Millisecond Pulsars

Abstract

Time scales based on an ensemble of atomic clocks realize the Earth's reference to date events. In recent years a number of technological advances have significantly improved the stability and accuracy of atomic time scales. These improvements are described and their impact on pulsar timing is analyzed. Reciprocally, the regularity of the period of rotation of millisecond pulsars can provide some information on the long-term stability of atomic time scales.

I Introduction

The frequency stability of a periodic phenomenon may be quantified by evaluating the relative changes in frequency within a given time interval. For this, a useful quantity is the Allan deviation (Allan 1987) which is denoted $\sigma_y(t)$ for an averaging time t. As an example, the fractional frequency stability of some of the clocks and time scales discussed in this paper is presented in Figure 1. Stability should be distinguished from accuracy, which is defined as the conformity of a value to its definition. Frequency accuracy is therefore only meaningful for a clock or a time scale when it explicitly aims at complying with a frequency implied by a conventional definition.

Soon after the discovery of the first millisecond pulsar in 1982, it was recognized that the periodicity of its pulses is extremely stable. As the pulses are sharp, their arrival could be timed to about one microsecond so it was possible, within a few years, to demonstrate that the stability of rotation of this millisecond pulsar rivals that of atomic clocks (Rawley et al. 1987): The relative frequency instability for averaging durations above one year is of order 10^{-14}. It is difficult, however, to interpret the instability of the timing data in terms of instability of the pulsar rotation itself because many other phenomena could contribute. Moreover, because many parameters of the pulsar systems are not known *a priori*, but have to be determined by measurement, pulsars cannot intrinsically define a time scale. These ideas have been developed by many authors (Blandford et al. 1984; Guinot & Petit 1991), but have sometimes been overlooked.

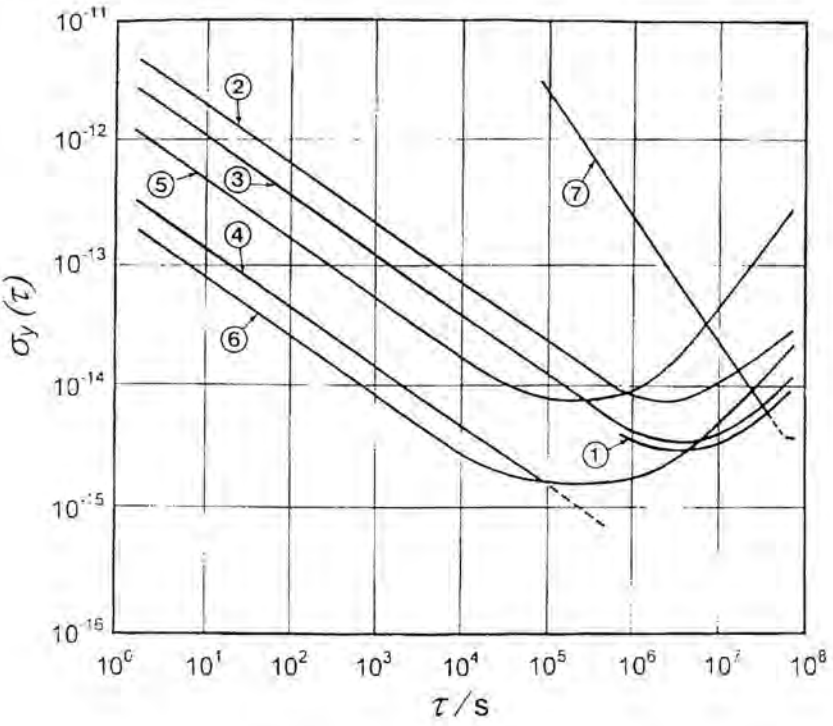

Allan standard deviation (estimate of relative stability)
for TAI and various clocks

① TAI
② Commercial caesium clock
③ PTB CS2 primary caesium clock
④ BNM-LPTF caesium fountain
⑤ Passive hydrogen maser
⑥ Active hydrogen maser
⑦ Pulsar

Figure 1. Estimate of the relative stability, in terms of Allan standard deviation, $\sigma_y(t)$, for various clocks and time scales: 1=TAI, 2=commercial caesium clock, 3=PTB-CS2 primary standard, 4=LPTF-FO1 caesium fountain, 5=passive hydrogen maser, 6=active hydrogen maser, 7=pulsar (from Thomas 1996).

Since 1982 more than seventy millisecond pulsars have been discovered, thanks to a number of systematic radio surveys and this effort continues, as only a fraction of the sky and of the possible space of the defining parameters has been searched. Many of the pulsars discovered are candidates for precise timing and a number of them are regularly observed by many research groups. It is known that several phenomena may corrupt the timing data, among them errors in the atomic time scale used as reference, in the solar system ephemeris and in the model of interstellar propagation. It is interesting to note that errors in atomic time would produce similar effects for all pulsars and so correlation studies should reveal them. It has been proposed (Petit & Tavella 1996) to take advantage of the independence of the noise sources (other than atomic time) among pulsars to average them out in forming an ensemble pulsar time scale.

Clocks and time scales based on atomic transitions have been the basis of time keeping since 1955, and of the official definition of the second since 1967. Until very recently, their long term stability and accuracy was estimated to be about 2×10^{-14} and was challenged by the expected long term stability of the rotation of millisecond pulsars. In consequence it has sometimes been predicted that astronomy will once again take some part of the definition of time references. Recent achievements and expected improvements in clock technology and in the generation of atomic time scales now suggest that, in addition to providing the practical realization of time, atomic devices will remain the fundamental time reference in the foreseeable future. Millisecond pulsars could however provide some information on the long term instabilities in atomic time scales. They could also be used as a flywheel to transfer the accuracy of future atomic clocks back to present and past atomic time.

II Clocks and time scales

A clock is a physical device which realizes its proper time, while a time scale is a reference against which events may be dated. Nowadays, clocks based on atomic transitions are considered to be the most stable devices available and they form the basis of the atomic time scales to which time on Earth is referenced. Although a time scale can be realized by the output of a single clock, the best time scales are based on data from many atomic clocks linked as an ensemble. A time scale can be judged in terms of several properties, accuracy, stability, reliability, availability, all of which are of importance when choosing a reference time scale for the analysis of pulsar timing data.

In its Resolution A4 (IAU 1991) the International Astronomical Union defined relativistic systems of space-time coordinates. The time coordinate of the barycentric (solar system) and geocentric systems are denominated TCB (Barycentric Coordinate Time) and TCG (Geocentric Coordinate Time), respectively. Recommendation IV of Resolution A4 then defines Terrestrial Time TT as a geocentric coordinate time scale whose rate differs from that of TCG by a constant amount (difference of order

7×10^{-10}), so that the scale unit of TT agrees with the SI second on the geoid. Apart from a constant offset of 32.184 s introduced for historical reasons (Guinot 1995), International Atomic Time TAI is a realization of TT. Finally, the basis for all legal time references is provided by the Universal Time Coordinated, UTC, which differs from TAI by an exact number of seconds. The introduction of leap seconds is decided by the International Earth Rotation Service so as to keep UTC within 0.9 s of the scale UT1 which represents the rotation of the Earth.

The Time section of the Bureau International des Poids et Mesures is in charge of establishing and distributing International Atomic Time. The calculation of TAI (Thomas & Azoubib 1996) makes use of an intermediate free-running time scale, EAL, computed from the data of more than two hundred atomic clocks spread world-wide. EAL is then steered in frequency to produce TAI, so that its scale unit is in agreement with the SI second on the geoid as realized by several primary frequency standards. The properties of these two time scales are similar. Their stabilities are comparable (see estimates in the next section), although the steering process slightly degrades that of TAI. By definition, however, TAI is accurate while EAL is not. Finally they are very reliable, being based on more than 200 different clocks, and available with a delay of one month.

The time scales TAI and UTC are made available by providing, with a 5-day interval (10-day until December 1995), the difference between TAI and TA(k) and between UTC and UTC(k), where TA(k) and UTC(k) represent time scales maintained by laboratory k. At present there are 17 laboratories keeping a TA(k) and more than 45 keeping a UTC(k). These data are published in the monthly BIPM circular T and in the annual report of the BIPM time section. They are also available electronically (anonymous `ftp` on `145.238.2.2`, subdirectory TAI).

Because it is computed in near real time, TAI is subject to certain stability limitations. Each year, therefore, the BIPM Time section establishes another realization of TT, denoted TT(BIPMxx), which covers the period 1975.5 to 19xx.0 where xx are the last two digits of the year of computation. The computation of TT(BIPMxx) is based on a different algorithm (Guinot 1988), and makes use of all available data from all primary frequency standards. Each new realization is a complete recalculation differing from, and taking precedence over, the previous one for the common dates. It is provided in the form TT(BIPMxx)−TAI for the dates of publication of TAI.

The time scales to be used as a reference for the analysis of pulsar timing have already been reviewed by Guinot & Petit (1991). Their conclusions remain valid and suggest that the best choice is a deferred-time realization of TT such as TT(BIPMxx). It is also advisable to use the most recent version of TT(BIPM) as new data and upgrades of the algorithms are expected to improve the whole time scale. Alternately, a free-running atomic time scale, for example TA(PTB), may be used. Estimates of the stability of most TA(k) relative to TAI may be found in the annual report of the BIPM Time section. When using a TA(k), it is advisable to check with the organization

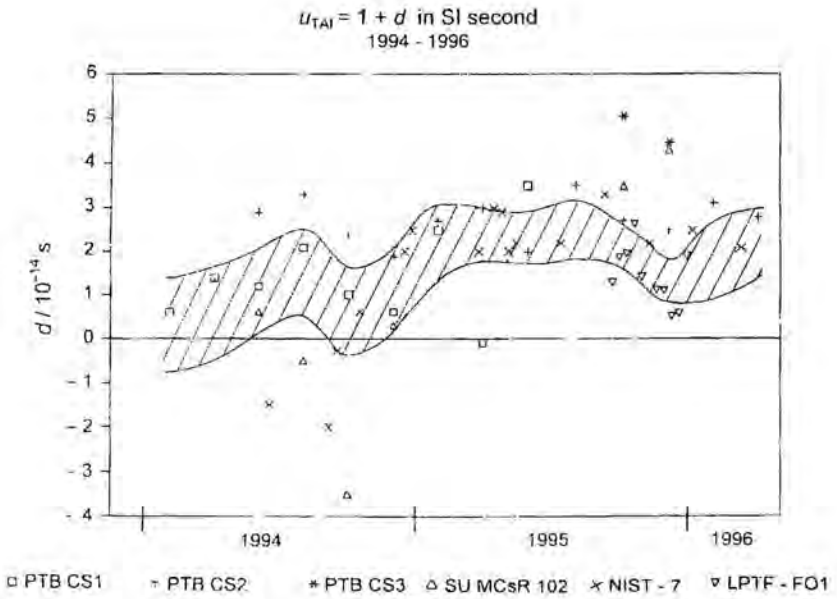

Figure 2. Departure d of the TAI scale unit from the SI second as produced by six primary frequency standards, and as computed by the BIPM (shaded area represents the one sigma confidence interval), over the period January 1994 to April 1996 (from Thomas 1996).

providing the time scale as changes may occur in the realization over the period considered. Steered time scales, and those available in real time, are less likely to match the stability requirements for the analysis of pulsar timing measurements.

III Recent and future progress in atomic time scales

In the period 1993–1995 great progress has been made. As a result atomic time scales show improved stability for all averaging durations.

First, the general use of GPS time transfer has decreased the measurement noise of clock comparisons, so that the instabilities it introduces do not exceed $1–2 \times 10^{-15}$ for an averaging duration of 10 days. The short and medium term stability (for an averaging duration ranging from 10 days to 160 days) has also improved due to a combination of factors: the introduction of many new commercial caesium clocks with improved stability; the development of cavity auto-tuned H-masers which are not subject to frequency drift; the use of better algorithms. As a result, it is estimated that the stability of EAL is about $2–3 \times 10^{-15}$ for an averaging duration of 20 days to 80 days (Thomas 1996).

For long averaging durations (one year and over), the concepts of stability and accuracy are intricately linked. Progress arises from the operation of new primary frequency standards of unprecedented accuracy. At the LPTF in Paris (France) a caesium fountain, LPTF-FO1, has been under evaluation since the fall of 1995. Its stability is $\sigma_y(t) = 2 \times 10^{-13} t^{-1/2}$ for t up to 10000 s and its accuracy is estimated to be 3×10^{-15} (Clairon et al. 1995). The NIST-7, an optically pumped caesium beam standard developed at the NIST in Boulder (Colorado, USA), has been in regular operation since 1994. Its accuracy is estimated to be 1×10^{-14}, with improvements expected (Shirley et al. 1995). The PTB-CS3, a caesium beam standard developed at the PTB in Braunschweig (Germany), has an accuracy of 1.4×10^{-14} (Bauch et al. 1996) and began operation in 1996. In addition PTB- CS2, which has an accuracy of 1.5×10^{-14}, has been in regular operation since 1986. As a result, the uncertainty in the determination of the scale unit of TAI is below 1×10^{-14} for recent years (BIPM 1996). Figure 2 shows the departure of the scale unit of TAI from the SI second on the geoid over recent years, which presents a global shift of about 2×10^{-14}. This discrepancy results from the recent decision by the Consultative Committee for the Definition of the Second (CCDS 1996) to apply a correction for the black-body radiation frequency shift to the data of all primary frequency standards, and it will be progressively reduced. Similarly it is estimated that the long term stability and accuracy of the realization of TT computed by the BIPM since 1996 (TT(BIPMxx) with xx < 96) is also below 1×10^{-14} for recent years (1994 and later). In addition TT(BIPM96) incorporates the black-body correction so this realization of TT is consistent with the new decision of the CCDS.

The limitations of conventional caesium beam standards originate mainly from phase shifts in the Ramsey cavity where the atoms interact, from side effects of the magnetic fields used for state selection and detection of the atoms, and from the uncertainty in the velocity of the atoms in the beam. In addition, the high velocity of the atoms limits the intrinsic width of the Ramsey fringes. These difficulties are all overcome when low velocity atoms interact at the same place in a small cavity, and optical pumping is used for state selection and detection. For neutral caesium atoms, such conditions can be realized in a fountain or in zero gravity. They can also be realized for ions by confining them in an electromagnetic trap. Based on these techniques, a great number of frequency standards are being developed throughout the world.

Further improvements in the LPTF's fountain and the development of a second device capable of operating either as a fountain on Earth or as a low velocity beam in zero gravity should make attainable an accuracy of 1×10^{-16} (Clairon et al. 1995). Linear Hg+ ion traps are being developed at the JPL in Pasadena (California, USA). Measurements of their stability give $\sigma_y(t) = 7 \times 10^{-14} t^{-1/2}$ for t up to 10000 s and $\sigma_y(t)$ remains below 10^{-15} for t up to 10 days (Tjoelker et al. 1995). Linear Yb+ ion traps are being developed at the CSIRO in Sydney (Australia) (Fisk et al. 1996). Recent measurements give $\sigma_y(t) = 5 \times 10^{-14} t^{-1/2}$ for t up to 20000 s (Figure 3). Such developments promise that the medium term stability of atomic time scales will

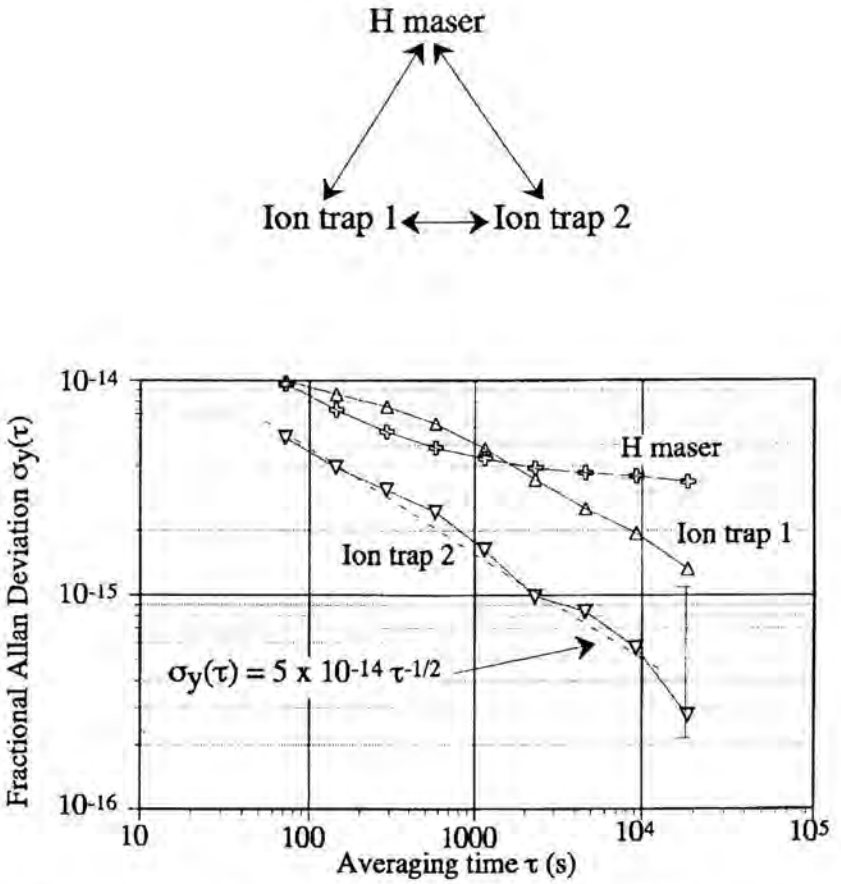

Figure 3. Estimate of the relative stability, in terms of Allan standard deviation $\sigma_y(t)$ determined by a "three- cornered hat" analysis, for two Yb+ ion traps and a hydrogen maser used to compare them (courtesy of P. Fisk and M. Lawn, CSIRO).

approach 10^{-16} in coming years. Similar long term stability is expected from the new frequency standards, but it will take some time for this to be acknowledged.

IV Pulsars and time scales

The application of pulsar measurements to time scales can be viewed from three different perspectives (Petit & Tavella 1996). In the first, the rotation of the pulsar itself is the source of a dynamical time scale PT (Pulsar Time) which can be read by counting the pulses received by a radio telescope. In the second, pulsar timing is an access to Ephemeris Time, the dynamical time resulting from the orbital motion of the Earth,

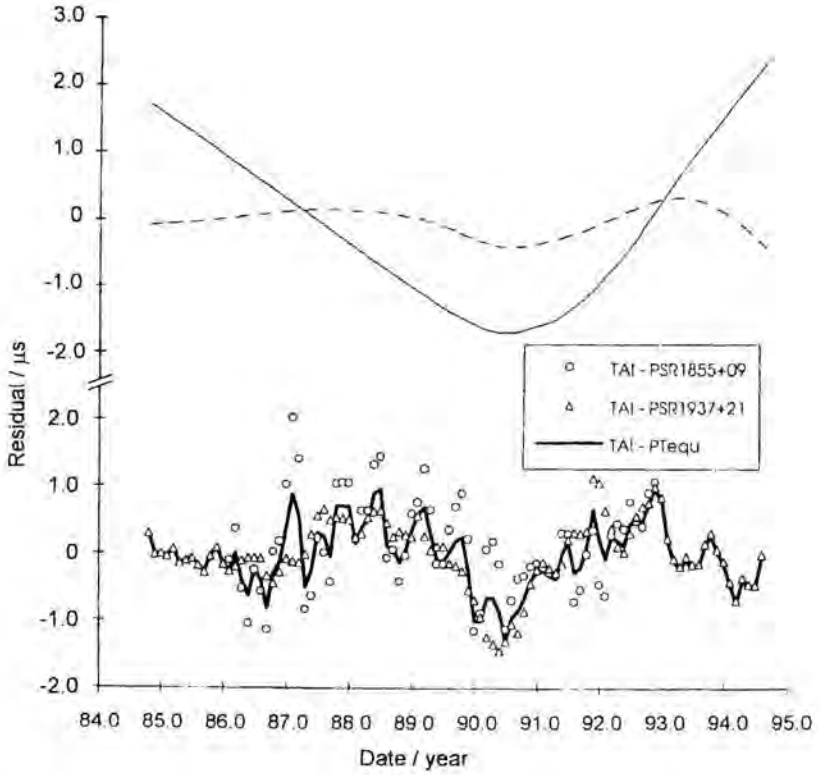

Figure 4. TAI-PT_i for pulsars B1937+21, after removal of a cubic term (triangles), and B1855+09 (circles), and for an equal weight average PT_{equ} (solid line). The effect that the frequency steering corrections applied to TAI would have on an ideal time scale is also shown on the same scale before (soild light curve) and after (dashed curve) the adjustment of a cubic term (Petit & Tavella 1996).

with a reading uncertainty of a few milliseconds. This is a considerable improvement over classical measurements of Ephemeris Time. In the third, pulsar timing provides access to the orbital motion of a pulsar in a binary system, which is described by a dynamical time parameter BPT (Binary Pulsar Time). For no averaging duration are the time scales generated in the last two applications expected to be as stable as atomic time, but the comparison of BPT with atomic time provides exciting perspectives for cosmology, gravitation and the dynamics of our galaxy (Taylor 1992).

A millisecond pulsar has the potential to provide a time scale whose long-term stability compares favorably with current atomic time. Using data from many pulsars, it is possible to derive an average pulsar time scale which is better than a scale derived from individual pulsar data and may have a stability better than atomic time. This improvement holds for averaging times well above one year but still much smaller

than the total period of observation. A simple algorithm which realizes such a scale is described by Petit & Tavella (1996), along with a tentative application to real data. This paper shows that data from pulsars B1937+21 and B1855+09 seem to indicate some instability in TAI for the period 1989–1992 when repeated frequency steerings were applied (Figure 4).

Further studies can produce only limited improvements because very few pulsars with low timing noise have been observed regularly, and because the time span of the observations never exceeds ten years. Among the presently known pulsars, B1937+21 has low timing noise, but demonstrates long-term instability of unknown origin. For B1855+09, no low frequency noise can clearly be identified on the available 8-year data span (Kaspi et al. 1994). Of the more recently discovered pulsars, J1713+0747 seems very promising because the timing noise is low (Camilo et al. 1994). Other candidates include B1257+12 (Wolszczan 1994), although the presence of companions of planetary mass implies multi-parameter adjustment, B1534+12 (Wolszczan 1991), J2019+2425 and J2322+2057 (Nice & Taylor 1995), and J2317+1439 (Camilo et al. 1993). Observations of these pulsars began in the period 1990 to 1992, so observations covering 10 years will be completed at the beginning of the coming century, at which point the computation of an ensemble pulsar time should be reconsidered.

V Conclusions

Atomic time scales have provided the best time reference with which to date events since their introduction in the late 1950s. Since 1980, their long term stability and accuracy have been 2–3 $\times$ 10^{-14}, but since 1994–1995 progress has pushed these values to below 1×10^{-14}. Ongoing technical developments suggest that future atomic clocks may achieve stability and accuracy of about 10^{-16} in the near future.

The rotation rate of millisecond pulsars is the most regular astronomical phenomenon known and can provide a time scale that rivals current atomic time in stability. Presently, few pulsars with suitable properties have been observed for long enough to provide a scale that outperforms atomic time. Current programmes of observation should provide enough data in the early 2000s to establish an ensemble pulsar time scale from five to eight individual series. This would be helpful in assessing whether the long term stability of atomic time scales has indeed been a few parts in 10^{15} since 1994–1995, as appears to be the case from present analyses.

Acknowledgements

I am greatly indebted to my colleague C. Thomas (BIPM) for providing some figures and for her support. I thank M. Lawn and P. Fisk (CSIRO) for useful discussions and for providing Figure 3 prior to publication, and D. Blackburn (BIPM) for his help in improving the manuscript.

References

Allan, D.W. 1987, IEEE Trans. Ultras. Ferroelect. Freq. Contr., 34, 647

Bauch, A. et al. 1996, Metrologia, 33, 3, 249

BIPM 1996, Annual report of the BIPM time section, Vol. 6, Bureau International des Poids et Mesures, Sèvres

Blandford, R., Narayan, R. & Romani, R.W. 1984, J. Astrophys. Astr., 5, 369

Camilo, F., Nice, D.J. & Taylor J.H. 1993, ApJ, 412, L37

Camilo, F., Foster, R.S. & Wolszczan, A. 1994, ApJ, 437, L39

CCDS 1996, Report of the 13th CCDS meeting, Bureau International des Poids et Mesures, Sèvres

Clairon, A. et al. 1995, in Proc. Fifth Symp. on Frequency Standards and Metrology, ed. J. C. Bergquist (World Scientific), 49

Fisk, P.T.H. et al. 1995, in Proc. Fifth Symp. on Frequency Standards and Metrology, ed. J. C. Bergquist (World Scientific), 27

Guinot, B. 1988, A&A, 192, 370

Guinot, B. 1995, Metrologia, 31, 6, 431

Guinot, B. & Petit, G. 1991, A&A, 248, 292

IAU 1991, IAU Transactions Vol. XXIB, in Proc. 21st Gen. Assembly, ed. J. Bergeron (Kluwer: Dordrecht)

Kaspi, V.M., Taylor, J.H. & Ryba, M.F. 1994, ApJ, 428, 713

Nice, D.J. & Taylor, J.H. 1995, ApJ, 441, 429

Petit, G. & Tavella, P. 1996, A&A, 308, 290

Rawley, L.A., et al. 1987, Science, 238, 761

Shirley, J.H., Lee, W.D. & Drullinger, R. 1995, in Proc. Fifth Symp. on Frequency Standards and Metrology, ed. J.C. Bergquist (World Scientific), 380

Taylor, J.H. 1992, Phil. Trans. R. Soc. London Ser. A, 341, 117

Thomas, C. 1996, in Proc. 50th Frequency Control Symp., 1123

Thomas, C., Azoubib, J. 1996, Metrologia, 33, 3, 227

Tjoelker, R.J., Prestage, J.D. & Maleki, L. 1995, in Proc. Fifth Symp. on Frequency Standards and Metrology, ed. J. C. Bergquist (World Scientific), 33

Wolszczan, A. 1991, Nature, 350, 688

Wolszczan, A. 1994, Science, 264, 538

Authors' Address

Bureau International des Poids et Mesures, 92312 Sèvres Cedex, France

G. Esposito-Farèse

Binary-Pulsar Tests of Strong-Field Gravity

Abstract

This talk is based on my work in collaboration with Thibault Damour since 1991. Unified theories, like superstrings, predict the existence of scalar partners to the graviton. Such theories of gravity can be very close to general relativity in weak-field conditions (solar-system experiments), but can deviate significantly from it in the strong-field regime (near compact bodies, like neutron stars). Binary pulsars are thus the best tools available for testing these theories. This talk presents the four main binary-pulsar experiments, and discusses the constraints they impose on a generic class of tensor-scalar theories. It is shown notably that they rule out some models which are strictly indistinguishable from general relativity in the solar system. This illustrates the qualitative difference between binary-pulsar and solar-system tests of relativistic gravity.

I Introduction

The usual meaning of "testing a theory" is rather negative: one compares its predictions with experimental data, and a single inconsistency suffices to rule it out. On the other hand, it is difficult to determine what features of the theory are correct when it passes a given test. In order to extract some positive information from experiment, it is useful to embed the theory into a class of alternatives. Indeed, by contrasting their predictions, it is easier to understand in what way they differ, and to determine the common features which make them pass or not the available tests. Moreover, this approach can suggest new experiments to test the other features of the theories.

The best known example of such an embedding of general relativity into a space of alternatives is the so-called Parametrized Post-Newtonian (PPN) formalism, which is extremely useful for studying gravity in weak-field conditions, at order $1/c^2$ with respect to the Newtonian interaction. The original idea was formulated by Eddington (1923), who wrote the usual Schwarzschild metric in isotropic coordinates, but introduced some phenomenological parameters $\beta^{\rm PPN}$, $\gamma^{\rm PPN}$, in front of the different

powers of the dimensionless ratio Gm/rc^2 :

$$-g_{00} = 1 - 2\frac{Gm}{rc^2} + 2\beta^{\rm PPN}\left(\frac{Gm}{rc^2}\right)^2 + O\left(\frac{1}{c^6}\right) , \tag{1a}$$

$$g_{ij} = \delta_{ij}\left[1 + 2\gamma^{\rm PPN}\frac{Gm}{rc^2} + O\left(\frac{1}{c^4}\right)\right] . \tag{1b}$$

General relativity, which corresponds to $\beta^{\rm PPN} = \gamma^{\rm PPN} = 1$, is thus embedded into a two-dimensional space of theories parametrized by all real values of $\beta^{\rm PPN}$, $\gamma^{\rm PPN}$. (The third parameter that one may introduce in front of $2Gm/rc^2$ in g_{00} can be reabsorbed in the definition of the mass m.) The constraints imposed in this space by solar-system experiments are displayed in Figure 1, and give the following 1σ limits on the Eddington parameters:

$$|\beta^{\rm PPN} - 1| < 6 \times 10^{-4} , \tag{2a}$$

$$|\gamma^{\rm PPN} - 1| < 2 \times 10^{-3} . \tag{2b}$$

The PPN formalism has been further developed by Schiff, Baierlin, Nordtvedt and Will to describe any possible relativistic theory of gravity at order $1/c^2$. In particular, Will & Nordtvedt (1972) introduced up to 8 extra parameters (besides $\beta^{\rm PPN}$ and $\gamma^{\rm PPN}$), each of them describing a particular violation of the symmetries of general relativity, like local Lorentz invariance, or the conservation of energy and momentum. Since these 8 parameters do not have any really natural field-theoretic motivation (as opposed to $\beta^{\rm PPN}$ and $\gamma^{\rm PPN}$; see below), we will not consider them any longer in this paper. Let us just mention that they are even more constrained than $(\beta^{\rm PPN} - 1)$ and $(\gamma^{\rm PPN} - 1)$ by solar-system experiments. (See the contribution of J. Bell to the present Proceedings for a discussion of the tight bounds on some of these parameters imposed by binary-pulsar data.) In the 10-dimensional space of all these PPN parameters ($\beta^{\rm PPN}$, $\gamma^{\rm PPN}$, and the 8 others), only a tiny neighborhood of Einstein's theory is thus allowed by solar-system experiments: the intersection of the three strips of Fig. 1 and a very thin 8-dimensional slice parallel to the plane of this figure. One can therefore conclude that general relativity is essentially the only theory which passes all these tests, and one may naturally ask the question: is it worth testing it any further ?

The reason why solar-system tests do not suffice is the extreme weakness of the gravitational field in these conditions. Indeed, the largest deviation from the flat metric is found at the surface of the Sun, and is proportional to its gravitational binding energy $(Gm/Rc^2)_\odot \approx 2 \times 10^{-6}$ (where R denotes the radius of the considered body). In the vicinity of the Earth, the gravitational field is of order $(Gm/Rc^2)_\oplus \approx 7 \times 10^{-10}$. This explains why only the first terms of the expansion (1) are tested by solar-system experiments. Two theories which are extremely close in weak-field conditions can differ significantly in the strong-field regime. For instance, the typical self-energy of a neutron star is $Gm/Rc^2 \approx 0.2$, and therefore one cannot justify any more the PPN

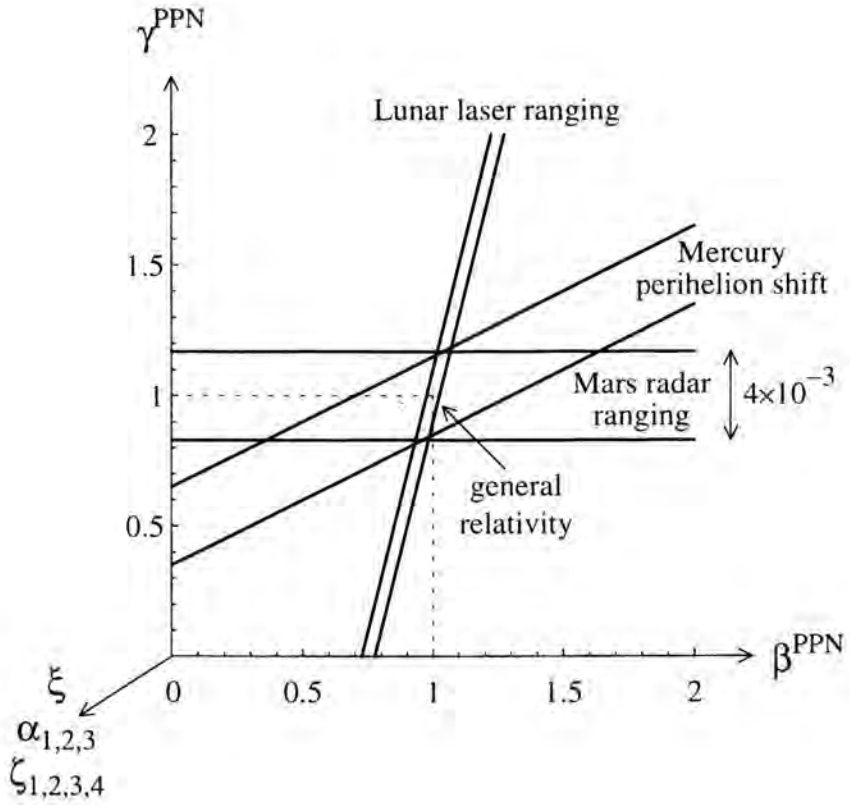

Figure 1. Solar-system constraints on the PPN parameters. The widths of the strips have been enlarged by a factor 100. The allowed region is shaded.

truncation of the theory at order $1/c^2$. (A more rigorous definition of the binding energy is $-\partial \ln m/\partial \ln G$. This expression takes its maximum value, 0.5, for black holes. The value ≈ 0.2 found for neutron stars should therefore be understood as a rather *large* number.) Binary pulsars are thus ideal tools for testing relativistic theories of gravity in strong-field conditions.

Before embedding general relativity into a class of contrasting alternatives, and comparing their predictions with experimental data, let us first describe the four main binary-pulsar tests presently available.

II Binary-pulsar tests

The aim of this talk is not to explain what is a pulsar to specialists of the question. For our purpose, it is sufficient to note that an isolated pulsar is essentially a (very stable) clock. A binary pulsar (a pulsar and a companion orbiting around each other) is thus a

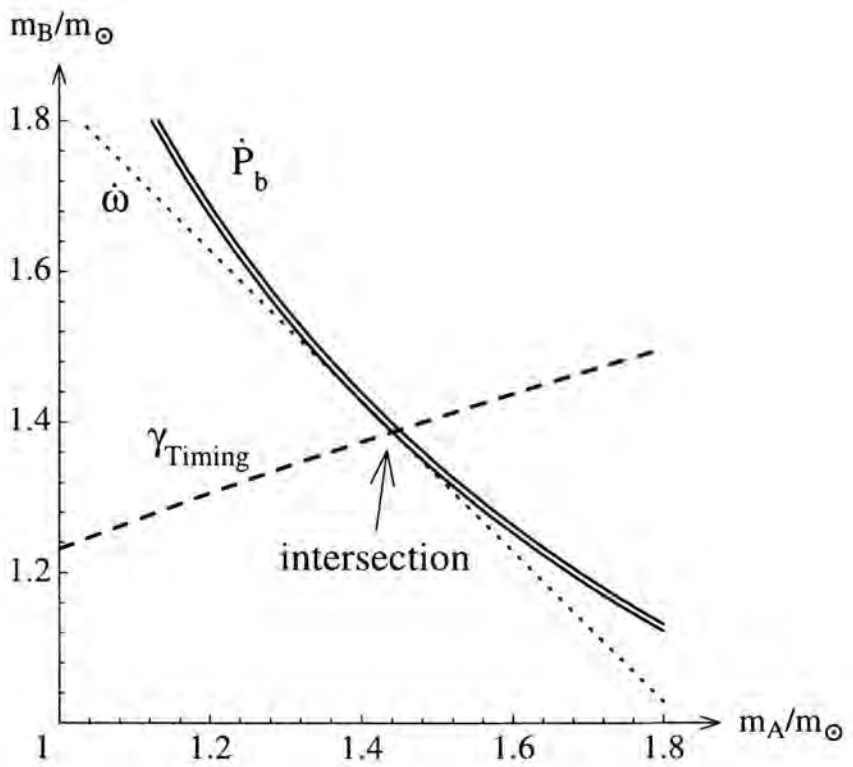

Figure 2. General relativity passes the $(\gamma\text{-}\dot{\omega}\text{-}\dot{P}_b)_{1913+16}$ test.

moving clock, the best tool that one could dream of to test a relativistic theory. Indeed, the frequency of the pulses is modified by the motion of the pulsar (Doppler effect), and one can extract from the Times Of Arrival many information concerning the orbit. For instance, the orbital period P_b can be obtained from the time between two maxima of the pulse frequency. One can also measure several other Keplerian parameters, like the eccentricity e of the orbit, the angular position ω of the periastron, etc.

In the case of PSR B1913+16, which has been continuously observed since its discovery in 1974 (Hulse & Taylor 1975), the data are so precise that one can even measure three relativistic effects with great accuracy. (i) The redshift due to the companion[1] $\propto Gm_B/r_{AB}c^2$ and the second-order Doppler effect $\propto v_A^2/2c^2$ are combined in an observable which has been denoted γ_{Timing}. (The index "Timing" is written to avoid a confusion with the Eddington parameter γ^{PPN} introduced in

[1] A denotes the pulsar, B the companion, and r_{AB} the distance between them.

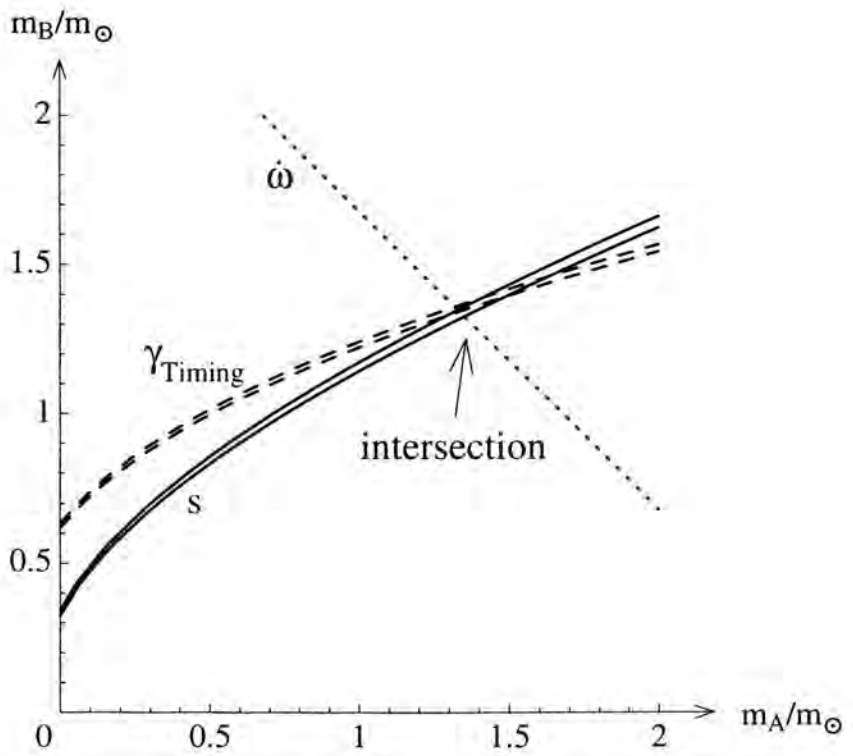

Figure 3. General relativity passes the $(\gamma\text{-}\dot{\omega}\text{-}s)_{1534+12}$ test.

Eq. (1b).) Since the Keplerian parameters P_b and ω have been measured accurately during two decades, their time derivatives are also available: (ii) $\dot{\omega}$ gives the periastron advance (a relativistic effect of order v^2/c^2), and (iii) the variation of the orbital period, $\dot{P}_b$, can be interpreted as a consequence of the energy loss due to the emission of gravitational waves (an effect of order v^5/c^5 in general relativity, but generically of order v^3/c^3 in alternative theories; see below). The three "post-Keplerian" observables $\gamma_{\rm Timing}$, $\dot{\omega}$, $\dot{P}_b$ can thus be compared with the predictions of a given theory, which depend on the unknown masses $m_{\rm A}$, $m_{\rm B}$ of the pulsar and its companion. However, 3 observables minus 2 unknown quantities is still 1 test. The equations $\gamma^{\rm th}(m_{\rm A}, m_{\rm B}) = \gamma^{\rm obs}$, $\dot{\omega}^{\rm th}(m_{\rm A}, m_{\rm B}) = \dot{\omega}^{\rm obs}$, $\dot{P}_b^{\rm th}(m_{\rm A}, m_{\rm B}) = \dot{P}_b^{\rm obs}$, define three curves (in fact three *strips*) in the two-dimensional plane of the masses $(m_{\rm A}, m_{\rm B})$. If the three strips meet in a small region, there exists a pair of masses $(m_{\rm A}, m_{\rm B})$ which is consistent with all three observables, and therefore the theory is consistent with the binary-pulsar data. If they do not meet, the theory is ruled out. Figure 2 displays these strips in the case of general relativity, which passes the test with flying colors. (We will see below that some other theories can also pass this test.)

The binary pulsar PSR B1534+12 has been observed only since 1991 (Wolszczan 1991) but it is much closer to the Earth than PSR B1913+16, and three post-Keplerian observables have already been measured with good precision: $\gamma_{\rm Timing}$, $\dot{\omega}$, and a new parameter denoted s. It is involved in the shape of the Shapiro time delay (an effect $\propto 1/c^3$ due to the propagation of light in the curved spacetime around the companion), and it can be interpreted as the sine $s = \sin i$ of the angle between the orbit and the plane of the sky. (The range r of this Shapiro time delay is also measured but with less precision.) Here again, the three strips "predictions$(m_{\rm A}, m_{\rm B})$ = observed values" can be plotted for a given theory, and if they meet each other, the test is passed. Figure 3 displays the case of general relativity, which passes the test at the 1σ level (Taylor et al. 1992).

As shown in §III below, generic theories of gravity predict a large dipolar emission of gravitational waves (of order v^3/c^3) when the masses of the pulsar and its companion are very different, whereas the prediction of general relativity starts at the much weaker quadrupolar order ($\propto v^5/c^5$). Several dissymmetrical systems, like the neutron star–white dwarf binary PSR B0655+64, happen to have very small observed values of $\dot{P}_b$, consistent with general relativity but not with a typical dipolar radiation. This is the third binary-pulsar test that we will use to constrain the space of gravity theories.

We will also see in §III below that in generic theories of gravity, the acceleration of a neutron star towards the center of the Galaxy is not the same as the acceleration of a white dwarf. This violation of the strong equivalence principle causes a "gravitational Stark effect" on the orbit of a neutron star–white dwarf system: its periastron is polarized towards the center of the Galaxy. (This is similar to the effects discussed in J. Bell's contribution to the present Proceedings.) More precisely, the eccentricity vector $\mathbf{e}$ of the orbit is the sum of a fixed vector $\mathbf{e}_F$ directed towards the Galaxy center (proportional to the difference of the accelerations of the bodies), and of a rotating vector $\mathbf{e}_R(t)$ corresponding to the usual periastron advance at angular velocity $\dot{\omega}_R$. Several dissymmetrical systems of this kind (such as PSRs 1855+09, 1953+29, 1800−27) happen to have a very small eccentricity. The only explanation would be that the rotating vector $\mathbf{e}_R(t)$ is precisely canceling the fixed contribution $\mathbf{e}_F$ at the time of our observation: $\mathbf{e}_F + \mathbf{e}_R(t) \approx \mathbf{0}$. However, this is very improbable, and one can use a statistical argument to constrain the space of theories (Damour & Schäfer 1991). Moreover, by considering several such systems, the probability that they have simultaneously a small eccentricity is the product of the already small individual probabilities. This idea has been used by Wex (1997) to derive a very tight bound on the difference of the accelerations of the bodies. This is the fourth binary-pulsar test that we will use in the following. Of course, general relativity passes this test, since it does satisfy the strong equivalence principle (universality of free fall of self-gravitating objects).

These four tests are presently the most precise of all those which are available. It should be noted that many other tests are *a priori* possible: Damour & Taylor (1992) have shown that 15 tests are in principle possible for each binary pulsar, if the pulses are measured precisely enough.

III Tensor-scalar theories of gravity

Introduction and action

We saw in the previous section that several tests of gravity can be performed in the strong-field regime, and that general relativity passes all of them. As discussed in §I, our aim is now to embed Einstein's theory into a class of alternatives, in order to determine what features have been tested, and what can be further tested. A generalization of the PPN formalism to all orders in $1/c^n$ would need an infinite number of parameters (cf. Eq. (1)). We will instead focus on the most natural class of alternatives to general relativity: "tensor-scalar" theories, in which gravity is mediated by a tensor field ($g_{\mu\nu}$) and one or several scalar fields (φ). Here are the main reasons why this class is privileged. (i) Scalar partners to the graviton arise naturally in theoretical attempts at quantizing gravity or at unifying it with other interactions (superstrings, Kaluza-Klein). (ii) They are the only consistent massless field theories able to satisfy the weak equivalence principle (universality of free fall of laboratory-size objects). (iii) They are the only known theories satisfying "extended Lorentz invariance" (Nordtvedt 1985), i.e., such that the physics of subsystems, influenced by external masses, exhibit Lorentz invariance. (iv) They explain the key role played by $\beta^{\rm PPN}$ and $\gamma^{\rm PPN}$ in the PPN formalism (the extra 8 parameters quoted in the Introduction vanish identically in tensor-scalar theories). (v) They are general enough to describe many different deviations from general relativity, but simple enough for their predictions to be fully worked out (Damour & Esposito-Farèse 1992).

Like in general relativity, the action of matter is given by a functional $S_m[\psi_m, \tilde{g}_{\mu\nu}]$ of some matter fields ψ_m (including gauge bosons) and one second-rank symmetric tensor[2] $\tilde{g}_{\mu\nu}$. The difference with general relativity lies in the kinetic term of $\tilde{g}_{\mu\nu}$. Instead of being a pure spin-2 field, it is here a mixing of spin-2 and spin-0 excitations. More precisely, it can be written as $\tilde{g}_{\mu\nu} = \exp[2a(\varphi)]g_{\mu\nu}$, where $a(\varphi)$ is a function of a scalar field φ, and $g_{\mu\nu}$ is the Einstein (spin 2) metric. The action of the theory reads thus

$$S = \frac{c^3}{16\pi G}\int d^4x\sqrt{-g}\,(R - 2g^{\mu\nu}\partial_\mu\varphi\partial_\nu\varphi) + S_m\left[\psi_m, e^{2a(\varphi)}g_{\mu\nu}\right] . \qquad (3)$$

(Our signature is $-+++$, R is the scalar curvature of $g_{\mu\nu}$, and g its determinant.)

Our discussion will now be focused on the function $a(\varphi)$, which characterizes the coupling of matter to the scalar field. It will be convenient to expand it around the

[2]To simplify, we will consider here only theories which satisfy exactly the weak equivalence principle, and we will restrict our discussion to a single scalar field except in §IV.

background value φ_0 of the scalar field (i.e., its value far from any massive body):

$$a(\varphi) = \alpha_0(\varphi - \varphi_0) + \frac{1}{2}\beta_0(\varphi - \varphi_0)^2 + \frac{1}{3!}\beta_0'(\varphi - \varphi_0)^3 + \cdots , \tag{4}$$

where α_0, β_0, β_0', ... are constants defining the theory. General relativity corresponds to a vanishing function $a(\varphi) = 0$, and Jordan-Fierz-Brans-Dicke theory to a linear function $a(\varphi) = \alpha_0(\varphi - \varphi_0)$. We will see in §V below that interesting strong-field effects occur when $\beta_0 \neq 0$, i.e., when $a(\varphi)$ has a nonvanishing curvature.

Weak-field constraints

Before studying the behavior of these theories in strong-field conditions, it is necessary to take into account the solar-system constraints (2). A simple diagrammatic argument (Damour & Esposito-Farèse 1996a) allows us to derive the expressions of the effective gravitational constant between two bodies, and of the Eddington PPN parameters in tensor-scalar theories:

$$G^{\text{eff}} = \mathrm{G}(1 + \alpha_0^2) , \tag{5a}$$

$$\gamma^{\text{PPN}} - 1 = -2\alpha_0^2/(1 + \alpha_0^2) , \tag{5b}$$

$$\beta^{\text{PPN}} - 1 = \frac{1}{2}\frac{\alpha_0\beta_0\alpha_0}{(1 + \alpha_0^2)^2} . \tag{5c}$$

(The factor α_0^2 comes from the exchange of a scalar particle between two bodies, whereas $\alpha_0\beta_0\alpha_0$ comes from a scalar exchange between three bodies.) The bounds (2) can therefore be rewritten as

$$\alpha_0^2 < 10^{-3} , \tag{6a}$$

$$|\alpha_0^2\beta_0| < 1.2 \times 10^{-3} . \tag{6b}$$

The first equation tells us that the slope of the function $a(\varphi)$ cannot be too large: the scalar field is linearly *weakly* coupled to matter. The second equation does not tell us much, since we already know that α_0^2 is small. In particular, it does not tell us if β_0 is positive ($a(\varphi)$ convex) or negative ($a(\varphi)$ concave).

The same diagrammatic argument can also be used to show that any deviation from general relativity at order $1/c^n$ ($n \geq 2$) involves at least two factors α_0, and has the schematic form

$$\begin{matrix}\text{deviation} \\ \text{from G.R.}\end{matrix} = \alpha_0^2 \times \left[\lambda_0 + \lambda_1 \frac{\mathrm{G}m}{R\mathrm{c}^2} + \lambda_2 \left(\frac{\mathrm{G}m}{R\mathrm{c}^2}\right)^2 + \cdots\right] , \tag{7}$$

where $\mathrm{G}m/R\mathrm{c}^2$ is the compactness of a body, and λ_0, λ_1, ... are constants built from the coefficients α_0, β_0, β_0', ... of expansion (4). Since α_0^2 is known to be small, we

thus expect the theory to be close to general relativity at any order. (We do not wish to consider models involving unnaturally large dimensionless numbers in the expansions (4) or (7).) However, in two different cases that will be discussed in §IV and V, the theory can exhibit significant strong-field deviations from general relativity: (i) If the theory involves more than one scalar field, Eq. (6a) does not necessarily imply that the slope of $a(\varphi)$ is small. (ii) Some nonperturbative effects can develop in strong-field conditions, and the sum of the series in the square brackets of Eq. (7) can be large enough to compensate even a vanishingly small α_0^2.

Strong-field predictions

The predictions of tensor-scalar theories in strong-field conditions have been derived in Damour & Esposito-Farèse (1992). They mimic the weak-field predictions with the important difference that the constants α_0, β_0 must be replaced by body-dependent parameters $\alpha_A \equiv \partial \ln m_A/\partial\varphi_0$, $\beta_A \equiv \partial\alpha_A/\partial\varphi_0$ (and similarly for the companion B). These parameters can be interpreted essentially as the slope and the curvature of $a(\varphi)$ at the center of body A (or body B). (In the weak-field regime, one has $\varphi \approx \varphi_0$, therefore $\alpha_A \approx \alpha_0$, $\beta_A \approx \beta_0$.) In particular, the effective gravitational constant between two self-gravitating bodies A and B reads

$$G_{AB}^{\rm eff} = G(1 + \alpha_A\alpha_B) \,, \tag{8}$$

instead of (5a). The acceleration of a neutron star A towards the center C of the Galaxy is thus proportional to $(1 + \alpha_A\alpha_C)$, whereas a white dwarf B is accelerated with a force $\propto (1 + \alpha_B\alpha_C)$. Since $\alpha_A \neq \alpha_B$ in general, there is a violation of the strong equivalence principle which causes the "gravitational Stark effect" discussed in §II.

The strong-field analogues of $\gamma^{\rm PPN}$ and $\beta^{\rm PPN}$ are given by formulas similar to (5b), (5c), but α_0^2 is replaced by $\alpha_A\alpha_B$ and $\alpha_0\beta_0\alpha_0$ by a combination of $\alpha_A\beta_B\alpha_A$ and $\alpha_B\beta_A\alpha_B$. The prediction for the periastron advance $\dot{\omega}$ can thus be written straightforwardly.

The expression of the observable parameter $\gamma_{\rm Timing}$ involves again the body-dependent parameters α_A, α_B, but also a subtle contribution proportional to $\alpha_B \times \partial \ln I_A/\partial\varphi_0$, where I_A is the inertia moment of the pulsar. This term is due to the modification of the equilibrium configuration of the pulsar due to the presence of its companion at a varying distance. We have shown in Damour & Esposito-Farèse (1992b) how to compute this effect, which happens to be particularly large in some models (see §V below).

The energy flux carried out by gravitational waves has been computed in Damour & Esposito-Farèse (1992). It is of the form

$$\text{Energy flux} = \left\{ \frac{\text{Quadrupole}}{c^5} + O\left(\frac{1}{c^7}\right) \right\}_{\text{helicity 2}}$$

$$+\left\{\frac{\text{Monopole}}{c}+\frac{\text{Dipole}}{c^3}+\frac{\text{Quadrupole}}{c^5}+O\left(\frac{1}{c^7}\right)\right\}_{\text{helicity 0}}. \tag{9}$$

The first curly brackets contain the prediction of general relativity. The second ones contain the extra terms predicted in tensor-scalar theories. The powers of $1/c$ give the orders of magnitude of the different terms. In particular, the monopolar and dipolar helicity-0 waves are generically expected to be much larger that the usual quadrupole of general relativity. However, the scalar monopole has the form

$$\frac{\text{Monopole}}{c}=\frac{G}{c}\left\{\frac{\partial(m_A\alpha_A)}{\partial t}+\frac{\partial(m_B\alpha_B)}{\partial t}+O\left(\frac{1}{c^2}\right)\right\}^2, \tag{10}$$

and it reduces to order $O(1/c^5)$ if the stars A and B are at equilibrium ($\partial_t(m_A\alpha_A)=0$), which is the case for all binary pulsars quoted in §II. (It should be noted, however, that this monopole would be huge in the case of a collapsing star, for instance.) The dipole has the form

$$\frac{\text{Dipole}}{c^3}=\frac{G}{3c^3}\left(\frac{G_{AB}m_Am_B}{r_{AB}^2}\right)^2(\alpha_A-\alpha_B)^2+O\left(\frac{1}{c^5}\right), \tag{11}$$

and is usually much larger than a quadrupole which is of order $1/c^5$ (see the third test discussed in §II). However, when the two stars A and B are very similar (e.g., two neutron stars), one has $\alpha_A\approx\alpha_B$ and this dipolar contribution almost vanishes. (A dipole is a vector in space; two identical stars do not define a preferred orientation.)

IV Tensor-multi-scalar theories

In order to satisfy the weak-field constraints (6) but still predict significant deviations from general relativity in the strong-field regime, the first possibility is to consider tensor-scalar theories involving at least two scalar fields (Damour & Esposito-Farèse 1992). Indeed, there can exist an exact compensation between the two fields in the solar system, although both of them can be strongly coupled to matter. If the kinetic terms of the scalar fields read $-(\partial_\mu\varphi_1)^2+(\partial_\mu\varphi_2)^2$, Eq. (6a) becomes $|\alpha_1^2-\alpha_2^2|<10^{-3}$, and none of the coupling constants α_1, α_2 needs to be small. However, one of the fields (here φ_2) must carry negative energy for this compensation to occur. Therefore, these tensor-bi-scalar theories can be considered only as *phenomenological* models, useful as contrasting alternatives to general relativity but with no fundamental significance.

We have constructed in the above reference the simplest tensor-bi-scalar model which has the following properties: (i) It has the same post-Newtonian limit as general relativity ($\beta^{\text{PPN}}=\gamma^{\text{PPN}}=1$), and therefore passes all solar-system tests. (ii) It does not predict any dipolar radiation $\propto 1/c^3$ ($\forall A,\forall B,\ (\alpha_A-\alpha_B)^2=0$), and therefore passes the third binary-pulsar test discussed in §II. Moreover, it depends on two

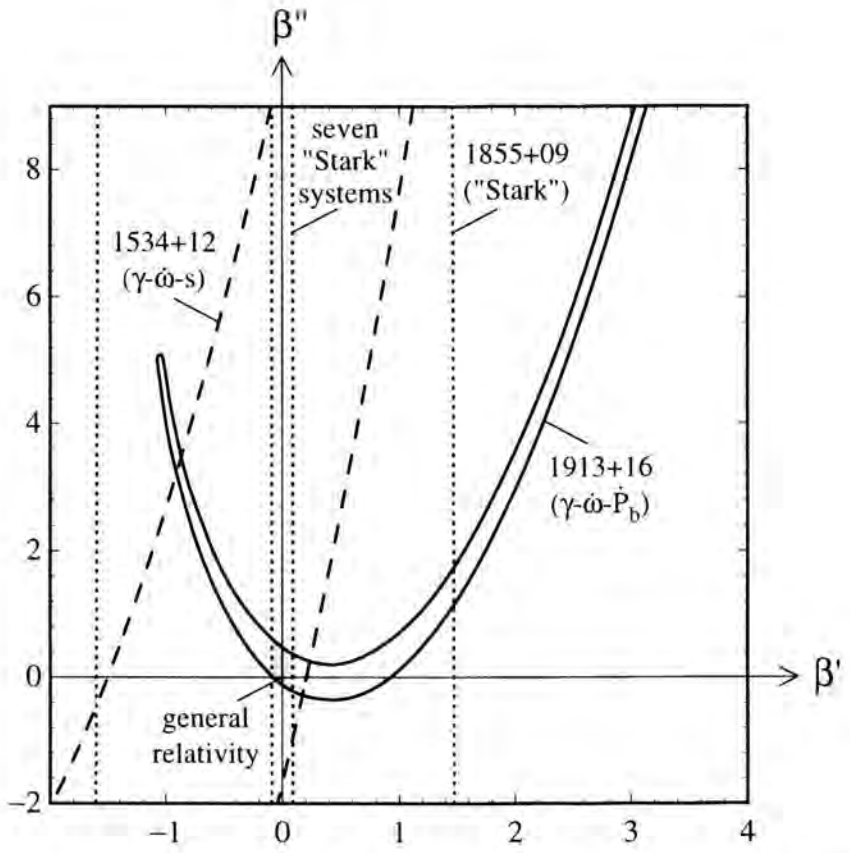

Figure 4. Constraints imposed by the four binary-pulsar tests of §II on the tensor-bi-scalar model of §IV. The two dotted strips illustrate how the precision of the "Stark" test is increased when several binary pulsars are considered simultaneously. The region allowed by all tests is the small shaded diamond around general relativity ($\beta' = \beta'' = 0$).

parameters β', β'', and general relativity corresponds to $\beta' = \beta'' = 0$. Figure 4 displays the constraints imposed by the three other binary-pulsar tests of §II in the plane of the parameters (β', β''). The theories passing the 1913+16 test are inside the long strip plotted in solid lines. Note that theories which are very different from general relativity can pass this test. For instance, Figure 5 displays the mass plane (m_A, m_B) for the (fine-tuned) model $\beta' = 8$, $\beta'' = 69$. The three strips are significantly different from those of Fig. 2, but they still meet each other in a small region (corresponding to values of the masses m_A, m_B different from those found in general relativity). To illustrate how much the theory differs from general relativity, let us just mention that the effective gravitational constant G_{AB}^{eff} between the pulsar and its companion is 1.7

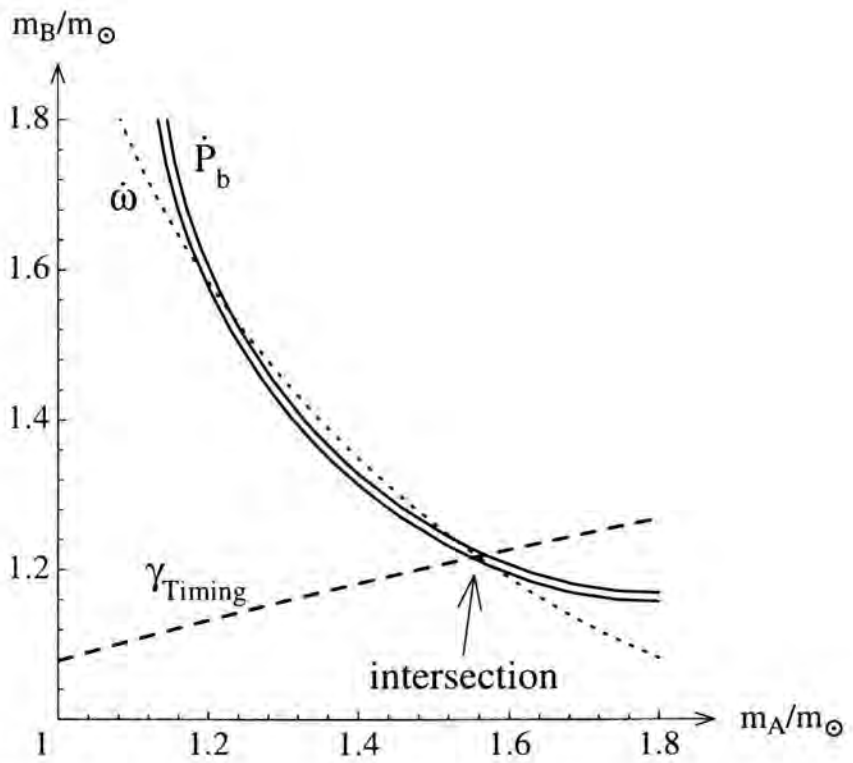

Figure 5. The tensor-bi-scalar model $\beta' = 8$, $\beta'' = 69$, passes the $(\gamma\text{-}\dot{\omega}\text{-}\dot{P}_b)_{1913+16}$ test, although the three curves are significantly different from those of Fig. 2.

times larger than the bare Newtonian constant G. We have thus exhibited a model which deviates by 70 % from Einstein's theory, but passes (i) all solar-system tests, (ii) the "no-dipolar-radiation" test of PSR 0655+64, and (iii) the "$\gamma_{\rm Timing}$-$\dot{\omega}$-$\dot{P}_b$" test of PSR 1913+16. Before our work, this 1913+16 test was usually considered as enough to rule out any theory but general relativity. We have proven that other binary-pulsar tests are also necessary. In particular, Fig. 4 shows clearly that the "$\gamma_{\rm Timing}$-$\dot{\omega}$-s" test of PSR 1534+12 and the "Stark" test complement it usefully. For instance, the model of Fig. 5 is easily ruled out by the 1534+12 test: the $\gamma_{\rm Timing}$ and s curves do not even meet each other (so that the observable $\dot{\omega}$ is not even useful here).

Thanks to the four binary-pulsar tests discussed in §II, this class of tensor-bi-scalar models is now essentially ruled out. We have achieved a similar result as in the weak-field regime of Fig. 1: only a tiny neighborhood of general relativity is still allowed. This is a much stronger result than just verifying that Einstein's theory passes these four tests.

V Nonperturbative strong-field effects

We now discuss the second way to satisfy the constraints (6) while predicting significant deviations from general relativity in the strong-field regime. As opposed to the models of the previous section, we consider here well-behaved theories, with only positive-energy excitations (of the type that is predicted by superstrings and extra-dimensional theories). To simplify, we will also restrict our discussion to the case of a single scalar field φ.

The simplest tensor-scalar theory, Jordan-Fierz-Brans-Dicke theory, cannot give rise to nonperturbative effects for an obvious reason. It corresponds to a linear coupling function $a(\varphi) = \alpha_0(\varphi - \varphi_0)$, and even if the field φ_A at the center of body A is very different from the background φ_0, one has anyway $\alpha_A \approx a'(\varphi_A) = \alpha_0$. Therefore, the deviations from general relativity, proportional to $\alpha_A \alpha_B \approx \alpha_0^2$, are constrained by the solar-system limit (6a) to be $\lesssim 0.1\ \%$ even in the vicinity of neutron stars.

On the contrary, if we consider a quadratic coupling function $a(\varphi) = \frac{1}{2}\beta_0\varphi^2$, the field equation for φ in a body of constant density ρ is of the form $\mathrm{d}^2(r\varphi)/\mathrm{d}r^2 \approx \beta_0\rho \cdot (r\varphi)$. Therefore, the solution involves a sinh if $\beta_0 > 0$, and a sin if $\beta_0 < 0$. More precisely, one finds

$$\alpha_A \approx \alpha_0 / \cosh \sqrt{3\beta_0 G m/Rc^2} \quad \text{if } \beta_0 > 0\,, \tag{12a}$$

$$\alpha_A \approx \alpha_0 / \cos \sqrt{3|\beta_0| G m/Rc^2} \quad \text{if } \beta_0 < 0\,. \tag{12b}$$

In the case of a convex coupling function $a(\varphi)$ (i.e., $\beta_0 > 0$), the deviations from general relativity are thus smaller in strong-field conditions than in the weak-field regime: $\alpha_A \alpha_B < \alpha_0^2 < 10^{-3}$. On the other hand, a concave $a(\varphi)$ can give rise to significant deviations: if $\beta_0 \lesssim -4$, the argument of the cosine function is close to $\pi/2$ for a typical neutron star ($Gm/Rc^2 \approx 0.2$), and α_A can thus be large even if α_0 is vanishingly small. To understand intuitively what happens when $\alpha_0 = 0$ strictly (i.e., when the theory is strictly equivalent to general relativity in weak-field conditions), it is instructive to compute the energy of a typical configuration of the scalar field, starting from a value φ_A at the center of body A and tending towards 0 as $1/r$ outside. One gets a result of the form

$$\begin{aligned} \text{Energy} &\approx \int \left[\frac{1}{2}(\partial_i\varphi)^2 + \rho\, e^{\beta_0\varphi^2/2}\right] \\ &\approx mc^2 \left(\frac{\varphi_A^2/2}{Gm/Rc^2} + e^{\beta_0\varphi_A^2/2}\right)\,. \end{aligned} \tag{13}$$

When $\beta_0 < 0$, this is the sum of a parabola and a Gaussian, and if the compactness Gm/Rc^2 is large enough, the function $\text{Energy}(\varphi_A)$ has the shape of a Mexican hat; the value $\varphi_A = 0$ now corresponds to a local *maximum* of the energy. It is therefore energetically favorable for the star to create a nonvanishing scalar field φ_A, and thereby

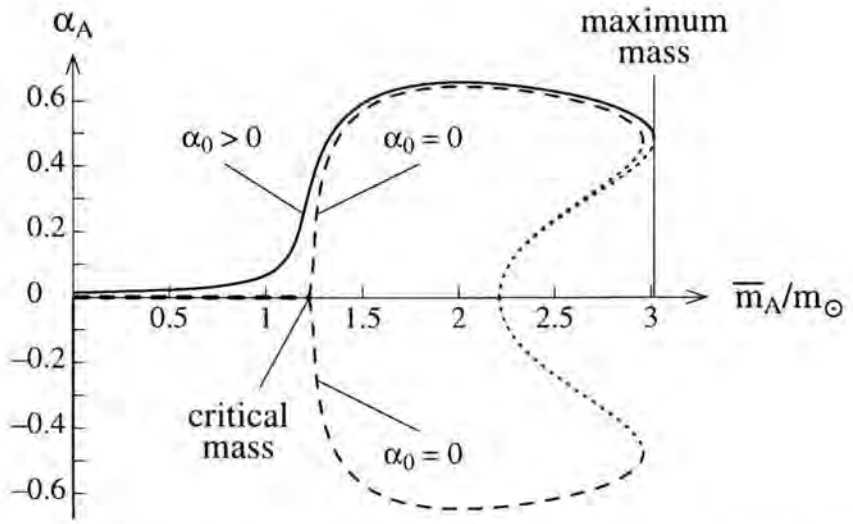

Figure 6. Scalar charge α_A versus baryonic mass $\overline{m}_A$, for the model $a(\varphi) = -3\varphi^2$ (i.e., $\beta_0 = -6$). The solid line corresponds to the maximum value of α_0 allowed by solar-system experiments, and the dashed lines to $\alpha_0 = 0$ ("zero-mode"). The dotted lines correspond to unstable configurations of the star.

a nonvanishing "scalar charge" $\alpha_A \approx \beta_0 \varphi_A$. This phenomenon is analogous to the spontaneous magnetization of ferromagnets.

We have verified the above heuristic arguments by explicit numerical calculations, taking into account the coupled differential equations of the metric and the scalar field, and using a realistic equation of state to describe nuclear matter inside a neutron star. We found that there is indeed a "spontaneous scalarization" above a critical mass, whose value depends on β_0. Figure 6 displays the scalar charge α_A for the model $\beta_0 = -6$. Note that the deviations from general relativity are of order $\alpha_A \alpha_B \approx 35\ \%$ for a wide range of masses from $\approx 1.25\, M_\odot$ to the maximum mass; therefore, no fine tuning is necessary to get large deviations in a particular binary pulsar. Note also that the nonperturbative effects do not vanish with α_0: even if the theory is *strictly* equivalent to general relativity in the solar system, it deviates significantly from it near compact bodies. In fact, an even more surprising phenomenon occurs for the term $\alpha_B \partial \ln I_A / \partial \varphi_0$ involved in the observable $\gamma_{\rm Timing}$ (see §II): this term blows up as $\alpha_0 \to 0$. In other words, a theory which is closer to general relativity in weak-field conditions predicts larger deviations in the strong-field regime!

The "$\gamma_{\rm Timing}$-$\dot{\omega}$-$\dot{P}_b$" test of PSR 1913+16 is displayed in Figure 7 for the model $\beta_0 = -6$ and the maximum value of α_0 allowed by solar-system experiments. (The "$\gamma_{\rm Timing}$-$\dot{\omega}$-s" test of PSR 1534+12 gives curves similar to those of Fig. 7 for the first two observables, while the s strip is only slightly deviated from that of Fig. 3.) The

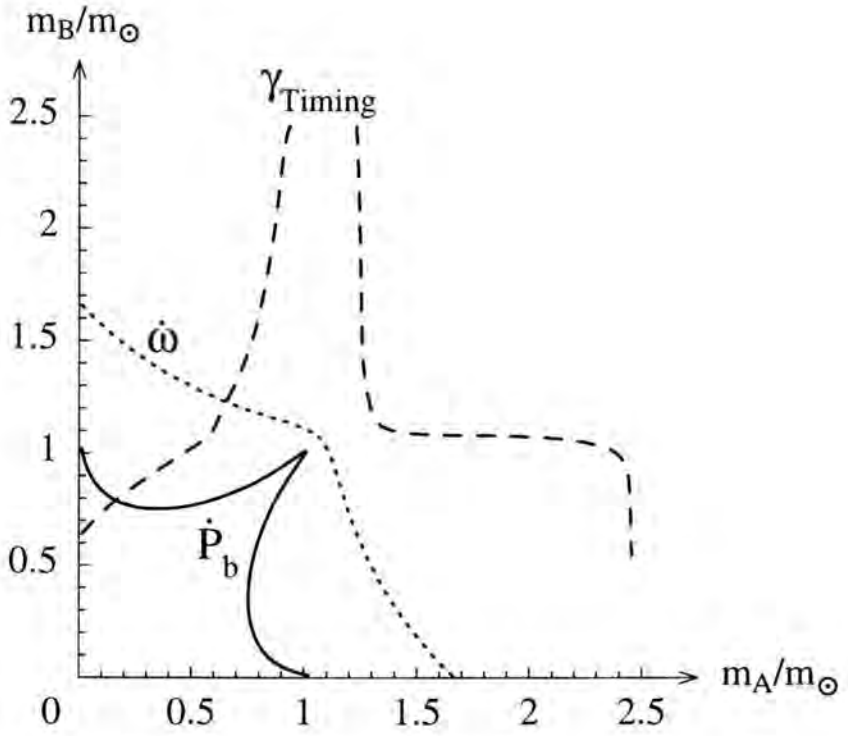

Figure 7. The model $a(\varphi) = -3\varphi^2$ does not pass the $(\gamma\text{-}\dot{\omega}\text{-}\dot{P}_b)_{1913+16}$ test.

great deformation of the $\dot{P}_b$ curve, as compared to the general relativistic prediction, Fig. 2, is due to the emission of dipolar waves in tensor-scalar theories. The fact that this dipolar radiation vanishes on the diagonal $m_A = m_B$ explains the shape of this curve. As expected, the $\gamma_{\rm Timing}$ curve is also very deformed because of the contribution $\alpha_B \partial \ln I_A / \partial \varphi_0$. When β_0 is not too negative (e.g., $\beta_0 \approx -4$), a smaller value of α_0 allows the test to be passed: the three curves finally meet in one point. On the contrary, when $\beta_0 < -5$, we find that the test is never passed even for a vanishingly small α_0 (because the term $\alpha_B \partial \ln I_A / \partial \varphi_0$ blows up). In other words, this binary pulsar rules out all the theories $\beta_0 < -5$, $\alpha_0 = 0$, although they are strictly equivalent to general relativity in weak-field conditions. This illustrates the *qualitative* difference between binary-pulsar and solar-system tests.

Generic tensor-scalar theories can be parametrized by the first two derivatives, α_0 and β_0, of their coupling function $a(\varphi)$, cf. Eq. (4). It is instructive to plot the constraints imposed by all kinds of tests in the plane (α_0, β_0). Figure 8 shows that solar-system experiments do not constrain at all the curvature β_0 of $a(\varphi)$ if its slope α_0 is small enough. On the contrary, binary pulsars impose $\beta_0 > -5$, independently of α_0.

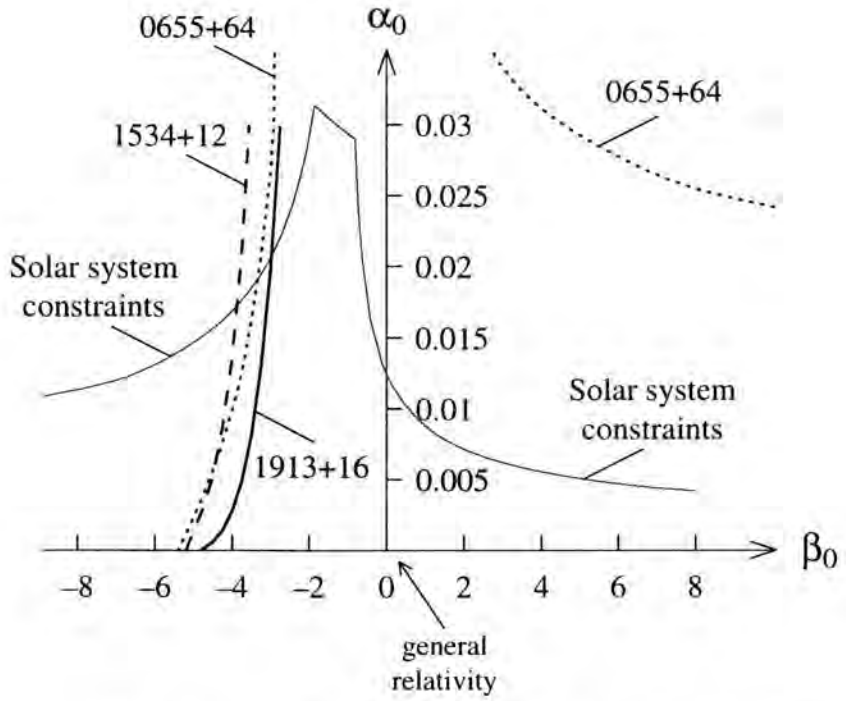

Figure 8. Constraints imposed by solar-system and binary-pulsar experiments in the plane (α_0, β_0). In view of the reflection symmetry $\alpha_0 \to -\alpha_0$, only the upper half plane is plotted. The allowed regions are below and on the right of the different curves. The shaded region is allowed by all the tests.

Using Eq. (5b), (5c), this bound can be expressed in terms of the Eddington parameters:

$$\frac{\beta^{\rm PPN} - 1}{\gamma^{\rm PPN} - 1} < 1.3 \,. \tag{14}$$

The singular $(0/0)$ nature of this ratio vividly expresses why such a conclusion could not be obtained in weak-field experiments.

Recent cosmological studies, notably Damour & Nordtvedt (1993), have shown that theories with a positive β_0 are easily consistent with observational data, whereas some fine-tuning would be required if $\beta_0 < 0$. It is fortunate that binary pulsars precisely privilege the positive values of this parameter.

VI Conclusions

Tensor-scalar theories of gravity are the most natural alternatives to general relativity. They are useful as contrasting alternatives, and can suggest new experimental tests. For instance, the tensor-bi-scalar model of §IV proved that a single binary-pulsar test does not suffice. Well-behaved tensor-scalar theories (with no negative energy, no large dimensionless parameters, and no fine tuning) can develop nonperturbative strong-field effects analogous to the spontaneous magnetization of ferromagnets. Their study illustrates the qualitative difference between binary-pulsar and solar-system experiments: binary pulsars have the capability of testing theories which are strictly equivalent to general relativity in the solar system.

References

Damour, T. & Schäfer, G. 1991, Phys. Rev. Lett., 66, 2549
Damour, T. & Taylor, J.H. 1992, Phys. Rev. D, 45, 1840
Damour, T. & Esposito-Farèse, G. 1992, Class. Quantum Grav., 9, 2093
Damour, T. & Nordtvedt, K. 1993, Phys. Rev. Lett., 70, 2217
Damour, T. & Esposito-Farèse, G. 1993, Phys. Rev. Lett., 70, 2220
Damour, T. & Esposito-Farèse, G. 1996, Phys. Rev. D, 53, 5541
Damour, T. & Esposito-Farèse, G. 1996, Phys. Rev. D, 54, 1474
Eddington, A.S. 1923, The Mathematical Theory of Relativity, Cambridge University Press
Hulse, R.A. & Taylor, J.H. 1975, ApJ, 195, L51
Nordtvedt, K. 1985, ApJ, 297, 390
Taylor, J.H. et al. 1992, Nature, 355, 132
Wex, N. 1997, A&A, 317, 976
Will, C.M. & Nordtvedt, K. 1972, ApJ, 177, 757
Wolszczan, A. 1991, Nature 350, 688

Authors' Address

Centre de Physique Théorique, CNRS Luminy, Case 907, F 13288 Marseille Cedex 9, France

J. Bell

Tests of Relativistic Gravity Using Millisecond Pulsars

Abstract

General relativity asserts that: energy and momentum conservation laws are valid, preferred frames do not exist, and the strong equivalence principle is obeyed. In this paper recent progress in testing these important principles using millisecond pulsars is summarized.

I Introduction

The fundamental physics and principles that can be observed and tested by the exceptional precision of pulsar timing includes (Bell 1997):

- Relativistic precession
- Shapiro delay
- Einstein delay
- Gravitational waves
- Variation in G
- Chandrasekhar mass
- Spin-orbit coupling
- Ultra low frequency gravitational waves
- Strong Equivalence Principle
- Lorentz Invariance
- Conservation laws

At this meeting Esposito-Farèse gave an update on the first 4 items and summary of the parametrised post-Newtonian formalism (PPN). Will (1993) also discusses the PPN formalism in detail and gives limits on many of the ten PPN parameters. Taylor et al. (1992) discuss many other relativistic effects which could in principle be measured with sufficient precision. Limits on the PPN parameters α_1, α_2, α_3 and ξ will be discussed here in relation to the last two items. Tests of the strong equivalence principle (SEP) giving limits on Δ (defined below) will also be discussed due to the similar nature of the tests. These tests are null tests and it is the 90% confidence level limits which are quoted.

In placing such limits, one wishes to know the extent to which strong field effects are contributing. Measurement of a given PPN parameter $\hat{\alpha}$ contains both a weak field contribution α and a strong field contribution α' (Damour & Esposito-Farèse 1992)

$$\hat{\alpha} = \alpha + \alpha'(c_1 + c_2 + \cdots) + \cdots \tag{1}$$

Here c_1, c_2 represent the compactness ($E_{\rm grav}/mc^2$) of the bodies involved. For the sun, $c_i \sim 10^{-6}$, for a neutron star $c_i \sim 0.2$ and for a black hole $c_i \sim 0.5$. Therefore, strong field effects are poorly constrained by solar system experiments, while pulsars provide comparable sensitivity and ease of study when compared to black holes.

The cosmic microwave background (CMB) has been chosen as the absolute frame in most studies. While some recent results (Lauer & Postman 1994) have questioned this, it is the magnitude, not the direction of the absolute velocity $\mathbf{w}$ that is most relevant; this is similar for both the CMB and Lauer & Postman data.

One might ask whether the similar nature (i.e., upper limits from low eccentricity orbits) of the tests discussed below (which constrain Δ, α_1 and α_3) makes them degenerate. This is not the case; there are sufficient degrees of freedom and different figures of merit for each test so that different pulsars are being used for each test.

II Lorentz Invariance, $|\alpha_2| < 2.4 \times 10^{-7}$

If a gravitational interaction is not Lorentz invariant (PPN $\alpha_2 \neq 0$, due to some long-range tensor field), an oblate spinning body will feel a torque (Nordtvedt 1987):

$$\tau \propto \alpha_2 \mathbf{w} \times \mathbf{\Omega}, \tag{2}$$

where $\mathbf{\Omega}$ is the angular velocity. This torque would cause the spin axis to precess about $\mathbf{w}$. Since the spin-orbit coupling between the sun and planets is weak, the close alignment ($\sim 6^\circ$) of the spin and orbital angular momenta means that the above torque is weak. Quantitatively, the limit is $|\alpha_2| < 2.4 \times 10^{-7}$, showing that the gravitational interaction is Lorentz invariant to high precision (Nordtvedt 1987).

There are two important assumptions made here: primordial alignment of the spin and orbital angular momenta and that the sun has not made many rotations and by

chance is closely aligned at the present epoch. Pulsars play a role in confirming that the second assumption is valid since if the torque was sufficiently large to cause the sun to make many rotations it would also be large enough to cause the fastest pulsars to precess out of view (Nordtvedt 1987), assuming they do not have fan beams.

Nordtvedt (1987) also considered preferred location effects as distinct from the above preferred frame effects. The resulting Lagrangian for a three-body interaction contains the PPN parameter ξ. Using the Galactic center as a distant third body yields $\tau \propto \xi \mathbf{w} \times \mathbf{\Omega}$, giving a limit on ξ similar to the limit on α_2 by the same arguments.

III Polarised orbits and relativistic precession

The tests discussed in sections IV, V, and VI search for the presence of eccentricities induced in pulsar orbits. These are gravitational analogues of the Stark effect, with the orbits being polarised in particular directions. However there is a non-zero probability that the relativistic precession of the orbit may cause cancellation with the intrinsic eccentricity of the system.

The problem of the possible cancellation was first considered by Damour and Schäfer (1991). They noted that, if the binary pulsar system is old compared to the time scale for precession, so that many rotations had been completed, then a statistical treatment of the probability of cancellation was sufficient since the goal was an upper limit rather than a measurement. A more precise statistical treatment was derived by Wex (1997) who also demonstrated the power of using multiple systems to improve the limits.

IV Strong Equivalence Principle, $|\Delta| < 0.004$

The SEP requires the universality of the free fall of self-gravitating objects, i.e. in the same gravitational potential, two bodies should feel the same acceleration regardless of their mass, composition and density. Nordtvedt (1968) showed that if SEP did not hold for the Earth-Moon-Sun system, the Moon's orbit would be eccentric and polarised with the semi-major axis pointing towards the Sun. So began the now famous lunar-laser-ranging experiments which searched for this polarisation using the Apollo 11 reflector and measurement uncertainties of ~ 1 ns in the time of flight.

Damour and Schäfer (1991) pointed out the need for such a test in a strong field regime and showed that it is possible using binary pulsars. They suggested that the Earth-Moon-Sun system be replaced with a pulsar-companion-Galaxy system. If the companion is a white dwarf, the composition, density and self gravity is very different to the pulsar giving sensitivity to strong field effects. Damour and Schäfer (1991) showed that the figure of merit for choosing the best test systems is $f_\Delta = P_b^2/e$ and used PSR B1953+29 to obtain the limit $|\Delta| = |1 - M_I/M_G| < 0.01$.

Arzoumanian (1995) suggested that PSR B1800−27 could be used to improve this limit to $|\Delta| < 0.004$, however it is not clear that this system is sufficiently old (Wex 1997). If several pulsars are used simultaneously the multiplication of small probabilities leads to the very rigorous bound of $|\Delta| < 0.004$ (Wex 1997).

V Lorentz Invariance, $|\hat{\alpha}_1| < 1.7 \times 10^{-4}$

If preferred reference frames exist and $\alpha_1 \neq 0$, then there is a constant forcing term in the time evolution of the eccentricity vector of a binary system. For a very low eccentricity orbit, this tends to "polarize" the orbit, aligning the eccentricity vector with the projection onto the orbital plane of the absolute velocity of the system. Hence, the orbital parameters of very low eccentricity binary pulsars such as PSR B1855+09 may be used to set an upper bound of $|\hat{\alpha}_1| < 5 \times 10^{-4}$ (Damour & Esposito-Farèse 1992). This compares with limits from solar system data of $\alpha_1 = 2.1 \pm 1.9 \times 10^{-4}$ (Hellings 1984).

The most circular orbit known ($e \sim 10^{-6}$), that of PSR J2317+1439 (Camilo, Nice & Taylor 1996) has a figure of merit $f_{\alpha_1} = P_b^{1/3}/e$ 10 times better than PSR B1855+09. However, the more unfortunate orientation with respect to the CMB and poorly constrained radial velocity means that only a factor of 3 improvement was possible, giving a limit of $|\hat{\alpha}_1| < 1.7 \times 10^{-4}$ (Bell, Camilo & Damour 1996).

VI Conservation laws and Lorentz invariance, $|\alpha_3| < 2.2 \times 10^{-20}$

As shown by Nordtvedt and Will (1972) , a non-zero α_3 induces a contribution to the perihelion precession of the planets in the solar system. The two planets with the best measurements of periastron advance were Earth and Mercury. By combining the observations for two planets it is possible to eliminate the terms involving other parameters, obtaining $|49\alpha_1 - \alpha_2 - 6.3 \times 10^5 \alpha_3 - 2.2\xi| < 0.1$ (Will 1993). Using the limits on α_1, α_2, ξ a limit of $|\alpha_3| < 2 \times 10^{-7}$ was thus obtained.

Single pulsars

A tighter limit on α_3 has been obtained by considering the effect of the acceleration

$$\mathbf{a}_{\rm self} \propto \alpha_3 \mathbf{w} \times \mathbf{\Omega} \tag{3}$$

on the observed pulse periods of isolated pulsars. The observed pulse period $P \simeq P_0(1 + v_r/c)$, contains a contribution from the Doppler effect due to the radial velocity v_r. Similarly any radial acceleration a_r contributes to the observed period derivative $\dot{P} \simeq \dot{P}_0 + P a_r/c$.

Self accelerations are directed perpendicular to both $\mathbf{w}$ and $\mathbf{\Omega}$. If self accelerations were contributing strongly to the observed period derivatives of pulsars, roughly equal numbers of positive and negative observed period derivatives would be expected, since the spin axes and therefore the self accelerations are randomly oriented. The observed distribution of normal pulsars (excluding those pulsars in globular clusters) contains only positive period derivatives, allowing a limit of $|\alpha_3| < 2 \times 10^{-10}$ to be placed (Will 1993). Using millisecond pulsars, Bell (1996) obtained a limit of $|\alpha_3| < 5 \times 10^{-16}$.

Binary pulsars

For a binary pulsar with a white dwarf companion, we again have two bodies with very different self gravities and sensitivities to strong field effects. If $\alpha_3 \neq 0$, the induced self-acceleration of the white dwarf would be negligible compared to that of the pulsar. Hence, we now have a rocket in a binary system. Since $\mathbf{a}_{\rm self}$ is perpendicular to $\mathbf{\Omega}$ and since the spin and orbital angular momenta are aligned for recycled systems, the $\mathbf{a}_{\rm self}$ is in the plane of the orbit. The resulting effect is a polarised orbit similar to those predicted by SEP violations (section IV) and Lorentz invariance violations (section V) (Bell & Damour 1996).

The figure of merit for choosing the best test systems is $f_{\alpha_3} = P_b^2/eP$. Selecting appropriate systems and applying the statistical treatment of relativistic precession (section III) gives a limit of $|\alpha_3| < 2.2 \times 10^{-20}$ (Bell & Damour 1996). The only other ultra-high-precision null experiments (giving limits of order 10^{-20} on a dimensionless theoretical parameter) of which we are aware, are the recent Hughes-Drever-type tests (Prestage et al. 1985, Lamoreaux et al. 1986, Chupp et al. 1989), shown in Figure 14.2 of Will (1993). It is remarkable that tests involving binary pulsars can rank, together with modern laser-cooled trapped atom experiments, among the most precise null experiments of physics.

VII Prospects for further improvements

The figures of merit indicate how strongly these tests depend on the orbital periods and eccentricities of binary pulsars. The dotted lines in Figure 1 indicate the relative slopes of $f_\Delta \propto P_b^2/e$ and $f_{\alpha_1} \propto P_b^{1/3}/e$. There are also strongly evolutionary links expected between P_b and e (Phinney 1992) as shown by the solid line. Comparison of the slope of this curve, with the figure of merit dependence on P_b and e indicates that scope for improvements of the SEP test is small unless more longer orbital period systems can be found. A similar conclusion for the α_3 limit can be drawn but the additional dependence on P, ($f_{\alpha_3} \propto P_b^2/eP$) makes it less clear.

The flatter dependence on P_b of f_{α_1} means that short orbital period systems are preferable. However, only upper limits are presently available for many of these (the

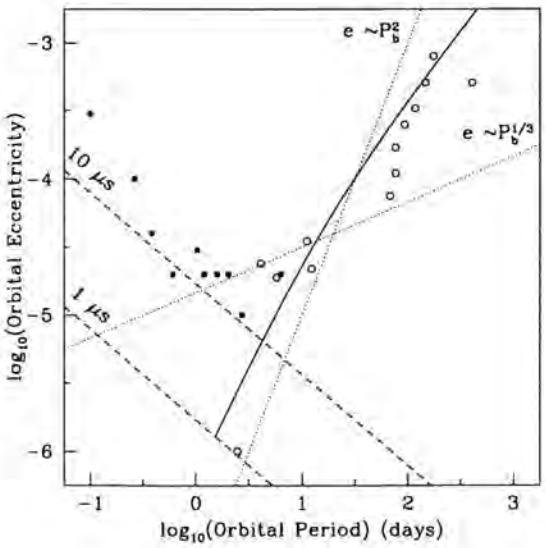

Figure 1. Orbital eccentricities of low-mass binary radio pulsars. Circles: measured values; squares: upper limits. Dashed lines—approximate limits obtainable on eccentricities for RMS timing residuals of 10 μs and 1 μs.

filled squares in Fig. 1). If these upper limits could be reduced substantially, it should be possible to usefully improve the limit on α_1, especially if several systems are used.

The limits on α_2 and ξ may be improved slightly, by careful consideration of pulse profile changes of the fastest pulsars to obtain limits on the precession. However there is another more promising approach. If the orientation of the spin and orbital angular momenta could be determined for binary millisecond pulsars it would be possible to improve the limits on α_2 and ξ by several orders of magnitude. The inclination of the PSR J1012+5307 orbit has been determined from optical observations (van Kerkwijk, Bergeron & Kulkarni 1996). It may be possible to obtain the orientation of the pulsar spin axis from polarization observations. With only one system, the ambiguity of many rotations would remain, but with several such binary systems, statistical arguments similar to those used for Δ and α_3 could provide very strict limits.

Acknowledgements

I thank the organizers for an excellent meeting and G. Esposito-Farèse for useful discussions.

References

Arzoumanian, Z. 1995, Ph.D. Thesis, Princeton Univ.

Bell, J.F. 1996, ApJ, 462, 287

Bell, J.F. 1997, in Satellite and Ground Based Studies of Radio Pulsars, Proceedings of Section E1.5 of the 31st Scientific Assembly of COSPAR, ed. P. Caraveo (Amsterdam: Elsevier), in press

Bell, J.F., Camilo, F. & Damour, T. 1996, ApJ, 464, 857

Bell, J.F. & Damour, T. 1996, Classical Quantum Gravity, 13, 3121

Camilo, F., Nice, D.J. & Taylor, J.H. 1996, ApJ, 461, 812

Chupp, T.E. et al. 1989, PRL, 63, 1541

Damour, T. & Esposito-Farèse, G. 1992, PRD, 46, 4128

Damour, T. & Schäfer, G. 1991, PRL, 66, 2549

Hellings, R.W. 1984, in General Relativity and Gravitation, Proceedings of the Tenth International Conference, ed. B. Bertatti, F. de Felice, & A. Pascolini, (Dordrecht: Reidel), 365

Lamoreaux, S.K. et al. 1986, PRL, 57, 3125

Lauer, T.R. & Postman, M. 1994, ApJ, 425, 418

Nordtvedt, K. 1968a, Phys. Rev., 169, 1014

Nordtvedt, K. 1968b, Phys. Rev., 170, 1186

Nordtvedt, K. 1987, ApJ, 320, 871

Nordtvedt, K. & Will, C.M. 1972, ApJ, 177, 775

Phinney, E. S. 1992, PTRSA, 341, 39

Prestage, J.D. et al. 1985, PRL, 54, 2387

Taylor, J.H. et al. 1992, Nature, 355, 132

van Kerkwijk, M.H., Bergeron, P. & Kulkarni, S.R. 1996, ApJ, 467, L89

Wex, N. 1997, A&A, 317, 976

Will, C.M. 1993, Theory and Experiment in Gravitational Physics, (Cambridge: Cambridge University Press)

Authors' Address

The University of Manchester, NRAL, Jodrell Bank, Cheshire SK11 9DL, UK;
jb@jb.man.ac.uk

D.C. Backer and T. Wong

Interstellar Weather—Radio Wave Propagation Through the Turbulent Ionized Interstellar Medium

Abstract

Turbulence, or turbulent-like structures, in the interstellar medium when combined with motions of the medium and the pulsar-earth line of sight lead to observable changes in pulse arrival time via dispersion measure changes and multipath propagation or pulse broadening. In the Vela (PSR B0833−45) and Crab (PSR B0531+21) pulsars the column density variations are dominated by structures within the high density material associated with the surrounding supernova remnants and pre-stellar matter. In the millisecond pulsar B1937+21 the effects are much smaller and are associated with the general intervening interstellar medium. Precision timing in the presence of unstable interstellar weather require multifrequency observations at the highest possible radio frequencies with dense sampling in time.

I Radio wave propagation primer

Useful references on radio wave propagation through the turbulent interstellar medium include: Rickett (1977); Cordes, Pitwerbetsky & Lovelace (1986); Hu et al. (1991); Foster & Cordes (1990).

The index of refraction in a dilute, thermal plasma contains a term dependent on the electron density divided by the radio frequency ($\nu = c/\lambda$) squared. The medium is thus dispersive. A path integral of the inverse of the group velocity at any frequency provides the dispersive delay, $\tau_{\rm DM}$, which depends on the column density of electrons. Radio astronomers call this column density the Dispersion Measure, or DM, and use units of pc cm^{-3},

$$\mathrm{DM(pc\ cm^{-3})} = \int n_e \mathrm{d}l$$

$$\tau_{\rm DM} \propto \mathrm{DM}/\nu^2.$$

The interstellar plasma density is not uniform. There are fluctuations on all scales—from kpc down to 10^8 m or less. On scales below one parsec the fluctuations in some

regions may be described by a single power law wave number spectrum. Furthermore this spectrum may indicate the operation of a Kolmogorov-like turbulent cascade with injection of density and velocity fluctuations at an outer scale and dissipation of turbulent energy after the cascade at an inner scale. One goal of the pulsar observations described below is better understanding of the location and spectrum of the interstellar plasma fluctuations.

The transverse motion of the pulsar-earth line of sight at $v_\perp$ through turbulent plasma leads to variations in the DM. The structure function of DM(t) is a useful statistical summary:

$$D_{\rm DM}(\tau) \equiv \langle [({\rm DM}(t+\tau) - {\rm DM}(t)]^2 \rangle \propto \tau^\delta.$$

Here δ is 2 for $\tau/v_\perp$ less than the inner scale and 0 when greater than the outer scale. For intermediate length scales the slope is related to the slope of the power spectrum and has been shown to be near 2.

The dispersive delay can be written as radio wave phase by multiplying by the radio frequency. (In a dilute plasma the phase velocity and group velocity are very near c and inversely proportional to each other.) The phase fluctuations are much larger than one radian on transverse length scales equal to the first Fresnel radius for most pulsar observations. Consequently diffraction plays an important role. We can define a transverse coherence length $l_\circ$ from the phase structure function, $D_\phi(l_\circ) \equiv 0$. This coherence length is roughly proportional to radio frequency,

$$l_\circ \propto \nu.$$

The presence of a power law wave number spectrum (3D) of density fluctuations with an index near -4 will change this dependence slightly.

Consider a slab of turbulent plasma along the line of sight as shown in Figure 1. A plane wave incident upon this slab will be scattered by the phase fluctuations into a cone of dimension $\Theta_s = \lambda/l_\circ$. This scattering angle is a property of the slab independent of its location. As an aside the scattering here is by plasma waves and not single electron Thompson scattering. Fig. 1 provides the geometry of scattering for source and observer at finite distances. The apparent size of a point source seen through the slab is

$$\Theta_\circ = x\Theta_s \propto \nu^2.$$

The observable effect of scattering by the slab decreases as it is moved toward the emitter.

The angular scattering results in multipath propagation and a broadening of sharp impulses sent through the slab by a time

$$\tau_s = x(1-x)D\Theta_s^2/2{\rm c} \propto \nu^4.$$

Pulse broadening is maximized when the slab is half way between the pulsar and the observer. A further effect of scattering is that the region of the slab through which

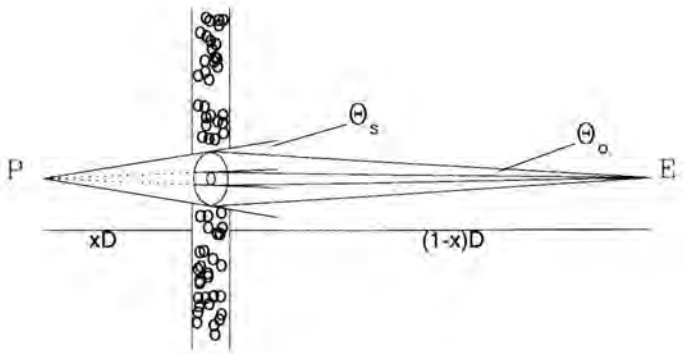

Figure 1. Geometry of interstellar scattering. Inner cone corresponds to scattering at 610 MHz and outer to scattering at 327 MHz.

radiation is received has a transverse scale of

$$l_d = x(1-x)\Theta_s D.$$

The DM that we measure is then an average of the column density over this scale. This averaging smooths the DM(t) that would be observed in the absence of scattering. In the case illustrated in Fig. 1 the smoothing time scale is $l_d/(1-x)v_\perp = x\Theta_s/v_\perp$.

Finally those phase fluctuations on scales larger than a Fresnel radius lead to refraction effects such as small (25%) intensity modulation. The time scale for changes in the refractive effects is the same as that just described for smoothing of DM changes. Refraction also changes the effective scattering angle, and thereby modulates angular (Θ_o) and temporal (τ_s) broadening. The paths of signals through the slab in Fig. 1 will be bent by refraction and the bending will be frequency dependent. For steep power law density irregularity spectra the refraction angles can exceed the scattering cone angle Θ_s while for shallow spectra refraction is small with respect to Θ_s.

II Observations

Most of the observations described below were obtained with the 85 ft pulsar monitoring telescope in Green Bank, WV. Receivers with linearly polarized feeds at 327 and 610 MHz are mounted off axis for continuous use by offset pointing. The bandwidths are 10 and 40 MHz respectively. Average pulse profiles are obtained after 5–10 minutes of integration with the Green Bank-Berkeley Pulsar Processor (e.g., Backer et al. 1997). The multichannel data from this processor are reduced to flux calibrated average pulse profiles. Further reduction includes estimation of flux, pulse broadening in some cases and arrival times.

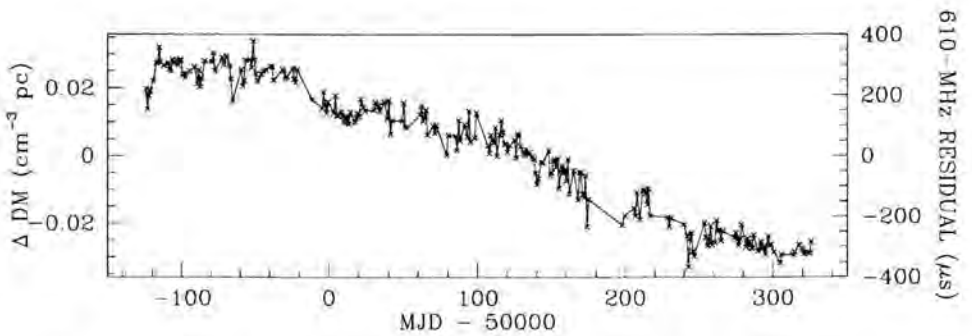

Figure 2. Dispersion measure variations for PSR B0833−45 from Green Bank pulsar monitoring telescope.

PSR B0833−45, the Vela pulsar

Figure 2 shows that the DM of the Vela pulsar continues to decline at the rate of -0.04 pc cm^{-3} y^{-1} first reported by Hamilton et al. (1977). Apparently a large wedge of plasma is exiting the line of sight. Given the pulsar's proper motion of 115 km s^{-1} (Bailes et al. 1989) and assuming a factor x of 0.5, we can infer a typical density in this wedge of 10^3 cm^{-3} and a transverse scale exceeding 10^{16} cm. Gradients of DM are seen in other pulsars (Phillips & Wolszczan 1992; Backer et al. 1993). The gradient for the Vela pulsar is very large by comparison. One can conclude that the DM changes for the Vela pulsar are the result of dense material in the Gum nebula within which the Vela pulsar resides. The gradient will lead to a frequency dependent source position (about 10 mas at 1 m λ) that could be detected by astrometric observations with a global VLBI array.

Small changes in the pulse broadening of the Vela pulsar at 327 MHz are also observed. The amplitude and time scale of these changes suggest an origin in the refractive properties of the intervening medium as discussed in the primer section. A useful followup study to our monitoring of pulse broadening would be contemporaneous angular broadening measurements. The combined measurements should show correlated changes and can determine the location of the scattering slab if the effects are dominated by a single portion of the line of sight (see Gwinn, Bartel, & Cordes 1993).

PSR B0531+21, the Crab pulsar

Rankin & Counselman (1973) reported on changes in the DM and pulse broadening of the Crab pulsar. Their analysis of pulse broadening led to the conclusion that the line of sight was dominated by two scattering slabs and that one was highly variable. The natural conclusion was that the highly variable slab was in or around the Crab nebula.

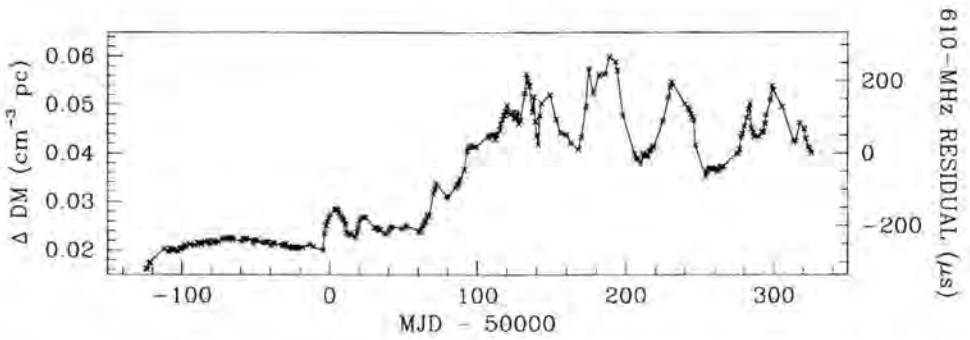

Figure 3. Dispersion measure variations for PSR B0531+21 from Green Bank pulsar monitoring telescope. A large dispersion and scattering event began around MJD 50000, 1995 October 10.

Lyne & Thorne (1975) and Rankin et al. (1988) reported on extreme variations of the scattering during 1974. Again these variations were attributed to Crab nebula plasma.

Figure 3 displays the DM record from our observations over the past 1.5 yr. Extreme variations similar to the event in 1974 are evident in this DM record as well as in the pulse broadening. Conversion of time scales to transverse length scales leads to density estimates around 10^3 cm^{-3} which is comparable to the densities in the web of filaments that surround the optical synchrotron nebula (Lawrence et al. 1995; Hester et al. 1996). We conclude that this is the likely site for the extreme scattering material and that $x = 10^{-3}$. Note that this small value of x means that the apparent size of the pulsar may not have changed very much. In a more complete report (Wong, Backer & Lyne 1997) we present a structure function for the DM variations both from the results in Fig. 3 and from the historic record kept at Jodrell Bank. The structure function has a rather flat index, near +1, that also distinguishes these variations from those in the general interstellar medium.

PSR B1937+21, a millisecond pulsar

In Green Bank we are conducting precision timing of PSR B1937+21 at four radio frequencies: 327, 610, 800 & 1395 MHz. Figure 4 displays the timing residuals from a model fit to the 1395 MHz data. Deviations of the 800 MHz data with microsecond amplitude are expected from DM variations along the line of sight through the general interstellar medium (Backer et al. 1993; Kaspi, Taylor & Ryba 1994). The figure also displays the 610 MHz residuals from the same timing model. These residuals are larger as expected from the radio frequency dependence of the dispersion. The dotted lines in Fig. 4 follow the 800 MHz data with scaling by the ratio of $(1/610^2 - 1/1395^2)/(1/800^2 - 1/1395^2)$ to show what the effects of dispersion would be assuming that the 800 MHz residuals are dispersive. There is good agreement

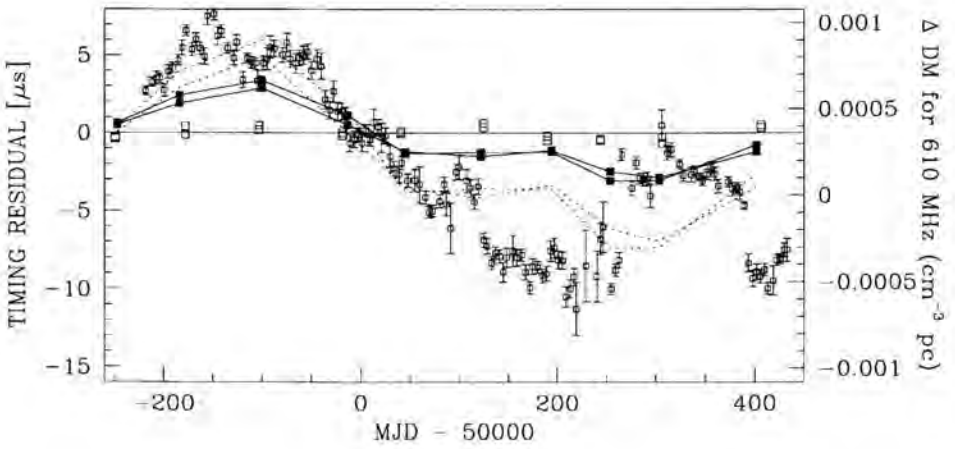

Figure 4. Dispersion measure variations for PSR B1937+21 from Green Bank pulsar monitoring and 140 ft telescopes. Open squares are 1395 MHz data; solid squares are 800 MHz data and densely sampled open squares with error bars are 610 MHz data. A model is fit to the 1395 MHz data to produce near zero residuals. The deviations of the 800 MHz data from zero are interpreted as dispersive and the dashed lines represent how this dispersive delay would scale to 610 MHz. There is an arbitrary zero for the three sets of residuals, and some uncertainty surrounds the continuity of 610 MHz residuals at MJD 50228 owing to equipment changes.

through about MJD 50120 (1996 February 07). After this date there appear to be several swings of the 610 MHz residuals above and below the dispersive extrapolation. Inspection of other data from this telescope show no evidence for equipment problems. In particular the residuals for PSR J0437−4715 in the interval since MJD 50228 are smaller than that shown in Fig. 4. Furthermore there is evidence in the 327 MHz data (not shown here) for events with different temporal behavior associated with the abrupt changes in the 610 MHz residuals shown in Fig. 4. Cognard et al. (1993) report on sudden changes in the propagation effects of B1937+21 which they conclude are the result of crossing a caustic.

There is a good reason for the lack of agreement of the four frequency data with a simple model of variable plasma dispersion. As discussed in the primer the effects of angular scatteringmean that *the* dispersion measure (column density of electrons) is in fact an average over a volume of the intervening path established by the diffractive and refractive properties along the path. In the simplest case this volume is a tube of growing diameter out to the midpath point and then contracting as the observer is approached (see Fig. 1). (In the absence of scattering the tube diameter would be established by the Fresnel radius along the line of sight.) The diameter of this volume

is set by the path geometry and the scattering angle. The total volume of this averaging tube is thus dependent approximately on $-nu^{-4}$. As a consequence, *the* dispersion measure is *not* an accurately defineable quantity at any instant—the column density of electrons depends to some extent on frequency. The inaccuracy is most evident on the refractive time scale, the time scale for the averaging volume to displace itself, and this time scale is itself frequency dependent as stated above. At 610 MHz we estimate that the refractive time scale is 40 d.

Precision timing of millisecond pulsars, if limited by dispersive effects, can best be improved both by going to higher observing frequency and with dense sampling in time to average over independent samples. On time scales less than the refractive time scale, the variance of the variations will increase as t^2.

Acknowledgements

We are grateful for the Naval Research Laboratory's support of the Green Bank pulsar monitoring telescope, and assistance from the NRAO operators and David Nice.

References

Backer, D.C. et al. 1997, PASP, 109, 61
Backer, D. . et al. 1993, ApJ, 404, 636
Bailes, M. et al. 1989 ApJ, 343, L53
Cognard, I. et al. 1993, Nature, 366, 320
Cordes, J.M., Pitwerbetsky, A. & Lovelace, R.V.E. 1986, ApJ, 310, 737
Foster, R.S. & Cordes, J.M. 1990, ApJ, 364, 123
Gwinn, C.R., Bartel, N. & Cordes, J.M. 1993, ApJ, 410, 673
Hamilton, P.A. et al. 1977, Nature, 265, 224
Hester, J.J. et al. 1996, ApJ, 456, 225
Hu, W., Romani, R.W. & Stinebring, D.R. 1991, ApJ, 366, L33
Kaspi, V.M., Taylor, J.H. & Ryba, M.F. 1994, ApJ, 428, 713
Lawrence, S.S. et al. 1995, AJ, 109, 2885
Lyne, A.G. & Thorne, D.J. 1975, MNRAS, 172, 97
Phillips, J.A. & Wolszczan, A. 1992, ApJ, 385, 273
Rankin, J.M. & Counselman, C.C. 1973, ApJ, 181, 875
Rankin, J.M. et al. 1988, AA, 202, 166
Rickett, B.J. 1977, ARAA, 15, 479
Wong, T., Backer, D.C. & Lyne, A.G. 1997, in preparation

Authors' Addresses

Astronomy Department, University of California, Berkeley, CA 94720, USA

M. Kramer, O. Doroshenko and K.M. Xilouris

Prospects of Pulsar Timing at High Frequencies Including Polarization Measurements

Abstract

We have been exploring the possibility of high frequency pulsar timing with the Effelsberg radio telescope. We describe briefly the instrumentation for such a project and discuss its advantages in comparison to low frequency timing. Successful observations of some millisecond pulsars at 4.85 GHz as well as the results from an ongoing timing experiment at 1.4 GHz give further confidence in the proposed scheme.

I Introduction

Pulsar timing has long been used to determine crucial parameters such as pulsar position and proper motion and, in the case of binary systems, orbital elements and relativistic parameters. It obviously requires high precision in the determination of the times-of-arrival (TOAs) of pulses. In most cases the TOA measurements are limited by effects intrinsic to the pulsar known as timing noise (e.g., Arzoumanian et al. 1994), or extrinsic effects caused by the interstellar medium (ISM). In order to be able to make full use of the information provided by timing, perturbations introduced by the ISM onto the TOAs must be removed. Since these time perturbations are frequency dependent, becoming less severe at high radio frequencies, we have been exploring the possibility of timing observations at frequencies higher than 1.4 GHz. The *Effelsberg Pulsar Observing System* (EPOS) has been continuously improved, enabling us to make regular high precision timing (e.g., Wolszczan, these proceedings; Doroshenko et al. 1997) and polarization observations (Xilouris et al. 1998) of millisecond pulsars since April 1994.

II Observations

Our observations have been made at the 100-m radiotelescope of the MPIfR near Effelsberg, using a highly sensitive 1.4/1.7 GHz HEMT-receiver ($T_{\rm sys} \approx 25$ K). During all regular timing sessions we have obtained full polarization information by

an adding polarimeter preceding a 4-channel 60 × 667 kHz post-detection hardware dedisperser called *PSE* (Von Hoensbroech & Xilouris 1997). The data were sampled with a maximum resolution of 0.2 μs. Sub-integrations of 15-sec duration were time stamped with signals provided by the station H-maser, itself synchronized to UTC via GPS. Recently, we have installed aside the PSE a clone of the *Coherent Dispersion Removal Processor* constructed by the Berkeley pulsar group. This wide bandwidth system called *Effelsberg-Berkeley-Pulsar-Processor* will allow high frequency work, obtaining also full polarization information (for details see Backer et al. 1997).

III High frequency observations

Kaspi et al. (1994) and Backer (these proceedings) have nicely demonstrated the impact of observed DM variations on the obtained timing residuals. We propose to make regular timing observations at frequencies higher than 1.4 GHz to minimize the disturbing effects of the ISM. Observations by Kijak et al. (1997) show that a number of the strongest millisecond pulsars are detectable at 4.85 GHz. Observing time and signal-to-noise ratio can, however, be optimized at an intermediate frequency like 2.7 GHz at which the impact of DM variation would be effectively reduced by a factor of almost four compared to 1.4 GHz. We have made first observations with a new, high sensitivity HEMT receiver centered at 2.7 GHz ($T_{\rm sys} \approx 25$ K, $G = 1.5$ K/Jy), which have shown that large portions of this band are unusable due to radio interference. However, observations at 2.7 GHz revealed that free bands are existing at the lower edges of the used bandwidth, so that tuning of the receiver is currently investigated.

IV Polarization measurements

Obtaining full polarization information during timing observations as done with EPOS, provides a unique chance to extract additional information about the observed source in particular for binary systems (Damour & Taylor 1992). Polarization data can, for instance, be used to derive the relative orientation of spin and magnetic axis, allowing a study of the spin-orbital coupling in binary systems. Simultaneous measurements of pulsar structure parameters deriving the emission beam geometry (e.g., Kramer et al. 1998) can be used to separate relativistic effects incorporated into observed values of classical parameters. For an excellent review the interested reader is referred to Damour & Taylor (1992). For the purpose of precise timing it is important to emphasize the significance of correct gain calibration and guaranteed gain stability for the observing session. The general high degree of millisecond pulsar polarization, in particular the circular component, can impose spurious TOA variations if the gains between the two polarizations are not properly balanced. The polarimetric properties of our instrumental set-up have been extensively explored by Von Hoensbroech & Xilouris (1997). Here, the emphasis was to minimize the instrumental polarization and to

guarantee proper gain calibration. Regular checking of the polarization characteristics of the instrumental set-up can be done by tracking well known slow rotating pulsars guaranteeing the polarization purity of the signals. Additionally, frequent observations of unpolarized continuum sources enable a reliable gain calibration, which in turn is checked by injecting noise diode signals of known strength in the signal path after each pulsar scan.

V Conclusions

The possibility of regular timing observations at high frequencies have been explored using the Effelsberg radio telescope. Regular timing observations at a frequency as high as 2.7 GHz, could provide information capable of eliminating the "interstellar weather" effects on pulsar timing (see the contribution by D. C. Backer). Although further investigation is required as to find the exact frequency range that will be free of interference, the sensitivity of the Effelsberg receivers and the time stability of the pulsar data taking system have proven so far that such an enterprise is feasible. In turn, it can be used to investigate the properties of the ISM. As has been shown by Xilouris et al. (1998), one of the striking features in millisecond pulsar profiles is their weak evolution with frequency, e.g., between 430 MHz and 1400 MHz. Observations at 4.85 GHz (Kijak et al. 1997) show that major profile changes are not expected any further. This would allow a straightforward interpretation of profile features at a wide frequency range. Our current results suggest that extremely valuable information can be obtained by tracing also the polarization characteristics of the received emission at high frequencies. Since millisecond pulsars appear to be much weaker sources and significantly depolarized at 4.85 GHz, we conclude that a frequency of 2.7 GHz looks indeed as a very good compromise as a future standard timing frequency.

Acknowledgements

OD acknowledges a fellowship from the Max-Planck-Gesellschaft. Arecibo Observatory is operated by Cornell University under cooperative agreement with NSF.

References

Arzoumanian, Z. et al. 1994, ApJ, 422, 671
Backer, D.C. 1998, these proceedings
Backer, D.C. et al. 1997 PASP, 109, 1
Damour, T. & Taylor., J.H. 1992, Phys. Rev. D, 45, 1840
Doroshenko, O.V. et al. 1997, in preparation
Jessner, A. 1994, MPIfR internal report
Kaspi, V.M., Taylor, J.H. & Ryba, M.F. 1994, ApJ, 428, 713

Kijak, J. et al. 1997, A&A, 318, L63
Kramer, M. et al. 1996, in Pulsars: Problems and Progress, IAU Colloquium 160, ed. S. Johnston, M.A. Walker & M. Bailes (San Francisco: ASP), 95
Kramer, M. et al. 1998, ApJ, 501, 270
Taylor, J.H. 1992, Philos. Trans. Roy. Soc. London A, 341, 117
Von Hoensbroech, A. & Xilouris, K.M. 1997, A&AS, 126, 121
Wolszczan, A. 1997 these proceedings
Xilouris, K.M. Kramer, M. 1996, in Pulsars: Problems and Progress, IAU Colloquium 160, ed. S. Johnston, M.A. Walker & M. Bailes, (San Francisco: ASP), 245
Xilouris, K.M. et al. 1998, ApJ, 501, 286

Authors' Addresses

M. Kramer and O. Doroshenko: Max-Planck-Institut für Radioastronomie, Auf dem Hügel 69, D-53121 Bonn, Germany

O. Doroshenko: on leave from Astro Space Centre of P.N. Lebedev Physical Inst. of the Academy of Science, Leninski pr. 53, Moscow 117924, Russia

K.M. Xilouris: NAIC, Arecibo Observatory, P.O. Box 995, Arecibo, Puerto Rico 00613

Part II:

Timing Binary and Millisecond Pulsars

R.N. Manchester

Binary and Millisecond Pulsars

Abstract

Recent surveys for millisecond pulsars (MSPs) have been exceptionally productive. In particular, the recently completed Parkes southern survey discovered 17 MSPs in the Galactic disk. Results from this survey are reviewed. Precision timing results for the strongest MSP discovered in the survey, PSR J0437−4715, are described. For MSPs, the kinematic or 'Shklovskii' contribution to the period derivative is often a significant fraction of the observed period derivative, and its effect on computed ages and magnetic fields is discussed. Observed correlations between orbital period, orbital eccentricity and companion mass for binary pulsars are described.

I Introduction

Of the approximately 750 pulsars known, 73 are either members of a binary (or higher order) system or have periods in the millisecond range, defined here to be less than 30 ms, and 37 have both these properties. Of these pulsars, 28 are members of a globular cluster system. These very close relationships, well illustrated by the Venn diagram of Figure 1, strongly support the idea that millisecond pulsars are 'recycled' by mass transfer in a binary system and resultant spin-up of an old and moribund neutron star (Bhattacharya & van den Heuvel 1991, Phinney & Kulkarni 1994). Pulsars of this type are preferentially found in globular clusters because the dense cores of these clusters provide significant opportunities for an evolved star or binary system to capture a passing neutron star and subsequently to spin it up (Sigurdsson & Phinney 1995).

The study of binary and millisecond pulsars is undoubtedly the most interesting and exciting area of current pulsar research. Millisecond pulsars are extraordinarily good clocks, with a stability rivalling that of the best terrestrial clocks (Rawley et al. 1987, Kaspi, Taylor & Ryba 1994). The presence of these objects in binary systems allows the detection of many subtle effects, and these effects often have significant implications. Important examples are the verification of Einstein's general theory of relativity and detection of the effects of gravitational radiation in the PSR B1913+16

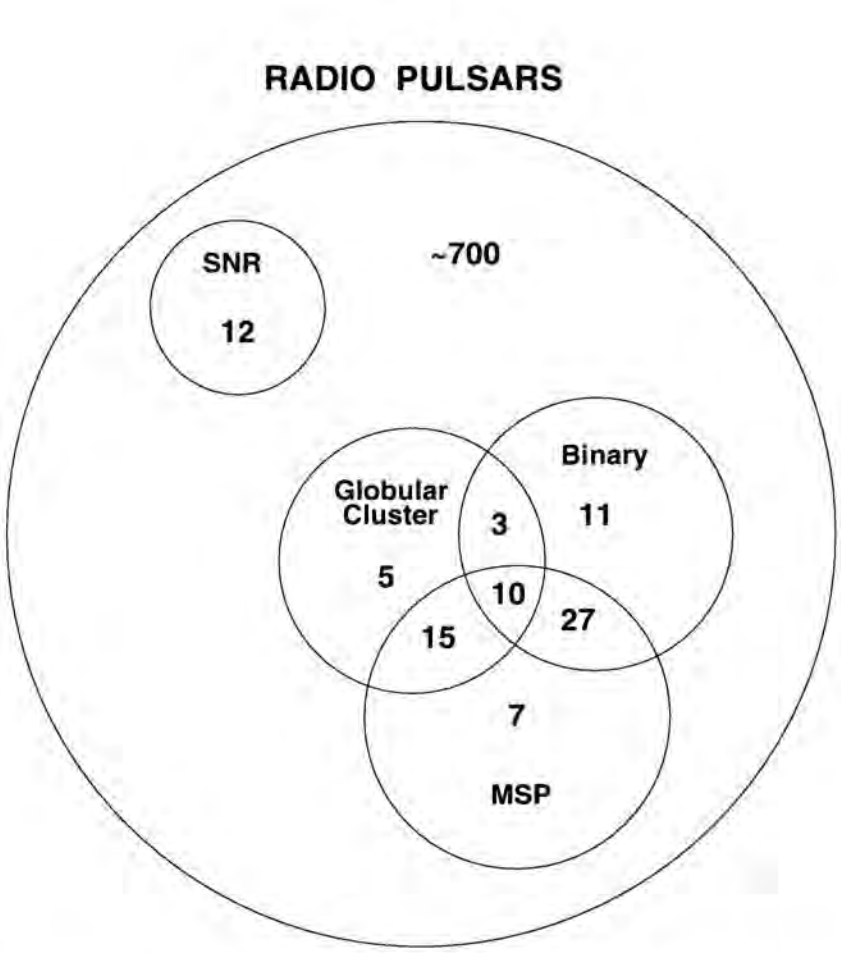

Figure 1. Venn diagram for radio pulsars showing the close relationship between binary, millisecond and globular-cluster pulsars.

system (Taylor et al. 1992) and the first detection of extra-Solar-system planets (Wolszczan & Frail 1992, Wolszczan 1994).

In this review, I first give a brief description of the recently completed Parkes southern pulsar survey, and describe some results from timing studies of pulsars detected in the survey. In Section 3, I describe some general properties of the observed population of binary and millisecond pulsars. I do not discuss in any detail the two known pulsars with massive binary companions, PSR B1259−63 and PSR J0045−7319, as these are the subject of separate presentations at this Colloquium by Simon Johnston and Vicky Kaspi, respectively.

II The Parkes Southern Survey

The Parkes southern survey was a large-scale survey of the entire southern sky for millisecond and other low-luminosity pulsars made using the Parkes 64-m radio telescope. The project was a collaboration, with the ATNF and the University of Manchester, Jodrell Bank, as principal partners. A total of nearly 45,000 beam positions were observed for about 2.5 min each. The observing frequency was 436 MHz with 256 channels across the 32-MHz bandwidth. After summing orthogonal polarizations, each channel was one-bit sampled every 0.3 ms and the data recorded on Exabyte tape. Work-station networks at the ATNF, Jodrell Bank and the Istituto di Radioastronomia del CNR, Bologna, were used to process the data; more than 600 512K-point FFTs were required for each beam position. The survey was very successful, detecting a total of 298 pulsars, including 19 millisecond pulsars. Of these, 17 millisecond pulsars and 84 'long-period' pulsars were new discoveries. Twelve of the new millisecond pulsars are members of binary systems but, so far, none of the new long-period pulsars has been shown to be binary. A more detailed description of the survey system and results from the first half of the survey are given by Manchester et al. (1996). Results from the second half of the survey and implications of the survey results for the Galactic population of pulsars are described by Lyne et al. (1998).

Figure 2 shows the clearly bimodal period distribution of the new discoveries and of all pulsars detected in the survey. The new discoveries have a much higher proportion of millisecond pulsars, reflecting the fact that most of the southern sky had not been effectively searched for this class of pulsar. This is also shown by the extraordinary discovery of PSR J0437−4715 (Johnston et al. 1993), by far the strongest millisecond pulsar known, which was detected with a signal-to-noise ratio of 510, far above the limiting value of 7.5.

Figure 3 shows the distribution of the newly discovered pulsars in Galactic coordinates. The long-period pulsars are clearly concentrated toward the Galactic equator, but the distribution of the millisecond pulsars is close to isotropic over the search area. There are several reasons for this difference. As Figure 4 shows, the detected millisecond pulsars have a much smaller range of dispersion measure (DM) than the long-period pulsars and hence are, on average, closer to the Sun. This is partly a result of sensitivity – few millisecond pulsars were detected with a DM greater than 50 cm^{-3} pc, where the instrumental broadening was two sample intervals or 0.6 ms. It is also partly a result of the generally low luminosity of millisecond pulsars – they are difficult to detect at large distances. The third factor that is important in accounting for this difference is the long lifetime of millisecond pulsars. With active lifetimes often in excess of 10^9 yr (Camilo, Thorsett & Kulkarni 1994), millisecond pulsars have plenty of time to move away from the Galactic plane.

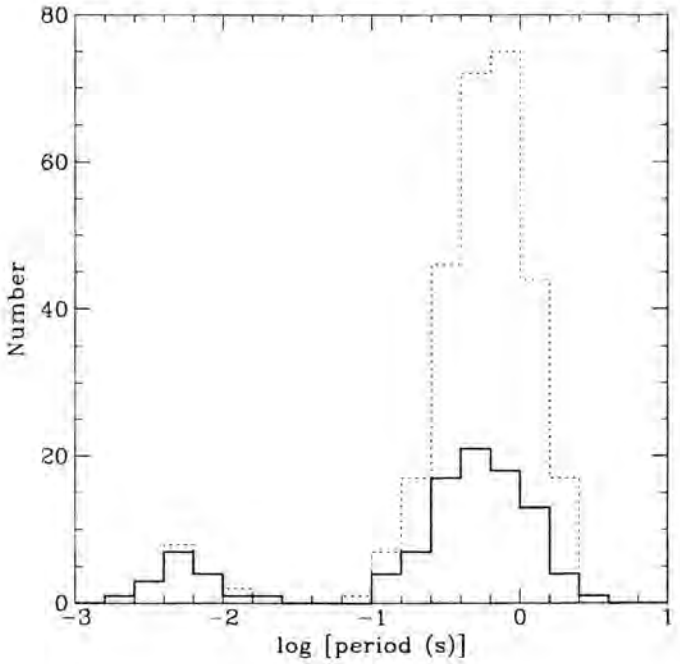

Figure 2. Period distribution of pulsars discovered in the Parkes southern survey (full line) and all pulsars detected by this survey (dotted line).

PSR J2051−0827 — an eclipsing binary pulsar

One of the more interesting pulsars discovered in the Parkes southern survey is PSR J2051−0827. This pulsar has a pulse period of 4.5 ms and is a member of a binary system with the very short orbital period of 2.38 h (Stappers et al. 1996). The companion is a low-mass white dwarf which is evidently being ablated by the pulsar wind, creating a gaseous envelope which, at least at low radio frequencies, eclipses the pulsar every orbit. At 1.4 GHz, the pulsar can frequently be seen through the whole orbital period. There are substantial variations in the column density of electrons in the eclipsing plasma both as a function of orbital phase for one orbit, and at the same orbital phase on different orbits (Stappers et al. 1996). Typical column densities are $\sim 4 \times 10^{17}$ cm^{-2} which, for reasonable values of outflow velocity, correspond to mass-loss rates $\sim 10^{-14}$ M$_\odot$ yr^{-1}. Even though the companion mass is only ~ 0.03 M$_\odot$, it is clear that mass loss at this rate is never going to destroy the companion.

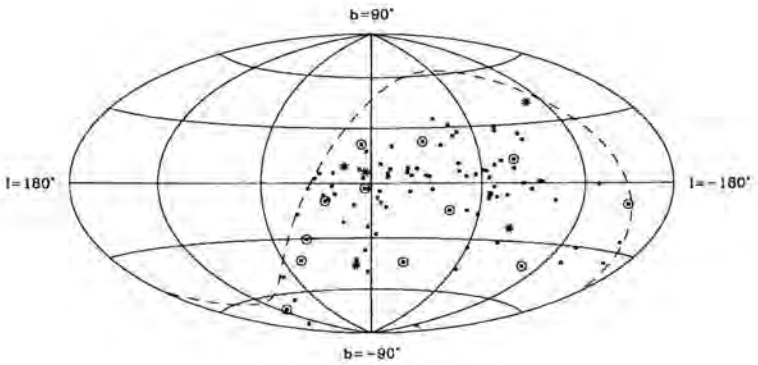

Figure 3. Galactic distribution of the 101 pulsars discovered in the Parkes southern survey. Binary MSPs are marked by ⊙ and single MSPs by ∗. The dashed line is the celestial equator and the northern limit of the survey.

Either substantial mass loss occurs in the form of neutral gas or in directions not traversed by the line of sight to the pulsar. If neither of these possibilities is true, ablation is not a viable mechanism for creating single millisecond pulsars.

PSR J0437−4715 — recent timing results

As part of a collaborative program with Shri Kulkarni and his group at Caltech, the Caltech correlator (Navarro 1994) has been used at Parkes to obtain timing data for PSR 0437−4715 from 1994 January to 1996 August. For these observations, the correlator system recorded two bands, each of width 128 MHz and normally centered at 1410 and 1660 MHz. Auto-correlation functions were folded with 1024 bins across the period for 90 s and then transferred to a work-station for subsequent processing. After transforming to the frequency domain, the data were dedispersed and pulse times of arrival (TOAs) computed by cross-correlation with a standard template. Over the 2.5 yr, a total of nearly 5000 TOAs were recorded. Times were referred to UTC(NIST) using GPS links.

TOAs were analyzed using TEMPO (Taylor & Weisberg 1989) and the DE200 Solar system ephemeris (Standish 1990). The position of PSR J0437−4715 relative to the DE200 reference frame is determined to a precision of about 50 micro-arcsec. This allows a precise determination of the proper motion of the system, which is quite large, $\sim$ 140 mas yr^{-1} (Bell et al. 1995a) and, more importantly, a significant measurement

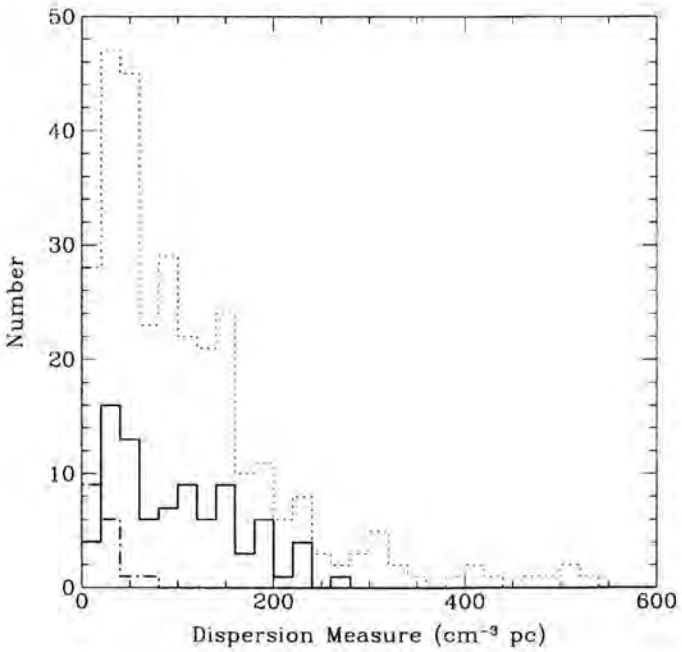

Figure 4. Distribution in dispersion measure of newly discovered millisecond pulsars (dot-dash line), long-period pulsars (full line) and all pulsars detected in the Parkes southern survey (dashed line).

of the annual parallax. The derived value, 5.6 ± 0.8 mas, corresponds to a distance of 180 ± 25 pc. This compares with 140 pc based on the DM and the Galactic electron density model of Taylor & Cordes (1993).

As was first described in the context of pulsars by Shklovskii (1970), the changing Doppler shift resulting from transverse motion of the pulsar makes a positive contribution to the observed period derivative,

$$\begin{aligned} \dot{P}_s &= \frac{P\mu^2 d}{\mathrm{c}} \\ &= 2.43 \times 10^{-27} \left(\frac{P}{\mathrm{ms}}\right) \left(\frac{\mu}{\mathrm{mas\ yr^{-1}}}\right)^2 \left(\frac{d}{\mathrm{pc}}\right) \end{aligned}$$

where P is the pulsar period, μ is its proper motion and d is the pulsar distance. Actually, this kinematic effect has been known for a long time in classical astronomy as *secular acceleration* – the first reference given by van de Kamp (1981) is to Bessel (1844)! If we assume that the observed period derivative for PSR J0437−4715 is entirely due to this kinematic effect, we can place an upper limit on the distance of 204 pc, consistent with the parallax distance. Alternatively, if we take the parallax distance as correct, the kinematic effect contributes 85% of the observed period derivative and the intrinsic period derivative is very small, $\sim 7 \times 10^{-21}$. The implied surface magnetic field is also very small, $B_0 \sim 2 \times 10^8$ G, and the characteristic age is very large, $\tau_c \sim 2.5 \times 10^{10}$ yr.

As pointed out by Bell & Bailes (1996), the changing Doppler shift also affects the binary orbital period. If the expected intrinsic orbital period derivative is negligible (as is the case for the PSR J0437−4715 system), then a further and potentially accurate distance estimate can be obtained from the observed orbital period derivative. For PSR J0437−4715, $\dot{P}_b = (5.3 \pm 0.9) \times 10^{-12}$, giving a distance in the range 180 to 255 pc, also consistent with the parallax value.

The large proper motion of the system has another observable effect: the plane of the orbit remains fixed in space as the system moves across the sky, but our view of it changes. This change in orbit inclination angle i results in a change in the projected semi-major axis of the pulsar orbit $x \equiv a_p \sin i$. The observed value of $\dot{x} = (8.0 \pm 0.4) \times 10^{-14}$ sets a limit on $\cot i$ (Kopeikin 1996) and implies $i < 43^\circ$ and a companion mass $m_2 > 0.2$ M$_\odot$.

After fitting for these parameters, the final rms residual was 500 ns. While this is close to the best timing precisions so far obtained (e.g., Kaspi et al. 1994), it is many times the formal TOA uncertainties based on the cross-correlation analysis. With further observations and the elimination (or at least reduction) of remaining systematic errors, there is potential for refining these results and detection of even more subtle effects.

These results and their implications are discussed in more detail by Sandhu at this Colloquium and by Sandhu et al. (1997).

III The binary and millisecond pulsar population

Over the past few years, there has been a large increase in the number of known millisecond and binary pulsars, especially in the Galactic disk. Mostly as a consequence of this, there has also been an increase in the number of pulsars with significant measurements of parameters such as proper motion and orbital eccentricity. This allows a more thorough examination of various correlations suggested on the basis of either empirical evidence or models for stellar or binary evolution.

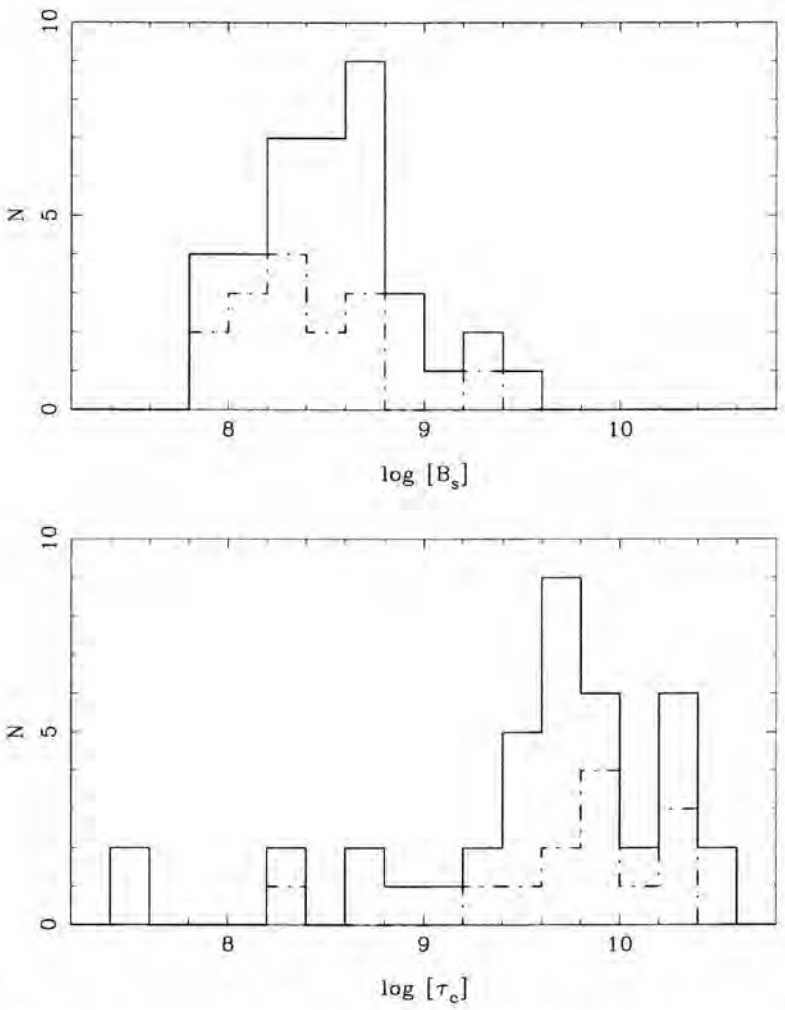

Figure 5. Distributions of dipole surface magnetic field B_s and characteristic age τ_c for millisecond pulsars ($P < 30$ ms). For pulsars with known and significant proper motions, the intrinsic period derivative $\dot{P}_i$ has been used to compute B_s and τ_c. The distributions for those pulsars where this correction has been made are marked with dot-dash lines.

Intrinsic period derivatives

As mentioned above, the 'Shklovskii' or kinematic term makes a positive contribution $\dot{P}_s$ to the observed period derivative, $\dot{P}$. When computing characteristic ages and surface magnetic fields, the intrinsic period derivative, $\dot{P}_i = \dot{P} - \dot{P}_s$ should

be used. This correction is especially important for MSPs because of their small $\dot{P}$; it is significant for a few longer-period pulsars, but it makes an insignificant contribution to the observed period derivative. Distributions of B_0 and τ_c for MSPs are plotted in Figure 5 showing that many have weak surface magnetic fields, $\sim 10^8$ G, and characteristic ages of greater than 10^{10} yr. The low magnetic fields have implications for pulse emission models and the large characteristic ages have implications for stellar and binary evolution. In particular, the large characteristic ages, many greater than the age of the Galaxy, mean either that magnetic fields of isolated or non-accreting binary pulsars decay on timescales of gigayears or that many millisecond pulsars are born with periods not too much less than their current value. In turn, this latter conclusion would mean that many millisecond pulsars are born (or reborn) with periods well below the conventionally defined spin-up line (Bhattacharya & van den Heuvel 1991). Even ignoring the more radical alternative, that millisecond pulsars are formed directly and not by spin-up in an accreting binary system (e.g., Michel 1987), there are many assumptions in the definition of the spin-up line (Ghosh & Lamb 1992, Arons 1993) and hence considerable room for movement in it.

Binary evolution

Probably the clearest of the various relationships between binary parameters is the correlation between orbital eccentricity and orbital period for binary systems with low-mass white dwarf companions (Phinney 1992, Phinney & Kulkarni 1994). For these systems, if the companion was a red giant filling its Roche lobe during the spin-up phase, there is a coupling between convective instabilities in the red-giant envelope and the orbital motion. The predicted relationship between orbital eccentricity and orbital period agrees well with recent discoveries and improved measurements (Figure 6), confirming that Roche-lobe overflow was indeed the spin-up mechanism. Systems with companions of intermediate mass, most likely CO white dwarfs, have followed a different evolutionary path, probably involving common-envelope evolution and spiral-in (van den Heuvel 1994). All of the high-mass systems have high eccentricity. Two of them (PSRs J0045−7319 and B1259−63) have main-sequence companions and at least four and probably all six of the others are double-neutron-star systems. Eccentricities are generally higher for systems in globular clusters, reflecting interactions with other cluster stars (Phinney 1993).

As first pointed out by Joss, Rappaport & Lewis (1987), if Roche-lobe overflow is maintained during spin-up, then a relationship is expected between the final orbital period and the final mass of the companion star. This relationship was further refined by Rappaport et al. (1995). Figure 7 shows the current correlation between these two quantities.

Pulsars with CO white-dwarf companions lie well to the right of the line, reflecting their different evolutionary history as mentioned above. There is now a significant

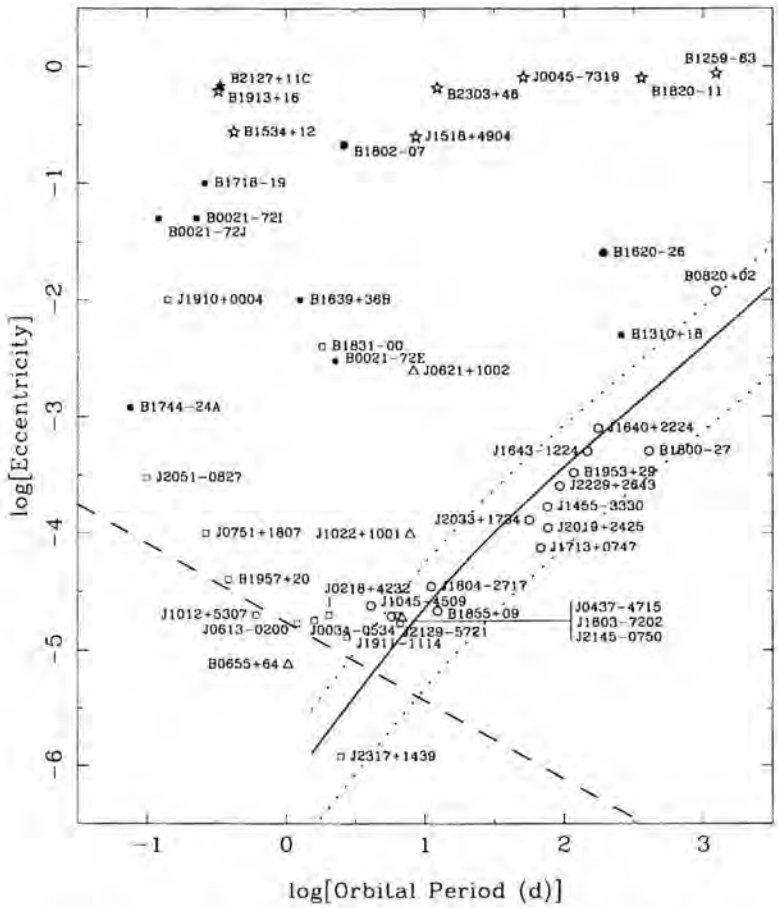

Figure 6. Orbital period versus orbital eccentricity for known binary pulsars. Systems with low-mass white dwarf companions are marked with a circle, other low-mass companions by squares, intermediate-mass companions by a triangle and high-mass companions by a star. Upper limits on the eccentricity are marked by a square. Systems in globular clustersre marked by filled symbols. The approximate limit on eccentricity for pulsars with TOA uncertainties of 10 μs is indicated by the dashed line. (After Bell et al. 1997)

group of pulsars with long orbital periods which lie well to the left of the line. It is statistically unlikely that all of these pulsars have the low inclination angles necessary to allow them to fit on the predicted correlation.

Fig. 7 also shows that the orbital-period 'gap' at around 50 d, first mentioned by Camilo (1995), persists with the latest data. This suggests that it represents a real difference in evolutionary paths. A possible mechanism is discussed by Tauris (1996).

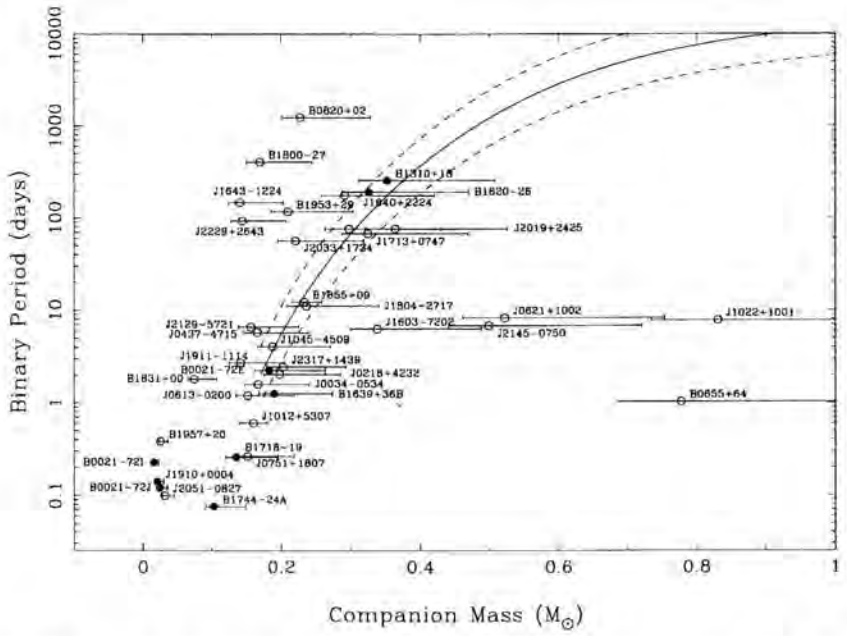

Figure 7. Binary period versus companion mass for binary pulsars. For all pulsars except PSR B1855+09 (Ryba & Taylor 1991) and PSR J1012+5307 (van Kerkwijk, Bergeron & Kulkarni 1996) where direct measurements of companion mass exist, error bars are plotted for $1 - \cos i = 0.2$ and 0.8, that is, the points where the probability of an inclination less than i is 20% and 80% respectively. The line is the predicted relationship according to Rappaport et al. (1995), valid for companion masses $\gtrsim 0.2$ $M_\odot$.

IV Conclusions

Recent discoveries of binary and millisecond pulsars have greatly enriched the subject of pulsar astronomy and astrophysics. With planned surveys and follow-up observations of both newly discovered and previously known pulsars, many new and interesting results can be expected in the next few years.

Authors' Address

Australia Telescope National Facility, CSIRO, P.O. Box 76, Epping NSW 2121, Australia

References

Arons, J. 1993, ApJ, 408, 160
Bell, J.F. & Bailes, M. 1996, ApJ, 456, L33
Bell, J.F. et al. 1997, MNRAS, 286, 483
Bell, J.F. et al. 1995, ApJ, 440, L81
Bessel, F.W. 1844, Astron. Nachr., 22, 145
Bhattacharya, D. & van den Heuvel, E.P.J. 1991, Phys. Rep., 203, 1
Camilo, F. 1995, in The Lives of the Neutron Stars (NATO ASI Series), ed. A. Alpar, Ü. Kiziloğlu & J. van Paradis (Dordrecht: Kluwer), 243
Camilo, F., Thorsett, S.E. & Kulkarni, S.R. 1994, ApJ, 421, L15
Ghosh, P., & Lamb, F.K. 1992, in X-ray Binaries and Recycled Pulsars, ed. E.P.J. van den Heuvel & S.A. Rappaport, (Dordrecht: Kluwer), 487
Johnston, S. et al. 1993, Nature, 361, 613
Joss, P.C., Rappaport, S. & Lewis, W. 1987, ApJ, 319, 180
Kaspi, V.M., Taylor, J.H. & Ryba, M. 1994, ApJ, 428, 713
Kopeikin, S.M. 1996, ApJ, 467, L93
Lyne, A.G. et al. 1998, MNRAS, 295, 743
Manchester, R.N. et al. 1996, MNRAS, 279, 1235
Michel, F.C. 1987, Nature, 329, 310
Navarro, J. 1994. Ph.D. Thesis, California Inst. of Technology
Phinney, E.S. 1992, Phil. Trans. Roy. Soc. A, 341, 39
Phinney, E.S. 1993, in Structure and Dynamics of Globular Clusters, ed. S.G. Djorgovski & G. Meylan (San Francisco: ASP), 141
Phinney, E.S. & Kulkarni, S.R. 1994, ARA&A, 32, 591
Rappaport, S. et al. 1995, MNRAS, 273, 731
Rawley, L.A. et al. 1987, Science, 238, 761
Ryba, M.F. & Taylor, J.H. 1991, ApJ, 371, 739
Sandhu, J.S. et al. 1997, ApJ, 478, L95
Shklovskii, I.S. 1970, Soviet Astron., 13, 562
Sigurdsson, S. & Phinney, E.S. 1995, ApJS, 99, 609
Standish, E.M. 1990, A&A, 233, 252
Stappers, B.W. et al. 1996, ApJ, 465, L119
Tauris, T.M. 1996, A&A, 315, 453
Taylor, J.H. & Cordes, J.M. 1993, ApJ, 411, 674
Taylor, J.H. & Weisberg, J.M. 1989, ApJ, 345, 434
Taylor, J.H. et al. 1992, Nature, 355, 132
van de Kamp, P. 1981, Stellar Paths, (Dordrecht: Reidel)
van den Heuvel, E.P.J. 1994, A&A, 291, L39
van Kerkwijk, M.H., Bergeron, P. & Kulkarni, S.R. 1996, ApJ, 467, L89
Wolszczan, A. 1994, Science, 264, 538
Wolszczan, A. & Frail, D.A. 1992, Nature, 355, 145

J.-F. Lestrade, I. Cognard and V. Maitia

Timing of Millisecond Pulsars at Nançay

Abstract

We summarize the timing observations of millisecond pulsars conducted at the Nançay radiotelescope since 1988 with a coherent dedisperser based on a swept frequency oscillator.

I Introduction

The large collecting area of the Nançay radio telescope (1 K/Jy and $T_{\rm sys} = 45$ K) has been used to conduct a timing program of the millisecond pulsars B1937+21 and B1821−24 since 1988, and B1713+07, B1643−12, B1620−26 and B1744−24A more recently. The observations are conducted at 1.28, 1.41, 1.68 and 1.7 GHz at least 10 times per month for the first 4 pulsars of this list. The best timing precision is 0.4 μsec for B1937+21 at 1.4 GHz for 1 hour of integration.

It is well established that the measured topocentric Time of Arrival (TOA) can be written as:

$$\mathrm{TOA} = NP + \frac{\vec{r}.\vec{\sigma}}{\mathrm{c}} + \tau_S + \frac{k\mathrm{DM}_0}{\nu^2} + \delta\tau_D + \delta\tau_{\rm geo}$$

where N is the number of pulses, P the pulsar rotation period, $\vec{r}$ the Solar System barycentric position of the radiotelescope on the Earth crust, $\vec{\sigma}$ the unit-direction of the pulsar, τ_S the General Relativity Shapiro delay, DM_0 the Dispersion Measure at some epoch and ν the frequency of observation. The additional terms $\delta\tau_D$ and $\delta\tau_{\rm geo}$ correspond to propagation perturbations of radio wave caused by scintillation in the inhomogeneous ionized interstellar medium (Rickett 1990). The dispersion delay perturbation $\delta\tau_D$ depends directly on the amplitude of the electron density fluctuations δn_e and the geometric delay perturbation $\delta\tau_g$ depends on the refractive angle. These two delay perturbations are derived in Cordes, Pidwerbetsky & Lovelace (1986) and can reach 1 μsec at 1.4 GHz over time scale comprised between a few days and a few tens days (Blandford & Narayan 1985). The dense timing series of Nançay are well

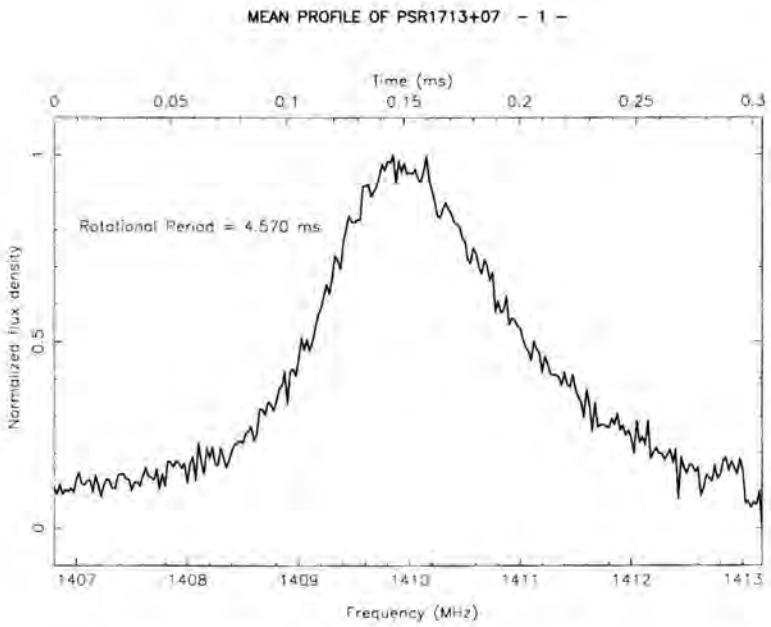

Figure 1. Mean profile of B1713+07 from thirty 7-minute observations at Nançay at 1.4 GHz. The full width at half maximum is 108 μsec

suited to study interstellar refractive scintillation and, eventually, could contribute to its modeling to improve the timing accuracy.

We shall briefly describe the coherent pulsar dedisperser built at Nançay to conduct timing observations and present the mean profile of B1713+07, recently determined at Nançay. We shall discuss the long timing series of B1937+21 and B1821−24 conducted since 1988 where Extreme Scattering Events and anti-correlation between flux density and TOA variations are apparent.

II Coherent dedisperser for pulsar timing at Nançay

At Nançay, the pulsar signal is de-dispersed by using a swept frequency local oscillator around 80 MHz in the receiver IF chain. This oscillator was a VCO (Voltage Control Oscillator) slaved to a parabolic saw-tooth synthesized by step of 100 ns until September 1996 and is now a DDS (Digital Direct Syntheziser) directly controlled by the saw-tooth and needs no feed back loop. The dispersion band B_d, matching in the frequency domain the pulsar period, ranges from a few MHz to a few hundreds MHz for most pulsars ($B_d = 1/2P\nu^3/k$ DM, e.g., 7.55 MHz for B1937+21 and 95 MHz for B1713+07 at 1.4 GHz). The effective integration bandwidth at Nançay is

presently limited to 12 MHz because of an IF limitation that will be removed soon. After dedispersion, the pulse spectra are produced by the station digital autocorrelator with a frequency resolution of 12.5 or 25 kHz. The station UT time scale is provided by a Rhode and Schwarz XSRM Rubidium Frequency standard. The offset relative to the conventional UTC time scale was measured daily at 14 UT via the Observatory of Paris by a special purpose receiver using TV signals until 1995. The accuracy of this daily monitoring is at the level of 40 nanosec as shown by various consistency cross-checks and several Global Positioning System (GPS) measurements conducted in parallel. The station UT is now monitored directly via GPS. The frequency of arrival for our system is determined by cross-correlation between the daily spectrum and a template. The profile of B1713+07 in Figure 1 is an example of a dedispersed profile by our coherent dedisperser. This profile is the summation of 30 observations 7 minutes long at Nançay. The full width at half maximum from Fig. 1 is 108 μsec and the pulse is narrower than the earlier measurement with an instrumental smearing of 80 μsec by Camilo (1995).

III Timing series of B1937+21 and B1821−24

The TOA analysis is carried out with our software ANTIOPE that can fit all the relevant parameters for single or binary pulsars. ANTIOPE uses the Jet Propulsion Laboratory Ephemerides DE200 or DE202 (Standish 1993). The astrometric parameters solved for B1937+21 with ANTIOPE and the Nançay data have been compared to the parameters determined with Arecibo data and the software TEMPO (Taylor 1992). We found a very satisfactory agreement (Cognard et al. 1993a).

The pulsars B1937+21 and B1821−24 have been timed at Nançay about 10 times or more per month since 1988 at 1.4 GHz. The flux density was recorded with a precision of about 15% and the TOA with a precision of 0.4 μsec for B1937+21 and 3 μsec for B1821−24 over 1 hour long integration. Figure 2 and Figure 3 show the flux densities and the post-fit TOA residuals of these 2 pulsars after solving for the rotation period, the first time derivative of the period, position and proper motion. The systematic behavior of these residuals for B1937+21 has already been recognized in the Arecibo data and termed "red noise" whose origin is not clearly identified. We have found that B1821−24 exhibits similar behavior (Cognard et al. 1996 and Fig. 3). It is worth noticing that 1855+09 observed at Arecibo over 8 years do not display such a red noise (Kaspi, Taylor & Ryba 1994) and that its characteristic age is 3 Gy and significantly greater than the age of B1937+21 (150 My) and B1821−24 (10 My). The red noise of the TOA residuals of B1937+21 and B1821−24 can be whitened rather arbitrarily by solving for the second and higher order time derivatives of the rotation period. These higher order time derivatives can be used to calculate the stability index Δ_8 used for normal pulsars to quantify their rotation irregularities by Azoumanian et al. (1994). It is interesting to notice that the indices Δ_8 for B1937+21 and B1821−24 fall on the empirical relationship found for the stability index $\Delta_8 = 6.6 + 0.6\dot{P}_0$ by Arzoumanian et al. (1994). The millisecond pulsars B1937+21 and B1821−24 might

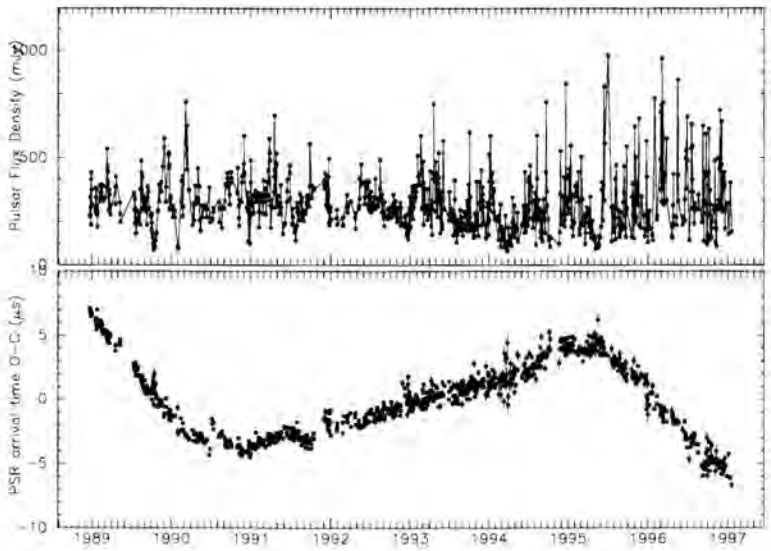

Figure 2. Flux density and post-fit timing residuals of B1937+21 at Nançay at 1.4 GHz. The period, position, proper motion and first period derivative only have been solved for. This results in the red noise apparent in these residuals. DM was held constant.

exhibit some rotation irregularities similarly to normal pulsars but scale down with their characteristic age.

In addition to the red noise observed over the observation span of 8 years, the dense timing series of Nançay exhibit systematic behavior in the flux density and TOA residuals of B1937+21, and possibly of B1821−24, over shorter time scales. About once a year, the flux density monotonically decreases and then increases back to the mean level over a few weeks while the TOA residuals are significantly more scattered. This was shown with daily timing observation of B1937+21 at Nançay for an event in October 1989. We could identify a systematic behavior in the TOA residuals of B1937+21 with two positive peaks (TOA delayed) while the flux density is constantly depressed over two weeks. This has been interpretated as an Extreme Scattering Event or more properly a Strong Refractive Event (Cognard et al. 1993b).

Another finding in the dense timing series of B1937+21 is the inverse correlation between TOA residuals and flux density variations at 1.4 GHz presented in Lestrade, Cognard & Biraud (1995). This negative correlation at zero-lag shown in Figure 4 corresponds to flux/TOA variations correlated over 15 days as expected from interstellar refractive scintillation (RISS). The negative correlation means that late pulses are weaker than early ones. We have a paper in preparation with B.J. Rickett to show that this sense is expected when the TOA fluctuations due to the dispersive perturbations $\delta\tau_D$ dominate over geometric perturbations $\delta\tau_g$. These dispersive perturbations are due

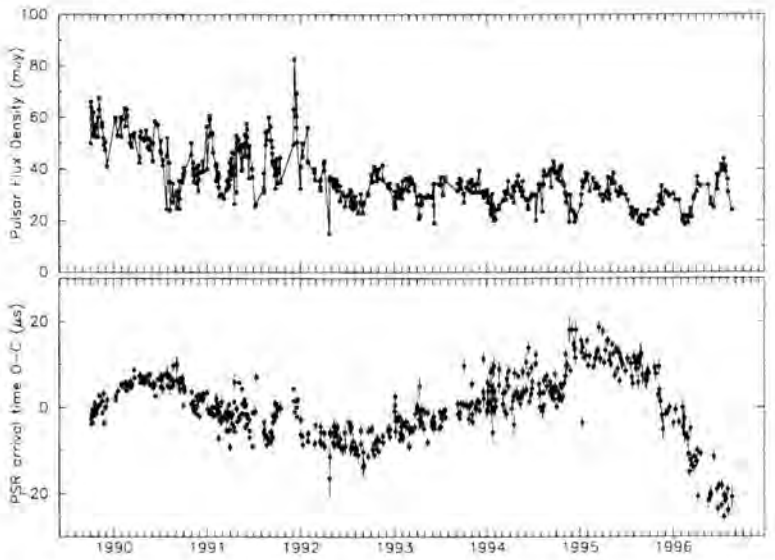

Figure 3. Flux density and post-fit timing residuals of B1821−24 at Nançay at 1.4 GHz. The period, position, proper motion and first period derivative only have been solved for. This results in the red noise apparent in these residuals. DM was held constant.

to intervening plasma clouds with scale size of $\sim$ 1/4 AU in the direction of B1937+21. The DM variations currently monitored by dual frequency timing observations at Arecibo and Nançay are smoothed over about 50 days in the analysis process. This smoothing is long compared to the RISS fluctuations over 15 days and the DM series can not correct adequately the timing data.

Our timing series of B1821−24 have revealed long-term DM variations as high as 0.005 pc cm^{-3} yr^{-1} in the direction of this pulsar, i.e., about 10 times larger than for B1937+21, (Cognard & Lestrade 1997) and that are consistent with the trend reported earlier by Backer et al. (1993). Cognard & Lestrade (1997) provide also a new proper motion for this low ecliptic latitude pulsar whose right ascension and declination components are inconsistent with the value zero for the first time. This proper motion is useful to discuss the diffractive and refractive properties of the interstellar medium in the direction of this pulsar.

IV Prospects

The timing program at Nançay should be enhanced in the near future by making our DDS coherent dedispersion system sweep over 100 MHz rather than 12 MHz presently. The upgrade of the telescope over the next 2 years will provide an additional improvement of the sensitivity by a factor 2.4. Another improvement sought is to

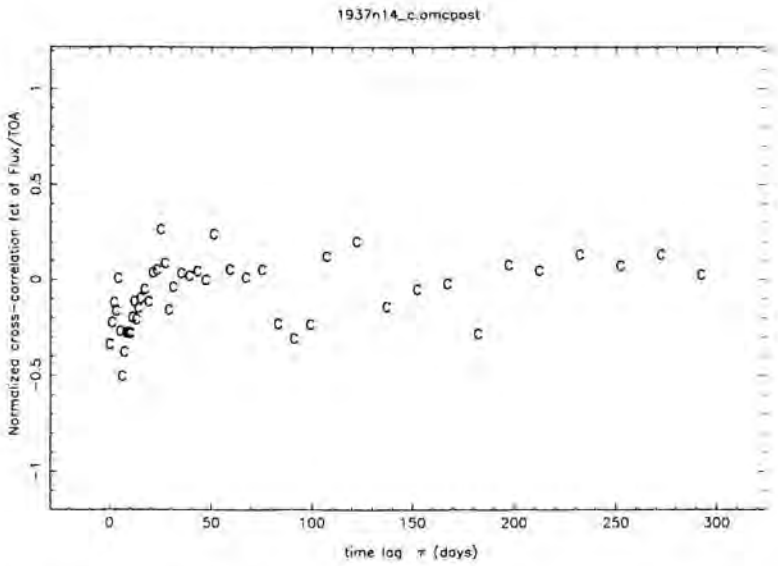

Figure 4. Cross-correlation of the flux density and post-fit timing residuals of B1937+21 at Nançay at 1.4 GHz.

extend our station autocorrelator bandwidth from 6.4 MHz, presently, to 50 MHz with 8000 point spectra.

Our scientific motivations are 1) to establish a timing array of pulsars for the study of the stochastic background of gravitational waves, 2) to study the interstellar medium and 3) to contribute to the discrimination of the relativistic theories of gravitation.

We have also started a survey of pulsars at 1.4 GHz of the galactic plane with the Navy-Berkeley-Pulsar-Processor (NBBP) in a collaboration with R.S. Foster, P.S. Ray at NRL and D.C. Backer at Berkeley. The time constant of the NBPP used for the survey is 60 μsec and should provide good sensitivity to millisecond pulsars.

Acknowledgements

We are in debt to F. Biraud, D. Aubry, J.-P. Drouhin and B. Darchy for their crucial help in building and maintaining the dedisperser at the Nançay radiotelescope.

References

Arzoumanian, Z. et al. 1994, ApJ, 422, 671
Backer, D.C. et al. 1993, ApJ, 404, 636
Blandford, R. & Narayan, R. 1985, MNRAS, 213, 591
Camilo, F. 1995, Ph.D. Thesis, Princeton Univ.
Cognard, I. et al. 1993a, Nature, 366, 320
Cognard, I. et al. 1993b, A&A, 296, 169
Cognard, I. et al. 1996, A&A, 311, 179
Cognard, I. & Lestrade, J.-F., 1997, A&A, 323, 211
Cordes, J.M., Pidwerbetsky, A. & Lovelace, R. V. E. 1986, ApJ, 310, 737
Foster, R.S. & Cordes, J. M., 1990, ApJ, 364, 123
Foster, R.S. et al. 1997, in Pulsars: Problems and Progress, IAU Symposium 160, ed. S. Johnston, M.A. Walker & M. Bailes (San Francisco: ASP), 25
Kaspi, V.M., Taylor, J.H. & Ryba, M. 1994, ApJ, 428, 713
Lestrade, J.-F., Cognard, I. & Biraud, F. 1995, in Millisecond Pulsars: A Decade of Surprise, PASP Conf. Ser. 72, ed. A.S. Fruchter, M. Tavani & D.C. Backer (San Francisco: ASP), 357
Rickett, B.J. 1990, ARAA, 28, 561
Standish, E.M. 1993, AJ, 105, 2000
Taylor, J.H. 1992, Phil. Trans. R. Soc. Lond. A., 341, 117

Authors' Addresses

J.-F. Lestrade and V. Maitia: Observatoire de Paris-Meudon and CNRS-URA1757

I. Cognard: Laboratoire de Physique et Chimie de l'Environnement - UPR4010

S.E. Thorsett and Z. Arzoumanian

The Pulsar Triple System PSR B1620−26: A Status Report

Abstract

The pulsar PSR B1620−26, in the globular cluster M4, has a low-mass stellar companion and a large frequency second derivative that has been ascribed to acceleration of the binary system in the gravitational field of a second companion object. Recently, we have reported the detection of a decrease in the projected size of the semimajor axis of the binary, which we believe is caused by precession of the binary in the tidal field of the second companion. The implied mass of the second companion is only $\sim 0.01\ M_\odot$. In this work, we summarize recent observations of B1620−26, as well as results from modeling the time evolution of the apparent pulsar spin frequency and orbital elements in a hierarchical triple system.

I Introduction

The millisecond radio pulsar PSR B1620−26, in the globular cluster M4, has a binary companion, probably a $\sim 0.3\ M_\odot$ white dwarf, in a 191 day, low-eccentricity orbit (Lyne et al. 1988). Unlike other known millisecond pulsars, it has a very large frequency second derivative $\ddot{f}$, implying that the spin-down rate varies on a timescale of ~ 10 yrs (Backer 1993). Neither intrinsic rotational instabilities nor acceleration in the gravitational field of the cluster is likely to produce such a large $\ddot{f}$; the most attractive explanation appears to be a second companion, of either stellar or planetary mass, in a bound, hierarchical orbit around the neutron-star–white-dwarf binary (Backer 1993; Thorsett, Arzoumanian & Taylor 1993; Backer & Thorsett 1995).

The best test of the triple system hypothesis would be a predictive Keplerian fit to data spanning more than one orbit of the outer body. However, because the inferred orbital period is of order a century or more, such a demonstration is beyond our ability: at best, we can observe only a small portion of an orbit, essentially measuring successively higher-order derivatives of the acceleration at a single point.

Of course, even in a hierarchical triple the orbits are not truly Keplerian, because of gravitational interactions between the inner and outer companions. Another test of the triple system hypothesis is therefore to seek perturbations induced on the inner orbit

Table 1: Timing parameters of PSR B1620−26.

Right ascension (J2000.0)	$16^{\rm h}23^{\rm m}38\overset{\rm s}{.}2212(3)$
Declination (J2000.0)	$-26°31'53\overset{''}{.}79(2)$
Proper motion RA (mas yr^{-1})	−11.6 (assumed)
Proper motion Dec (mas yr^{-1})	−15.7 (assumed)
Dispersion measure (pc cm^{-3})	62.8626(6)
Spin period P (ms)	11.075750914220(4)
Spin frequency f (Hz)	90.2873320053(3)
$\dot{f}$ (s^{-2})	$-5.4703(7)\times10^{-15}$
$\ddot{f}$ (s^{-3})	$1.930(3)\times10^{-23}$
$\dddot{f}$ (s^{-4})	$6.7(6)\times10^{-33}$
$\ddddot{f}$ (s^{-5})	$-2.1(3)\times10^{-40}$
Epoch of f (MJD)	48725.0
Projected semi-major axis $x = a_1 \sin i$ (s)	64.809459(6)
Orbital period P_b (s)	16540653(5)
Eccentricity e	0.0253154(2)
Time of periastron T_0 (MJD)	48728.2625(2)
Angle of periastron ω	117.1292(4)
Mass function ($M_\odot$)	7.975×10^{-3}
Advance of periastron $\dot{\omega}$ (°yr^{-1})	$(-2.8\pm2.0)\times10^{-4}$
$\dot{P}_b$	$(1.4\pm1.9)\times10^{-9}$
$\dot{e}$ (s^{-1})	$3(3)\times10^{-15}$
$\dot{x}$	$-6.6(0.8)\times10^{-13}$

NOTE — Position is relative to the JPL DE202 solar system ephemeris. Numbers in parentheses are uncertainties in the final digits quoted. Proper motion is from Cudworth & Hansen 1993. Formal uncertainties are relative to model fit with above parameters. Covariances with unfit parameters (e.g., the fifth frequency derivative) may increase true uncertainties, particularly of $\ddot{f}$ and $\dddot{f}$.

by the more distant third body. For example, the gravitational tidal force of the outer body on the inner orbit will cause the inner orbit to precess around the normal to the outer orbit. This effect is well known in the solar system, where it is called planetary precession; it may be made manifest through the changing projected size of the inner orbit.

II Observations

We report on observations made at Green Bank and the Very Large Array between March 1988 & August 1996. Details of the observing systems and techniques may be found elsewhere (e.g., Thorsett, Arzoumanian & Taylor 1993).

A timing model was fit to the data using standard techniques. The resulting parameters are given in Table 1.

III Discussion

The early suggestion that the anomalously large second frequency derivative was evidence of a varying gravitational acceleration of the B1620−26 binary has proven robust. The apparent frequency derivative of the pulsar has changed by a factor of three since its discovery; at this pace, the pulsar will appear to begin spinning up in April 2001. Such large fractional variations strongly argue against a model dependent on intrinsic timing noise (Figure 1). Similarly, the timescale of the variation rules out the mean field contribution of the cluster or galaxy, and the probability of a near enough (unbound) close encounter by another cluster star is low (Thorsett, Arzoumanian & Taylor 1993).

Further evidence for the triple hypothesis comes from the very significant measurement of a variation in the projected semimajor axis of the orbit, with timescale $x/\dot{x} \sim 3\,\mathrm{Myr}$. No corresponding variation in P_b is seen, suggesting that $\dot{x}$ is due to a change in the inclination angle i. The simplest understanding of this observation is that the plane of the inner orbit is precessing in the tidal gravitational field of another, noncoplanar, object.

If PSR B1620−26 is a member of a hierarchical triple, then the four measured frequency derivatives provide information about the curvature of a nearly Keplerian orbit. Recently, Joshi & Rasio (1997) have demonstrated how the measurements can be inverted to solve Kepler's equation, with a single free parameter (such as the eccentricity of the outer orbit). Such timing measurements only probe the projection of the motion on the line of sight, so a number of angles (the inclinations and relative orientation of the orbits) remain unresolved. Orbital perturbations, however, depend upon these angles as well. Using Monte Carlo techniques, Joshi and Rasio have used the spin frequency derivatives, the measured $\dot{x}$, and limits on changes in the other orbital elements to conclude that the most likely second companion has a mass of only $0.01 \pm 0.005\ \mathrm{M}_\odot$, and an orbital radius of $\sim 40\,\mathrm{AU}$.

The birth and survival of such a system pose substantial theoretical challenges (Sigurdsson 1995; Joshi & Rasio 1997). Ionization of the "planet" or brown dwarf will occur by close encounters between the triple and other cluster stars in a timescale of $\sim 2 \times 10^7$ yr (Joshi & Rasio 1997). The planet may have been formed around

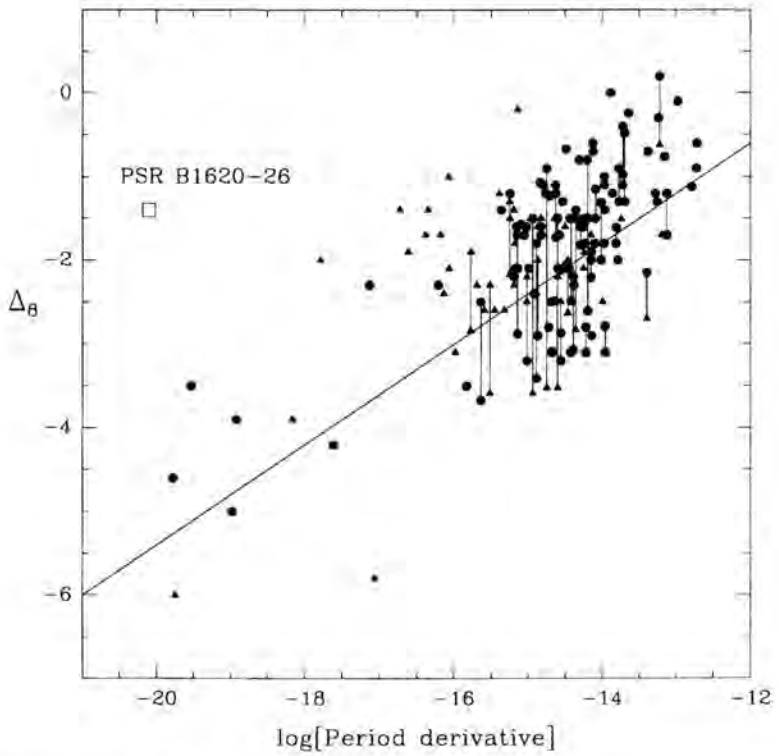

Figure 1. PSR B1620−26 $\ddot{f}$ relative to intrinsic timing noise observed in a sample of pulsars (after Arzoumanian et al. 1994). The parameter $\Delta_8 \propto \log|\ddot{P}|$ is a measure of residual timing noise after subtraction of a quadratic phase model. Triangles are upper limits, and the open box is the location of B1620−26, assuming a typical millisecond pulsar magnetic field of 3×10^8 G.

another star, and exchanged recently into the preexisting pulsar binary during a close encounter, but because the likelihood of the planet remaining bound after the encounter is small, the implied number of such planets orbiting stars in globular clusters must be correspondingly large.

Because such a system is so unexpected, it is very important to continue to improve the observations. Measurement of higher order frequency derivatives, as well as time variations of ω and e, will further constrain the nature of the outer companion, and measurement of an orbital period derivative will test the basic acceleration picture, since we expect $\dot{P}_b/P_b = \dot{P}/P$.

Acknowledgements

We thank Don Backer, Fred Rasio, Kris Joshi, and Steinn Sigurdsson for numerous valuable discussions, David Nice for frequent help with observations at Green Bank, and Joe Taylor for the TEMPO analysis software. The Very Large Array and Green Bank are both parts of the National Radio Astronomy Observatory, a facility of the U.S. National Science Foundation. Grant support for various phases of this project has been provided by Princeton, Caltech, and the N.S.F.

References

Arzoumanian, Z. et al. 1994, ApJ, 422, 671
Backer, D.C. 1993, in Planets around Pulsars, ASP Conf. Ser. Vol. 36, ed. J.A. Phillips, S.E. Thorsett & S.R. Kulkarni (San Francisco: ASP), 11
Backer, D.C. & Thorsett, S.E. 1995, in Millisecond Pulsars: A Decade of Surprise, ASP Conf. Ser. Vol. 72, ed. A.S. Fruchter, M. Tavani & D.C. Backer (San Francisco: ASP), 387
Cudworth, K.M. & Hansen, R.B. 1993, AJ, J., 105, 168
Joshi, K.J. & Rasio, F.A. 1997, ApJ, 479, 948
Lyne, A.G. et al. 1988, Nature, 332, 45
Sigurdsson, S. 1995, ApJ, 452, 323
Thorsett, S.E., Arzoumanian, Z. & Taylor, J.H. 1993, ApJ, 412, L33

Authors' Addresses

S.E. Thorsett: Joseph Henry Laboratories and Department of Physics, Princeton University

Z. Arzoumanian: Center for Radiophysics and Space Research, Cornell University

D.J. Nice, J.H. Taylor and R.W. Sayer

Timing Observations of the J1518+4904 Double Neutron Star System

Abstract

We summarize timing observations of PSR J1518+4904, a recently discovered pulsar in a double neutron star binary. New measurements include (1) periastron advance of $0^\circ.0113 \pm 0^\circ.0001\ \mathrm{yr}^{-1}$, for a total system mass of $2.69 \pm 0.04\ \mathrm{M}_\odot$; (2) period derivative of 2×10^{-20}, yielding an age comparable to that of the Galaxy and a magnetic field substantially lower than other pulsars in double neutron star binaries; and (3) proper motion of $8 \pm 2\ \mathrm{mas\,yr}^{-1}$, or a transverse velocity of $27 \pm 8\ \mathrm{km\,s}^{-1}$, among the lowest pulsar velocities measured.

I Observations

PSR J1518+4904 is a 40.9 ms pulsar in a moderately eccentric, 8.6 day orbit with a second neutron star. It was discovered in the course of a recent survey of the northern sky for fast pulsars (Sayer, Nice & Taylor 1997). We have made timing observations of this pulsar with the Green Bank 140 Foot Telescope at regular intervals since its discovery. The dataset extends from December 1994 to November 1996, and includes observations made at 370, 575, and 800 MHz. Further details of the data acquisition system, as well as results from an early portion of the data, are given in Nice, Sayer & Taylor (1996).

The pulse arrival times were measured using standard techniques and were fit to a model of pulsar rotation, astrometry, and binary motion using the TEMPO software package. As expected for a moderately sized, eccentric binary, the orbit exhibits relativistic precession (Figure 1). Thus the binary model incorporates periastron advance along with the usual five Keplerian orbital parameters. The best-fit timing model is described in Table 1.

Observed pulse period derivatives are biased by the relative acceleration of pulsars and the earth (Damour & Taylor 1991). This bias can be broken into three components, as quantified in Table 2. For PSR J1518+4904, the intrinsic period derivative turns out to be close to the observed value.

Table 1: Timing Model of J1518+4904

Observed Parameters	
Period (ms)	40.93498826871(2)
Period Derivative	$2.75(6) \times 10^{-20}$
Right Ascension (J2000)	$15^{h}18^{m}16\overset{s}{.}7979(2)$
Declination (J2000)	$+49°04'34\overset{''}{.}292(2)$
Proper Motion in α (mas yr^{-1})	$-1(3)$
Proper Motion in δ (mas yr^{-1})	$-8(2)$
Epoch (MJD)	49894.00
Dispersion Measure (pc cm^{-3})	11.61
Orbital Period (days)	8.63400494(5)
Projected Semi-Major Axis (light sec)	20.044005(3)
Eccentricity	0.2494849(2)
Angle of Periastron	$342\overset{\circ}{.}46221(5)$
Time of Periastron (MJD)	49896.246990(1)
Rate of Advance of Periastron (deg yr^{-1})	0.0113(1)
Derived Parameters	
Distance (kpc)	$0.70^{+0.13}_{-0.07}$
Magnetic Field (G)	1×10^{9}
Age (yr)	2×10^{10}
Total System Mass ($M_{\odot}$)	2.69(4)
Orbit Decay Time (yr)	2400×10^{9}
Composite Proper Motion (mas yr^{-1})	8(2)
Transverse Velocity (km s^{-1})	27(8)

II Discussion

The characteristics of J1518+4904 and other double neutron star systems are compared in Table 3 and Figure 2. Tight binary systems B1913+16, B1534+12, and B2127+11C have remarkably similar ages and magnetic fields. (The ages in this population are, of course, influenced by short coalescence times due to relativistic orbital decay.) The wider J1518+4904 system has a very similar pulse period, but a much smaller period derivative, indicative of a very large age (comparable to the age of the Galaxy, like many low-mass millisecond pulsar systems), and a relatively small magnetic field. The origin of this small magnetic field, and its relation to the evolution of the system, is not clear.

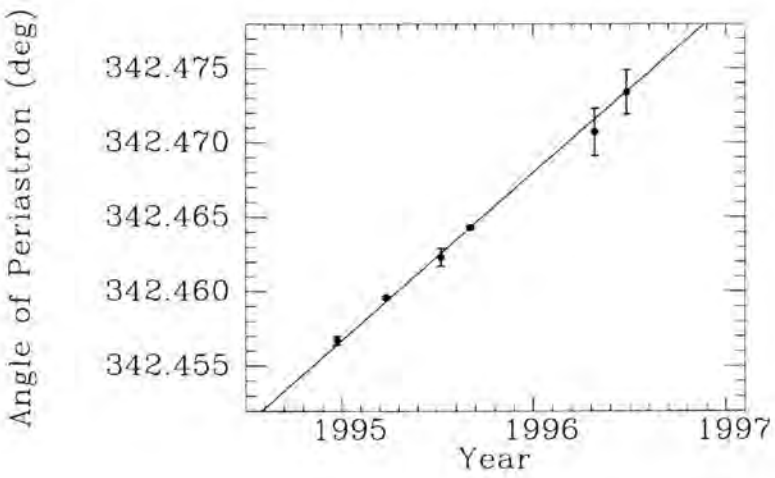

Figure 1. Angle of periastron measured at different epochs by analyzing independent subsets of the data.

The rate of orbital precession, $0^\circ.0113 \pm 0^\circ.0001\ \mathrm{yr}^{-1}$, yields a total system mass of $2.69 \pm 0.04\ \mathrm{M}_\odot$. This is slightly less than the total mass of the B1913+16 system (2.83 $\mathrm{M}_\odot$), but it is indistinguishable from masses of the other systems. The differences in mass must reflect differences in the evolution of the systems. We expect that future observations will refine the mass measurement of J1518+4904. However, given the range of masses in the tight systems (2.69 to 2.83 $\mathrm{M}_\odot$), the interpretation of the J1518+4904 mass will not be simple.

From the proper motion of $8 \pm 2\ \mathrm{mas\ yr}^{-1}$, we estimate the transverse space velocity to be $27 \pm 8\ \mathrm{km\ s}^{-1}$. This is remarkably low compared with pulsars in general and even compared with binary pulsars. (For example, B1913+16 has transverse velocity $100 \pm 40\ \mathrm{km\ s}^{-1}$ and 1534+12 has velocity $80 \pm 20\ \mathrm{km\ s}^{-1}$.) Given the relatively wide orbit, any event, such as an asymmetric supernova, which would have substantially boosted the system velocity would also likely have disrupted the binary. Thus a low space velocity seems like a necessary condition for the survival of such a system.

Table 2: Period Derivative

Observed Period Derivative		$2.75 \pm 0.06 \times 10^{-20}$
Acceleration	Towards Galactic disk	$0.55 \pm 0.02 \times 10^{-20}$
	Galactic rotation	$0.08 \pm 0.01 \times 10^{-20}$
	Transverse motion	$-0.5 \pm 0.3 \times 10^{-20}$
Intrinsic Period Derivative		$2.9 \pm 0.3 \times 10^{-20}$

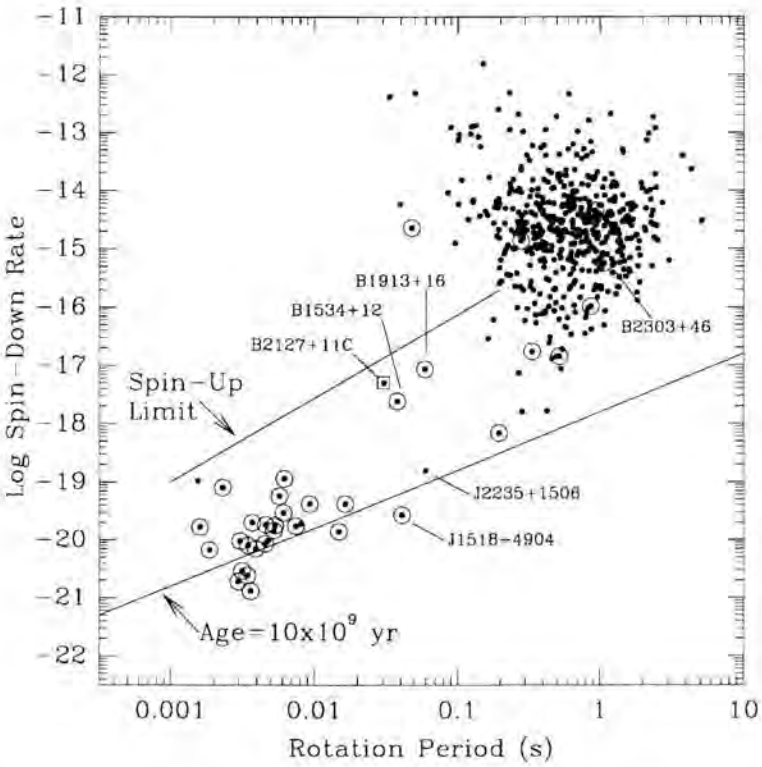

Figure 2. Spin parameters of disk pulsars. Binaries are indicated by circles; one cluster pulsar (B2127+11C) is included. Pulsars likely formed in double neutron star systems are labeled; see text for discussion.

Finally, we comment that parameters of J1518+4904 make it the pulsar closest to PSR J2235+1506 on the P-$\dot{P}$ diagram. This circumstantial evidence suggests that J2235+1506 was formed in a high mass neutron star binary which was disrupted upon the second supernova explosion.

Acknowledgements

We thank Z. Arzoumanian for assistance with collection of some of the pulsar timing data. The 140 Foot telescope is a facility of the National Radio Astronomy Observatory, operated by Associated Universities, Inc., for the National Science Foundation.

Table 3: Double Neutron Star Systems[a]

PSR	Orbital Period (d)	Characteristic Age (yr)	Magnetic Field (G)	System Mass ($M_\odot$)
J1518+4904	8.6	2×10^{10}	1×10^{9}	2.69 ± 0.04
B1534+12	0.4	2×10^{8}	1×10^{10}	2.6784
B1913+16	0.3	1×10^{8}	2×10^{10}	2.8284
B2127+11C	0.3	1×10^{8}	1×10^{10}	2.712
B2303+46	12.3	3×10^{7}	8×10^{11}	2.60 ± 0.06

[a]See Nice et al. (1996) for references.

References

Damour, T. & Taylor, J.H. 1991, ApJ 366, 501
Nice, D.J., Sayer, R.W. & Taylor, J.H 1996, ApJ 466, L87
Sayer, R.W., Nice, D.J. & Taylor, J.H. 1997, ApJ 474, 426

Authors' Address

Physics Department, Princeton University, Box 708, Princeton, NJ 08544, USA

Z. Arzoumanian, J.H. Taylor and A. Wolszczan

Evidence for Relativistic Precession in the Pulsar Binary B1534+12

Abstract

We report the detection of a long-term change in the integrated pulse profile of the relativistic binary pulsar B1534+12. The rate of change over 2.5 years is consistent with that expected from geodetic precession of the pulsar's spin axis in the gravitational field of the companion neutron star.

I Introduction

The curvature of space-time around a massive star results in precession of the spin axis of an orbiting gyroscope or, equivalently, a rotating companion star. The magnitude of this "geodetic" precession, the larger of two relativistic effects, is calculable in any metric theory of gravity and generally depends on the masses of the two stars and the nature of the orbit. For the double neutron-star system PSR B1534+12, General Relativity predicts a geodetic precession rate for the pulsar's spin axis of 0.5 deg yr^{-1}, a prediction based on component star mass measurements made through the dependence of other strong-field relativistic effects on those same masses (Damour & Taylor 1992, and references therein). As a result, detection and measurement of pulsar precession in a relativistic system promise a new and stringent self-consistency test of General Relativity, or any other relativistic theory of gravity, in the strong-field regime.

As a neutron star's magnetosphere sweeps through the line of sight, variation of the radiated beam's polarization angle with rotational phase establishes the angle that the magnetic axis makes with the line of sight at closest approach, the "impact parameter" (Radhakrishnan & Cooke 1969). For relativistic binary pulsars, changes in this viewing geometry are the most promising means of detecting precession of the pulsar spin axis, which would reveal itself in evolving pulse intensity and polarization profiles. A long-term change in the intensity profile of PSR B1913+16, the original relativistic binary pulsar, has in fact been observed at a rate consistent with geodetic precession (Weisberg, Romani & Taylor 1989); the constancy of the polarization profile over the same epoch, however, is surprising (Cordes, Wasserman & Blaskiewicz 1990).

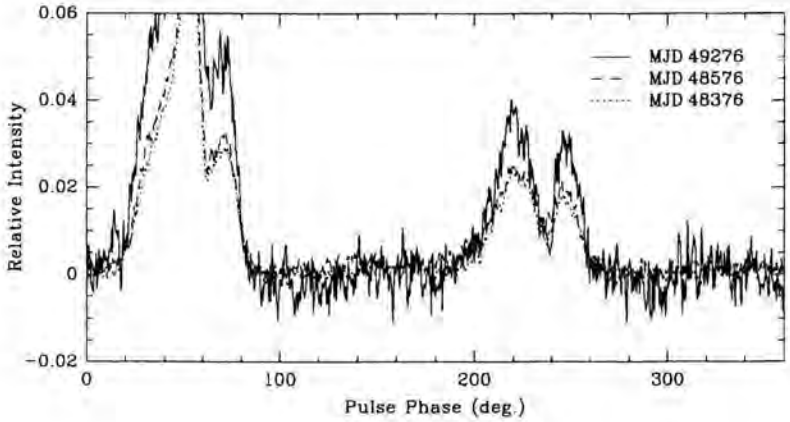

Figure 1. Integrated 1400 MHz pulse profiles of PSR B1534+12 at three epochs, scaled to unit peak intensity.

The opening angle of the cone traced out by the precessing spin axis, i.e., the misalignment between the pulsar's spin and orbital angular momentum vectors, ultimately determines whether the effects of pulsar precession are detectable. For PSR B1534+12, pulse polarization measurements (Arzoumanian et al. 1996) constrain this misalignment to be small, but likely non-zero. Here, we report the detection of a long-term, monotonic change in the pulsar's intensity profile, evidence for precession of the pulsar spin axis.

II Observations and Results

We examined the pulse shape of PSR B1534+12 using a large number of intensity profiles collected during dual-frequency (430 MHz and 1400 MHz) timing observations made at biweekly intervals between October 1990 and January 1994 with the Arecibo radiotelescope (see Arzoumanian 1995 for details). Low-noise integrated profiles were formed from the single-epoch observations by combining them into thirteen 100 day averages.

Figure 1 plots 1400 MHz integrated profiles for B1534+12 at three epochs. Each profile is averaged over all orbital phases and normalized to unit peak intensity. The dotted and dashed lines represent low-noise profiles from two early 100 day groupings, and the highest-quality late-epoch profile is plotted with a solid line. The increasing relative intensity of the "off-pulse" emission with time is clear. Figure 2 depicts the same trend in a different manner: intensity contours are plotted versus pulse phase and date for averaged profiles from each of the thirteen intervals.

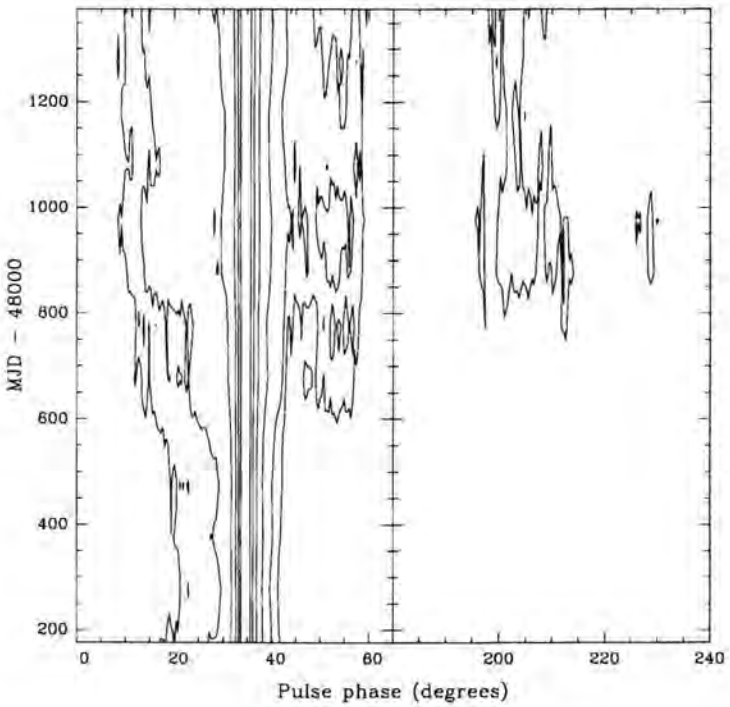

Figure 2. Evolution of the 1400 MHz integrated profiles of PSR B1534+12 at 100 day intervals. Contours represent intensities between 3% and 75% of the peak value.

III Discussion

The stability of average pulse shapes over long periods of time has been quantitatively studied for a number of pulsars (Blaskiewicz 1991). Excepting the "moding" phenomenon (the switching, at irregular intervals, between two or three distinct emission patterns) and the relativistic binaries B1534+12 and B1913+16, the pulse waveforms of only three objects (all isolated) are known to evolve: PSRs B2217+47 (Suleymanova & Shitov 1994), B0833−45 and B1642−03 (Blaskiewicz 1991). These authors have proposed models invoking free precession to explain the profile changes they observe; since the models depend on changes in the internal structure of the neutron stars, it seems unlikely that they would apply to either B1913+16 or B1534+12, which are at least two orders of magnitude older, and therefore cooler and less active, than the others. No compelling explanation for long-term changes in pulse shape other than precession has ever been advanced, and while other effects cannot be ruled out, the observed profile shape evolution of PSR B1534+12 is evidence for spin-orbit precession of the pulsar spin axis.

If the shape change at 1400 MHz is assumed to be due to precession, we can estimate the angular displacement of the pulsar's spin axis. We assume that the central component of the main pulse is circularly symmetric, and note that the observed change can be simply described as a gradual decrease in the intensity of the main pulse relative to the other profile components. The difference in impact parameter between early and late epochs is then roughly the phase on the main pulse of the early profile at which the peak intensity of the late profile is reached. Scaling the average 1400 MHz profiles at MJDs 48376 and 49276 (Fig. 1) by the peak intensity of the interpulse, we find that the main pulse has dropped to 66% of its original intensity. This level is reached on the early-epoch profile at 3.3 phase bins from the peak, both preceding and following it, a value obtained by simple-mindedly interpolating between bins ($360^\circ/1024\,\mathrm{bins} = 0.^\circ35/\mathrm{bin}$). The implied angular displacement of approximately $1.^\circ2$ is clearly consistent with geodetic precession of the spin axis over 2.5 years.

No evolution of the 430 MHz pulse profile similar to that at the higher frequency is observed. The lack of a clear shape change does not necessarily rule out precession. The central component of the main pulse is twice as wide at 430 MHz as it is at 1400 MHz—the larger width at the lower frequency may be masking changes at the level observed in the high-frequency profile. More importantly, the low-frequency data is known to suffer from systematic effects, such as scintillation slopes (Arzoumanian 1995; Stairs et al. 1998), which would tend to smear profile features in pulse phase.

References

Arzoumanian Z. 1995, Ph.D. Thesis, Princeton University
Arzoumanian, Z. et al. 1996, ApJ, 470, 1111
Cordes, J.M., Wasserman, I. & Blaskiewicz M. 1990, ApJ, 349, 546
Damour, T. & Taylor J.H. 1992, Phys. Rev. D, 45, 1840 (DT92)
Radhakrishnan, V. & Cooke D.J. 1969, Ap. Lett., 3, 225
Stairs, I.H. et al. 1998, ApJ, 505, 352
Weisberg, J.M., Romani, R.W. & Taylor J.H. 1989, ApJ, 347, 1030

Authors' Addresses

Z. Arzoumanian: Center for Radiophysics and Space Research, Cornell University, Ithaca, NY 14853-6801, USA; arzouman@spacenet.tn.cornell.edu

J.H. Taylor: Joseph Henry Laboratories and Physics Department, Princeton University, Princeton, NJ 08544, USA; joe@pulsar.princeton.edu

A. Wolszczan: Department of Astronomy and Astrophysics, Pennsylvania State University, University Park, PA 16802, USA; alex@astro.psu.edu

N. Wex and S. Johnston

Recent Timing Results for PSR B1259−63

Abstract

The binary pulsar PSR B1259−63 is in a highly eccentric 3.4 yr orbit around the Be star SS 2883. Timing observations of this pulsar, made over a 7 yr period using the Parkes 64 m radio-telescope, cover two periastron passages, in 1990 August and 1994 January. The timing observations of PSR B1259−63 clearly show evidence for timing noise which is dominated by a cubic term. Unfortunately, the large amplitude timing noise and data over only two complete orbits make it difficult to produce a unique timing solution for this pulsar. However, if the long term behavior of timing noise is completely modeled by a cubic term, both $\dot{\omega}$ and $\dot{x}$ terms are required in the timing model which could be a result of a precessing orbit caused by the quadrupole moment of the tilted companion star. In this paper we summarise the timing observations for the PSR B1259−63 system; full details are given in Wex et al. (1997).

1 Introduction

The binary pulsar PSR B1259−63 is part of a unique system. Discovered at Parkes in a survey of the Galactic plane at 1.5 GHz (Johnston et al. 1992a), it was shown by Johnston et al. (1992b) to be in a highly eccentric 3.4 yr orbit around a $10^{\rm th}$ magnitude Be star, SS 2883. The pulsar period P is relatively short, 47.8 ms, and the measured period derivative gives a pulsar characteristic age, $\tau_c = P/(2\dot{P})$, of 3.3×10^5 yr and a surface magnetic field, $B = 3.2 \times 10^{19}(P\dot{P})^{1/2}$, of $3.3{\times}10^{11}$ G. This therefore is a young system, which may evolve through an accretion phase to form a single or binary millisecond pulsar. The companion star is of spectral type B2e, with a mass of $M_* \sim 10$ M$_\odot$ and radius $R_* \sim 6$ R$_\odot$ (Johnston et al. 1994). A companion mass of 10 M$_\odot$ and a pulsar mass of 1.4 M$_\odot$ imply an orbital inclination $i \sim 35°$. The orbital eccentricity is very high, 0.87, and for $\sin i \sim 0.5$, the pulsar approaches within 25 R_* of the companion star at periastron, passing through the circumstellar disk.

In this paper we report timing observations made using the Parkes radio telescope over a 7 year interval covering both the 1990 and 1994 periastron passages and discuss their interpretation.

II Timing observations and data analysis

A total of more than 300 pulse times of arrival (TOAs) were measured at the Parkes radio telescope between 1990 January and 1996 October. Most of the observations were at frequencies around 1.5 GHz, giving TOA uncertainties of $\lesssim 100\mu$s. Observations at 0.43, 0.66, 4.8 and 8.4 GHz were also made. Details of the observing systems are given in Johnston et al. (1996).

Pulsar and binary parameters were obtained using the least-squares fitting program TEMPO (Taylor & Weisberg 1989) with the Jet Propulsion Laboratory solar-system ephemeris DE200 (Standish 1982). TEMPO was extended by a timing model for binary pulsars that orbit a companion star with a significant quadrupole moment (Wex 1997).

As discussed by Johnston et al. (1996), significant dispersion and scattering changes were observed around periastron. Because of this, data from 1990 July and 1993 December were omitted from the analysis. The pulsar was eclipsed during 1994 January. Thus there is a gap in the TOAs around the first periastron (August 1990) from day -107 to day $+22$ and a gap around the second periastron (January 1994) from day -51 to day $+25$. Unfortunately this is a crucial problem when searching for the correct timing model for PSR B1259−63. One consequence of this is that the timing models are quite insensitive to extra phase-jumps added to the TOAs at each periastron.

The data were first fitted for pulsar position, period, period derivative, dispersion measure and the five Keplerian orbital parameters. The best results give a RMS of 2030 μs. Systematic variations in the residuals are observed at all orbital phases, showing that this set of parameters does not satisfactorily model the timing behavior of the system.

Observations made between 1990 January and 1994 October appeared to be well explained by step changes in the pulsar period at the two periastrons (Manchester et al. 1995), which could originate from a propeller-torque spindown caused by the interaction of the pulsar with the circumstellar matter at the Alfvén radius (Illarionov & Sunyaev 1975). This timing solution now fails to model the TOAs obtained during timing observations from 1995 and 1996.

One could still try to fit for a pure Keplerian motion and the effects of spin-down (modeled as a $\Delta P/P$ term) at each periastron. The best fit for this has an RMS residual of 360 μs. The resulting two period steps for this fit emerge to have opposite signs, certainly a problem if one looks for a physical interpretation.

PSR B1259−63 is a comparatively young pulsar with a period derivative $\dot{P}$ of 2.3×10^{-15}. According to Lyne (1996) such a pulsar should suffer a timing noise which is usually dominated by a cubic term. This can be modeled by a period second derivative $\ddot{P}$ of the order of $\pm 10^{-26}$ ss^{-2}. Fitting for a $\ddot{P}$, the pulsar spin parameters and the Keplerian parameters for the orbital motion leads to a RMS of 950 μs, but there are still strong systematics in the residuals.

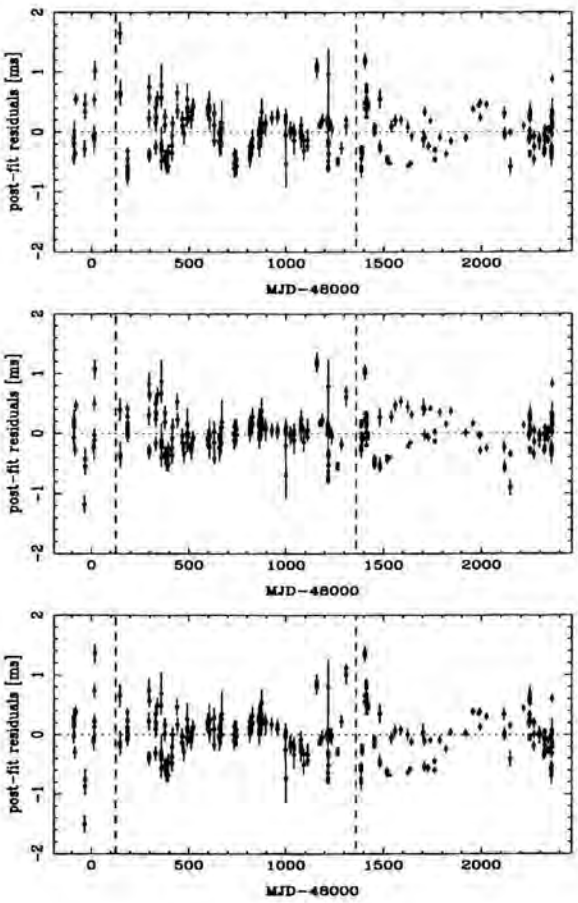

Figure 1. Post-fit residuals for MODEL 1, MODEL 2A, MODEL 2B (unweighted fits). The vertical dashed lines indicate the two times of periastron passage.

A straight forward assumption is that the timing noise is not fully modeled by a $\ddot{P}$ and additional frequency derivatives are needed to account for it. Adding just a third derivative leads to some improvement but does not give a satisfactory fit. So we add a fourth frequency derivative and obtain a fit with a RMS residual of 390 μs (MODEL 1). Figure 1 shows the corresponding post-fit residuals. The resulting fit still shows systematics which of course could result from un-modeled contributions from timing noise. Fitting for even higher frequency derivatives does not improve the fit and does not give significant values for these higher frequency derivatives.

For a pulsar in orbit about a Be star, one expects changes in the longitude of the periastron ω and the inclination of the orbit i (Lai et al. 1995). The latter manifests itself as a change of the projected semi-major axis $x = a_p \sin i$. The physical cause of these changes is the so called "classical spin-orbit coupling," i.e., the fact that the spin-induced quadrupole of the fast rotating companion leads to a $1/r^3$ term in the gravitational potential which leads to apsidal motion and precession of the binary orbit (see Kopal 1978, Smarr & Blandford 1976, and Lai et al. 1995 for details). Fits for the pulsar position, spin parameters (including $\ddot{P}$ to model the timing noise), Keplerian parameters for orbital motion, and the two post-Keplerian parameters, $\dot{\omega}$ and $\dot{x}$, lead to two timing solutions, MODEL 2A (RMS $= 340\,\mu$s, $\dot{\omega} = -0.000019(1)$ deg/yr, $\dot{x} = -0.21(1) \times 10^{-12}$) and MODEL 2B (RMS $= 410\,\mu$s, $\dot{\omega} = -0.000041(1)$ deg/yr, $\dot{x} = -2.42(1) \times 10^{-12}$). The corresponding post-fit residuals are shown in Fig. 1. Realistic errors for the parameters were obtained by adding (or subtracting) an integer number of phase turns at each periastron until the fit deviated from the best fit by about 20 per cent (in RMS residual). These fits are still not perfect, e.g., there are clearly systematic trends in the residuals between MJD 49500 and MJD 50200. But so far these are the best fits for PSR B1259−63. The systematic behavior could be a result of un-modeled timing noise or a physical process so far overlooked in this system.

In conclusion, we have four fits that give reasonably good residuals. We feel the solutions which involve a step change in the period can be ruled out on the grounds of their opposite sign. If we have completely modeled the timing noise with a cubic term then the fact that $\dot{\omega} < 0$ implies that the companion is tilted at least $54\overset{\circ}{.}7$ with respect to the orbital plane. This is an important result with consequences both for the theory of binary evolution and pulsar kick velocities but also for the interpretation of the radio and high-energy emission from the system at periastron. For a detailed discussion of the various timing fits, the full set of parameters derived for the binary system and the implications and restrictions of the orientation of the companion see Wex et al. (1997).

Observations of this pulsar continue to be made in the lead up to the next periastron predicted for 1997 May 29. This periastron passage should enable us to determine which of the above models is the correct description of the PSR B1259−63 system.

Acknowledgements

We thank Ed van den Heuvel for his hospitality during the conference. We thank our co-collaborators R.N. Manchester, A.G. Lyne, B.W. Stappers and M. Bailes for their on-going commitment to the project. We are grateful to J.H. Taylor for valuable comments.

References

Illarionov, A.F. & Sunyaev, R.A. 1975, A&A, 39, 185
Johnston, S. et al. 1992a, MNRAS, 255, 401
Johnston, S. et al. 1992b, ApJ, 387, L37
Johnston, S. et al. 1994, MNRAS, 268, 430
Johnston, S. et al. 1996, MNRAS, 279, 1026
Lai, D., Bildsten, L. & Kaspi, V.M. 1995, ApJ, 452, 819
Lyne, A.G. 1996, in Pulsars: Problems & Progress, IAU Coll. 160, ed. S. Johnston, M.A. Walker & M. Bailes (San Francisco: ASP), 73
Manchester, R.N. et al. 1995, ApJ, 445, L137
Smarr, L.L. & Blandford, R.D. 1976, ApJ, 207, 574
Taylor, J.H. & Weisberg, J.M. 1989, ApJ, 345, 434
Wex, N. 1997, MNRAS, 298, 67
Wex, N. et al. 1997, MNRAS, 298, 997

Authors' Addresses

N. Wex: Max-Planck-Institut für Radioastronomie, Auf dem Hügel 69, D-53121 Bonn, Germany

S. Johnston: Research Centre for Theoretical Astrophysics, University of Sydney, NSW 2006, Australia

V.M. Kaspi

The Pulsar/B-Star Binary PSR J0045−7319

Abstract

A surprisingly rich variety of astrophysical results has emerged from observations of PSR J0045−7319, a 926-s pulsar in a 51-day eccentric binary orbit with a B star. Here we review these results, which include tight limits on the B-star's mass-loss rate, well-defined constraints on the inclination of the B-star's spin axis with respect to the orbital angular momentum through the detection of classical periastron advance and spin-orbit coupling, strong evidence for a birth kick to the neutron star from an asymmetric supernova, as well as evidence for retrograde differential rotation of the B star.

I Basic properties of the PSR J0045−7319 binary

PSR J0045−7319, the only known pulsar in the Small Magellanic Cloud, was discovered as part of a large survey for radio pulsars in the Magellanic Clouds (McConnell et al. 1991). Timing observations of the pulsar demonstrated that it is in an eccentric 51-day binary orbit with a companion having minimum mass 4 $M_\odot$ (Kaspi et al. 1994). The same timing observations also determined the pulse period derivative for this 926-ms pulsar, which implied a timing age of $\sim 3 \times 10^6$ yr and a surface magnetic field of $\sim 2 \times 10^{12}$ G. Optical observations revealed the presence of a main sequence 16-mag B1V star at the pulsar timing position. Follow-up spectroscopy revealed radial velocity variations of the B star, consistent with Doppler shifts of the expected magnitude and at the predicted orbital phase, confirming the association (Bell et al. 1995b). Those observations also measured the width of He I lines and measured the stellar projected rotation velocity, $v \sin i = (113 \pm 10)$ km s^{-1}, typical of B stars (Allen 1963). The B-star's colors and luminosity at the distance of the SMC implied a temperature of (24000±1000) K and a radius of (6.4 ± 0.7) $R_\odot$ (Bell et al. 1995b). The B-star radial velocity curve determined its mass to be (8.8 ± 1.8) $M_\odot$ and the inclination angle of the orbit $i = 44^\circ \pm 5^\circ$, assuming a 1.4 $M_\odot$ neutron star. This implies that the pulsar approaches its companion very closely at periastron: to within (3.7±0.5) B-star radii.

II Deviations from a Keplerian orbit and the B-star wind

Continued timing observations of the pulsar revealed that a simple Keplerian orbit provided a poor fit to the pulse arrival times (Kaspi et al. 1996b). Although no eclipses of the radio data were observed at any orbital phase, the proximity of the pulsar to the B star at periastron suggested that the pulsar's radio emission could be dispersed by the ionized component of the B-star's wind, resulting in apparent delays of the single-frequency timing signal. To investigate this possibility, multiple frequency observations were performed near and away from periastron. No significant increase in the pulsar's dispersion measure (DM) was observed near periastron, with a 3σ upper limit of $\Delta\mathrm{DM} < 0.9$ pc cm^{-3} (Kaspi, Tauris & Manchester 1996). This permitted a limit to be placed on the mass-loss rate for the B star, $\dot{M} < (3.4 \times 10^{-11})(v_\infty/v_{\rm esc})$ M$_\odot$ yr^{-1}, where v_∞ is the terminal wind velocity and v_{esc} is the stellar escape velocity. Though significantly smaller than what is predicted by empirical mass-loss/luminosity relations, derived from Galactic B stars for which $\dot{M}$ has been measured (e.g., de Jager, Nieuwenhuijzen & van der Hucht 1988), so low an $\dot{M}$ is not surprising given the low SMC metallicity and the importance of metals in radiation-driven winds of early-type stars (Lucy & Solomon 1970, Castor, Abbott & Klein 1976, Kudritzki, Pauldrach & Puls 1987).

III Classical periastron advance and spin-orbit coupling

Lai, Bildsten & Kaspi (1995) showed (see also Smarr & Blandford 1976) that a rapidly rotating B star such as the companion to PSR J0045−7319 should have a substantial equatorial bulge, and that the quadrupolar term in the interaction potential should result in classical precession of the line of apsides, i.e., periastron advance ($\dot{\omega}$). In addition, Lai et al. showed that for a B-star spin axis significantly inclined with respect to the orbital angular momentum, the net torque on the B star would force it to precess; since total angular momentum is conserved, the orbital angular momentum would be forced to precess as well, and the inclination of the orbital plane should vary (di/dt), observable as a changing projected semi-major axis, d(a sin$i$)/dt. Kaspi et al. (1996a) showed that the timing model including a Keplerian orbit plus $\dot{\omega}$ and d(a sin$i$)/dt fit the data well. The fitted values $\dot{\omega} = (0\overset{\circ}{.}0259 \pm 0\overset{\circ}{.}0005)$ yr^{-1} and d(a sin$i$)/dt $= (1.17 \pm 0.02) \times 10^{-9}$ lt s s^{-1} require the B-star spin axis to be inclined with respect to the orbital angular momentum by at least 25°.[1] The true value of the inclination angle depends on the unknown precession phase. As the precession period is probably several hundred years, the inclination angle is not likely to be better constrained soon.

[1] Kaspi et al. (1996) constrained the inclination angle to be less than 41°, however it has recently been pointed out (Norbert Wex, personal communication) that a region of phase space exists in which the angle could be as large as 54$\overset{\circ}{.}$7.

IV Neutron star birth kicks

Birth kicks to neutron stars resulting from asymmetric supernova explosions have been hypothesized on the basis of large observed pulsar proper motions (e.g., Cordes, Romani & Lundgren 1993, Lyne & Lorimer 1994) but remained unproven because scenarios could be envisioned in which binary disruption in symmetric supernovae resulted in the high pulsar velocities (Iben & Tutukov 1996). Prior to the formation of the pulsar in the PSR J0045−7319 system, the binary must have been very close (see Kaspi et al. 1994), so tidal and/or mass-transfer forces should have aligned the angular momenta. Therefore, the non-zero inclination angle observed today via the detected spin-orbit coupling provides strong, new evidence for a birth kick to the neutron star out of the original plane of the orbit (Kaspi et al. 1996a). The size of the kick required to achieve the minimum possible misalignment is poorly constrained, but was probably $\sim$100 km s^{-1}.

V Orbital period derivative and retrograde differential B-star rotation

From the timing data, Kaspi et al. (1996a) showed that in addition to the classical post-Keplerian parameters $\dot{\omega}$ and di/dt, the best timing model included a significant orbital period derivative $\dot{P}_b = (-3.03 \pm 0.09) \times 10^{-7}$. The implied time scale for orbital evolution is only $\sim$0.5 Myr, comparable to that observed in accreting neutron star/B-star binaries (e.g., Levine et al. 1993); however, in PSR J0045−7319, the evolution is necessarily of a different origin, given the tiny B-star mass-loss rate. Energy dissipation is expected because of oscillation modes excited in the B star by the neutron star's orbit (the so-called "dynamical tide"), however Kumar, Ao & Quataert (1995) showed that the effect should be small, because low-frequency (hence low-energy) modes should be excited most. Lai (1996) proposed retrograde rotation of the B star as a way of exciting high-frequency modes, since in this case, in the B-star's rest frame, the neutron star's relative angular velocity is much larger, thereby exciting high frequency modes. Kumar & Quataert (1997) argued that although higher frequency modes would be excited as Lai suggested, his assumed dissipation rate was too high, and the excited modes would be damped insufficiently quickly to account for the large observed $\dot{P}_b$. However, Kumar & Quataert also show that differential rotation of the B star could result in significantly smaller damping times, and could explain the observed $\dot{P}_b$. Retrograde rotation demands a larger birth kick velocity to the neutron star in order to have made it reverse the direction of the pre-supernova orbital motion; the magnitude, again poorly constrained, was most likely $\sim$200 km s^{-1}.

VI Future observations

We expect future observations of PSR J0045−7319 to yield additional interesting information. Continued timing will determine if the observed orbital period derivative is indeed secular, as opposed to variable as in the eclipsing binary pulsar PSR B1957+20 (Arzoumanian, Fruchter & Taylor 1994). An improved optical light curve for the B star could reduce the uncertainties on the mass ratio significantly, and possibly help determine the apsidal constant for use in comparing with models of the stellar interior. Polarization measurements of the radio pulsar as a function of orbital phase could help map the B-star magnetic field, as has been done for the pulsar/Be-star binary PSR B1259−63 (see Wex & Johnston, this volume). Finally, the wide range of interesting results that has emerged from observations of PSR J0045−7319 (and PSR B1259−63) makes it highly desirable to discover and observe other such systems. Although a number of searches designed specifically with this purpose in mind (Sayer, Nice & Kaspi 1996, Vasisht 1996, Philp et al. 1996, Kaspi, Manchester & D'Amico 1997) have discovered no new binaries, future Galactic-plane pulsar searches hold the most hope for success.

Acknowledgements

I am grateful to my numerous collaborators and co-authors who have been involved in various aspects of PSR J0045−7319 observations and theory. I thank Norbert Wex for pointing out the possibility of a B-star inclination angle as large as 54°.7.

References

Allen, C.W. 1963, Astrophysical Quantities, (London: Athlone Press)
Arzoumanian, Z., Fruchter, A.S. & Taylor, J.H. 1994, ApJ, 426, L85
Bell, J.F. et al. 1995, ApJ, 447, L117
Castor, J.I., Abbott, D.C. & Klein, R.I. 1976, ApJ, 195, 157
Cordes, J.M., Romani, R.W. & Lundgren, S.C. 1993, Nature, 362, 133
de Jager, C., Nieuwenhuijzen, H. & van der Hucht, K.A. 1988, A&AS, 72, 259
Iben, I. & Tutukov, A.V. 1996, ApJ, 456, 738
Kaspi, V.M. et al. 1996a, Nature, 381, 584
Kaspi, V.M. et al. 1994, ApJ, 423, L43
Kaspi, V.M. et al. 1996b, in Compact Stars in Binaries, IAU Symp. 165, ed. J. van Paradijs, E.P.J. van den Heuvel & E. Kuulkers, (Dordrecht: Kluwer), p. 271
Kaspi, V.M., Tauris, T. & Manchester, R.N. 1996, ApJ, 459, 717
Kaspi, V.M., Manchester R.N., D'Amico, N. 1997, in preparation
Kudritzki, R.P., Pauldrach, A. & Puls, J. 1987, A&A, 173, 293
Kumar, P., Ao, C.O. & Quataert, E.J. 1995, ApJ, 449, 294
Kumar, P. & Quataert, E.J. 1997, ApJ, 479, L51

Lai, D. 1996, ApJ, 466, L35
Lai, D., Bildsten, L. & Kaspi, V.M. 1995, ApJ, 452, 819
Levine, A. et al. 1993, ApJ, 410, 328
Lucy, L.B. & Solomon, P. 1970, ApJ, 159, 879
Lyne, A.G. & Lorimer, D.R. 1994, Nature, 369, 127
McConnell, D. et al. 1991, MNRAS, 249, 654
Philp, C.J. et al. 1996, AJ, 111, 1220
Sayer, R.W., Nice, D.J. & Kaspi, V.M. 1996, ApJ, 461, 357
Smarr, L.L. & Blandford, R. 1976, ApJ, 207, 574
Vasisht, G. 1996. Ph.D. Thesis, California Inst. of Tech.

Authors' Address

MIT 37-621, 70 Vassar Street, Cambridge, MA, USA 02139

A. Wolszczan

Detecting Planets Around Pulsars

Abstract

We review the results of searches for planet-mass bodies around neutron stars using the pulse timing technique. The precision of pulsar timing allows a detection of terrestrial-mass bodies orbiting slow pulsars and asteroidal-mass companions to millisecond pulsars. A planetary and asteroidal "noise" may be a precision-limiting factor in other uses of the pulse timing method. At present, PSR B1257+12, the 6.2-millisecond pulsar, remains the only neutron star accompanied by confirmed planets. There is a possibility for a fourth distant planet in this system.

I Introduction

The first planets beyond the Solar System have been detected around a billion year old neutron star, a 6.2-millisecond radio pulsar, PSR B1257+12 (Wolszczan & Frail 1992; Wolszczan 1994). The three companions to PSR B1257+12 remain the only known system of terrestrial mass planets orbiting a star other than the Sun. More recent results include growing evidence for a Jupiter-mass object orbiting a binary pulsar, PSR B1620−26, in the globular cluster M4 (Arzoumanian et al. 1996; Thorsett & Arzoumanian, these proceedings) and a possibility for an Earth-mass body around PSR B0329+54 (Shabanova 1995). The existence of pulsar planets, and a series of spectacular discoveries of giant planetary-mass objects around solar-type stars (e.g., Mayor & Queloz 1995; Marcy & Butler 1996; see Bos 1996 for a recent review) provide compelling evidence that extrasolar planetary systems can exist in a surprising, entirely unanticipated multitude of forms.

Radio pulsars, especially those of the millisecond period variety, are extremely stable rotators (see Phinney & Kulkarni 1994 for a recent review). The intrinsic rotational stability of these objects and the corresponding steady repetition rate of the observed pulses of radio emission makes them the most precise "cosmic clocks" known, with performance rivaling that of the best terrestrial time standards. Searches for extrasolar planets are the latest of the many applications of the pulsar clocks as probes of a wide range of astrophysical phenomena (e.g., Blandford 1992).

In this paper, we present the pulse timing as a high-precision method of detection of planetary mass bodies around neutron stars and summarize the results of searches for pulsar planets using this technique.

II Planets and pulse timing precision

Accurate measurements of the pulse time-of-arrival (TOA) variations generated by reflex motion of a pulsar due to orbiting planets provide a powerful method of the indirect planet detection. This method is closely related to single-line Doppler spectroscopy and astrometry which are widely used in planetary searches around ordinary stars. For a circular orbit and the pulsar mass, $M_{\rm psr} = 1.35$ M$_\odot$, a relationship between the planetary mass, m_2, the planet's orbital period, P_b, and the semi-amplitude, Δt, of the corresponding TOA variations is:

$$m_2 \sin i = 21.3 \mathrm{M}_\oplus \left(\frac{\Delta t}{1\ \mathrm{ms}}\right) \left(\frac{P_b}{1\ \mathrm{day}}\right)^{-2/3}, \qquad (1)$$

where M$_\oplus$ is the Earth mass, i is the orbital inclination and $m_2 \ll M_{\rm psr}$.

A practical demonstration of the consequences of this relationship is presented in Figure 1 which shows timing residuals from simulated observations of the Solar System planets with the Sun replaced by a 1.35 M$_\odot$ neutron star. Clearly, the Jovian planets generate large residuals, the terrestrial planets are detectable with $a \leq 1$ ms precision provided by "normal," slowly rotating pulsars ($P \sim 1$ s) and they are extremely easy to recognize with millisecond pulsars due to their microsecond timing accuracy. Moreover, as demonstrated in Figure 1c, with a sub-microsecond timing precision attainable with the best pulsar clocks, the largest asteroids become barely detectable as well! In fact, this raises a disturbing possibility that the timing noise generated by circumpulsar asteroids may be one of the elements of the pulsar "weather" which delimit a precision of the TOA measurements.

It is illuminating to compare a planet detection power of the pulsar timing with the current capabilities of optical methods. Radial velocity precision required to detect a Moon-like body in an inner planet orbit around a solar-mass star would be ~ 1 mm s^{-1}. This corresponds to a timing residual amplitude of a few microseconds (Eq. 1) which is measurable with millisecond pulsars (e.g., Wolszczan 1994). The most advanced Doppler searches for planets around normal stars have recently achieved a ≤ 5 m s^{-1} accuracy (Butler et al. 1996) which is sufficient to detect Jupiters and "super-Jupiters." Further technical improvements may make it possible to lower this limit to ~ 1 m s^{-1} and gain access to Saturn-mass bodies. Undoubtedly, in a foreseeable future, the pulse timing method will remain unique in its ability to detect low-mass planetary objects outside the Solar System and to study their dynamics.

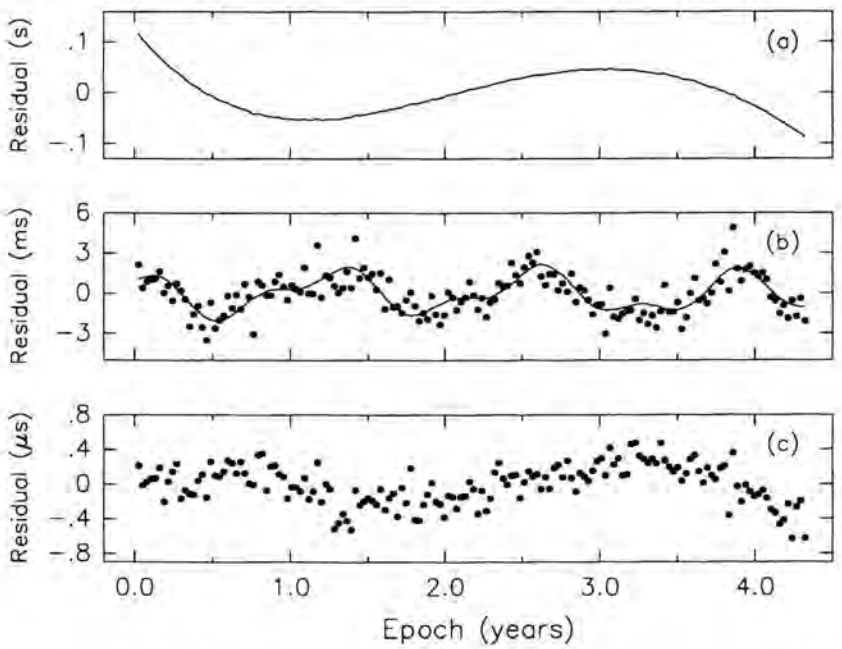

Figure 1. Simulated timing residuals from observations of the Solar System planets around a 1.4 $M_\odot$ pulsar, after subtraction of the best-fit model including the initial phase, the pulsar rotation period, P, and its slowdown rate, $\dot{P}$. *(a)* All planets present, the residuals are dominated by Jupiter. *(b)* Outer planets fitted out, the residuals for a slow pulsar (filled circles, timing accuracy 0.5 ms) show the presence of the Earth and Venus. The solid line represents the same detection with a slow pulsar replaced with a millisecond pulsar (0.1 μs timing precision). *(c)* All planets removed, the residuals from a millisecond pulsar (defined as above) reveal the presence of Ceres, the largest asteroid.

III Methods of pulsar planet detection

Practical methods of detection of the TOA variations caused by orbiting planets include direct fits of Keplerian and real orbits (e.g., Thorsett & Phillips 1992; Wolszczan 1994; Lazio & Cordes 1995) and model-independent frequency domain approaches based on Fourier transform techniques (Konacki & Maciejewski 1996; Bell et al. 1997). In fact, it appears that it is best to search for periodicities in TOAs (or residuals) by examining periodograms of the data and then refine the search by fitting orbits in time domain using the initial orbital parameters derived from frequency domain analysis. The Lomb-Scargle algorithm (Lomb 1976; Scargle 1982) provides an efficient way to compute spectra of unevenly spaced data.

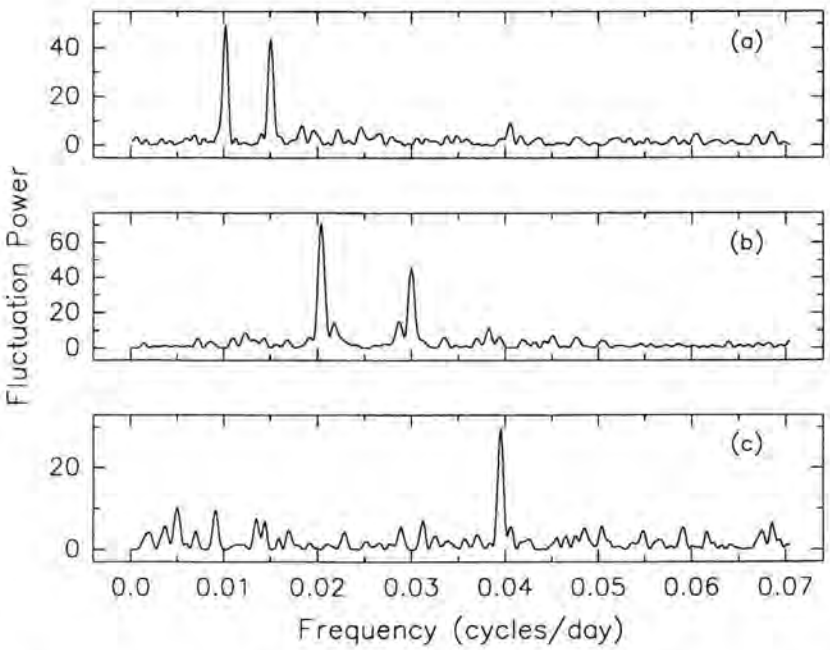

Figure 2. An example of the frequency domain analysis of pulse arrival times from the planet pulsar, PSR B1257+12, observed with the Arecibo telescope at 430 MHz. *(a)* A periodogram of the original TOA set, the two spectral peaks correspond to the orbits of planets B and C. *(b)* A periodogram of TOA variations with the fundamental frequencies of planets B and C removed, the peaks are first harmonics due to non-zero eccentricities of the orbits. *(c)* The fundamental frequencies and their first harmonics removed, a periodicity due to planet A becomes clearly visible (courtesy of M. Konacki).

This combination of methods has been successfully applied by Wolszczan & Frail (1992) and Wolszczan (1994) to detect planets around PSR B1257+12. Further refinements include a promising implementation of the frequency domain analysis in which contributions from any periodic TOA variations are successively subtracted from the data to reveal lower level fluctuations (Konacki & Maciejewski 1996; Figure 2).

IV Planets around PSR B1257+12

A 6.2 millisecond pulsar, PSR B1257+12, was discovered in 1990 during a pulsar search conducted with the 305 m Arecibo radiotelescope (Wolszczan 1991). The analysis of the follow-up timing observations of this pulsar has led to a detection of the first extrasolar planetary system (Wolszczan & Frail 1992) later confirmed by a detection of planetary perturbations between planets B and C (Wolszczan 1994). The

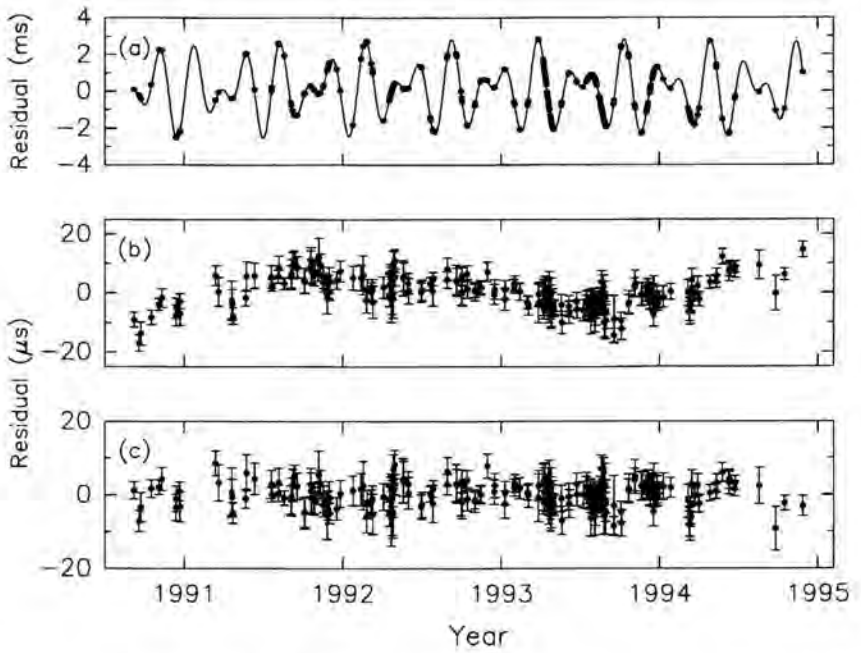

Figure 3. Timing residuals for PSR B1257+12 at 430 MHz. *(a)* A fit for the spin parameters and astrometric parameters only. *(b)* A fit including standard pulsar parameters, three planets and perturbations between planets B and C. *(c)* A fit with the second period derivative taken into account.

system consists of three planet-mass bodies, A, B, and C, with orbital characteristics listed in Table 1. Timing residuals due to planets B and C are shown in Figure 3a (planet A is not discernible on this scale).

Residuals from the least-squares fit of a model including the spin parameters and astrometric parameters of the pulsar, three orbits, and planetary perturbations are shown in Figure 3b. Clearly, the three-planet timing model for PSR B1257+12 requires a fit for a second-order derivative of the pulsar spin period, $\ddot{P}$, to remove unmodeled slow variations in the timing residuals (Figure 3c). A very intriguing possibility is that the observed $\ddot{P}$ is due to a dynamical influence of a distant, long-period fourth planet in the pulsar system (Wolszczan 1996).

As discussed in detail by Joshi & Rasio (1997), one can establish analytical relationships between the measured pulsar spin frequency derivatives and orbital elements of an outer planet, and use them to constrain its orbit in a straightforward manner. For PSR B1257+12, numerical values of the spin frequency and its first three derivatives are: $f = 160.8$ Hz, $\dot{f} = -8.6 \times 10^{-16}$, $\ddot{f} = (-1.25 \pm 0.05) \times 10^{-25}$, and $\dddot{f} = (1.1 \pm 0.3) \times 10^{-33}$, respectively.

Table 1: Parameters of the PSR B1257+12 planetary system.

	A	B	C
Keplerian orbital parameters			
Semi-major axis (light-ms)	0.0035(6)	1.3106(6)	1.4121(6)
Eccentricity	0.0	0.0182(9)	0.0264(9)
Epoch of periastron (JD)	2448754.3(7)	2448770.3(6)	2448784.4(6)
Orbital period (s)	2189645(4000)	5748713(90)	8486447(180)
Longitude of periastron (deg)	0.0	249(3)	106(2)
Parameters of the planetary system			
Planet mass ($M_\oplus$)	$0.015/\sin i_1$	$3.4/\sin i_2$	$2.8/\sin i_3$
Distance from the pulsar (AU)	0.19	0.36	0.47
Orbital period (days)	25.34	66.54	98.22

With the pulsar mass of 1.35 $M_\odot$, and the assumption that the observed $\dot{f}$ is dominated by the effect of orbital acceleration, these values of spin parameters give a planet in a $\sim$ 170 year orbit, with the orbital radius of $\sim$ 35 AU and the planetary mass of $\sim$ 95 $M_\oplus$, which would be a Saturn-mass object at a Pluto-like distance from the pulsar. Obviously, smaller acceleration contributions to $\dot{f}$ will lead to correspondingly different planetary masses and orbital elements. For example, a hypothetical fourth planet could have a low, Mars-like mass and orbit the pulsar at $\sim$ 9 AU (Joshi & Rasio 1997).

Another type of microsecond-level variability in the timing residuals of PSR B1257+12 is related to gravitational perturbations between planets B and C (e.g., Rasio et al. 1993; Malhotra 1993; Peale 1993). The detection of this effect in the timing residuals of PSR B1257+12 (Wolszczan 1994) has provided a final proof that the pulsar is indeed orbited by at least two planetary companions. The best-fit perturbation model constrains the minimum pulsar mass to be $\sim$ 1.2 $M_\odot$ and it implies that the masses of planets B and C must be similar to their respective "canonical", Earth-like values of 3.4 $M_\oplus$ and 2.8 $M_\oplus$ (Tab. 1). Another related dynamical constraint provided by the perturbation analysis is that inclinations of the planetary orbits are unlikely to be less than 60° for any reasonable choice of a neutron star mass.

V Planets around other pulsars

The discovery of planets around PSR B1257+12 has stimulated further searches for planetary companions to other neutron stars observable as radio pulsars. In addition to pulse timing measurements which allow a detection of isolated orbiting bodies, there

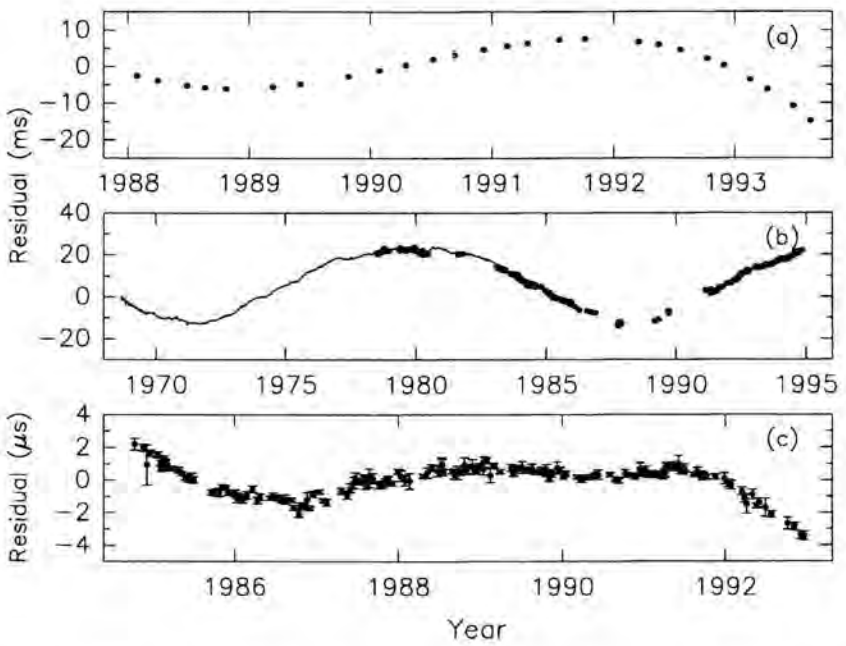

Figure 4. Long-term variations of pulse timing residuals for three pulsars. *(a)* PSR B1620−26 (courtesy of D. Backer), *(b)* combined JPL data (solid line) and Pushchino data (filled circles) for PSR B0329+54 (courtesy of V. Shabanova), and *(c)* PSR B1937+21 (Princeton public-access data base).

have been several attempts to make direct observations of possible debris disks around nearby pulsars (e.g., Zuckerman 1993; Phillips & Chandler 1993).

It is important to emphasize that there are a number of phenomena related to physics of the neutron star interiors and magnetospheres, the interstellar propagation, and the Solar System dynamics, which can affect pulse arrival times and are capable of mimicking planetary signatures in the timing residuals. In particular, a "timing noise" due to seismology of a neutron star and a precession-induced wobble of its rotation axis may lead to quasiperiodic TOA variations (see Cordes 1993 for an extensive review).

At the time of this writing, the best candidate for another planet pulsar is PSR B1620−26, the 11 ms pulsar in a 191 day neutron star-white dwarf binary system located in the globular cluster M4 (Arzoumanian et al. 1996, and references therein; Thorsett & Arzoumanian, these proceedings). The timing residuals for this pulsars (Figure 4a) show a deterministic, non-linear behavior that is most naturally accounted for by the presence of another orbiting mass around the inner binary. Arzoumanian et al. (1996) and Joshi and Rasio (1997) make a compelling case for a substellar (10^{-3}–10^{-2} $M_\odot$) companion, but they also demonstrate that a stellar mass object cannot be entirely ruled out.

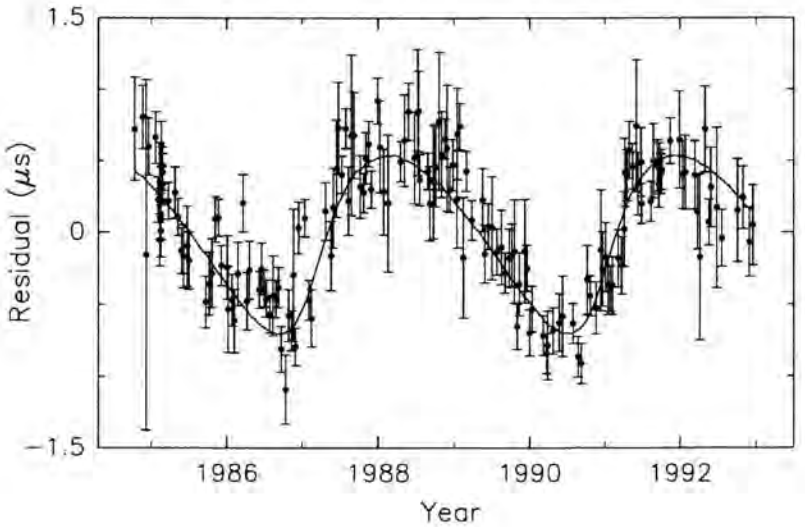

Figure 5. Timing residuals for PSR B1937+21 after subtraction of the standard model including the second order period derivative, $\ddot{P}$ (filled circles). The residual variation expected from a Ceres-mass asteroid in a 3.8 yr, 2.71 AU, eccentric orbit around the pulsar is denoted with the solid line (reproduced after Fukushima (1995), using the Princeton public-access data base).

A case for a terrestrial-mass planet around a relatively young, "slow" pulsar, PSR B0329+54, has been recently made by Shabanova (1995). Curiously, the first suggestion that this object can have a planetary companion has appeared as early as 1979. It was based on the detection of a $\sim$ 3 year periodicity in the timing residuals of the pulsar (Demiański & Prószynski 1979) later confirmed by Bailes, Lyne, & Shemar (1993). Shabanova's analysis suggests that the 3 year periodicity of residuals has practically disintegrated after 3–4 cycles, and that the data collected until 1995 are best explained in terms of a $\sim 2\ M_{\oplus}$ planet in a 17 year, eccentric orbit around the pulsar (Figure 4b). Of course, in view of a distinct possibility that other effects, most notably a timing noise, can contribute to the observed TOA behavior of PSR B0329+54, further long-term observations are necessary to either confirm or dismiss this intriguing case.

Another millisecond pulsar which has been considered as a possible candidate for planetary companions is the 1.57 ms pulsar, PSR B1937+21. This apparently isolated object has been shown by Kaspi, Taylor, & Ryba (1994) to exhibit microsecond-level, long-term TOA fluctuations (Figure 4c). In an unpublished analysis, Fukushima

(1995) has demonstrated that it is possible to remove these fluctuations by including a second-order period derivative and a 3.8 yr, eccentric orbit of a Ceres-mass asteroid in the timing model of this pulsar. To illustrate Fukushima's model, its reconstruction is shown in Figure 5. As in the case of PSR B0329+54 discussed above, a verification of this model will require many more TOA measurements and a much longer data span.

VI Discussion

At present, among more than thirty known millisecond pulsars, there are eight solitary objects that have either managed to dispose of their binary stellar companions, or they have been created without the aid of binary evolution (Bailes et al. 1997). If a missing stellar companion to the pulsar indicates a possibility of "leftover" planets around it, PSR B1257+12 remains the only confirmed case. Clearly, the pulsar planet formation is a low-efficiency process, but the available statistics are still insufficient to reliably constrain it.

The observed characteristics of PSR B1257+12 and its planets, when confronted with standard ideas concerning planetary formation (Levy 1993; Ruden 1993) and the origin and evolution of millisecond pulsars (Phinney & Kulkarni 1994), indicate that the planets have probably evolved in a circumpulsar disk of matter created from the remains of the pulsar's binary stellar companion. In addition, there is a large body of over 700 younger, "slow" pulsars, some of which may have retained planets of their parent stars (Thorsett & Dewey 1993).

Most of the scenarios of the millisecond pulsar planet formation concern themselves with possible ways to transform a fraction of the companion's mass into a protoplanetary disk, implying that the planets would subsequently form in a manner similar to that envisioned for the origin of planetary systems around normal stars (Podsiadlowski 1993; Phinney & Hansen 1993). One such scenario envisions that pulsar planets could be created as a by-product of a white dwarf merger which may produce a rapidly rotating neutron star and a suitable debris disk (Livio, Pringle & Saffer 1992). Another interesting alternative, described by Phinney & Hansen (1993), postulates a stellar companion disruption triggered by a close encounter with the pulsar formed in an asymmetric supernova explosion. This mechanism could produce a high-velocity single neutron star with a planetary system created from the remnants of the former binary companion. In this context, it is conceivable that the exceptionally high proper motion of PSR B1257+12 ($\sim$ 300 km s^{-1}) and the fact that this pulsar has planets are actually related.

One possible consequence of the existence of pulsar planets is that asteroid belts around neutron stars, if sufficiently common, may become a serious limiting factor of the pulse timing precision at submicrosecond levels. However, it is much more exciting to speculate that, even though the planetary systems around solar-type stars and pulsars are very likely to differ in their physical and chemical characteristics, the

fundamental features of their dynamics should be similar. This possibility alone makes further searches for neutron star planets and the detailed studies of their dynamics with the pulse timing technique an important branch of astronomy of the extrasolar planets.

Acknowledgements

This research was supported by NASA under grant NAGW-3405 and by the NSF under grant AST-9317757.

References

Arzoumanian, A. et al. 1996, in Pulsars: Problems and Progress, IAU Coll. 160, ed. S. Johnston, M.A. Walker & M. Bailes (San Francisco: ASP), 525
Bailes, M., Lyne, A.G. & Shemar, S.L. 1993, in Planets around Pulsars, ed. J.A. Phillips, S.E. Thorsett & S.R. Kulkarni (San Francisco: ASP), 19
Bailes, M. et al. 1997, ApJ, 481, 386
Bell, J.F. et al. 1997, MNRAS, 286, 463
Blandford, R.D., 1992, Phil. Trans. R. Soc. Lond. A, 341, 177
Bos, A.P., 1996, Physics Today, 49, 32
Butler, R.P. et al. 1996, PASP, 108, 500
Cordes, J.M. 1993, in Planets around Pulsars, ed. J.A. Phillips, S.E. Thorsett & S. R. Kulkarni (San Francisco: ASP), 43
Demiański, M. & Prószyński, M. 1979, Nature, 282, 383
Joshi, K.J. & Rasio, F.A. 1997, ApJ, 479, 948
Kaspi, V.M., Taylor, J.H. & Ryba, M. 1994, ApJ, 428, 713
Konacki, M. & Maciejewski, A.J. 1996, Icarus, 122, 347
Lazio, T.J.W. & Cordes, J.M. 1995, Mercury, March/April, 23
Levy, E.H. 1993, in Planets around Pulsars, ed. J.A. Phillips, S.E. Thorsett & S.R. Kulkarni (San Francisco: ASP), 181
Livio, M., Pringle, J.E. & Saffer, R.A. 1992, MNRAS, 257, 15P
Lomb, N.R. 1976, Ap&SS, 39, 447
Malhotra, R. 1993, ApJ, 407, 266
Marcy, G.W. & Butler, R.P. 1996, ApJ, 464, L147
Mayor, M. & Queloz, D. 1995, Nature, 378, 355
Peale, S.J. 1993, AJ, 105, 1562
Phillips, J.A. & Chandler, C.J. 1993, ApJ, 420, L83
Phinney, E.S. & Hansen, B.M.S. 1993, in Planets around Pulsars, ed. J.A. Phillips, S.E. Thorsett & S.R. Kulkarni, (San Francisco: ASP), 371
Phinney, E.S. & Kulkarni, S.R. 1994, ARA&A, 32, 591
Podsiadlowski, P. 1993, in Planets around Pulsars, ed. J.A. Phillips, S.E. Thorsett & S.R. Kulkarni (San Francisco: ASP), 149
Rasio, F.A. et al. 1993, in Planets around Pulsars, ed. J.A. Phillips, S.E. Thorsett &

S.R. Kulkarni, (San Francisco: ASP), 107
Ruden, S.P. 1993, in Planets around Pulsars, ed. J.A. Phillips, S.E. Thorsett & S.R. Kulkarni, (San Francisco: ASP), 197
Scargle, J.D. 1982, ApJ, 263, 835
Shabanova, T.W. 1995, ApJ, 453, 779
Thorsett, S.E. & Dewey, R.J. 1993, ApJ, 419, L65
Thorsett, S.E. & Phillips, J.A. 1992, ApJ, 387, L69
Wolszczan, A. 1991, Nature, 350, 688
Wolszczan, A. & Frail, D.A. 1992, Nature, 355. 145
Wolszczan, A. 1994, Science, 264, 538
Wolszczan, A. 1996, in Pulsars: Problems and Progress, IAU Coll. 160, ed. S. Johnston, M.A. Walker & M. Bailes (San Francisco: ASP), 91
Zuckerman, B. 1993, in Planets around Pulsars, ed. J.A. Phillips, S.E. Thorsett & S.R. Kulkarni (San Francisco: ASP), 303

Authors' Address

The Pennsylvania State University, Department of Astronomy & Astrophysics, 525 Davey Laboratory, University Park, PA 16802, USA

Part III:

Searches

F. Camilo

Pulsar Searches in the Northern Hemisphere

Abstract

We summarize the main parameters of all searches for radio pulsars known to us carried out in the northern hemisphere since about 1990, including searches of supernova remnants (SNRs), OB runaway stars, γ- and X-ray error boxes, and compact radio sources, in addition to undirected "all-sky" surveys. We also tabulate some parameters of the 47 binary and recycled pulsars known in the disk of the Galaxy.

I Introduction

One of two general approaches may be adopted in deciding where to search for pulsars: if we believe we know where pulsars are located (e.g., in SNRs, near their birthplaces), we may carry out *directed searches* of the appropriate targets; alternatively we may search "blindly" over large areas of sky, carrying out *undirected searches*. Both approaches have yielded exciting discoveries, such as that of PSR B1937+21, the first millisecond pulsar (Backer et al. 1982), and that of PSR B1913+16, the first binary pulsar (Hulse & Taylor 1975), respectively.

In the tables that follow we include the radio frequency used in each search, the sampling interval used (the minimum detectable pulse period is at least $2\,T_{\rm samp}$), the time spent pointing in each direction, and the minimum flux density detectable in the search. This quantity, $S_{\rm min}$, is usually appropriate only for long period pulsars observed at the telescope beam center and in directions where the sky temperature is as low as it can be within the search area. For a fuller discussion of sensitivity issues see, e.g., Camilo, Nice & Taylor (1996).

II Directed Searches

The *supernova remnant* searches summarized in Table 1 have not discovered many associated pulsars, but it is not easy to infer how many SNRs actually have associated pulsars: many remnants are large and have not been fully surveyed, the high remnant

Table 1: Directed Searches

Telescope	Number of Targets	Frequency (MHz)	$T_{\rm samp}$ (ms)	$T_{\rm int}$ (min)	$S_{\rm min}$ (mJy)	Pulsars Found
		Supernova Remnants				
Arecibo	18[a]	430/1420	0.5–1.0	30–90	0.2–1.0	0
Arecibo	10	1400	0.5	5	> 0.2	1[b]
Jodrell Bank[c]	33	606	1.0	$\simeq 35$	> 2	2
		OB Runaway Stars				
VLA	44	1400[d]	2.6	12	0.2	0
NRAO 140′	40	575/770	1.0	72	1	1[e]
		EGRET (γ-ray) Error Boxes				
Arecibo	7	430	0.2	3	0.2	1[f]
NRAO 140′	27[g]	370/770/1390	0.5–2.0	36–143	0.4–3.6	0
		Einstein (X-ray) IPC Sources				
Arecibo	1300[h]	430	0.2	3.1	> 0.2	3[i]
		Steep Spectrum Compact Radio Sources				
WSRT	1[j]	325/410	$\simeq 0.2$	$\simeq 30$	$\simeq 1$	1[k]

[a] Many only partially surveyed (Gorham et al. 1996).

[b] PSR B1853+01 in W44 (Wolszczan, Cordes & Dewey 1991).

[c] See contribution by Lorimer et al. in these proceedings.

[d] Also used maps made at 5 GHz (Philp et al. 1996).

[e] Pulsar unrelated to OB star (Sayer, Nice & Kaspi 1996).

[f] Millisecond pulsar J0751+1807 unrelated to EGRET source (Lundgren, Zepka & Cordes 1995).

[g] 19 sources are in the second EGRET catalog (Nice & Sayer 1997).

[h] Total area surveyed $\simeq 27$ deg^2 (Zepka et al. 1996).

[i] One young pulsar, J0631+1036, possibly related to X-ray source.

[j] Linear polarization of $\sim 40\%$, spectral index of ~ -3 (WENS survey continuing; Kouwenhoven et al., in prep.).

[k] Pulsations from the millisecond pulsar J0218+4232 detected at Jodrell Bank (Navarro et al. 1995).

temperatures are non-uniform resulting in highly variable $S_{\rm min}$, pulsars with high velocity can escape the remnant boundaries, and many SNR properties (such as distance and age) are poorly constrained. For a survey of southern SNRs with the Parkes telescope see Kaspi et al. (1996), and see Kaspi (1996) for a discussion of pulsar/SNR associations.

OB runaway stars are thought to acquire their high velocities when their binary companions explode in SNe. If some of the newly-formed neutron stars remain bound, and the radio emission is not quenched in the winds of the OB stars, one may detect pulsars in these systems. None have been found to date, placing constraints on the binary survival fraction (see references from Tab. 1).

All identified Galactic γ-ray point sources are pulsars. There are some 40 unidentified unresolved sources detected by the *EGRET* instrument. Searches of some of these have proven unfruitful to date (Tab. 1), somewhat constraining models of the γ-ray source population (see references).

Some young radio pulsars emit substantial amounts of X-rays, making *unidentified X-ray sources* intriguing targets for the search of this distinctive class of pulsars. A recent search used a new algorithm for identifying X-ray sources, and surveyed 2/3 of those visible from Arecibo (Tab. 1).

Pulsars are virtually the only *steep spectrum compact radio sources* with high degrees of linear polarization. Follow-up work on one such source resulted in the discovery of PSR J0218+4232 (see Tab. 1), mimicking in several aspects the discovery of PSR B1937+21. Curiously these two are among the most luminous and have the largest period derivatives, $\dot{P}$, of any millisecond pulsars.

Other projects have included the search for radio pulsations from the γ-ray pulsar Geminga (Arecibo); the search of several Be/X-ray transients (Jodrell Bank); follow-up of compact, polarized candidates from the 21 cm Northern VLA Sky Survey (Green Bank); and a search of $\sim$ 150 low-mass white dwarfs that must have evolved in binary systems (Jodrell Bank & Parkes). No positive results have been reported, with some projects continuing.

III Undirected Searches

While most large-area pulsar surveys have been conducted at low radio frequencies, surveying the Galactic plane can be done to great advantage at high frequencies, reducing the deleterious effects of dispersion and scattering. Two very successful surveys at 1400 MHz were carried out in the late 1980s at Jodrell Bank and Parkes (Clifton et al. 1992; Johnston et al. 1992a). The *Effelsberg* high-frequency survey of the Galactic center region aims to detect pulsars that are severely scatter-broadened even at 1400 MHz. Such surveys, and those using a large telescope like *Arecibo* at high frequencies, have very small rates of sky coverage (see Table 2).

The "piggyback" survey searched most of the sky visible from *Arecibo* several times by using the 430 MHz feed slaved to the 1400 MHz feed being used to track sources in other programs (Tab. 2).

Table 2: Undirected Searches

Telescope	Search Area	Frequency (MHz)	$T_{\rm samp}$ (ms)	$T_{\rm int}$ (sec)	$S_{\rm min}$ (mJy)	Pulsars Found
		Assorted Searches				
Effelsberg	$\|b\| < 0.5°, \|l\| < 0.5°$	4850	0.5	540	0.2	0[a]
Arecibo	1 deg^2 at $b = 0°$	1400	0.25	300	0.2	1[b]
Arecibo	$-1° < \delta < +39°$	430	0.3	10	> 1	...[c]
		All-Sky Surveys for Millisecond Pulsars				
Jodrell Bank	$\delta > +35°$	408	0.3	314	3	1[d]
Green Bank	$\delta > +0°$	370	0.256	134	8	8[e]
Cambridge[f]	$\delta > -20°$	81.5	0.768	100–400	> 200	0
Bologna	$\delta > +0°$	408	0.064	67	9	0[g]

[a] About 25% of search area covered to date (Kramer et al., in preparation).

[b] $l \simeq 50°$, DM $= 400\,{\rm cm}^{-3}$ pc (Wolszczan).

[c] Piggyback survey: 8 known pulsars detected; about 400 candidates to reobserve (Cordes & Backer, in preparation).

[d] 4,000 deg^2 searched so far (Nicastro et al. 1995).

[e] Relativistic binary PSR J1518+4904 discovered (see Nice, these proceedings). $15,900 + 1,500$ deg^2 searched and 76 known pulsars detected (Sayer, Nice & Taylor 1997).

[f] 30,300 deg^2 searched. $S_{\rm min}$ varies *greatly* as a function of δ. 20 known pulsars detected (Shrauner 1996).

[g] 1,100 deg^2 searched so far (D'Amico).

By far the most successful pulsar searches in the 1990s have been the large-area surveys for millisecond pulsars. Those summarized in Tab. 2 aim to cover about 2π sr in a relatively short period of time, sometimes with unusual parameters like very low radio frequency or very fast sampling rate.

The Arecibo surveys (Table 3) have discovered nearly half of all disk millisecond pulsars known. They are complementary to the very successful survey of the southern sky at the Parkes telescope that discovered 17 millisecond pulsars (Manchester et al. 1996; Lyne et al. 1997; see also Manchester, these proceedings): they are more sensitive (the numbers of pulsars found in the two surveys are comparable, while the area covered so far at Arecibo is 1/4 that at Parkes), but proceed more slowly. Several groups carry out the surveys at Arecibo; at present each of five groups is assigned eight disjoint 1°-wide declination strips with central declinations given in Tab. 3. After a long hiatus caused by a telescope upgrade, the searches will soon resume, with a four-fold improvement in frequency- and time-resolution that will increase sensitivity to the shortest-period pulsars. (For a more complete review of millisecond pulsar surveys see Camilo 1996.)

Table 3: Arecibo Millisecond Pulsar Surveys*

Group	Search Area	New Pulsars (MSP/Total)
Princeton	$\|b\| < 8°$ (260 deg^2)	2/24[a†]
	$21^h < \alpha < 02^h$ (680)	4/12[b]
	$\delta = (0.5 + 5n)°$ (1428)	2/21[c]
Penn State/NRL[d]	$13^h < \alpha < 18^h$(828)	4/17 †
	$\delta = (3.5 + 5n)°$ (527)	1/2
Caltech[e]	$08^h < \alpha < 13^h$ (360)	0/2
	$\delta = (2.5 + 5n)°$ (600)	1/12
CIT/PSU/UCB[f†]	$01^h < \alpha < 09^h$ (448)	0/0
STScI/Arecibo	$\delta = (1.5 + 5n)°$ (500)	1[g]/9
Arecibo Total	5,630 deg^2	15/99[h]

*Frequency = 430 MHz, $T_{samp} = 250\ \mu$s, $T_{int} = 33$ s, $S_{min} > 0.5$ mJy; $2 \times 32 \times 250$ kHz filterbank used.

†Higher-frequency-resolution correlator used for at least a portion of the survey.

[a] Nice, Fruchter & Taylor 1995.

[b] Camilo, Nice & Taylor 1996.

[c] Camilo et al. 1996.

[d] 230 deg^2 searched with high-time-resolution PSPM (Foster et al. 1995).

[e] Ray et al. 1996.

[f] $8 < T_{int} < 67$ s (Ray et al. 1995).

[g] PSR J0418+16 ($P = 25.7$ ms; Fruchter et al., in preparation).

[h] About 5,000 deg^2 of Arecibo sky uniquely searched. The 15 "MSP" include PSRs B1534+12 and J2235+1506.

Table 4 lists some parameters for all binary and recycled pulsars known in the disk of the Galaxy. Here we regard isolated pulsars as recycled if they have periods $P < 60$ ms and low surface magnetic field strengths, as inferred from their $\dot{P}$. We list observed $\dot{P}$s, although these differ significantly from the intrinsic ones for many millisecond pulsars (Camilo, Thorsett & Kulkarni 1994). The companion masses, m_2, are derived from the pulsar mass function for an assumed pulsar mass of 1.4 $M_\odot$ and "median" inclination angle of $i = 60°$, with the exception of PSRs B1855+09, B1534+12, and B1913+16, for which they are measured with the help of relativistic orbital effects, and PSR J0045−7319, from optical measurements (Bell et al. 1995b). Distances are obtained from the dispersion measure and the Taylor & Cordes (1993) model. Thirty-four of the 47 pulsars listed were discovered in the last 6 years in the surveys summarized in this paper and in the Parkes southern sky survey. For these pulsars we provide the discovery reference and the most up-to-date source of parameters, if different.

Table 4: Parameters of binary and recycled pulsars known in the disk of the Galaxy.

PSR	P (ms)	$\dot{P}$ (10^{-18})	P_b (d)	$a_1 \sin i/c$ (s)	e	m_2 ($M_\odot$)	d (kpc)	$\lvert z \rvert$ (kpc)	Refs.*
Circular Orbit Pulsars ($e \lesssim 0.01$)									
J0034−0534	1.88	0.0051	1.589	1.438	<0.00002	0.17	1.0	0.9	[3,8]
J0218+4232	2.32	0.08	2.029	1.984	<0.00002	0.20	>5.8	>1.8	[22]
J0437−4715	5.76	0.057	5.741	3.367	0.000019	0.17	0.1	0.1	[14,6]
J0613−0200	3.06	0.0096	1.199	1.091	<0.00002	0.15	2.2	0.4	[19,5]
J0621+1002	28.85	0.04	8.319	12.032	0.0025	0.54	1.9	0.1	[9,†]
J0751+1807	3.48	0.008	0.263	0.397	<0.0001	0.15	2.0	0.8	[20]
J1012+5307	5.26	0.015	0.605	0.582	<0.00002	0.13	0.5	0.4	[23,17]
J1022+1001	16.45	0.04	7.805	16.765	0.000098	0.87	0.6	0.5	[9]
J1045−4509	7.47	0.017	4.084	3.015	0.000024	0.19	3.3	0.7	[3,5]
J1455−3330	7.99	0.024	76.175	32.362	0.00017	0.30	0.7	0.3	[19,8]
J1603−7202	14.84	0.014	6.309	6.881	<0.00002	0.33	1.6	0.4	[18]
J1640+2224	3.16	<0.003	175.461	55.330	0.00080	0.30	1.1	0.7	[12]
J1643−1224	4.62	0.018	147.017	25.073	0.00051	0.14	>4.9	>1.8	[19,5]
J1709+23	4.63						1.9	1.0	[12]
J1713+0747	4.57	0.0085	67.825	32.342	0.000075	0.33	0.9	0.4	[13,7]
J1804−2717	9.34	0.042	11.129	7.281	0.000035	0.24	1.2	0.1	[18]
B1855+09	5.36	0.018	12.327	9.231	0.000022	0.26	1.0	0.1	[16]
J1911−1114	3.63	0.013	2.717	1.763	<0.00001	0.14	1.6	0.3	[18]
B1953+29	6.13	0.030	117.349	31.413	0.00033	0.21	5.4	0.0	[29]
B1957+20	1.61	0.017	0.382	0.0892	<0.00004	0.03	1.5	0.1	[2]
J2019+2425	3.93	0.0070	76.512	38.768	0.00011	0.37	0.9	0.1	[26,25]
J2033+1734	5.95	0.011	56.308	20.163	0.00013	0.22	1.4	0.3	[27,‡]
J2051−0827	4.51	0.013	0.099	0.045	<0.0003	0.03	1.3	0.6	[28]
J2129−5721	3.73	0.020	6.625	3.501	<0.00002	0.16	>2.6	>1.8	[18]
J2145−0750	16.05	0.030	6.839	10.164	0.000019	0.51	0.5	0.3	[3,8]
J2229+2643	2.98	0.0019	93.016	18.913	0.00025	0.15	1.4	0.6	[11]
J2317+1439	3.45	0.0024	2.459	2.314	0.000001	0.21	1.9	1.3	[10,11]
B0655+64	195.67	0.69	1.029	4.126	<0.00003	0.81	0.5	0.2	[1]
B0820+02	864.87	104.3	1232.395	162.145	0.012	0.23	1.4	0.5	[1]
J1803−2712	334.42	17.3	406.781	58.940	0.00051	0.17	3.6	0.2	[29]
B1831−00	520.95	10.7	1.811	0.723	<0.004	0.08	2.6	0.2	[1]
Other Binary Pulsars ($e \gtrsim 0.25$)									
J0045−7319	926.28	4486.	51.169	174.254	0.808	8.8	57.		[15]
B1259−63	47.76	2280.	1236.81	1296.00	0.870	4.19	4.6	0.1	[21]
J1518+4904	40.93	0.027	8.634	20.044	0.249	1.01	0.7	0.6	[24]
B1534+12	37.90	2.43	0.421	3.729	0.274	1.34	0.7	0.5	[30,1]
B1820−11	279.83	1376.	357.762	200.673	0.795	0.80	6.3	0.1	[1]
B1913+16	59.03	8.63	0.323	2.342	0.617	1.39	7.1	0.3	[29]
B2303+46	1066.37	569.1	12.340	32.688	0.658	1.46	4.2	0.9	[1]

Table 4: *(cont.)*

PSR	P (ms)	$\dot{P}$ (10^{-18})	P_b (d)	$a_1 \sin i/c$ (s)	e	m_2 ($M_\odot$)	d (kpc)	$\lvert z \rvert$ (kpc)	Refs.*
Other Recycled Pulsars									
J0711−6830	5.49	0.015	Isolated				1.0	0.4	[4]
J1024−0719	5.16	0.018	Isolated				0.3	0.2	[4]
B1257+12	6.22	0.11	Planets				0.6	0.6	[32,31]
J1730−2304	8.12	0.020	Isolated				0.5	0.1	[19,8]
J1744−1134	4.07	0.0086	Isolated				0.2	0.0	[4]
B1937+21	1.56	0.11	Isolated				3.6	0.0	[16]
J2124−3358	4.93	0.021	Isolated				0.2	0.2	[4]
J2235+1506	59.77	0.16	Isolated				1.2	0.7	[10,11]
J2322+2057	4.81	0.0097	Isolated				0.8	0.5	[26,25]

* Reference keys are decoded in the **References** section.
† $\dot{P}$ unpublished (author).
‡ Updated parameters obtained from Nice & Thorsett (private communication).

Of the 35 millisecond pulsars in Tab. 4 (5% of all known pulsars), 22 (3/5) are in nearly circular orbits with companions of mass $0.15 \lesssim m_2 \lesssim 0.45$ $M_\odot$, presumably helium white dwarfs. Seven (1/5) are isolated objects. Three have intermediate-mass companions ($m_2 \geq 0.45$ $M_\odot$), probably carbon-oxygen white dwarfs, 2 are in eclipsing systems with companions of very low mass ($m_2 \lesssim 0.05$ $M_\odot$), and one has at least three planetary-mass companions. It is not clear how the evolutionary histories of all these systems relate to each other.

Acknowledgements

I thank Ed van den Heuvel and the organizers of the Colloquium for a wonderful meeting, and David Nice and Joe Taylor for all the shared fun of the last few years searching for pulsars.

References

Arzoumanian, Z. 1995, Ph.D. Thesis, Princeton Univ. [1]
Arzoumanian, Z., Fruchter, A.S. & Taylor, J.H. 1994, ApJ, 426, L85 [2]
Backer, D.C. et al. 1982, Nature, 300, 615
Bailes, M. et al. 1994, ApJ, 425, L41 [3]
Bailes, M. et al. 1997, ApJ, 481, 386 [4]
Bell, J.F. et al. 1997, MNRAS, 286, 463 [5]
Bell, J.F. et al. 1995a, ApJ, 440, L81 [6]
Bell, J.F. et al. 1995b, ApJ, 447, L117

Camilo, F. 1996, in High Sensitivity Radio Astronomy, ed. N. Jackson & R.J. Davis (Cambridge: Cambridge Univ. Press), 14
Camilo, F., Foster, R.S. & Wolszczan, A. 1994, ApJ, 437, L39 [7]
Camilo, F. et al. 1997, ApJ, in preparation [8]
Camilo, F. et al. 1996, ApJ, 469, 819 [9]
Camilo, F., Nice, D.J. & Taylor, J.H. 1993, ApJ, 412, L37 [10]
Camilo, F., Nice, D.J. & Taylor, J.H. 1996, ApJ, 461, 812 [11]
Camilo, F., Thorsett, S.E. & Kulkarni, S.R. 1994, ApJ, 421, L15
Clifton, T.R. et al. 1992, MNRAS, 254, 177
Foster, R.S. et al. 1995, ApJ, 454, 826 [12]
Foster, R.S., Wolszczan, A. & Camilo, F. 1993, ApJ, 410, L91 [13]
Gorham, P.W. et al. 1996, ApJ, 458, 257
Hulse, R.A. & Taylor, J.H. 1975, ApJ, 195, L51
Johnston, S. et al. 1993, Nature, 361, 613 [14]
Johnston, S. et al. 1992, MNRAS, 255, 401
Kaspi, V.M. 1996, in Pulsars: Problems and Progress, IAU Colloqium 160, ed. S. Johnston, M.A. Walker & M. Bailes (San Francisco: ASP), 375
Kaspi, V.M. et al. 1994, ApJ, 423, L43 [15]
Kaspi, V.M. et al. 1996, Astron. J., 111, 2028
Kaspi, V.M., Taylor, J.H. & Ryba, M. 1994, ApJ, 428, 713 [16]
Lorimer, D.R. et al. 1995a, Nature, 376, 393 [17]
Lorimer, D.R. et al. 1996, MNRAS, 283, 1383 [18]
Lorimer, D.R. et al. 1995b, ApJ, 439, 933 [19]
Lundgren, S.C., Zepka, A.F. & Cordes, J.M. 1995, ApJ, 453, 419 [20]
Lyne, A.G. et al. 1997, MNRAS, 295, 743
Manchester R.N., et al. 1995, ApJ, 445, L137 [21]
Manchester R.N. et al. 1996, MNRAS, 279, 1235
Navarro, J. et al. 1995, ApJ, 455, L55 [22]
Nicastro, L. et al. 1995, MNRAS, 273, L68 [23]
Nice, D.J., Fruchter, A.S. & Taylor, J.H. 1995, ApJ, 449, 156
Nice, D.J. & Sayer, R.W. 1997, ApJ, 476, 261
Nice, D.J., Sayer, R.W. & Taylor, J.H. 1996, ApJ, 466, L87 [24]
Nice, D.J. & Taylor, J.H. 1995, ApJ, 441, 429 [25]
Nice, D.J., Taylor, J.H. & Fruchter, A.S. 1993, ApJ, 402, L49 [26]
Philp, C.J. et al. 1996, Astron. J., 111, 1220
Ray, P.S. et al. 1995, ApJ, 443, 265
Ray, P.S. et al. 1996, ApJ, 470, 1103 [27]
Sayer, R.W., Nice, D.J. & Kaspi, V.M. 1996, ApJ, 461, 357
Sayer, R.W., Nice, D.J. & Taylor, J.H. 1997, ApJ, 474, 426
Shrauner, J.A. 1996, Ph.D.. Thesis, Princeton Univ.
Stappers, B.W. et al. 1996, ApJ, 465, L119 [28]
Taylor, J.H. & Cordes, J.M. 1993, ApJ, 411, 674
Taylor, J.H., Manchester, R.N. & Lyne, A.G. 1993, ApJS, 88, 529 [29]
Wolszczan, A. 1991, Nature, 350, 688 [30]

Wolszczan, A. 1994, Science, 264, 538 [31]
Wolszczan, A., Cordes, J.M. & Dewey, R.J. 1991, ApJ, 372, L99
Wolszczan, A. & Frail, D.A. 1992, Nature, 355, 145 [32]
Zepka, A. et al. 1996, ApJ, 456, 305

Authors' Address

The University of Manchester, NRAL, Jodrell Bank, Macclesfield, Cheshire SK11 9DL, UK; fernando@jb.man.ac.uk

D.R. Lorimer, A.G. Lyne and F. Camilo

A Search for Pulsars in Supernova Remnants

Abstract

We have carried out a sensitive search for young pulsars associated with supernova remnants using the 76-m Lovell radio telescope at Jodrell Bank. The survey was conducted at 606 MHz and targeted 33 remnants in the northern hemisphere. Two pulsars, J0215+6217 and J1957+2833, were discovered during this survey and PSR B1952+29 was redetected. The new pulsars both lie towards the edge of their respective target remnants, G132.7+1.3 and G65.1+0.6. It is presently unclear whether the pulsars and the remnants are genuinely associated.

I Introduction

In the past five years, the number of proposed associations between pulsars and supernova remnants (SNRs) has risen to almost 30. This is a result of a number of different approaches: high frequency searches for young pulsars, cross–correlations of the pulsar and SNR catalogues, targeted searches for pulsars around remnants and for remnants around pulsars. The interested reader is referred to Kaspi (1996) for a recent review. The number of spurious associations in this sample, i.e., those cases where the pulsar and the SNR are merely in chance alignment along the line of sight, is likely to be rather large. Using statistical arguments, Gaensler & Johnston (1995) conclude that, at most, 10 associations are expected to be real.

The motivation for the present survey was to search a large sample of northern hemisphere SNRs with improved sensitivity than previous searches. Our search complements recent targeted searches of southern SNRs at Parkes (Kaspi et al. 1996), of those remnants visible from Arecibo (Gorham et al. 1996) as well as an earlier survey at Jodrell Bank (Biggs & Lyne 1996). In these proceedings, we give only a summary of our results. Complete details of this survey will be published elsewhere (Lorimer et al. 1997, in preparation).

II Observations & Results

All survey observations were made with the 76–m Lovell radio telescope operated by the University of Manchester, Jodrell Bank, on 5 separate observing sessions between 1994 June and 1996 April. We chose 33 SNRs from Green's (1996) catalogue primarily at declinations north of 30 degrees. The observations were made at 606 MHz using a filterbank system with a total bandwidth of 8 MHz and a noise temperature on cold sky of about 50 K. To maintain good sensitivity to rapidly rotating pulsars, incoming signals were sampled every millisecond. For those remnants larger than the telescope beamwidth (0.5 degrees FWHM) we covered the full area of the remnant using several beam positions. Three pulsars were detected by this survey, B1952+29 and two that were previously unknown, PSRs J0215+6217 and J1957+2833 which lie towards the edge of the target SNRs, G132.7+1.3 and G65.1+0.6 respectively.

III Discussion

The evidence that the newly discovered pulsars are associated with their target remnants is not clear. PSR J0215+6217 has a period of 549 ms and a DM of 84 cm^{-3} pc. The distance to this pulsar estimated from its DM and galactic coordinates using the Taylor & Cordes (1993) electron density model is 3.2 ± 1.0 kpc, consistent with the distance to G132.7+1.3 of 3.0 kpc derived from optical measurements (see Green 1996 and references therein). Timing measurements show that the characteristic age of PSR J0215+6217 is 13 Myr. Whilst the age of G132.7+1.3 is rather uncertain, we estimate it to be $\lesssim 3 \times 10^5$ yr, based on its angular size and distance and assuming it to be in a Sedov expansion phase with expansion velocity of 50 km-s^{-1}. If PSR J0215+6217 is associated with G132.7+1.3, we note that the anomalously large characteristic age requires the initial spin period of the pulsar to be similar to its present value.

For the 307 ms pulsar J1957+2833, the case for an association with G65.1+0.6 is even less clear, since there is neither an independent distance estimate to the remnant nor presently a measured period derivative for the pulsar. The size of G65.1+0.6 (~ 1 degree) suggests that it is certainly closer than the distance of 7.0 ± 2.3 kpc inferred from the dispersion measure of PSR J1957+2833 (139 cm^{-3} pc). The, admittedly uncertain, Σ–d relationship suggests that the distance to G65.1+0.6 is ~ 2 kpc.

To ultimately confirm/refute both these candidate associations, measurements of the pulsar proper motions are required in order to determine whether the pulsar velocities are of the correct magnitude and direction to carry them to their presently observed positions with respect to the remnant centers. We have recently begun such measurements using the multi–element radio linked interferometer network operated by the University of Manchester.

Acknowledgements

We thank Christine Jordan and Jon Bell for help with the observations. Both DRL and FC acknowledge financial support from the European Commission in the form of fellowships within the European Pulsar Network.

References

Biggs, J.D. & Lyne, A.G. 1996, MNRAS, 282, 691
Gaensler, B.M. & Johnston, S. 1995, MNRAS, 277, 1243
Gorham, P.W. et al. 1996, ApJ, 458, 257
Green, D.A. 1996. MRAO, Cambridge, UK. (available on the World-Wide-Web at URL `http://www.mras.cam.ac.uk/surveys/snrs/`)
Kaspi, V.M. et al. 1996, AJ, 111, 2028
Kaspi, V.M. 1996, in Pulsars: Problems and Progress, IAU Coll. 160, ed. S. Johnston, M.A. Walker & M. Bailes (San Francisco: ASP), 375
Taylor, J.H. & Cordes, J.M. 1993, ApJ, 411, 674

Authors' Addresses

D.R. Lorimer: Max Planck Institut für Radioastronomie, Auf dem Hügel 69, D–53121 Bonn, Germany

A.G. Lyne and F. Camilo: University of Manchester, NRAL, Jodrell Bank, Macclesfield, Cheshire SK11 9DL, UK

N. D'Amico and L. Burderi

On the Possibility to Probe the Interior Structure of Neutron Stars with a Submillisecond Pulsar-Search Experiment

Abstract

Searches for millisecond pulsars conducted up to now were strongly biased against the detection of periodicities near or below the period value ($\simeq 1.5$ ms) of the original millisecond pulsar PSR B1937+21. This value is remarkably close to the limiting spin period predicted by a "stiff" equation of state of the ultradense neutron matter. On the other hand, other equations of state, such as a "soft" one for neutron matter or one of those describing self-bound states like quark stars, predict a shorter spin period (< 1 ms). In particular the detection of a pulsar with spin period well below 1 ms could put severe constraints on the neutron star structure and on the absolute ground state for the baryon matter in nature. The observational properties of such an object could be such to allow its detectability with the present generation of radiotelescopes, provided that the experiment sensitivity is properly tuned in the ultrashort period range. An experiment specifically designed to probe the critical period range is in progress at the Italian Northern Cross radiotelescope near Bologna. We briefly discuss the capabilities of this experiment and the survey plan.

I The minimum rotational period for a neutron star

A neutron star (NS) is an intrinsic relativistic object, so all the classical quantities must be redefined in an adequate way. Its gravitational mass M is less than its baryon mass $M_{\rm B}$ by an amount equal to the binding energy ($\sim 10\%$), and its radius must be redefined by the circumferential equatorial radius R (i.e., the *proper* circumference in the equatorial plane divided by 2π).

The equation of state of the ultradense matter (ES) determine the NS structure and its behavior under rapid rotation. Depending on the ES adopted, the NS can be a gravitationally-bound (GBound) object in which the ultradense matter is held together by the action of gravity (as in the "classical" neutron matter ES, e.g., those proposed in Cook, Shapiro & Teukolsky 1994), and a self-bound (SBound) object in which the ultradense matter is self confined in a stable state (e.g., the "ground state" for strong interactions claimed by Witten 1985 for the strange quark stars).

A firm lower limit to the rotational period attainable for a spinning neutron star (NS) is set by its capability to resist to centrifugal disruption. Within an accuracy $\leq 20\%$ the so called Roche Model (Shapiro & Teukolsky 1983) allows the determination of this minimum period $P_{\rm K}$. In this model the equatorial radius of the NS inflates under the effect of rapid rotation while most of the mass remain concentrated near the center. The radius increase by 50% of its static value (determined for a given NS mass by the particular ES adopted) for *any* ES. Under these assumptions the classical Keplerian formula holds:

$$P_{\rm K} \approx (M/{\rm M}_\odot)^{-1/2}(R_0^{3/2}/10\,{\rm km})^{3/2} \quad {\rm ms}, \tag{1}$$

where R_0 is the radius of the non-rotating NS. The constant (1.0) in the above formula differs from 0.544 (appropriate for the Keplerian limit of a rigid body) because of the factor $(R(P_{\rm K})/R_0)^{3/2} = (1.5)^{1.5} = 1.84$ determined by the radius inflation. Given a baryon mass different GBound ESs predict different radii for the not spinning equilibrium configuration. The largest radii correspond to the stiffest ESs, the smallest to the softest. It is clear from Eq. (1) that the softest ESs allow the shortest spin periods. With Eq. (1) is possible to set an absolute lower limit against centrifugal disruption under extremely general conditions for the ES of a GBound NS. This limit is valid for *any* ES satisfying only few reasonable restrictions like the non violation of the causality (Glendenning 1992):

$$P_{\rm GBound} \approx 0.06 + 0.20 \times \left(\frac{M}{{\rm M}_\odot}\right) \quad {\rm ms}. \tag{2}$$

For a SBound object such limit does not hold. The firm lower limit is set by the requirement of the stability of the NS respect to the Einstein's Equations of general relativity and by Eq. (1):

$$P_{\rm SBound} \approx 0.167 \times \left(\frac{M}{{\rm M}_\odot}\right) \quad {\rm ms} \tag{3}$$

(Glendenning 1992). These limits are probably underestimates because there is no physical reason that requires that the true ES should minimize the rotational period. Moreover non-axisymmetric instabilities arise in a rapidly rotating fluid spheroid (see, e.g., Friedman & Ipser 1992 for a review). The oscillations induced by these instabilities can radiate angular momentum *via* gravitational radiation, rising the minimum period $P_{\rm min}$. This mechanism is dependent on the particular equation of state (ES) adopted for the NS matter as well as on the NS temperature and viscosity. However for a realistic range of NS temperatures and for several GBound ES the $P_{\rm min}$ limited by the non-axisymmetric instabilities are remarkably close to those determined by the effective centrifugal limit as observed in Burderi & D'Amico (1997). In Figure 1 $P_{\rm min}$ is plotted vs. the NS temperature for one of the softest GBound ES, i.e., the Reid core with hyperons, labeled as B in Cook, Shapiro & Teukolsky (1994), and for one of the stiffest, i.e., the Mean Field, labeled as L. For each ES two values of the NS mass are considered: the canonical 1.4 $\rm M_\odot$ corresponding to the Chandrasekhar limit, and

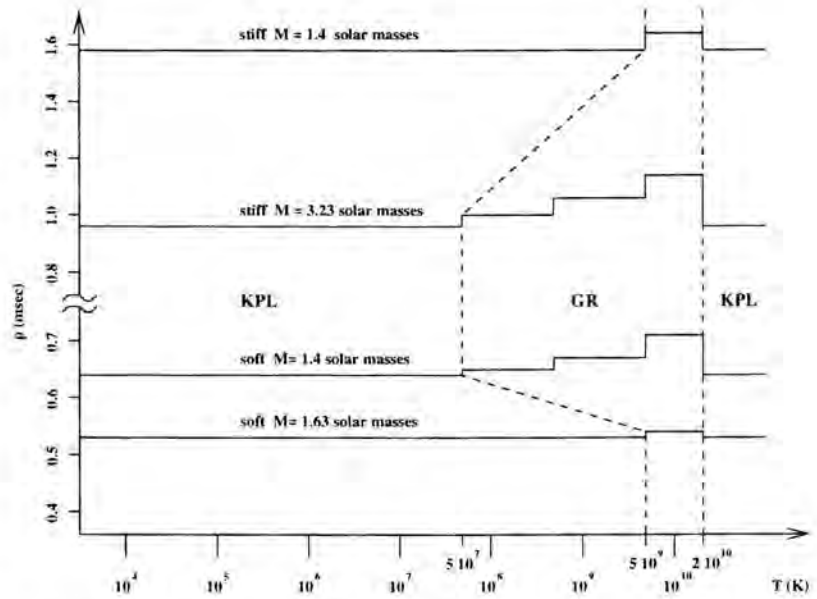

Figure 1. Schematic plot of the shortest possible periods for a rotating NS vs. the NS temperature. The curves labeled as **soft** refer to ES B, the curves labeled as **stiff** refer to ES L. **GR** indicates the zone (delimited by the first and the last dashed line) where the minimum period is determined by the gravitational radiation driven non-axisymmetric instability. **KPL** indicates the zones where the minimum period is determined by the effective centrifugal limit.

the extreme mass allowed before the gravitational collapse into a black hole. From this figure it's clear that a search for a submillisecond pulsar can distinguish whether the GBound ES is stiff or soft. The situation is different for SBound objects such as quark stars where the non-axisymmetric instabilities (if not damped by viscosity) could limit the minimum rotational periods well above their centrifugal limits (Colpi and Miller, 1992). If this is not the case, a pulsar of given mass found to have a spin period in the zone limited by Eqs. (2) and (3) would indicate the existence of strange quark (or even more exotic) matter.

II The Bologna submillisecond pulsar search experiment

Burderi & D'Amico (1997) and D'Amico (1998) have discussed the detectability of a submillisecond pulsar on the basis of the efficiency of the spin-up model, the expected luminosity, and the time spent in the submillisecond period range. They have shown that a population of submillisecond pulsars could exist and have significant possibility of being detected with the present generation of radiotelescopes.

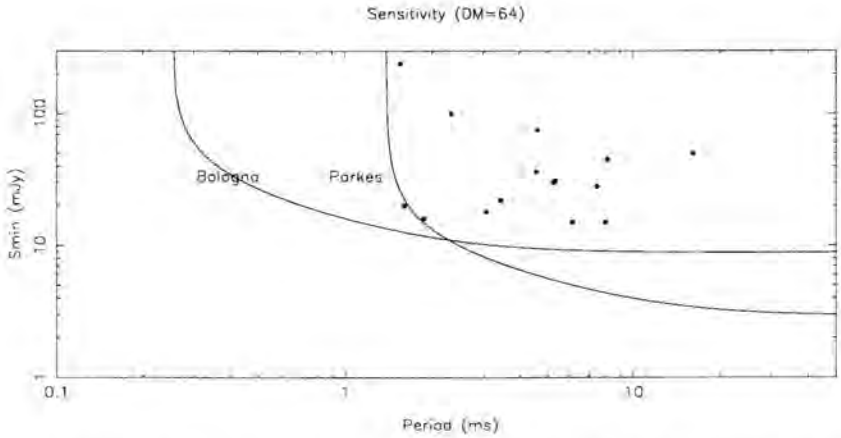

Figure 2. Minimum detectable pulsar mean flux density for the Bologna survey, compared with that of the Parkes survey. The dots indicate known millisecond pulsars.

A large scale pulsar-search experiment with high sensitivity in the submillisecond period range was commissioned recently (D'Amico 1998) at the Italian Northern Cross radiotelescope near Bologna, Italy. The technical requirements of an experiment designed to probe the ultrashort period range are described by D'Amico (1998), and by Burderi & D'Amico (1997). Roughly speaking, in order to detect narrow (< 100 μs) pulses, an adequate time resolution is required. Moreover, because the pulsar signal is dispersed by propagation in the interstellar medium, it requires to be resolved also in the frequency domain. The finite frequency resolution $\delta\nu/\nu$ adopted to sample the frequency domain results in a pulse smearing $\delta_{\rm DM} = 8.3 \times 10^3 {\rm DM}\, \nu^{-2} (\delta\nu/\nu)$ (where $\delta\nu$ and ν are the width of a single frequency channels and the center observing frequency in MHz respectively, DM is the dispersion measure in cm^{-3}pc, and $\delta_{\rm DM}$ is in seconds). The Bologna experiment adopts a sampling time of 64 μs and uses a high resolution filterbank (128 $\times$ 32 kHz) centered at a frequency of 408 MHz, in order to achieve an unprecedented sensitivity in the ultra short period range. Figure 2 shows the sensitivity of the Bologna experiment compared with that of the recent Parkes survey (Manchester et al. 1996, Lyne et al. 1997, D'Amico et al. 1997). The experiment requires the acquisition of 128×10^6 samples per beam position, and the entire survey calls for the observations of more than 100,000 beams. The raw data are not recorded, but they are rather processed online by a powerful multiprocessor system, and only the relevant suspect periodicities are recorded for future investigations. This experiment represents the first real attempt to probe the critical period range.

References

Burderi, L. & D'Amico, N. 1997, ApJ, 490, 343
Colpi, M. & Miller, J.C. 1992, ApJ, 388, 513
Cook, G.B., Shapiro, S.L. & Teukolsky, S.A. 1994, ApJ, 424, 823
D'Amico, N. 1998, in The Many Faces of Neutron Stars, ed. A. Alpar, R. Buccheri & J. van Paradijs (Dordrecht: Kluwer), 129
D'Amico, N. et al. 1997, MNRAS, 297, 28
Friedman, J.L. & Ipser, J.R. 1992, Phil. Trans. R. Soc. Lond., 340, 391
Glendenning, N.K. 1992, Phys. Rev. D, 46, 4161
Lyne, A.G. et al. 1997, MNRAS, 295, 743
Manchester, R.N. et al. 1996, MNRAS, 279, 1235
Proszynski, M. & Przybycien, D. 1985, in Millisecond Pulsars, ed. S.P. Reynolds & D.R. Stinebring (Green Bank: NRAO), 151
Shapiro, S.L. & Teukolsky, S.A. 1983, Black Holes, White Dwarfs & Neutron Stars (New York: Wiley)
Witten, E. 1984, Phys. Rev. D, 30, 272

Authors' Addresses

N. D'Amico: Osservatorio Astronomico di Bologna, via Zamboni 33, 40126 Bologna, Italy; and Istituto di Radioastronomia del CNR, via Gobetti 101, 40129 Bologna, Italy

L. Burderi: Astronomy Group, University of Leicester, Leicester LE1 7RH, UK; and Istituto di Fisica dell'Universita', via Archirafi 36, 90123 Palermo, Italy

T. Belloni, L. Zampieri and S. Campana

Search for Old Neutron Stars in Molecular Clouds

Abstract

We performed a systematic search for old neutron star (ONS) candidates in two giant molecular clouds (Cyg OB7 and Cyg Rift), making use of the ROSAT PSPC archive. Four of the soft X-ray sources in our fields could not be optically identified down to a limit of $m_v \sim 20$. A detailed theoretical calculation of the expected number of detections predicts a number of sources considerably larger than what observed, indicating that the assumptions and/or the range of parameters of theoretical models need to be revised.

I Introduction

The detection of old neutron stars (ONS) accreting from the interstellar medium is a long-sought goal of X-ray astronomy. Systematic studies of the observability of ONS with ROSAT were carried out by Treves & Colpi (1991), Blaes & Madau (1993) and Zane et al. (1995). To date, good evidence for ONS candidates has been presented by Stocke et al. (1995) and Walter, Wolk & Neuhäuser (1996). As shown by Blaes & Madau (1993), Colpi, Campana & Treves (1993) and Zane et al. (1995), some molecular clouds in the vicinity of the Sun represent the most favorable sites for the observability of these sources.

We have performed a systematic investigation of the X-ray sources detected by the ROSAT PSPC in the direction of the two molecular clouds Cygnus Rift and Cygnus OB7. A more exhaustive report can be found in Belloni, Zampieri & Campana (1997).

II Theoretical expectations

In order to calculate the number of ONS detectable in the direction of Cygnus Rift and OB7, a number of assumptions have been made:

- Structure of the ISM: we adopted three different ISM densities on the line of sight: $\sim$0.6 cm^{-3} for the local ISM ($<$ 100 pc), 1 cm^{-3} for the ISM $>$ 100 pc and $\sim$30 cm^{-3} for the molecular clouds.

- Space and velocity distribution of ONS: we adopted the distribution derived by Zane et al. (1995).

- Total number of ONS in the Galaxy: $N_{\rm tot} = 10^9$.

- Magnetic field: we assumed that a relic magnetic field, $B = 10^9$ G, is present. The B field channels the accretion flow into the polar caps, but all its radiative effects have been neglected.

- Emitted spectrum: we adopted the spectrum calculated by Zampieri et al. (1995) for a non-magnetized neutron star accreting well below the Eddington limit.

- Observational coverage: we took into account the uneven coverage of the clouds and the different sensitivity levels of different pointings.

In summary, our calculations predict the detection of a total of $\sim$40 sources in the fraction of the clouds covered by ROSAT pointings at the sensitivity limit of 10^{-3} c s^{-1}.

III Observations

We selected pointings from the ROSAT PSPC archive, for a total of $\sim$127 ksec of total exposure. The total spatial coverage was around 5% for both clouds. Sources were detected using the standard EXSAS procedure (see Zimmermann et al. 1994), limited to the central 20′ of the detector in order not to degrade the resulting positional accuracy. All sources were visually checked. *A total of 109 sources were detected.*

67 sources were identified with entries in the Guide Star Catalog (Lasker et al. 1990). 35 sources contained possible counterparts with $m_v < 20$ in the Palomar plates. Three of the remaining objects were known X-ray sources. *4 sources remained without possible optical identification* (two sources per cloud, see Table 1).

IV Results

All four sources are close to the sensitivity limit and have a good robust position. Three sources are hard and could be inside the clouds, while the remaining might be a foreground ONS.

Table 1: The four ONS candidates

Name	α (2000)	δ (2000)	Δr ($''$)
Rift–1	$20^h19^m27\overset{s}{.}96$	$+38°38'27\overset{''}{.}6$	10.5
Rift–2	$20^h19^m47\overset{s}{.}05$	$+41°12'01\overset{''}{.}3$	19.2
OB7–1	$20^h53^m07\overset{s}{.}35$	$+55°13'29\overset{''}{.}0$	13.4
OB7–2	$21^h25^m31\overset{s}{.}12$	$+51°48'31\overset{''}{.}5$	9.2

The values of $\log(f_x/f_o)$ for our four candidates are between -0.4 and $+0.1$. They could still be BL Lacs, clusters of galaxies, young SNRs or PMS stars. Deeper optical/IR observations are needed in order to establish their nature.

However, it is clear that the theoretical number of detectable ONS exceeds the number of candidates by roughly one order of magnitude. This means that the assumptions and/or the range of parameters of theoretical models need to be revised.

References

Belloni, T., Zampieri, L. & Campana, S. 1997, A&A, 319, 525
Blaes, O. & Madau, P. 1993, ApJ, 403, 690
Colpi, M., Campana, S. & Treves, A. 1993, A&A, 278, 161
Lasker B.M. et al. 1990, AJ, 99, 2019
Stocke, J.T. et al. 1995, AJ, 109, 1199
Treves, A. & Colpi, M. 1991, A&A, 241, 107
Walter, F.M., Wolk, S.J. & Neuhäuser, R. 1996, Nature, 379, 233
Zampieri, L. et al. 1995, ApJ, 439, 849
Zane, S. et al. 1995, ApJ, 451, 739
Zimmermann, H.U. et al. 1994, MPE Report 257

Authors' Addresses

T. Belloni: Astronomical Institute "Anton Pannekoek", University of Amsterdam and Center for High-Energy Astrophysics, Kruislaan 403, NL-1098 SJ Amsterdam, The Netherlands

L. Zampieri: Department of Physics, Loomis Laboratory of Physics, University of Illinois at Urbana-Champaign, 1110 West Green Street Urbana, Illinois 61801-3080, USA

S. Campana: Osservatorio Astronomico di Brera, Via Bianchi 46, I-22055 Merate, Italy

Part IV:

Timing Noise and Glitches — Observations

A. Lyne

Glitches and Timing Noise

Abstract

The rotational stability of pulsars is one of their most remarkable and valued properties, permitting their use as clocks in many astrophysical experiments in ways described by several other authors in this volume. For instance they allow us to determine the shapes and sizes of binary orbits, to study general relativistic effects in intense gravitational fields, to demonstrate the radiation of gravitational waves from binary systems, to detect extra-solar planets and to put limits on the long-period gravitational wave background. However, it is clear that many pulsars show significant departures from regular slow-down which make their rotation unpredictable. There are two main forms of irregularity, glitches and timing noise, which are most marked in, but not confined to, young pulsars. Here, we review the observational status and statistical aspects of the phenomena in so far as they limit studies in which the rotational stability is paramount and may limit their use as clocks. We do not discuss their implications for neutron star structure. Both timing noise and glitch activity depend roughly inversely as the frequency derivative, implying that even millisecond pulsars may be prone to these effects.

I Introduction

The spin-down of pulsars is believed to result from the loss of rotational kinetic energy in the form of low frequency electromagnetic waves or high-energy particles and radiation. We first discuss the process of regular spin-down before discussing departures from this monotonic behavior.

In a general slowdown, the braking torque depends upon the rotation rate ν according to the spin-down equation $\dot{\nu} = -K\nu^n$, where n is the braking index, which depends upon the physics of the braking mechanism. For magnetic braking by a dipolar field or particle loss from a completely aligned rotator, n has an expected value of 3 (Pacini 1968, Goldreich & Julian 1969). The value of the dipolar magnetic field B_0 at the surface of the star of radius R can be obtained in terms of the period, $P = 1/\nu$, giving $B_0 = \sqrt{3Ic^3 P\dot{P}/8\pi^2 R^6} = 3.3 \times 10^{19}(P\dot{P})^{1/2}$ Gauss, where the neutron star is taken

to have a radius $R = 10$ km and moment of inertia $I = 10^{45}$ gm cm^2. In the case where the initial rotation rate is much greater than the present one, the age of the pulsar can be estimated as $\tau = -\nu/(n-1)\dot{\nu} = +P/(n-1)\dot{P} = +P/2\dot{P}$, for $n = 3$. The latter estimate is commonly known as the characteristic age of the pulsar. For the Crab pulsar, the characteristic age is 1250 years, in reasonable agreement with the known age of 940 years. Since the initial period must have been finite, the characteristic age is usually regarded as an upper limit to the true age. Any decay in the magnetic field will also serve to make it an overestimate of the true age.

In principle, the value of n can be checked by differentiation of the spin-down equation, giving $n = \nu\ddot{\nu}/\dot{\nu}^2$. A stable value of n has been measured in this way for only 4 pulsars, the Crab (B0531+21), B0540−69, B1509−58 and Vela (B0833−45), giving values of 2.509±0.001 (Lyne et al. 1988), 2.01±0.02 (Manchester & Peterson 1989), 2.838±0.001 (Kaspi et al. 1994) and 1.4±0.2 (Lyne et al. 1996) respectively. These values are all somewhat less than 3. While these small values may result from the non-dipolar nature of the magnetic field or the presence of particles in the magnetosphere, it seems more likely that the magnetic field or effective moment of inertia of the pulsar may be evolving with time (Lyne et al. 1996; Camilo 1996). For older pulsars, timing noise and the recovery from glitches usually dominate the measured value of $\ddot{\nu}$ (see section 3), and the value of n is variable and is not related to the braking mechanism.

The normal slowdown described above is steady and predictable. However, some pulsars show erratic behavior of two types: glitches and timing noise. Both are apparently associated with the irregular transfer of angular momentum from the fluid interior (Lyne 1992) as the pulsar slows down and we discuss each of these in turn.

II Glitches

Glitches are seen as sudden increases in the rotation rate, often followed by an exponential recovery or relaxation back towards the pre-glitch frequency. For example, the slowdown of the Vela pulsar over a 14-year interval is shown in Figure 1a. During this time, 6 glitches can barely be seen in the top diagram against the normal slowdown but, after a slope is removed, they are clear, each step corresponding to a fractional increase in rotation rate of $\Delta\nu/\nu \sim 2 \times 10^{-6}$. The relaxations can be most clearly seen in Figure 1b which shows the variation in $\dot{\nu}$, over a 25-year period.

The Crab pulsar behaves rather differently (Lyne, Pritchard & Smith 1993) and has shown a series of glitches of magnitude $\Delta\nu/\nu \sim 10^{-8}$ to 10^{-7}. Following an initial short-term transient, the main effect of these glitches seems to be a persistent increase in slowdown rate amounting to about 0.1 % in total over a period of 23 years. This may be attributed to either a growing value of magnetic field or possibly to a decreasing moment of inertia.

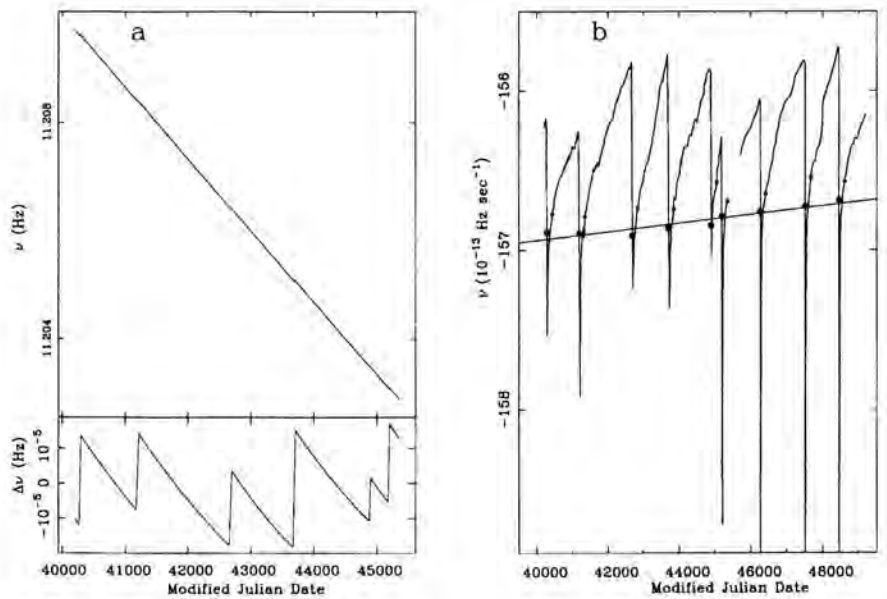

Figure 1. The slowdown of the Vela pulsar. *a)* The rotation frequency ν over 14 years, showing 6 glitches, before and after subtraction of a constant value of $\dot{\nu}$. *b)* The run of $\dot{\nu}$ over 25 years.

There are two main aspects of glitches which may or may not be related: firstly, the cause of the glitch, which might be either a starquake or the result of catastrophic superfluid vortex unpinning, and secondly, the post glitch relaxation, which gives information on the amount of fluid in the star and the physics of the angular momentum transfer from the core. First we discuss briefly the possible causes of the glitches and then the possible implications of the recovery.

A starquake might arise from changing ellipticity of the crust of the neutron star as it slows down (Ruderman 1969). The oblateness of an equilibrium spheroid will decrease as the rotation rate decreases. Stresses build up in the rigid crust as the departure from the equilibrium shape increases, until it cracks and assumes a shape closer to the equilibrium spheroid. The moment of inertia I decreases and conservation of angular momentum results in a spin-up given approximately in terms of the change in oblateness: $\Delta\epsilon = \Delta I/I = -\Delta\nu/\nu$.

While this explanation provided a satisfactory explanation for the glitches in the Crab pulsar, it soon became clear that the magnitude and frequency of the glitches in the Vela pulsar were too great to be sustained by this mechanism (Pines, Shaham &

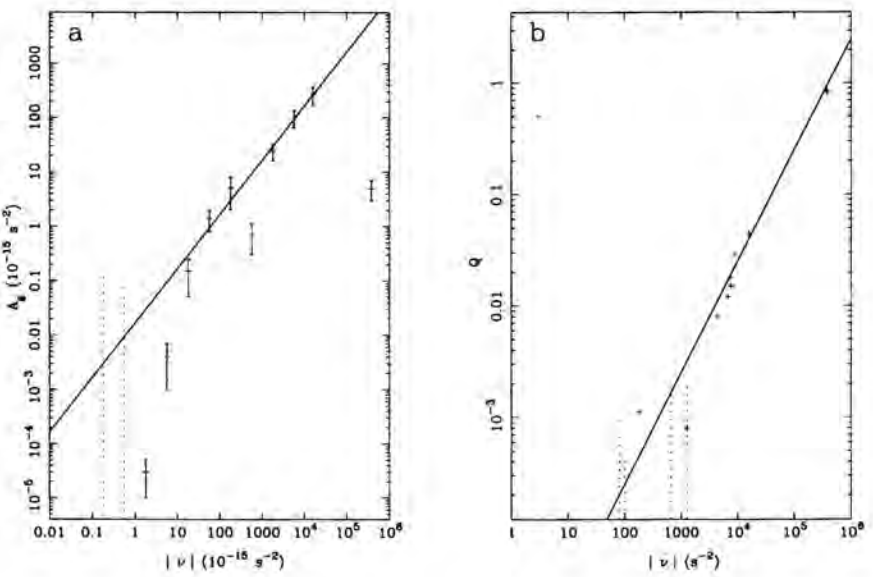

Figure 2. *a)* The glitch activity parameter, the rate of increase in frequency due to glitches, averaged over all observed pulsars in semi-decade ranges of frequency derivative. *b)* The fraction Q of the frequency step $\Delta\nu$ which is recovered in short-term, quasi-exponential post-glitch relaxation. In both diagrams, the dotted lines represent upper limits and the lines have slopes of unity.

Ruderman 1972). More likely, in this case it seems that the glitches result from the catastrophic unpinning of superfluid neutron vortices from the nuclei of the solid crust (Baym, Pethick & Pines 1969, Anderson & Itoh 1975).

III The frequency of glitches

Glitches are rare—only about 20 out of over 700 pulsars have suffered a total of 45 glitches and until recently the study of glitches has been limited by their small number. Excluding Vela, only about 10 glitches were observed in about 20 years up to 1987, mainly due to a lack of known young pulsars. Such pulsars are rare since they do not stay young for very long, and also because there are strong selection effects against the discovery of young pulsars in most searches. To combat such effects, two surveys have been conducted at low latitude and high radio frequency, with 40 pulsars found at Jodrell Bank (Clifton & Lyne 1986, Clifton et al. 1992) and 45 at Parkes (Johnston

Table 1: Known glitching pulsars

Pulsar	Age(kyr)	N_g	$\Delta\nu/\nu \times 10^6$	References
0355+54	560	2	.006, 4.4	A,U
0525+21	1480	2	.0013, .0003(?)	B,U
0531+21	1.3	4	.01, .04, .01, .08	C,D,E,F
0833−45	11	9	2.3, 2.0, 2.0, 3.1, 1.1, 2.0, 1.3, 1.8, 2.7	G,H,I,J,K,L,M,N,O
1325−43	2800	1	.12	P
1338−62	12	3	1.5, .03, 1.0	Q,U
1508+55	2340	1	.0002(?)	R
1535−56	790	1	2.8	S,U
1641−45	350	1	.2	T
1706−44	17	1	2.1	S,U
1727−33	26	1	3.1	S,U
1736−29	650	1	.003	U
1737−30	21	6	.43, .03, .03, .60, .64, .05, .02, .01, .17	V,U
1757−24	15	1	2.0	W
1758−23	59	3	.22, .23, .35, .06	X,U
1800−21	16	1	4.1	U
1823−13	21	2	2.7, 3.0	U
1830−08	150	1	1.9	U
1859+07	4360	1	.03	U
1907+00	2950	1	.0007(?)	Y
2224+65	1120	1	1.7	Z,U

REFERENCE KEYS:

A:Lyne (1987) B:Downs (1982) C:Boynton et al. (1972)
D:Lohsen (1975) E:Lyne & Pritchard (1987) F:Lyne et al. (1992)
G:Radhahrishnan & Manchester (1969) H:Reichley & Downs (1971)
I:Manchester et al. (1976) J:Manchester et al. (1983 K:Mculloch et al. (1983)
L:Cordes et al. (1988) M:Mculloch et al. (1987) N:Flanagan (1989)
O:Flanagan (1991) P:Newton et al. (1981) Q:Kaspi et al. (1992)
R:Manchester & Taylor (1974) S:Johnston et al. (1992) T:Manchester et al. (1978)
U:Shemar & Lyne (1996) V:McKenna & Lyne (1990) W:Lyne et al. (1996)
X:Kaspi et al. (1993) Y:Gullahorn et al. (1976) Z:Backus et al. (1982)

et al. 1992a). These new samples have a mean characteristic age of less than a million years compared with 6 million years for all pulsars found in previous surveys (Clifton et al. 1992). Already 20 glitches have occurred in these pulsars (Shemar & Lyne 1996).

Table 1 provides a summary of the 21 pulsars which have glitched, together with the their characteristic ages, the number of glitches, the fractional increase in rotational frequency at each glitch and the observational references. These data show that glitches have been observed in only about 3% of the known population, predominantly in young pulsars. The rest of this section describes the frequency of glitches and their recovery as a function of the pulsar spin-down parameters.

Apart from the youngest pulsars, most pulsars which have glitched have done so only once. The implication here is that the intervals between glitches in these objects and in similar ones is much greater than the observational timespan and, given enough time, many more will display glitch activity. For this reason, in order to understand the frequency of glitches, we have to consider the length of time that pulsars of similar characteristics have been observed. Dividing the total change in frequency occurring at glitches by the total observation time for a group of pulsars gives a rate of glitch activity, A_g, which is a measure of the amount of frequency derivative $\dot{\nu}$ which is "undone" by glitches (McKenna & Lyne 1990, Lyne, Shemar & Smith 1997). Figure 2a shows the pulsar glitch activity as a function of $\dot{\nu}$. We clearly see that A_g is greatest for pulsars with $|\dot{\nu}| \sim 10^{-11}$ s^{-2}, corresponding to ages between about 10,000 and 30,000 years. For greater ages, it seems that the activity falls off roughly as the frequency derivative, presumably as the flow of angular momentum from the interior decreases. To first order, this can be understood in terms of glitches undoing of a fixed fraction of the normal rotational slow-down. This fraction amounts to about 0.03, suggesting that about 3% of the angular momentum in these pulsars is carried by superfluid neutrons whose outward flow to the crust is held up by vortex pinning and only moves in a stepwise manner. Since there is little significant recovery between glitches (see next section), this implies that there is little drift occurring in these vortices.

Somewhat surprising is the low level of glitch activity in the youngest pulsars such as the Crab pulsar, PSR B1509−58 and PSR B0540−69 which are collectively responsible for the most extreme right-hand point in Fig. 2a. Although these pulsars have very large slow-down rates, the angular momentum flow seems to be reasonably continuous. One possible reason for this is the youth of these pulsars and their corresponding high internal temperature, which may allow the stresses to be relieved by thermal drift of the vortices from one pinning site to another in a gradual fashion (McKenna & Lyne 1990).

IV The recovery from glitches

There is a wide range of recovery from glitches and again this seems to be related approximately to the age of the pulsar. For glitches in the younger pulsars, both the frequency and frequency derivative steps of the glitch recover substantially over the following months, and there is often a persistent and non-decaying permanent offset in $\ddot{\nu}$, as seen between the Vela glitches (Fig. 1b). In those glitches which have been observed closely following the event, exponential recoveries on up to 3 timescales are often recorded (McCulloch et al. 1990, Alpar et al. 1993). For the older pulsars, the main effect of a glitch is a large step in frequency and there is very little recovery in this over the following years (Shemar & Lyne 1996). In fact the small amount of frequency recovery depends inversely upon the characteristic age, suggesting that, as discussed above, in older pulsars the vortex pinning is strong and little vortex drift occurs.

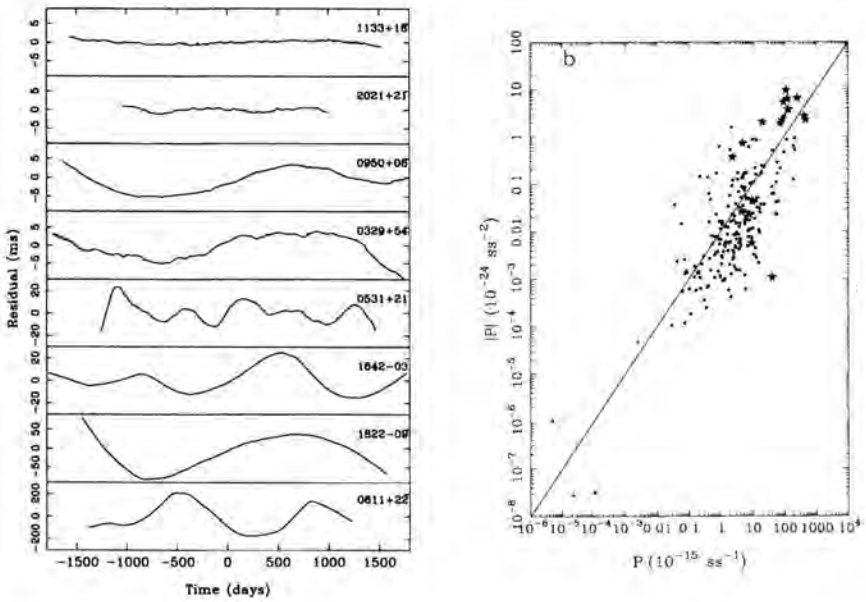

Figure 3. *a)* Examples of timing noise in 8 pulsars over about a 10 year period, showing increasing amounts of activity from the top to bottom. *b)* The magnitude of $\ddot{P}$, a measure of the amount of timing noise, plotted against $\dot{P}$, showing high level of timing noise in young, rapidly braking pulsars. Pulsars which glitch are shown by a star. The line has a slope of unity.

The short-term quasi-exponential behavior following each glitch can be explained by the presence of a fluid component in the interior of the neutron star (Baym et al. 1969) which is loosely coupled to the rigid crust whose rotation we observe through the emission beam which is tied to it. Alpar et al. (1993) have interpreted the recovery from these glitches in terms of both linear and non-linear relaxation in a number of regions within the crust.

V Timing noise

Timing noise is characterized by a continuous, unpredictable, phase wandering of the pulses relative to a simple slow down model. It is seen most prominently in the Crab and other pulsars with large period derivatives (Cordes & Helfand 1980). Some examples of timing noise in a number of pulsars are shown in Figure 3a where the unpredictability of the period in these pulsars is clear. The amount of this timing

noise can be quantified by measuring the residuals relative to a simple slow-down model as described above. On the whole, timing noise is very red and the timing residuals relative to a simple slow-down model are usually dominated by a cubic term which corresponds to a period or frequency second derivative. Figure 3b shows the magnitude of $|\ddot{P}|$ plotted against $\dot{P}$, for 218 pulsars (Lyne & Martin 1997). There are a few dozen additional upper limits, not included in this diagram, which lie mostly above the diagonal line, and which are for pulsars with short data timespans. This clearly confirms that young pulsars, with large slow-down rates, have much timing noise (see also Arzoumanian et al. 1994). While there are roughly equal numbers of positive and negative values of $\ddot{P}$ in this diagram, it is noteworthy that of the 30 pulsars with $\dot{P} \geq 3 \times 10^{-14}$, the 11 that have glitched all have negative values of $\ddot{P}$, as expected from the exponential form of the recoveries. Of the remaining 19, 14 have positive values, suggesting that the recovery from (unseen) glitches mostly dominates any timing noise present. While most millisecond pulsars, having very small period derivatives, are found to be very stable, note that PSR B1937+21, with a relatively high $\dot{P}$ for a millisecond pulsar, has shown significant timing noise (Kaspi, Taylor & Ryba 1994).

VI Conclusion

Glitches and timing noise are a widespread phenomenon in the pulsar population and are likely to be mostly due to an irregular flow of angular momentum from a neutron superfluid component in the interior of the stars. The trends described above are only recently becoming quantifiable and are still somewhat preliminary, but show clearly that over the bulk of the pulsar population, the amount of glitch activity, the amount of subsequent recovery and the amount of timing noise all depend approximately linearly on the magnitude of $\dot{\nu}$. However, as more glitches are observed in the newly discovered young pulsars, and the data spans for the study of timing noise increase, the study of neutron star interiors will become more detailed and may impose limits upon the equation of state of matter at the super nuclear densities within these objects (Pines 1991).

While glitches have affected only about 3% of the observed population since their discovery, it seems very likely that most pulsars will experience them in due course, the interval between glitches being much greater than the observation time hitherto. As for timing noise, the evidence of Fig. 3b suggests that most pulsars, even the millisecond pulsars, will display its effects in due course. For use as clocks, even those with the smallest derivatives are likely to be limited in their precision.

References

Alpar, M.A. et al. 1993, ApJ, 409, 345
Anderson, P.W. & Itoh, N. 1975, Nature, 256, 25
Arzoumanian, Z. et al. 1994, ApJ, 422, 671
Backus, P.R., Taylor, J.H. & Damashek, M. 1982, ApJ, 255, L63
Baym, G., Pethick, C. & Pines, D. 1969, Nature, 224, 673
Baym, G. et al. 1969, Nature, 224, 872
Boynton, P.E. et al. 1972, ApJ, 175, 217
Camilo, F. 1996, in Pulsars: Problems and Progress, IAU Colloqium 160, ed. S. Johnston, M.A. Walker & M. Bailes (San Francisco: ASP), 39
Clifton, T.R. & Lyne, A.G. 1986, Nature, 320, 43
Clifton, T.R. et al. 1992, MNRAS, 254, 177
Cordes, J.M., Downs, G.S. & Krause-Polstorff, J. 1988, ApJ, 330, 847
Cordes, J.M. & Helfand, D. J. 1980, ApJ, 239, 640
Downs, G.S. 1982, ApJ, 257, L67
Flanagan, C.S. 1989, IAU Circ. 4695
Flanagan, C.S. 1991, IAU Circ. 5311
Goldreich, P. & Julian, W.H. 1969, ApJ, 157, 869
Gullahorn, G.E. et al. 1976, ApJ, 205, L151
Johnston, S. et al. 1992a, MNRAS, 255, 401
Johnston, S. et al. 1992b, ApJ, 387, L37
Kaspi, V.M. et al. 1993, ApJ, 409, L57
Kaspi, V.M. et al. 1992, ApJ, 399, L155
Kaspi, V.M. et al. 1994, ApJ, 422, L83
Kaspi, V.M., Taylor, J.H. & Ryba, M. 1994, ApJ, 428, 713
Lohsen, E. 1975, Nature, 258, 688
Lyne, A.G. 1987, Nature, 326, 569
Lyne, A.G. 1992, Philos. Trans. Roy. Soc. London A, 341, 29
Lyne, A.G. et al. 1996a, MNRAS, 281, L14
Lyne, A.G. & Martin, C.E. 1997, MNRAS, submitted
Lyne, A.G. & Pritchard, R.S. 1987, MNRAS, 229, 223
Lyne, A.G. et al. 1996b, Nature, 381, 497
Lyne, A.G., Pritchard, R.S. & Smith, F.G. 1988, MNRAS, 233, 667
Lyne, A.G., Pritchard, R.S. & Smith, F.G. 1993, MNRAS, 265, 1003
Lyne, A.G., Shemar, S.L. & Smith, F.G. 1997, MNRAS, in preparation
Lyne, A.G., Smith, F.G. & Pritchard, R.S. 1992, Nature, 359, 706
Manchester, R.N., Goss, W.M. & Hamilton, P.A. 1976, Nature, 259, 291
Manchester, R.N. et al. 1978, MNRAS, 184, 35P
Manchester, R.N. et al. 1983, MNRAS, 202, 269
Manchester, R.N. & Peterson, B.A. 1989, ApJ, 342, L23
Manchester, R.N. & Taylor, J.H. 1974, ApJ, 191, L63
McCulloch, P.M. et al. 1990, Nature, 346, 822
McCulloch, P.M. et al. 1983, Nature, 302, 319

McCulloch, P.M. et al. 1987, Aust. J. Phys., 40, 725
McKenna, J. & Lyne, A.G. 1990, Nature, 343, 349
Newton, L.M., Manchester, R.N. & Cooke, D.J. 1981, MNRAS, 194, 841
Pacini, F. 1968, Nature, 219, 145
Pines, D. 1991, in Neutron Stars: Theory and Observation, ed. J. Ventura & D. Pines (Dordrecht: Kluwer), 57
Pines, D., Shaham, J. & Ruderman, M.A. 1972, Nature Phys. Sci., 237, 83
Radhakrishnan, V. & Manchester, R.N. 1969, Nature, 222, 228
Reichley, P.E. & Downs, G.S. 1971, Nature Phys. Sci., 234, 48
Ruderman, M. 1969, Nature, 223, 597
Shemar, S.L. & Lyne, A.G. 1996, MNRAS, 282, 677

Authors' Address

The University of Manchester, NRAL, Jodrell Bank, Cheshire SK11 9DL, UK;
agl@jb.man.ac.uk

F. Graham Smith

Glitches and the Vela Slowdown

I The basic model

In the superfluid component of a pulsar the angular momentum is represented by the area density of vortices. Slowing down therefore means that the vortices are moving outwards. If vortices in a component of the superfluid are pinned to the crystal lattice of the crust, that component does not participate in the slowdown.

The crust and the core are tightly linked: only the superfluid within the inner part of the crust can rotate independently.

II Glitches in all pulsars except the youngest

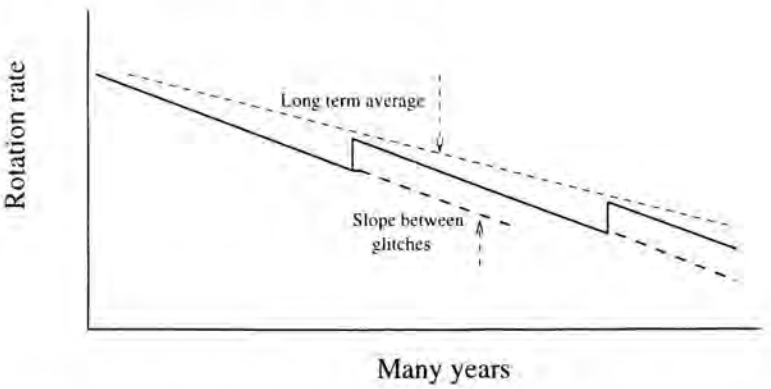

Figure 1. Sketch of the rotation rate of old glitching pulsars as a function of time.

There are three basic components of glitches in the older pulsars. The observations and interpretations can be summarized as follows:

Observation 1: The glitches are simply a step increase in rotation rate ν, reversing the predominant steady slowdown. The reversals, averaged over a long time, reduce the mean slowdown rate by about 1.7%. This fraction is independent of age and slowdown rate.

Interpretation: A region of superfluid with 1.7% of the total moment of inertia is fully pinned between glitches, and unpins completely at each glitch.

Observation 2: Part of the initial step recovers immediately following the glitch. This transient increase in ν amounts to around 1% of the glitch amplitude at most glitches. It decays in 10–100 days (see Figure 2).

Interpretation: A different region of superfluid is responding to the step in crustal rotation rate. In this region the vortices are not completely pinned, but their outward flow is impeded by the crustal lattice; they are 'creeping' outwards, and the rotation rate of this component is higher than in the crust. At the glitch the steady-state differential is disturbed and slowly re-established. In this model the moment of inertia of this component is around 1% of the total. Observations show that this proportion, which is of order 1% of the total, decreases with age.

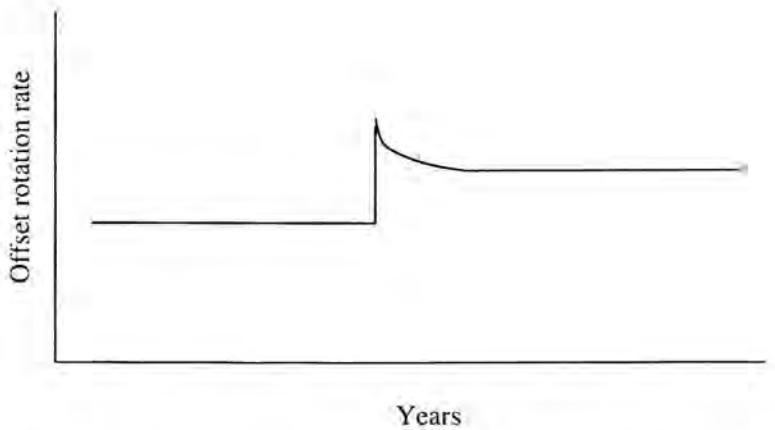

Figure 2. Transient increase in ν following a glitch (schematic). After a rapid decay following the glitch, an on average linear decay continues (see Figure 3).

Observation 3: Most pulsars show an approximately linear decrease of slowdown rate between glitches. This shows in a plot of slowdown rate, in which the mean slowdown rate has been removed (see Fig. 3).

Interpretation: Extending between the fully pinned region and the continuously creeping region is an intermediate region, all of which is fully pinned immediately after a glitch but which becomes progressively unpinned between glitches, like a zip fastener. The effective moment of inertia of this region increases as the unpinning spreads across it, giving a steady increase in slowdown rate. This component again represents about 1% of the total moment of inertia.

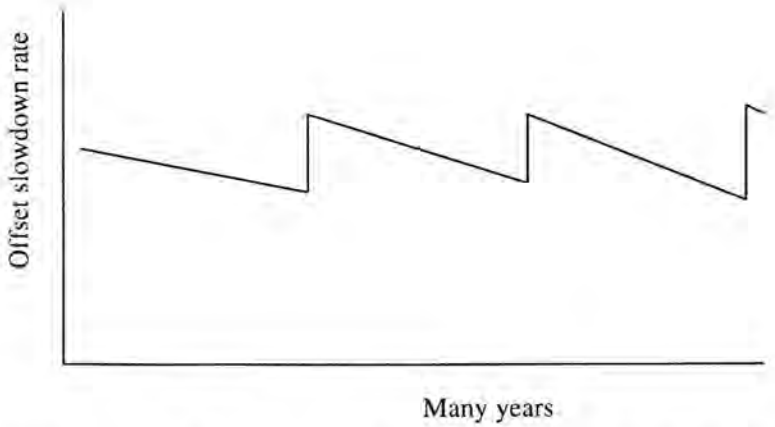

Figure 3. Mean trend of the slowdown rate between glitches (after subtraction of the mean slowdown rate).

III The young pulsars Crab and Vela

Glitches in the Vela pulsar show all three of the components described above, and in addition the slowdown rate shows an anomalous braking index. The short-term recovery has been resolved into several exponential components. Figure 4 shows the slowdown rate over 25 years (without any offset); the rate of change of slowdown rate is obtained from the long-term slope over the whole plot.

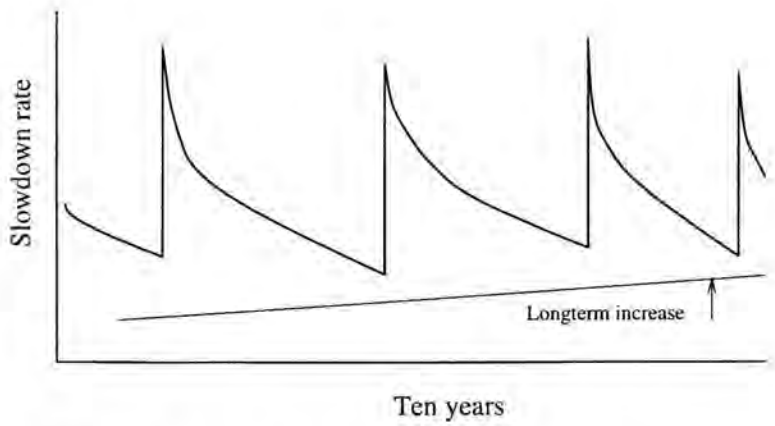

Figure 4. Slowdown rate of the Vela pulsar over a ten year period.

Crab glitches are completely different; as shown in Figure 5 they show primarily a step increase in slowdown rate which does not recover between glitches.

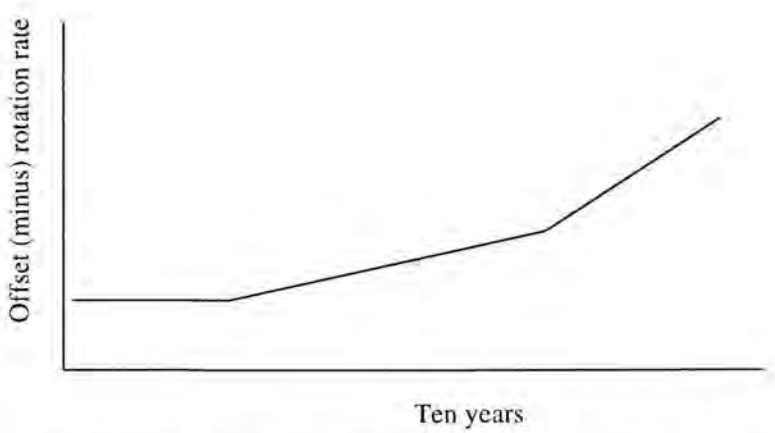

Figure 5. Offset slowdown rate of the Crab pulsar increases after each glitch.

Interpretation: The changes in slowdown rate in the Crab show a cumulative change in either moment of inertia or magnetic dipole moment. A decrease in moment of inertia would be due to a step decrease in pinning at each glitch, while an increase in dipole moment would be due to a rearrangement of the internal field.

IV The braking index of Vela

Why is the braking index of Vela 1.4 and not 3.0 as expected? The two possibilities are that either the magnetic moment M or the moment of inertia I changes in the slowdown process, averaged over many glitches. The slowdown law for magnetic dipole radiation gives

$$\frac{\mathrm{d}\dot{\nu}}{\dot{\nu}} = 3\frac{\mathrm{d}\nu}{\nu} + 2\frac{\mathrm{d}M}{M} - \frac{\mathrm{d}I}{I} \tag{1}$$

so that the braking index is

$$n = \frac{\nu\ddot{\nu}}{\dot{\nu}^2} = 3 - 2\tau_c M^{-1}\frac{\mathrm{d}M}{\mathrm{d}t} + \tau_c I^{-1}\frac{\mathrm{d}I}{\mathrm{d}t}, \tag{2}$$

where τ_c is the characteristic age,

$$\tau_c = -\frac{1}{2}\frac{\nu}{\dot{\nu}} \tag{3}$$

The low value of braking index $n = 1.4$ instead of the expected 3.0 might then be accounted for by a time-averaged change in either I or M; the required rates of change are

$$M^{-1}\frac{\mathrm{d}M}{\mathrm{d}t} = +0.8\tau_c^{-1} \tag{4}$$

and

$$I^{-1}\frac{\mathrm{d}I}{\mathrm{d}t} = -1.6\tau_c^{-1}, \tag{5}$$

i.e., either the effective moment of inertia is increasing on a time scale of 14 000 years or the total effective moment of inertia is decreasing on a time scale of 7 000 years. If this is to be explained in terms of incremental changes of I at the glitches, it must be related to the 2–3% of the total I that is involved in pinning. This rate of change could then only be sustained for less than 200 years. More reasonably, M might be increasing on a time scale comparable with the lifetime of the pulsar, either through a changing alignment angle or an internal organisation.

We suggest that this might occur at the glitches rather than as a continuous process. The step increase in the effective magnetic moment would then be one part in 5000 at each glitch.

This may also be occurring at Crab glitches, where the slowdown rate is observed to increase by about 1 in 5000 every 10 years.

Authors' Address

The University of Manchester, NRAL, Jodrell Bank, Cheshire SK11 9DL, UK;
fgs@jb.man.ac.uk

B.A. Jacoby and A. Wolszczan

Six Years of PSR B1853+01 Timing Observations

Abstract

We summarize the first six years of timing observations of PSR B1853+01, a young pulsar associated with the W44 supernova remnant. Our analysis has revealed two major rotational events: a step increase in the pulsar's period derivative, and a glitch. In addition, PSR B1853+01 exhibits large dispersion measure variations.

I Introduction

PSR B1853+01 was discovered in a search for pulsars in supernova remnants (SNR) with the 305-m Arecibo radio telescope (Wolszczan, Cordes & Dewey 1991). The pulsar's location within W44, and the agreement between the ages and distances of the pulsar and the SNR provided an early indication of their association. Further observations using the VLA (Frail et al. 1996) have detected a synchrotron nebula within W44 powered by the spin-down energy loss of the pulsar, as well as a cometary structure resulting from the pulsar's motion through the SNR. These observations constrain a transverse velocity of the pulsar to be between 300 and 500 km s^{-1}. This is consistent with the $\geq$ 200 km s^{-1} velocity which would be expected if the pulsar originated at the center of W44. Moreover, ASCA observations indicate synchrotron X-ray emission coincident with PSR B1853+01 (Harrus, Hughes & Helfand 1996). These observations point unambiguously to the association of PSR B1853+01 and the W44 SNR.

II Analysis of Timing Observations

We have timed PSR B1853+01 at approximately monthly intervals with the 305-m Arecibo radiotelescope and the 40 MHz, 3-level correlation spectrometer. Observations were conducted at 430 MHz and 1400 MHz, with dual-frequency data covering a 3-year period between 1992 and 1994. The detected, time-tagged input signals were folded at the topocentric pulse period, and cross-correlated with a high signal-to-noise pulse template to measure pulse arrival times (TOA). A conversion of the TOAs to the

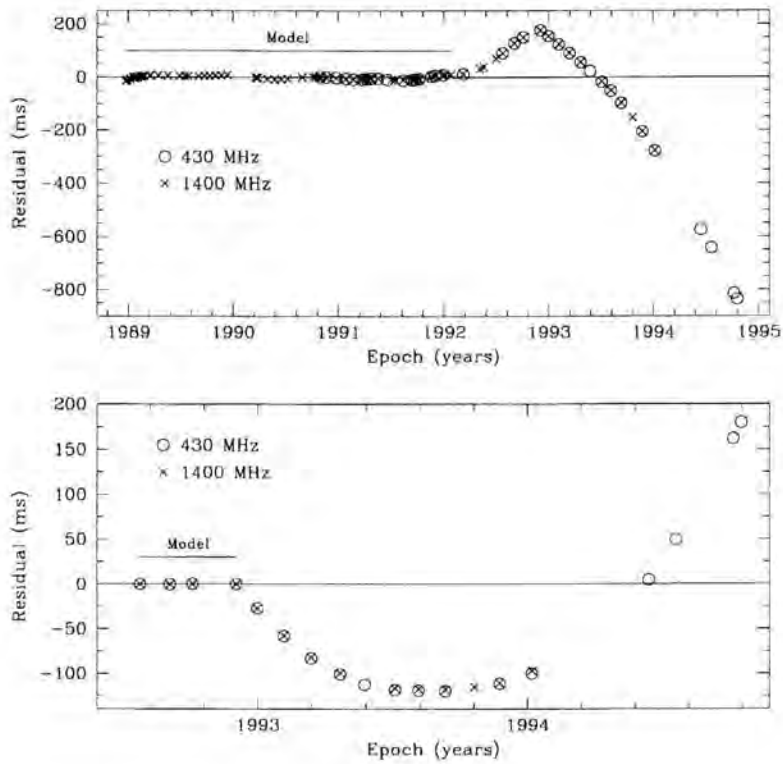

Figure 1. *Top:* Timing residuals for PSR J1853+01 at both observing frequencies, with the first 2.5 years of observations used as a model. *Bottom:* Timing residuals for PSR J1853+01 beginning in mid-1992, showing a large glitch. The timing model used here is based on the four observations previous to the glitch, during which the pulsar's spin parameters were relatively stable.

Solar System barycenter and the fits of timing models to data were performed with the standard timing package TEMPO.

PSR B1853+01 displays noisy rotational behavior. Figure 1 shows the residuals of the pulsar with respect to two different timing models. The first 2.5 years of observations are characterized by the timing noise typical of a young pulsar. In early 1992, an increase in the spin down rate of $\Delta\dot{P}/\dot{P} = 1 \times 10^{-3}$ was observed. After the spin parameters stabilized in late 1992, a glitch occurred. The values of $\Delta P/P = -1 \times 10^{-8}$ and $\Delta\dot{P}/\dot{P} = 7 \times 10^{-4}$ characterizing the fractional changes in the pulsar's spin parameters during this event are comparable to those of the Crab pulsar glitches (Lyne, Pritchard & Smith 1993). A recovery time scale for this

Table 1: Post-Glitch Parameters of PSR B1853+01

Parameter	Value
P (s)	0.26743520591(3)
$\dot{P}$ (10^{-15} s s^{-1})	208.477(1)
Epoch (MJD)	49535.4
α (J2000)	18 56 10.76(2)
δ (J2000)	01 13 28.0(6)
DM (pc cm^{-3})	96.6(3)

rotational discontinuity remains undetermined, because the pulsar's spin parameters following the glitch did not stabilize before the break in timing observations toward the end of 1994.

In young glitching pulsars, discontinuous changes in rotation period are usually followed by an exponential decay back toward the pre-glitch period (Shemar and Lyne 1996). However, in PSR B1853+01, either very little of the initial change in period has recovered, or a possible recovery trend has been concealed by the increased and unstable post-glitch value of $\dot{P}$. While glitches are common in young pulsars, PSR B1853+01's pre-glitch $\dot{P}$ increase, as well as its post-glitch $\dot{P}$ evolution make its rotational history untypical. Table 1 shows the best-fit values of the pulsar's spin parameters following the glitch.

In addition to the TOA measurements, changes in the dispersion measure (DM) of PSR B1853+01 were monitored at all epochs for which dual frequency data were available. The DM shows large, nonlinear variations, with an average rate of change $\Delta\mathrm{DM}/\Delta t = -0.07$ cm^{-3} pc yr^{-1}. A study of the propagation phenomena along the line of sight to this pulsar will be presented elsewhere.

Acknowledgements

This work was supported by the National Science Foundation under grant AST-9317757.

References

Backer, D.C. et al. 1993, ApJ, 404, 636
Frail, D.A.et al. 1996, ApJ, 464, L165
Harrus, I.M., Hughes, J.P. & Helfand, D.J. 1996, ApJ, 464, L161

Lyne, A.G., Pritchard, R.S. & Smith, F.G. 1993, MNRAS, 265, 1003
Shemar, S.L. & Lyne, A.G. 1996, MNRAS, 282, 677
Wolszczan, A., Cordes, J.M. & Dewey, R.J. 1991, ApJ, 372, L99

Authors' Address

The Pennsylvania State University, Department of Astronomy & Astrophysics, 525 Davey Lab, University Park, PA 16802, USA

Part V:

Neutron Star Interiors and Glitch Models

G.E. Brown

Equation of State of Dense Matter and the Upper Mass Limit for Neutron Stars

Abstract

We outline information that relativistic heavy ion collisions give about the equation of state (EOS) of supranuclear matter at densities $\rho \sim 3\rho_0$, where ρ_0 is nuclear matter density. We find $\sim 3\rho_0$ to be the critical density for both kaon condensation and chiral restoration. Calculations with a kaon condensed EOS give a maximum neutron star gravitational mass of $(M_{\rm NS})_{\rm max} \cong 1.5\ {\rm M}_\odot$ and a radius $R \simeq 7$ km.

I Introduction

The theory of dense matter at nuclear and supranuclear densities has developed over several decades and a multitude of papers have been devoted to this subject. Even though we can extrapolate the theory from fits to nuclear phenomena to a description of nuclear matter, basically the parameters must be fit to the known binding energy, compression modulus, etc., because the small $\sim$ 16 MeV net binding energy per nucleon results from near cancellation of large quantities, each of natural scale 1 GeV. Thus, the fit is a very sensitive one.

Extrapolation of theories of nuclear matter to supranuclear densities has had little empirical guidance. The masses and other properties of neutron stars have given some general conditions which must be fulfilled at high densities, but there are usually enough parameters in any of the theories to fulfill these. Unrealistically abrupt changes from hadronic matter undergoing extremely strong interactions to quark matter with weak interactions are generally made at densities of several times nuclear matter density. The chief trouble with the hadronic EOS's used to compute neutron star masses is that they do not soften sufficiently with increasing density, in preparation for making a transition to the relatively soft quark-matter EOS (asymptotic freedom).

The main point we wish to make here is that relativistic heavy ion collisions which reach densities of several times nuclear matter density can tell us about the equation of state of dense matter just in the region of densities relevant for phase transitions in neutron stars.

Study of the equation of state at high densities began in Berkeley in Bevalac heavy ion collisions. Following a lot of controversy, it was finally shown (Zhang, DasGupta & Gale 1994) that the compression modulus of nuclear matter is rather low,

$$K_0 \cong 210 \text{ MeV} . \tag{1}$$

Construction of SIS at GSI has given us facilities with much greater accuracy. In the collision of Au + Au at 1 GeV/Nucleon, densities of $3 - 4\rho_0$, where ρ_0 is nuclear matter density, are formed. As we shall show, in conventional descriptions the equation of state is dominated at these high densities by the repulsive vector interaction between nucleons, resulting in an extremely stiff EOS. This is, however, an ill preparation for transition to soft quark matter and asymptotic freedom at higher densities. We shall show that the measured flow in the relativistic heavy ion collisions requires less stiffness, less than obtained by extrapolating Walecka-type mean field equations from nuclear matter density.

Heavy ion collisions at 1 GeV/Nucleon create composite systems of temperatures $T \sim 75$ MeV, low compared with the masses of the exchanged σ- and ω-mesons which produce the main part of the nucleon-nucleon interaction. The CERN SPS experiments of 160 GeV/Nucleon Pb on Au create a temperature $T \sim 170$ MeV or more to begin with, which is high. Nonetheless, effects on meson masses stem chiefly from the high densities, and not from the high temperature. Study of the CERES experiment detection of dileptons tells us that the masses of the mesons, other than that of the pion, are density dependent. These effects have to be built into the EOS for neutron stars, even though we are working with essentially $T = 0$ cold matter here.

Most importantly for the EOS, we shall show that interactions of high density nuclear matter on the K^--meson are sufficiently attractive in dense matter to bring the K^- energy below that of the electron chemical potential μ_e by $\rho \sim 3\rho_0$. At this and higher densities, the electrons change into K^--mesons. The latter, being bosons, go into a condensate. The EOS for $\rho \gtrsim 3\rho_0$ is significantly softened by the kaon condensation, which limits the maximum mass of neutron stars to

$$(M_{\text{NS}})_{\text{max}} \sim 1.5 \text{ M}_\odot . \tag{2}$$

This has extremely important consequences.

II Chiral symmetry and scale invariance

We first discuss the density dependence of meson masses. In the absence of bare quark masses, the Yang-Mills theory possesses chiral symmetry. For our purposes here, this means that the underlying theory deals with massless quarks and gluons. In the world in which we live we know that particles have mass; e.g., the nucleon is usefully

described as consisting of three constituent quarks, so that

$$940 \text{ MeV} = m_n c^2 \cong 3 m_Q c^2 \,, \tag{3}$$

each of the quarks having approximately one-third of the nucleon mass. How these quarks acquire mass is interesting; this involves the dynamical breaking of the chiral symmetry.

We can study the behavior of the theory with increasing temperature (but only at zero density) by lattice gauge simulations on the computer. These tell us that the chiral symmetry restoration transition is a smooth one, either second order or very weakly first order. This means that the quark mass

$$m_Q^*(T_c) \simeq 0 \,, \tag{4}$$

i.e., that the constituent quark mass is essentially zero—the constituent quark has become essentially a bare quark—as $T \to T_c$. The star on the m_Q denotes that this is the mass at a finite temperature (or density). Since all quantities seem to change quite smoothly in the vicinity of the phase transition, we believe that $m_Q^*(T)$ goes smoothly to zero as $T \to T_c$, in the chiral limit in which bare quark masses are zero. These arguments are embodied in discussions of results of lattice calculations by Kocič and Kogut (1995a, 1995b).

Lattice gauge calculations cannot yet give us information about finite density. However, Brown and Rho (1991) were able to use the scale invariance of QCD to show that hadronic masses drop with increasing density.[1]

Brown and Rho proposed that

$$\frac{m_\omega^*}{m_\omega} \cong \frac{m_\rho^*}{m_\rho} \cong \frac{f_\pi^*}{f_\pi} \cong \frac{m_n^*}{m_n} = \cdots \tag{5}$$

as an approximate equality. Here f_π is the pion decay constant. The density dependence of f_π, needed to obtain f_π^*, can be calculated within the framework of chiral Lagrangians, but the usual procedure to date is to scale with m_n^*/m_n since this ratio is given in mean field theories. Such a procedure neglects loop corrections (Brown & Rho 1991). Now the vector mean field acting on either a nucleon or a kaon in dense matter is

$$V = \frac{g_{\omega NN}^2}{m_\omega^2} \rho \tag{6}$$

[1] It is well known that at quantum level QCD breaks scale invariance through developing a gluon condensate. The lowest glueball has a mass of $\sim$ 1.7 GeV, however, well beyond the scale $\Lambda_{\chi SB}$ (where χSB stands for "chiral symmetry breaking") $\simeq$ 1 GeV of low-energy nuclear physics. Thus, these gluon phenomena can be integrated out and treated as counter terms for low-energy nuclear physics.

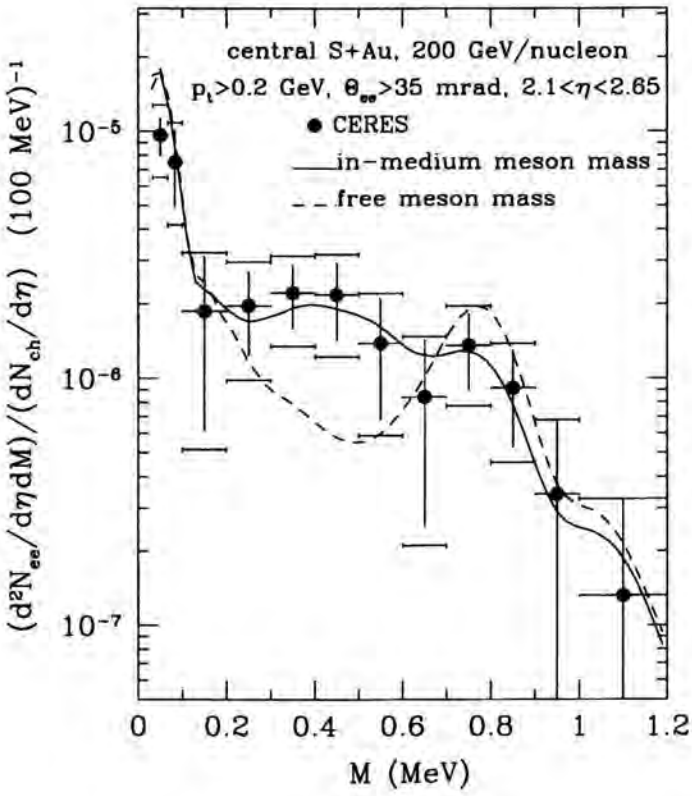

Figure 1. Ratio of dileptons to charged particles per rapidity interval in the CERN CERES experiments (Agakichiev et al. 1995) for 200 GeV/Nucleon S + Au collisions. The dashed line gives the theoretical results for free vector meson masses, whereas the full line gives those for density dependent masses (Li, Ko & Brown 1995, 1996; Li, Ko, Brown & Sorge 1997).

where ρ is the vector density. If, first, $m_\omega \to m_\omega^*$; i.e., m_ω becomes density dependent, and later $g_{\omega NN} \to g^*_{\omega NN}$ also becomes density dependent, so that

$$V \to \left(\frac{g^*_{\omega NN}}{m^*_\omega}\right)^2 \rho\,, \tag{7}$$

which actually decreases with density; this has strong consequences for dense matter.

Although, as we shall develop later, $g^*_{\omega NN}$ is expected to be quite density dependent, $g_{\sigma NN}$ should be taken to be independent of density, since our theory of the chiral restoration transition is a mean field one, and coupling constants change only at loop level. Since m^*_σ does decrease with density, the scalar mean field $S = -(g^2_{\sigma NN}/m^{*2}_\sigma)\rho_S$, where ρ_S is the scalar density, does become large in magnitude

at higher densities. This decrease in repulsive vector mean field and increase in magnitude of the attractive scalar mean field prepares the system for asymptotic freedom.

Rather direct evidence that m_ρ^*/m_ρ decreases with density as shown in equation (5) is given by the CERES dilepton experiments, as we now outline.

We show in Figure 1 results of dileptons in the recent CERES experiments (Agakichiev et al. 1995) for 200 GeV/Nucleon S + Au. Preliminary results for Pb + Au are similar (Ullrich, 1996). In these experiments one detects $e^+ + e^-$ dileptons from many agencies, most importantly those from decay of the ρ-meson,

$$\rho \rightarrow e^+ + e^- . \tag{8}$$

Although there is some spread in mass due to the high temperature, the invariant mass M of the dileptons, (M = summed total energy of the e^+ and e^-) tends to be close to the mass of the ρ-meson. The ρ-meson has a short lifetime, $\tau \sim 4/3$ fm/c, much shorter than the ~ 10 fm/c duration of the fireball. Thus most of the ρ-mesons decay while in the hot and dense nuclear medium. The large number of dileptons in the region of $M \sim 300 - 400$ MeV in Fig. 1 come from decay of ρ-mesons which had mass 300 MeV $< m_\rho^* <$ 400 MeV at the time they decayed.

III Determination of the equation of state of matter at supranuclear densities from the measured flow in relativistic heavy ion collisions

We shall discuss here relativistic heavy ion reactions such as Au + Au at energy 1 GeV/Nucleon. In these, densities $\sim 3\rho_0$ are reached, at temperatures $T \sim 70-80$ MeV. These temperatures are not much higher than those formed in the Helmholtz-Kelvin period of contraction of newly formed compact objects such as protoneutron stars. In particular, these temperatures are low enough so that the effect of the temperature on the effective masses of nucleons and mesons is not large. Therefore, our study of the equation of state in these reactions should be immediately relevant to neutron stars.

As a simple model for our discussion we shall use the Walecka linear $\sigma - \omega$ model (Serot & Walecka 1986). There are much improved models; e.g., see Furnstahl, Tang and Serot (1995). However, the important features are already contained in the linear $\sigma - \omega$ model, and it is easier to work with.

We now consider the flow produced in heavy ion reactions when two nuclei collide off center. The collision is shown in Figure 2.

The $\langle P_x \rangle$ is, of course, zero for y = 0 because of symmetry. If the EOS is very stiff, then high $\langle P_x \rangle$ will be produced as y increases, and large negative $\langle P_x \rangle$ will result as y

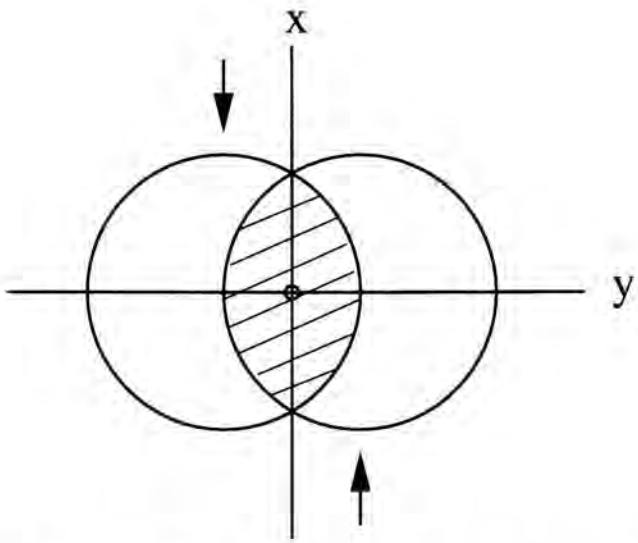

Figure 2. Nucleon flow. We look down on a collision of two equal size nuclei, say Au on Au, in the cm system. They collide off-center. The spectator nucleons, in the non-shaded region, go straight ahead and are discarded. The nucleons in the shaded region interact. Following the collision they will have a momentum distribution in the x direction, as shown in Figure 3.

moves to the left. The rate of increase of $\langle P_x \rangle$ with y at $y = 0$,

$$\left.\frac{\langle P_x \rangle}{dy}\right|_{y=0} = F \ , \tag{9}$$

i.e., the slope of the $\langle P_x \rangle$ at $y = 0$ is defined as the flow F. The stiffer the EOS, i.e., the greater the pressure in the shaded region, the greater the flow.

For Au-Au at 1 GeV/Nucleon collisions we can show that the main part of the flow develops at densities of $\rho \sim 3\rho_0$.

In all of the modern mean field models such as Furnstahl, Tang, and Serot (1995) the scalar attraction between nucleons is strong enough to bring the nucleon effective mass down to $m_n^* \sim 200 - 300$ MeV by $\rho \sim 3\rho_0$. On the other hand, the initial nucleon momentum is $p \simeq 1.7$ GeV/c, and even when equilibrated at this density, the Fermi momentum is $p_F \sim 400$ MeV. Thus, m_n^* is smaller than a typical momentum, so that the nucleons are, to a good approximation, massless. Corrections come only in order $(m_n^*/p)^2$, where p is a typical momentum.

Indeed, if one describes the finite density phase transition in the Nambu-Jona Lasinio model (Brown, Buballa & Rho 1996), which has the symmetries of QCD, then $m_n^* = 0$

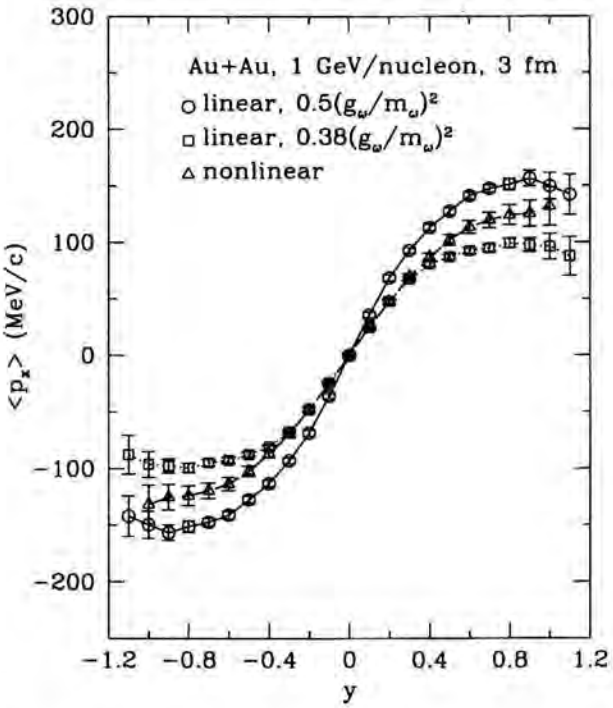

Figure 3. Flow in the Walecka linear $\sigma - \omega$ model (Serot & Walecka, 1986) which has $g_\omega^2/4\pi = 10.6$, but is reduced by the factors shown. Comparison is made with the nonlinear model of Ko, Li, and Wang (1987) and Ko and Li (1988). The Ko-Li model does not reproduce the dilepton data discussed in the last section, so we do not consider it to be a viable theoretical model. However, it does fit the flow, as measured in the EOS experiment (Partlan & EOS Collaboration 1995), so we consider the "nonlinear" curve to be essentially the empirically measured one.

for $\rho \sim 3\rho_0$, although inclusion of a bare quark mass of ~ 5 MeV is sufficient to bring m_n^* up to 100–200 MeV at $\rho \sim 3\rho_0$.

Consequently, the important point is that the flow in heavy ion collisions, which we discuss below, depends almost completely on the vector mean field. We now describe the measurement of the flow.

From the curves in Fig. 3 it might appear that the Walecka linear $\sigma - \omega$ model with g_ω^2/m_ω^2 reduced by a factor 0.38 is required by the flow. A major correction must, however, be made. In addition to the density dependence, an explicit momentum dependence must be introduced for the vector (and scalar) mean fields in order to fit nucleon-nucleus scattering (Cooper et al. 1993). Very roughly, this amounts to

multiplying the mean fields by a factor

$$f(\mathbf{p}) \sim \frac{1}{1 + E_{\rm kin}/m_n}, \tag{10}$$

where $E_{\rm kin}$ is the nucleon kinetic energy. For 1 GeV incident nucleons this gives a factor ~ 2 reduction, whereas for the equilibrated system formed later, this factor is not much less than unity. In going from the nonequilibrium glancing blow involved in the flow to the equilibrated system, the factor (10) must be included. Such inclusion (Li et al. 1997, in preparation) more than doubles the above factor of 0.38. Detailed calculations are given in Li et al. It turns out that the Furnstahl et al. (1995) EOS does quite a good job for the flow.

We are now ready to calculate the energy of a K^--meson at rest in neutron rich matter for $\rho \sim 3\rho_0$.

1. The nuclear vector mean field at $3\rho_0$ determined as discussed above, is $V_N \cong 675$ MeV. The K^- has one nonstrange antiquark. From G-parity the vector mean field is attractive. Since the vector field is assumed to couple to the baryon number in nonstrange quarks, the K^- vector mean field is

$$V_{K^-} \cong -225 \text{ MeV} \quad (\rho \sim 3\rho_0) . \tag{11}$$

2. The K^--neutron interaction is half of the K^--proton one, because of the differing couplings of the ρ-meson. For matter which is 85% neutrons, 15% protons, this means a correction of

$$\delta V_{K^-} = 53 \text{ MeV upwards} . \tag{12}$$

3. Short-range correlations raise the K^--energy ~ 30 MeV at $\rho \sim 3\rho_0$ (Waas, Rho & Weise 1996)

$$\delta\epsilon_{K^-} \cong +30 \text{ MeV} . \tag{13}$$

Finally, we discuss the scalar mean field. Brown and Rho (1996a) made the case that this could be obtained from the amount of lowering of the constituent quark mass of the nonstrange antiquark in the K^-. In our mean field model, the constituent quark mass is 1/3 of the nucleon effective mass. Furnstahl et al. (1995) find $m_n^*(3\rho_0) \cong 240$ MeV which means a constituent quark mass of

$$m_Q^* \simeq 80 \text{ MeV} \quad (\rho \sim 3\rho_0) . \tag{14}$$

The Furnstahl et al. (1995) EOS does quite a good job on the dileptons (Li et al. 1997, in preparation), although the low-mass production is slightly below the error bars,

indicating that the m_Q^* above is, if anything, too large. If we begin from $m_Q = 313$ MeV ($m_Q = \frac{1}{3}m_n$) then a scalar field

$$S_{K^-} = -(313 - 80)\ \text{MeV} = -233\ \text{MeV} \tag{15}$$

is needed to lower the constituent quark mass to 80 MeV. Adding (11), (12), (13), and (15) we obtain

$$M_{K^-}^* \cong 495 - 375\ \text{MeV} = 120\ \text{MeV}\ . \tag{16}$$

In fact, the electron chemical potential (Thorsson, Prakash & Lattimer 1994)

$$\mu_e = 214\ \text{MeV} \quad (\rho \simeq 3\rho_0) \tag{17}$$

so that it is energetically favorable by the density $\rho < 3\rho_0$ for electrons to change into K^--mesons

$$e^- \to K^- + \nu\ , \tag{18}$$

the neutrino leaving the neutron star.

In fact, the K^- *in-medium* energy is most sensitively measured in relativistic heavy ion reactions. The present ones reach densities up to $\sim 2.5\rho_0$. In Figure 4 we show the results of Cassing et al. (1997). In Ni + Ni at 1.8 GeV/Nucleon, many more K^--mesons are produced because of their lower *in-medium* energy, the productions being very roughly proportional to the Boltzmann factor $\exp[-(E_{K^-}/T)]$. The solid curve in Fig. 4 uses a parameterization for a K^- of zero momentum

$$m_{K^-}^*(\rho_B) = m_{K^-}\left(1 - 0.2\frac{\rho}{\rho_0}\right) \tag{19}$$

where m_{K^-} is really the K^- energy at zero momentum, the $m_{K^-}^*$ including effects of both scalar and vector fields.

As noted earlier, we expect the kaon condensation transition and the chiral restoration transition to both occur at $\rho_c \sim 3\rho_0$. They are by no means the same transition, as can be seen from the fact that the kaon condensation ρ_c can be changed by changing the electron chemical potential μ_{e^-}. In chiral restoration the nonstrange antiquark mass $m_{\bar{u}}^*$ goes to zero in the chiral limit at ρ_c. Not much happens to the mass m_s of the strange quark in the kaon, because the chiral restoration is chiefly in the nonstrange sector. The two transitions help, rather than compete, with each other, the kaon condensation one being aided by $m_{\bar{u}}^* \to 0$. There should be substantial binding energy from the hyperfine interaction between the $\bar{u}$ and strange quark s in the kaon, which will keep the $\bar{u}$ and s correlated in the K^--channel throughout the chiral restoration transition.

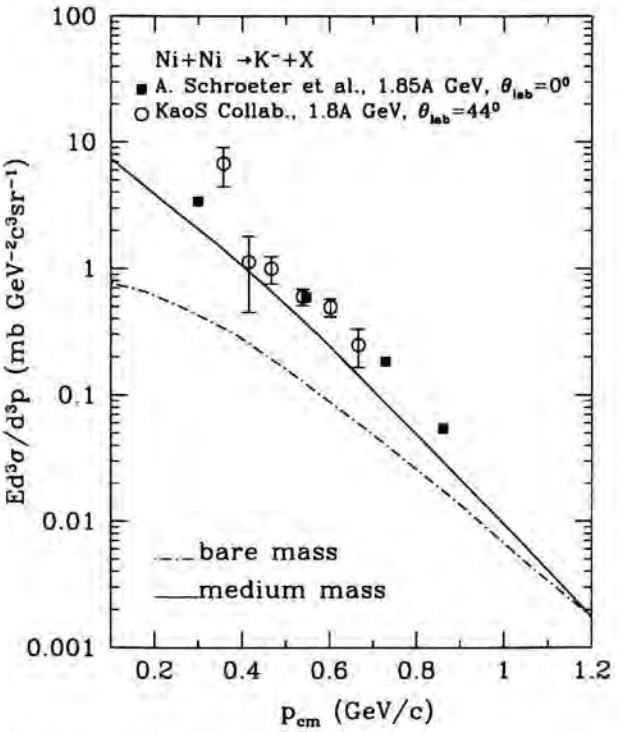

Figure 4. The inclusive cross section for K^- production as function of antikaon momentum in the nucleus-nucleus cms for K^--mesons at $\theta_{lab} = 0°$ for Ni + Ni at 1.85 GeV/Nucleon in comparisons with the experimental data from Schröter et al. (1994). Also shown is the preliminary data for Ni + Ni at 1.8 GeV/Nucleon from Senger (1996). The dashed line is calculated for the bare antikaon mass, the solid line for the *in-medium* mass. Note that the solid line with *in-medium* masses undershoots the data, indicating that the mass should drop more rapidly with ρ than in equation (18). On the other hand, the experiments are for nuclear matter rather than for neutron rich matter, where the K^- mass drops less rapidly, as shown by the δV_{K^-} in equation (12). We believe the parameterization (19) to be more appropriate for neutron rich matter than for nuclear matter.

IV Kaon condensation in neutron stars

In Figure 5 we show the behavior of the K^--meson energy ω_{K^-} as function of density in neutron-rich matter. We use the calculations of Thorsson, Prakash, and Lattimer (1994) with parameter $a_3 m_s = -222$ MeV, which has been determined since the calculations of these authors by lattice gauge calculations. (See Brown and Rho 1996 for a review.) This value of $a_3 m_s$ corresponds to Σ_{KN} = 343 MeV, where Σ_{KN} is the term which breaks chiral symmetry explicitly.

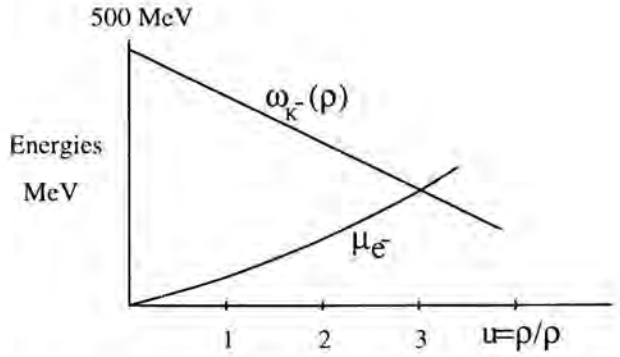

Figure 5. Schematic description of the kaon condensation found by Thorsson, Prakash, and Lattimer (1994). The K^- energy crosses the electron chemical potential at $\rho \simeq 3\rho_0$.

Once $\omega_{K^-}(\rho) = \mu_{e^-}(\rho)$, beyond this density the system energy can be lowered by electrons turning into K^--mesons

$$e^- \rightarrow K^- + \nu \,, \tag{20}$$

the neutrinos leaving the star.

V Consequences of a soft EOS for neutron star masses

We use as example of kaon condensed neutron stars the calculation of Thorsson, Prakash, and Lattimer (1994) with parameter $a_3 m_s = -222$ MeV. We take the compression modulus K_0 to be midway between the two values of 180 and 240 MeV which they use. Then the maximum neutron star mass is

$$(M_{\rm NS})_{\rm max} \sim 1.5 \ {\rm M}_\odot$$

as in equation (2). A kaon condensed neutron star is very compact, with a radius

$$R \sim 7 \ {\rm km} \,;$$

therefore a rotating one possesses rather less rotational energy $I\omega^2$ than would a neutron star with the same mass with the conventionally accepted $R \sim 10$ km. In Figure 6, taken from Thorsson et al. (1994) these results are shown. Note that the central densities of these neutron stars are great, $\rho_{\rm cent} > 10\rho_0$.

Given kaon condensation, the term neutron star is a misnomer, because in the kaon condensed region there are nearly as many protons as neutrons, the K^--mesons neutralizing the charge of the former. Brown and Bethe suggest using the name "nucleon star".

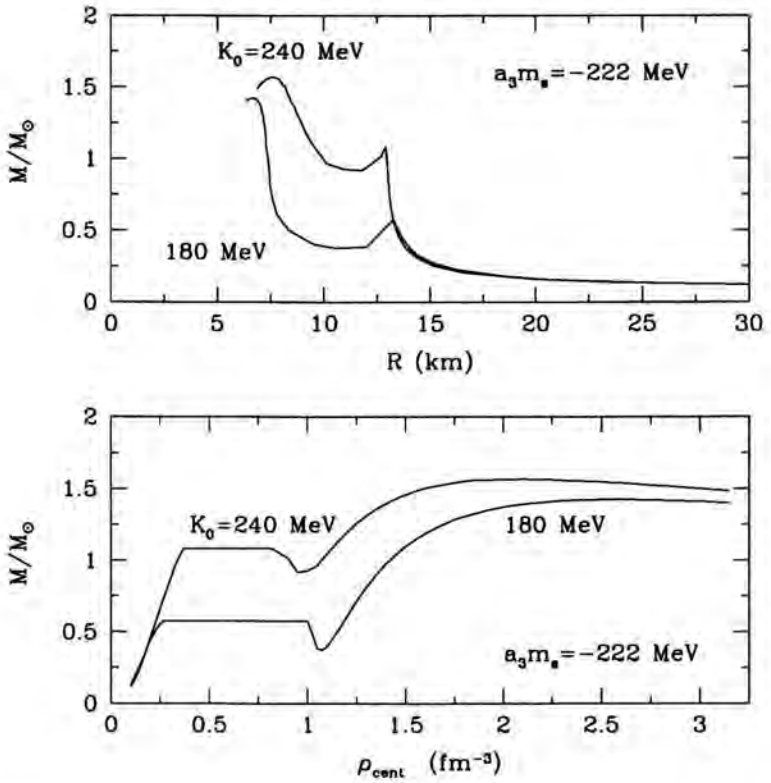

Figure 6. Mass curves for $a_3 m_s = -222$ MeV and $F(u) = u$. Lower panel: mass vs. central density. For the upper curve, the compression modulus is $K_0 = 240$ MeV, for the lower $K_0 = 180$ MeV. Upper panel: mass vs. radius for the same values of K_0.

It has been noted (Brown, Weingartner & Wijers 1996; see especially their Fig. 1) that in the evolution of pulsars from massive progenitors in either high mass X-ray binaries or in binary pulsars, the neutron star tends to end up at a mass not greater than 1.5 $M_\odot$.

In the case of SN 1987A, with progenitor of mass 18–20 $M_\odot$, the case has been made that the compact object (gravitational) mass did exceed 1.5 $M_\odot$, and that the core did go into a black hole (Brown & Bethe 1994). The kaon condensation can provide a scenario in which the compact object first emits neutrinos for some seconds, and then drops into a black hole (Thorsson, Prakash & Lattimer 1994; Brown & Bethe 1994).

The use of SN 1987A is, however, not so clear a proof that $\sim$ 1.5 $M_\odot$ is the maximum possible mass for a neutron star. It is possible that the neutron star existed for an hour or so. When the original shock wave enters the hydrogen envelope, it encounters an increased ρr^3, a situation which produces a reverse pressure which

sharpens into a reverse shock. Chevalier (1989) estimates that this reverse shock brings $\sim 0.15\ M_\odot$ back onto the compact object. Thus, even though most calculations of the gravitational mass of the compact object give masses $\sim 1.45 - 1.50\ M_\odot$, masses of up to $1.6 - 1.65\ M_\odot$ could be stable, and then sent into a black hole by the mass accretion from the reverse shock. This scenario applies only to the relatively dense blue supergiant progenitor of 1987A; a red giant progenitor would be much more diffuse, so that the mass accreted from the reverse shock would be only $\sim 0.01\ M_\odot$.

It is clear from my discussion here that in the scenario of kaon condensation, we would find it difficult to construct stable neutron stars of mass $1.6 - 1.65\ M_\odot$. In the coming year or two, data from relativistic heavy ion reactions should be much more accurate and precise. This will allow us to pin down our parameters better and achieve more definite results.

Acknowledgement

This work was supported by the U.S. Department of Energy under Grant No. DE-FG02-88ER40388.

References

Agakichiev, G. et al. 1995, Phys. Rev. Lett., 75, 1272
Brown, G.E. & Bethe, H.A. 1994, ApJ, 423, 659
Brown, G.E., Buballa, M. & Rho, M. 1996, Nucl. Phys. A, 609, 519
Brown, G.E. & Rho, M. 1991, Phys. Rev. Lett., 66, 2720
Brown, G.E. & Rho, M. 1996a, Nucl. Phys. A, 596, 503
Brown, G.E. & Rho, M. 1996b, Phys. Repts., 269, 334
Brown, G.E., Weingartner, J. C. & Wijers, R.A.M.J. 1996, ApJ, 463, 297
Cassing, W. et al. 1997, Nucl. Phys. A, submitted
Chevalier, R.A. 1989, ApJ, 346, 847
Cooper, E.D. et al. 1993, Phys. Rev. C, 47, 297
Furnstahl, R.J., Tang, H.-B. & Serot, B.D. 1995, Phys. Rev. C, 52, 1368
Ko, C.M. & Li, G.Q. 1988, Phys. Rev. C, 37, 2270
Ko, C.M., Li, G. Q. & Wang, R. 1987, Phys. Rev. Lett., 59, 1084
Kocič, A. & Kogut, J. 1995a, Phys. Rev. Lett., 75, 1272
Kocič, A. & Kogut, J. 1995b, Nucl. Phys. B, 455, 229
Li, G.Q. et al. 1997, in preparation
Li, G.Q., Ko, C.M. & Brown, G.E. 1995, Phys. Rev. Lett., 75, 4007
Li, G.Q., Ko, C.M. & Brown, G.E. 1996, Nucl. Phys. A, 606, 568
Li, G.Q., Ko, C.M., Brown, G.E. & Sorge, H., Nucl. Phys. A, submitted
Partlan, M.D. & EOS Collaboration 1995, Phys. Rev. Lett., 75, 2100
Schröter, A. et al. 1994, Z. Phys. A, 350, 101

Senger, P. 1996, APHN. S., Heavy Ion Physics, in press
Serot, B.D. & Walecka, J.D. 1986, Adv. Nucl. Phys., 16, 1
Thorsson, V., Prakash, M. & Lattimer, J.M. 1994, Nucl. Phys. A, 572, 693
Ullrich, Th. for the CERES Collaboration 1996, in Proc. Quark Matter '96, Nucl. Phys. A, in press
Waas, T., Rho, M. & Weise, W. 1966, Nucl. Phys. A, submitted
Zhang, J., DasGupta, S. & Gale, C. 1994, Phys. Rev. C, 50, 1617

Authors' Address

Department of Physics, State University of New York at Stony Brook, Stony Brook, NY 11794, USA

C.J. Pethick and D.G. Ravenhall

The Physics of Neutron Star Crusts

Abstract

The crust of a neutron star represents a small fraction of the star's volume and mass, yet it moderates or determines stellar processes, such as cooling and slowing down (glitches). The calculation of the upper density limit of the crust is discussed. An important ingredient in adjusting the nuclear effective interaction, the determination of the ground state energy of small neutron drops, is described. A simple planar approximation to the stellar constitutional equations appropriate for the crust is given.

I Introduction

Notwithstanding the fact that they constitute only a small fraction of the total stellar mass, the outer parts of a neutron star at densities less than about nuclear matter density are thought to play an important role in a number of observable phenomena. Perhaps the prime example is the sudden speed-ups, or glitches, in the pulse repetition rate of a number of radio pulsars. In models for glitches, the moment of inertia of a weakly coupled component, which in glitch models is often identified with superfluid neutrons in the crust of the neutron star, is an important parameter. In addition, the properties of matter in the outer parts of the star are a key ingredient in understanding surface thermal emission from neutron stars.

A striking development is the prediction that at densities just below that at which nuclei dissolve and the nuclear matter becomes spatially uniform, nuclei are not roughly spherical, as they are in laboratory situations, but rather they can be rod-like or plate-like (Lorenz, Ravenhall & Pethick 1993; Oyamatsu 1993). This is expected to have a strong influence on estimates of elastic properties of the star, and on pinning and transport properties that are important in modeling neutron star behavior.

Our purpose in this article is to review the underlying theoretical basis for estimates of fundamental properties of neutron stars, paying particular attention to the degree of confidence with which different quantities can be predicted. In particular we shall focus on the upper density limit to the neutron star crust, and the non-spherical phases. We begin by describing in Section II, the basic approaches used in calculating properties

of matter in neutron stars at subnuclear densities. Then in Section III we consider the question of how reliably one can predict the upper density limit at which nuclei exist. In Section IV we describe calculations for small clusters of neutrons, which are a valuable theoretical test system in the task of developing improved effective interactions. In Section V a simple planar approximation to the calculation of the crustal properties of a neutron star, the application of the nuclear physics we have discussed, is given. Section VI concerns open problems.

II Nucleon-nucleon interactions and the nuclear many-body problem

In neutron stars the proton fraction is very much less than in laboratory nuclei. The most neutron rich nuclei that can be investigated in the laboratory are close to the neutron drip line, and for all but the smallest nuclei the proton fraction at drip is about $1/3$. Consequently laboratory data on nuclear masses can be used directly in predicting properties of matter up to densities close to the neutron drip density, $\approx 4 \times 10^{11}$ gm cm^{-3}, as Haensel & Pichon (1994) demonstrate. However at higher densities matter in nuclei has an even smaller proton fraction, and the neutron liquid surrounding nuclei has no protons at all. The properties of such matter cannot be deduced directly from properties of systems that can be investigated experimentally. Rather one must resort to theory. In principle, one would like, as a first step, to develop a nucleon-nucleon interaction that can account for laboratory nucleon-nucleon scattering data, and then to use that interaction to predict, on the basis of many-body theory, properties of systems not directly accessible to experiment. Unfortunately, such a direct approach cannot be used, since for nuclei of the size encountered in neutron stars and for interactions that fit scattering data, it is at present not possible to perform the many-body calculations. Instead one has to adopt a two-stage approach in which one first constructs a simplified effective interaction, typically of the Skyrme type, which distills information about laboratory nuclei and about uniform neutron matter and possibly other neutron-rich systems whose properties can be calculated from many-body theory using interactions that fit two-body scattering data. The simplified interaction is chosen such that in Hartree-Fock theory it can account for the properties of known nuclei and the many-body calculations of the energy of uniform neutron matter.

Uniform nuclear matter is one of the most important examples of a system not accessible to experiment, but for which it is possible to make reliable calculations using many-body theory with a nucleon-nucleon interaction that fits scattering data. There is excellent agreement between the numerous calculations of the energy of neutron matter at subnuclear densities that have been made over the past quarter of a century using several different nucleon-nucleon interactions and a variety of different many-body techniques. The good understanding of the properties of neutron matter is due to the fact that at these densities the important interaction is the two-body one, which is well understood for the momentum transfers of interest, and the dominant correlations are

two-body ones. Higher-order correlations become important only at higher densities. The relative unimportance of the three-body interaction between nucleons is due to the low density, and to the fact that the probability of three neutrons being close is suppressed by the Pauli principle, which prohibits more than two neutrons (one for each spin state) being at the same point in space. In addition, the low density of the system is also responsible for the effects of three-body *correlations* being small, and consequently the important contribution to the energy arise from two-body correlations induced by the two-body interaction. Thus reliable answers for the energy can be obtained with any many-body method that treats these properly.

Armed with an expression for the energy of neutron matter, and with effective interactions of the Skyrme type that describe well the properties of laboratory nuclei, one is then in a position to construct an effective interaction which may be applied to calculate the properties of matter over a wider range of neutron excesses. The interaction of this type that we have used extensively in calculating properties relevant to neutron stars is the FPS21 interaction, the letters indicating that it is based on Friedman and Pandharipande's calculations of the energy of uniform neutron matter (Friedman & Pandharipande 1981), and that it is an interaction of the generalized Skyrme type. (The number 21 is for identification, with no physical significance.) Its properties are described in Pethick, Ravenhall & Lorenz (1995). The energy of Friedman and Pandharipande is plotted in Figure 1, together with the energies from FPS21 and some other effective interactions. We shall now describe how one may exploit effective interactions to make estimates of the inner boundary of the neutron star crust.

III The high-density boundary of the crust

The next question we wish to address is how reliably one may determine the inner boundary of the crust, given an effective nucleon-nucleon interaction. This problem is not a trivial one because of the complex character of the possible phases that are expected to exist near the boundary. However, as we shall now show, following Pethick, Ravenhall & Lorenz (1995), the location of the boundary can be determined rather precisely without the necessity of making calculations of the energy of phases with aspherical nuclei. This happy circumstance is due to the fact that the energy differences between the various possible phases are small compared with the total energy.

We now describe two relatively simple calculations that give upper and lower bounds on the density at which the transition to the uniform phase occurs. In the first of these we neglect Coulomb and surface energies in a generalized liquid drop description of the phases with nuclei. The problem of determining whether or not phases with nuclei have lower energy than the uniform phase is thus equivalent to determining whether equilibrium is possible between two bulk phases, with different densities and neutron excesses. This gives a lower bound on the energy of the non-uniform phase, since the Coulomb and surface energies that have been neglected can only increase the estimate

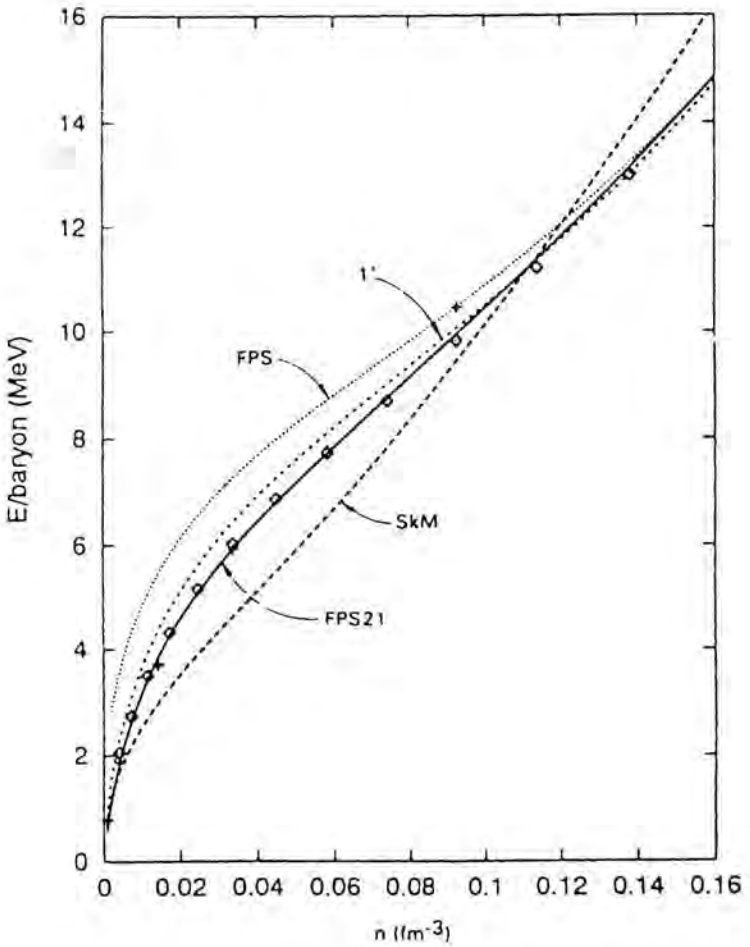

Figure 1. The energy per baryon of uniform neutron matter as a function of density. The diamonds are the values of Friedman and Pandharipande, with some additional points from the earlier work of Siemens and Pandharipande. The curves are from various effective interactions.

of the energy. Consequently, the highest density for coexistence of two phases gives an upper bound on the density at which the nonuniform phases can be the preferred state.

In the second approach one begins with the uniform phase and imagines lowering the density until matter becomes unstable to formation of infinitesimally small neutron and proton density waves. This would give the density at which the transition to the nonuniform state took place if it were a second-order transition. In fact, one knows on general grounds, from arguments given by Landau, that transitions of the liquid-gas

Table 1: Densities of Phase Transitions, and Pressure at Instability

Interaction	$n(Q)^a$ (fm^{-3})	n^b_{p-drip} (fm^{-3})	$n^c_{1\leftrightarrow 2}$ (fm^{-3})	p[n(Q)]^d (MeV fm^{-3})
SkM	0.0737	0.0769	0.0843	0.379
Skyrme 1′	0.0995	0.1066	0.1085	0.456
FPS	0.0957	0.1031	0.1056	0.373
FPS21	0.0983	0.1040	0.1081	0.500

[a] Onset of instability against proton clustering.
[b] Density of proton-drip in the two-fluid phase.
[c] Phase transition from two-fluid to one-fluid phase.
[d] Pressure at the onset of instability against proton clustering.

type (like the one we consider here) must be of first order. Thus the transition to the nonuniform phase must occur by a first-order transition, and this will occur at a higher density than that at which matter becomes unstable to a second-order transition. Thus the density at which a second-order transition will occur gives a lower bound on the density at which the transition to the uniform state occurs.

In Table 1 we show results for the conditions at the inner edge of the crust for a number of effective interactions. The first noteworthy point is that for a given interaction the upper and lower bounds are quite close, thereby giving one confidence in the result. The second point to notice is that the estimates of the bounds on the density of the boundary do not depend on the shape of nuclei at the inner boundary. A third point to notice is that the position of the inner boundary does depend on the equation of state used. As we have indicated, we believe the FPS21 interaction to be the most reliable one available, since it has been fitted most completely to the neutron matter data.

While the energy of uniform neutron matter is a valuable datum in constructing effective nucleon-nucleon interactions for neutron-rich matter, it does not enable one to pin down a number of the features of the effective interaction. One of these is the nature of the gradient terms in matter which is not isospin symmetric, and another is the spin-orbit interaction. Both of these may be investigated from a fundamental point of view by considering the energy of drops of matter composed entirely of neutrons, which is the topic of the next section.

IV Neutron drops

Effective interactions of the Skyrme type that are to be used to calculate crustal properties contain functionals of the densities, and parameters, whose values a knowledge of the properties of uniform neutron matter is insufficient to test: in particular, there are terms that depend on density derivatives, and there is a spin-orbit interaction. The density-gradient terms are related in a unique manner to the kinetic-density terms, for an interaction of zero range (delta-function interaction), the basic simplifying feature of such interactions, and the kinetic-density terms are well determined from the calculated properties of neutron matter at a range of densities and temperatures. (The physical quantity at question is the neutron effective mass in the neutron matter.) Consequently it would indeed be unfortunate if they were found to be incorrect. Studies of the nuclei ^{16}O and ^{15}N using the Cluster Variational Monte Carlo method (CVMC) and realistic inter-nucleon interactions have indicated that the spin-orbit splitting of the $J = 1/2$ and 3/2 states of ^{15}N comes only partially from two-nucleon correlations. Almost half of it appears to be due to correlations and interactions involving three or more nucleons. Because of the Pauli-principle suppression of three-neutron interactions mentioned earlier, one would expect therefore that spin-orbit effects in neutron systems would be weaker by a factor of order two compared with those for ordinary nuclei. Finite neutron systems that involve varying density are called for, and it is desirable that they contain as large a number of neutrons as possible, since the Hartree-Fock (HF) method employed with the effective interactions is more reliable for such systems.

Methods employed in exploring the predictions of realistic inter-nucleon interactions have usually been variational: trial wavefunctions for clusters of nucleons have their parameter values adjusted to minimize the Hamiltonian. In the CVMC mentioned in connection with ^{16}O and ^{15}N, the integrals involved are performed by the Monte Carlo method. The Green's Function Monte Carlo method (GFMC) uses the output of variational calculations as a starting wavefunction $|\Psi_V\rangle$ and improves on it. The principle is based on the following equation:

$$|\Psi_0\rangle = \lim_{\tau\to\infty} e^{-H\tau}|\Psi_V\rangle = \sum_n e^{-E_n\tau}|\Psi_n\rangle\langle\Psi_n|\Psi_V\rangle \tag{1}$$

where $|\Psi_n\rangle$ are the exact eigenstates of the Hamiltonian H, with corresponding energies E_n. As τ becomes larger, the ground state term of the sum, $|\Psi_0\rangle$, becomes the dominant one. In practice the exponential is applied in small increments, to permit approximation of the exponential, and the process takes the form of an integral equation

$$\Psi(R, \tau + \Delta\tau) = \int G(R, R')\Psi(R', \tau)\, \mathrm{d}R', \tag{2}$$

where $\Psi(R, \tau) = \langle R|\Psi_0\rangle$, R represents all of the nucleon coordinates, and

$$G(R, R') = \langle R|e^{-(H-E_0)\Delta\tau}|R'\rangle \tag{3}$$

is the Green's function. The manner in which the exponential operator in (3) is applied, including all of the operator dependence contained in H, is the heart, and art, of the method. The GFMC process permits improvement of the wavefunction beyond, and to some extent independent of, the constraints necessarily imposed on the variational wavefunction. For a Fermi system, however, the presence of nodes in the ground state wavefunction limits absolutely the total value of τ for which the equation may be usefully applied, and thus the improvement in accuracy over the variational starting point that can be achieved.

Although designed for few-body systems, the GFMC method can by careful program design be made to handle a 'nucleus' containing up to six nucleons, or up to eight neutrons. (The absence of isospin complexity in the latter case permits including more particles.) Nuclei composed entirely of neutrons do not exist in nature, since neutron matter is not self-bound, but as theoretical constructs they can exist inside an attractive external potential. This potential can be adjusted so as to provide a system that exhibits the properties of interest to us. Eight neutrons in a spherically symmetric confining environment have a shell structure that mirrors the neutrons in ^{16}O, with two neutrons in the $1s_{1/2}$ shell, four in the $1p_{3/2}$ shell and two in the $1p_{1/2}$ shell. The confining potential is made shallow enough that without the neutron-neutron interaction only the first two neutrons would be bound. The fact that the nucleus ^{8}n is bound in the shallow potential because of the $n-n$ interaction means that the behavior of this and lighter nuclei will reveal properties that are due to that interaction.

The GFMC energy and neutron density distribution of ^{8}n (Pudliner et al. 1996) are data with which the effective interaction can be tuned so far as the effect of varying density is concerned. The effective-interaction version of ^{8}n can be made to agree with both properties simultaneously by keeping unchanged the already determined gradient terms, and by adding a new delta-function term in the interaction that depends on the Laplacian of the density, a term that would not contribute to the properties of uniform neutron matter. The GFMC energies of the ground ($J = 1/2$) and first excited ($J = 3/2$) states of ^{7}n determine the p-shell spin-orbit splitting, which is found to be only about half of that expected from the usual density-independent spin-orbit part of the effective interaction. The remedy is to have the spin-orbit interaction depend on the nucleon density in such a way that it is suitably weakened when only one species of nucleon is present.

Recent GFMC results on the energy of the ground state of ^{6}n (Smerzi, Ravenhall & Pandharipande 1997) lead to a value of the pairing energy $\Delta_{\rm pairing} = (1/2)(E_{8n} - 2E_{7n} + E_{6n})$ for a pure neutron system. Customarily Skyrme-type effective interactions as applied to closed-shell nuclei or to infinite matter are represented by an energy functional of the matter and kinetic densities. Those one-body quantities vary smoothly with nuclear mass number, so that if, incorrectly, the energy functional is used to calculate the effective-interaction energies of all of the neutron nuclei, the resulting pairing energy is very small. If, however, the non-closed shell nuclei ^{7}n and ^{6}n are treated more correctly, by calculating the energy contributions

of the unclosed shells directly from the Skyrme t-matrix, one finds quite acceptable agreement with Δ_{pairing} from the GFMC calculations. Since the calculation of the ^{6}n energy using the effective interaction was made with no parameter adjustments, this result constitutes a useful test of the consistency of an effective interaction to reproduce the 'known' properties of low-density neutron systems. (The more correct calculations just discussed affect appreciably the energy of the ^{7}n states, but modify only slightly the calculated spin-orbit splitting.)

The modifications introduced in the effective interaction to bring about agreement with neutron-system properties are designed so as not to affect appreciably the properties of nuclei in the valley of stability. They may be expected to predict larger effects on properties of neutron drip-line nuclei. The systems encountered in the neutron-star inner crust, certainly now need further theoretical explorations.

V Crustal Engineering

The kind of matter for which our non-relativistic methods are useful occurs in the neutron star crust. This matter, which consists of neutron-rich nuclei, of various shapes and in various configurations, immersed in a neutron liquid, is believed to undergo a phase transition into a uniform fluid of neutrons and protons at a density somewhat less than nuclear saturation density. The depth below the neutron-star surface at which this occurs is $\lesssim 1$ km, and the fraction of the total mass that is in this outer skin is $\sim 2\%$. As with dynamics at the earth's surface, the region of interest appears locally as a plane. One can consider an appropriate technique for handling this rather special case of gravitational attraction in the Newtonian limit. Let us ask, for a spherically symmetric star of given mass M and radius R, how can one explore crustal properties without knowing in any detail what the interior structure of the star is? (General relativistic effects can cause very appreciable modifications, which we will give later, but for the essentially non-special-relativistic crust matter, the basic physics is contained in the Newtonian approximation.)

Static equilibrium of this assumed spherical mass distribution is given by pressure balance:

$$\frac{\mathrm{d}P}{\mathrm{d}r} = -\rho g(r), \tag{4}$$

where the local gravitational acceleration is

$$g(r) = \frac{\mathrm{G}m(r)}{r^2}. \tag{5}$$

The mass interior to the radius r, $m(r)$, can for the last couple of percent of the mass be approximated by the total mass M, and the radius r by the total radius R. Of radial dependences, only those of $\rho(r)$ and $P(r)$ remain, and equation (4) can be integrated

between two depths z_1 and z_2 (where the radial coordinate r has been replaced by z, the depth below the surface, $z = R - r$) to give

$$\int_1^2 \rho(r)\, dz \approx \frac{R^2}{GM} \int_1^2 \mathrm{d}P. \tag{6}$$

If z_1 is taken to be at the stellar surface, and z_2 at the boundary where the solid crustal matter dissolves, the left side becomes the column density of the crust, and leads to an approximation for the crustal mass:

$$\Delta M_{\mathrm{crust}} \approx 4\pi R^2 \int_{\mathrm{surface}} \rho \, \mathrm{d}z = \frac{4\pi R^4}{GM} P_{\mathrm{boundary}}. \tag{7}$$

The main effect of general relativity for the crustal region is to modify the $1/r^2$ of the gravitational attraction in (5), the result being to divide the right sides of (6) and (7) by $\Lambda(R) = 1/(1 - 2GM/Rc^2)$, the square of the red-shift factor. With this modification, (6) provides for a given M, R and equation of state an implicit relationship for the crust thickness. It can be used more generally to map out the matter properties of the crust as a function of the depth. Provided that M and R are assumed known, one may thus examine the structure of the crust without requiring knowledge of the equation of state in the interior of the star.

Using similar considerations on the general-relativistic equations for a slowly rotating star, one may also obtain an expression for the moment of inertia of the crust (Ravenhall & Pethic 1994), whose magnitude determines the size of the rotational speed-ups or glitches observed to occur at regular intervals in the rotation rates of younger pulsars:

$$\Delta I_{\mathrm{crust}} \approx \frac{2}{3} \Delta M_{\mathrm{crust}} R^2 \frac{1 - 2GI/R^3c^2}{1 - 2GM/Rc^2}, \tag{8}$$

where I is the stellar total moment of inertia. That quantity depends on the entire structure of the star, of course. For any given equation of state the constitutional equations whose Newtonian approximation we have considered may be solved in their full general relativistic form. For a wide selection of such equations of state, the moments of inertia may be shown to have a remarkably simple dependence on M and R, for masses $M \sim 1$–2 solar masses:

$$I \approx 0.21 \frac{MR^2}{1 - 2GM/Rc^2}. \tag{9}$$

One may recall that for a non-relativistic, incompressible ball, $I = (2/5)MR^2$. Neutron stars, however, are not incompressible, and general relativity does matter.

VI Concluding remarks

From the discussion we have given above, it may be seen that the physics of the crusts of neutron stars is relatively well understood compared with what is the case for the deep interior. The fundamental reason for this is that the relevant properties of nucleon-nucleon interactions are relatively well characterized, and the effects of nucleon-nucleon correlations can be calculated in detail. There are, however, still many unsolved problems, and we now mention some of these.

The first is whether the nonspherical phases are the thermodynamically stable ones. They are if one uses the FPS21 interaction, which is the one which we regard as being the most realistic available at present, but it is clearly important to improve estimates of surface energies using the information now becoming available from calculations of neutron drops in order to calculate the surface and Coulomb contributions to the energies of the nonspherical phases.

Another set of problems concerns superfluidity in the inner crust, where nuclei coexist with a neutron liquid. In the part of the inner crust near the inner boundary, where most of the mass in the crust resides, the superfluid coherence length is larger than the characteristic nuclear dimensions. Consequently, superfluid gaps are not well approximated by their values in bulk matter. Calculations of gaps are currently under way using a variety of techniques (Barranco et al. 1997; De Blasio et al. 1998).

A further set of issues arises when one turns to elastic properties of phases with non-spherical nuclei, which enter in important ways in problems of energy storage in the crust, including plate tectonics, and other aspects of the dynamics of the crust. Elastic properties of non-spherical phases have recently been considered in Pethick & Potekhin (1997).

Thus, while basic aspects of the static properties of the inner part of the crust, such as the equation of state, and the density at which it ends, can be predicted reliably, there is still much scope for improving understanding of other aspects of crustal behavior, including especially superfluid and dynamical properties.

Acknowledgements

This work was supported in part by the U. S. National Science Foundation under grants AST93-15133, AST94-21039, and AST96-18524, and by NASA under grant NAGW-1583.

References

Barranco, F. et al. 1997, Phys. Lett. B, 390, 13
De Blasio, F. et al. 1998, in preparation
Friedman, B. & Pandharipande, V.R. 1981, Nucl. Phys., A361, 502
Haensel, P. & Pichon, B. 1994, A&A, 283, 313
Lorenz, C.P., Ravenhall, D.G. & Pethick, C.J. 1993, PRL, 70, 379
Oyamatsu, K. 1993, Nucl. Phys., A561, 431
Pethick, C.J., Ravenhall, D.G. & Lorenz, C.P. 1995, Nucl. Phys., A584, 675
Pethick, C.J. & Potekhin, A. 1997, preprint
Pudliner, B.S. et al. 1996, PRL, 76, 2416
Ravenhall, D.G. & Pethick. C.J. 1994, ApJ, 424, 846
Smerzi, A., Ravenhall, D.G. & Pandharipande, V.R. 1997, Phys. Rev. C, submitted

Authors' Addresses

C.J. Pethick: Nordita, Blegdamsvej 17, DK-2100 Copenhagen Ø, Denmark

C.J. Pethick and D.G. Ravenhall: Department of Physics, University of Illinois at Urbana-Champaign, 1110 West Green Street, Urbana, Illinois 61801-3080, U.S.A.

A.B. Link and B.R.I. Epstein

Thermally-Driven Glitches

Abstract

During a neutron star's evolution, starquakes and other heating processes increase the frictional coupling between the crust and the neutron superfluid the star is expected to contain. We examine the thermal and dynamical response of an isolated neutron star to a sudden perturbation of the inner crust temperature, and show that internal heating can trigger sudden spin jumps resembling pulsar glitches.

I Introduction

Glitches have now been observed in more than 20 pulsars. Typical glitches in mature pulsars, e.g., the Vela pulsar, involve fractional jumps in the rotation rate of $\sim 10^{-6}$. Glitches in the relatively young Crab pulsar, on the other hand, are typically a factor of 10 to 100 smaller. The Crab glitch of 1989 was the first such spin-up to be partially time-resolved; following a jump in the spin rate (occurring in < 2 hours), the pulsar completed the remainder of the spin-up over ~ 1 d (Lyne, Smith, & Pritchard 1992; see Figure 2). By contrast, the Vela pulsar has shown very different behavior in at least one case. The giant "Christmas glitch" of December 24, 1989 (1.8×10^{-6} fractional spin-up), which occurred during an observing session, could not be time-resolved; most, or possibly all, of the spin-up took place in less than two minutes (McCulloch et al. 1990; see Fig. 2). Giant glitches seem to be typical behavior among mature pulsars, while the Crab appears to be unique in the smallness of its glitches.

Glitches might represent variable coupling between the neutron star crust, whose spin rate we observe, and the more rapidly rotating neutron superfluid the star is expected to contain. The coupling is related to the dynamics of the array of *vortices* that thread a rotating superfluid. The rotational state of the superfluid is determined by the distribution of vortices with respect to the rotation axis; hence, for the superfluid to change its angular momentum, vortices must move radially. In the inner crust, however, interactions between nuclei and vortex cores tend to *pin* the vortices to the lattice, nearly fixing the angular velocity of the superfluid there (see, e.g., Anderson & Itoh 1975). The inner crust superfluid is coupled to the crust to the extent that vortices can move through the lattice by thermally-activated *vortex creep* (see, e.g., Alpar et al. 1984; Link, Epstein, & Baym 1993). As the crust slows under the magnetic torque, the inner crust superfluid, because it is pinned, rotates more rapidly than the crust by

as much as ~ 1 rad s^{-1}. The excess angular momentum residing in the inner crust superfluid is more than enough to drive glitches (Anderson & Itoh 1975; Ruderman 1976). Here we show that sudden internal heating, perhaps from a modest starquake, can trigger angular momentum transfer to the crust, producing spin-up events that resemble pulsar glitches.

II The model

As a neutron star spins down, sudden structural relaxations, *starquakes*, are expected to occur which heat the crust (Ruderman 1969; Baym & Pines 1971). Owing to the enormous rigidity of the crust, these events should produce significant heating; the elastic energy released in a starquake could exceed 10^{42} ergs (see, e.g., Baym & Pines 1971). The seismic modes excited in the inner crust are efficiently damped by electron shear viscosity over time scales of ~ 1 minute, indicating that a large fraction of the energy released in a starquake goes quickly into heat. Starquakes could occur in accreting systems as well—matter accumulates on the surface until gravitational forces on the accreted matter exceed the yield strength of the neutron star crust.

The inner crust superfluid is very sensitive to starquake-generated temperature perturbations. The frictional coupling of the superfluid to the crust is a sensitive function of temperature (Link, Epstein, & Baym 1993), and so even small heating events, when processed by the superfluid-crust system, can noticeably affect the star's spin behavior. In particular, *sudden* inner crust heating from a moderate starquake would dramatically increase the frictional coupling between the superfluid and the crust, bringing the two components closer to corotation (see, e.g., Greenstein 1979); the superfluid spins down, while the crust spins up. We conjecture that glitches originate from the sudden deposition of thermal energy in the inner crust. Preliminary work on this question has been presented by Link & Epstein (1996).

III Dynamical description

Following a starquake, a thermal wave propagates through the crust over a thermal diffusion time scale. The resulting angular momentum transfer from the superfluid to the crust is controlled by the extent to which the pinned vortices can unpin through thermal activation and move through the inhomogeneous environment of the inner crust lattice (Link & Epstein 1991; Link, Epstein, & Baym 1993; Chau & Cheng 1993). The vortex mobility depends on the vortex-nucleus interaction potential (itself a function of density), the temperature, and the velocity difference between the superfluid and the crust. A description of the response of a star to internal heating would require solving for the superfluid hydrodynamics coupled to the propagation of the thermal wave and the motion of the crust. In general, this problem is three-dimensional and highly nonlinear.

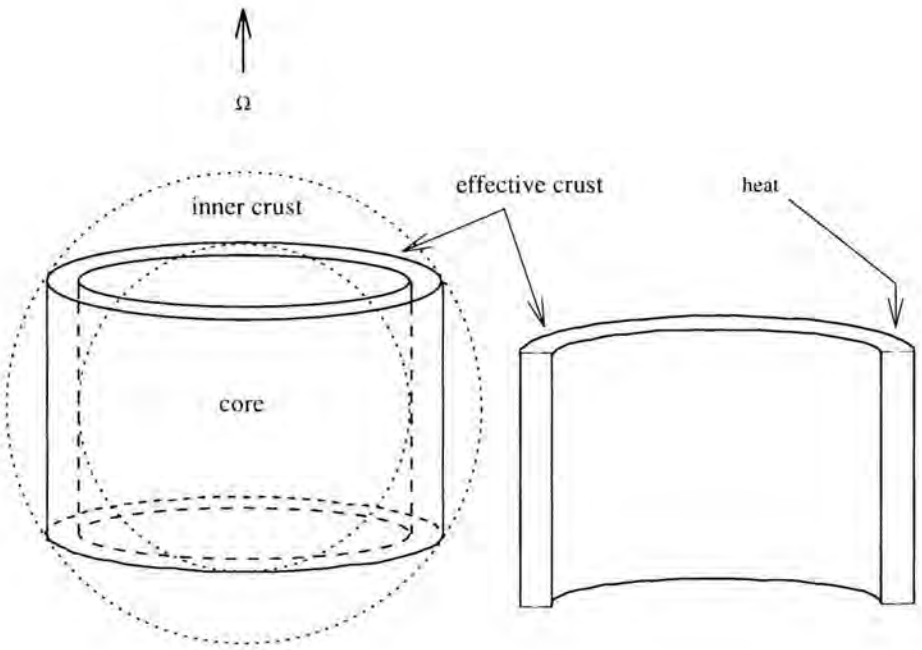

Figure 1. Model geometry. The inner crust superfluid is modeled as a cylindrical shell. Heat is deposited in a thinner cylindrical shell.

As a first step in addressing this problem, we have modeled the superfluid-crust system making several simplifying approximations (see Link & Epstein 1996 for details). First, we model the inner crust superfluid as a cylindrical shell of constant density (see Figure 1). We choose this geometry because the greatest contribution to the moment of inertia of the inner crust superfluid is in a band about the equator of the star. Second, we consider heating of a thin region within the cylindrical crust. Third, we neglect the generation of additional heat through friction between the superfluid and crust. We also assume that the core superfluid is rigidly coupled to the crust over short time scales ($\lesssim 10$ s), as recently argued by Abney, Epstein, & Olinto (1996) in their analysis of Vela's Christmas glitch; the effects of a more weakly-coupled core are straightforward to include.

For a given nuclear matter equation of state, the only important free parameters of the model are: 1) the initial energy deposition, 2) a coupling parameter that measures the frictional interaction between the superfluid and the normal matter (related to the vortex pinning energy per nucleus), and 3) the unperturbed inner crust temperature.

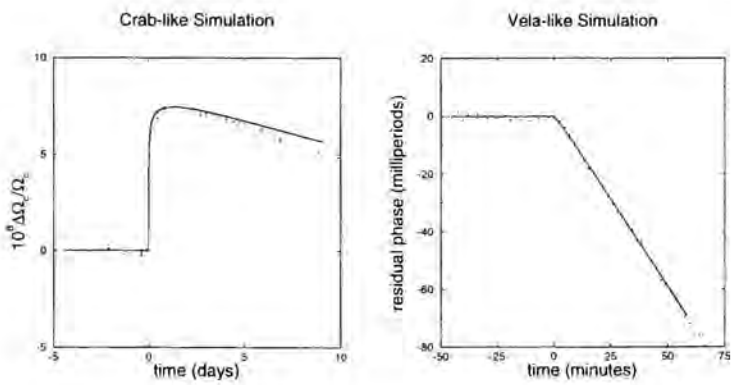

Figure 2. *Left panel:* simulation of the response of the Crab pulsar following the deposition of 2.2×10^{42} ergs in the inner crust. Shown is the excess spin rate relative to the pre-glitch extrapolated spin rate. Data from the large 1989 glitch are shown. *Right panel:* simulation of the response of the Vela pulsar following the deposition of 1.5×10^{42} ergs in the inner crust. Shown are the pulse arrival times minus the values extrapolated from a pre-glitch fit. Data from the Christmas glitch are shown.

IV Results

To illustrate the consequences of sudden inner crust heating, we show the results of two numerical simulations intended to represent the Crab and Vela pulsars. The models of the two stars differ only in the unperturbed spin rate, spin-down rate and inner crust temperature. Internal temperatures were calculated from surface emission data; we take 18 keV and 5 keV for the Crab and Vela, respectively. The value of the coupling parameter for the effective crust is the same for both simulations and was selected to give good fits to the Crab and Vela glitch data; its value is consistent with first-principles calculations (see, e.g., Epstein & Baym 1988) and observational constraints from surface emission measurements (see, e.g., Shibazaki & Lamb 1989; Van Riper, Link & Epstein 1995).

A deposition of $\sim 2 \times 10^{42}$ ergs in our simulation of the Crab pulsar triggers a small spin-up, taking place over ~ 1 day, remarkably similar to that seen during the partially time-resolved Crab glitch of 1989 (see Fig. 2). A slightly smaller energy deposition (1.5×10^{42}) ergs in the simulation of Vela produces a much larger and faster glitch, taking place over minutes, similar to the Christmas glitch (see Fig. 2). The differences in glitch magnitude and time scale between these two simulations are due mainly to the strong temperature dependence of the vortex mobility. For a star with a lower

temperature, e.g., Vela, a given energy deposition produces a much larger relative temperature change than in a hotter star. As a result, more vortices move, and they do so at a higher average velocity. The resulting spin jump is larger and faster than for a hotter star. Moreover, the higher thermal diffusivity of a cooler star causes the glitch to end sooner.

V Concluding remarks

The key result of this preliminary work is that *energy depositions of comparable magnitude to those expected from starquakes produce sudden spin jumps resembling pulsar glitches*. Moreover, the simple, one-dimensional model we have presented accounts naturally for the observed differences in glitch behavior between the Crab and Vela pulsars as being related to internal temperature alone. One prediction of this model is that the spin-up time scale for a given star should decrease with glitch magnitude. In the simulation of the Vela pulsar, for example, a glitch of $\Delta\Omega/\Omega = 10^{-6}$ occurs over minutes, while a glitch of 10^{-8} takes place over ~ 1 d. Data on the spin-up time scales for Vela's smaller glitches would be valuable in establishing the viability of this model.

If glitches are indeed triggered by internal heating, each spin-up is followed by the emergence of a thermal wave from the star's surface. Frictional heating between the superfluid and crust as the glitch proceeds augments the initial energy deposition. The magnitude and time scale of enhanced surface emission are sensitive to the nuclear matter equation of state and the depth of energy deposition. If the equation of state is fairly soft, and the star's surface temperature is 10^6 K, an energy deposition of 5×10^{42} ergs at an inner crust density of 3×10^{13} g-cm^{-3} would produce a 9% surface temperature enhancement peaking ~ 8 days after the glitch (Van Riper, Epstein & Miller 1991). Surface emission enhancements of this magnitude should be detectable with the ROSAT HRI, AXAF and possibly ASCA. A Target of Opportunity program led by F. Seward is already in place utilizing the ROSAT HRI.

References

Abney, M., Epstein, R.I. & Olinto, A. 1996, ApJ, 466, L91
Alpar, M.A., Anderson, P.W., Pines, D. & Shaham, J. 1984, ApJ, 276, 325
Anderson, P.W. & Itoh, N. 1975, Nature, 256, 25.
Baym, G. & Pines, D. 1971, Ann. Phys., 66, 816
Chau, H.F. & Cheng, K.S. 1993, Phys. Rev. B, B47, 2707
Epstein, R.I. & Baym, G. 1988, ApJ, 328, 680
Greenstein, G. 1979, ApJ, 231, 880
Link, B. & Epstein, R. I. 1991, ApJ, 373, 592
Link, B. & Epstein, R.I. 1996, ApJ, 457, 844

Link, B., Epstein, R.I. & Baym, G. 1993, ApJ, 403, 285
Lyne, A.G., Smith, F.G. & Pritchard, R.S. 1992, Nature, 359, 706
McCulloch, P.M. et al. 1990, Nature, 346, 822
Ruderman, M. 1969, Nature, 223, 597
Ruderman, M. 1976, ApJ, 203, 213
Shibazaki, N. & Lamb, F.K. 1989, ApJ, 346, 808
Van Riper, K.A., Link, B. & Epstein, R.I. 1995, ApJ, 448, 294
Van Riper, K.A., Epstein, R.I. & Miller, G.S. 1991, ApJ, 381, L47

Authors' Addresses

A.B. Link: Montana State University

A.B. Link & B.R.I. Epstein: Los Alamos National Laboratory

A. Muslimov and D. Page

Delayed Switch-on of the Vela Pulsar?

Abstract

We suggest that our modelling of the low braking indices of the young radio pulsars may be relevant to the recently reported anomalously low value of the braking index for the Vela pulsar (Lyne et al. 1996). We constrain the main unknown parameters, the initial spin period and historic age of the associated neutron star.

I Introduction

Recently Lyne et al. (1996; hereafter LPG-SC96) reported an analysis of the rotation rate of the Vela pulsar (known for its records in glitching activity) over 25 years from which they derived a very small value of the braking index $n = 1.4 \pm 0.2$. Earlier, we had suggested a model of field "submergence" (Muslimov & Page 1995, 1996; hereafter MP95, MP96) that may self-consistently explain braking indices $1 \lesssim n \lesssim 3$ in young pulsars. Our model favours the hypothesis that new born neutron stars (NS) may have low magnetization (see Michel 1994), and that their magnetic moments grow as they age. Though the very possibility that temporal evolution of the magnetic moment of a NS may affect pulsar braking index is known from the first theoretical works on pulsars (see, e.g., Manchester & Taylor 1977 and references therein), we suggested a concrete (and alternative to some other available explanations [see, e.g., Blandford & Romani 1988]) physical scenario that results in a secular increase in the magnetic moment of a NS which, in turn, may naturally explain the measured braking indices (that seem to be the least corrupted by timing noise) $n = 2, 2.5$, and 2.8 of the three youngest pulsars PSR 0540−69, 0531+21 (Crab), and 1509−58, respectively. The Vela pulsar obviously does not fit in this category of pulsars with relatively low timing noise and glitching activity, and if the analysis performed in LPG-SC96 is correct, it certainly shows an anomalously low braking index for its age.

In this paper we present the principal results of our calculations made for the parameters of the Vela pulsar within our field submergence model. Our modelling self-consistently constrains the initial spin period and the physical age of the Vela pulsar.

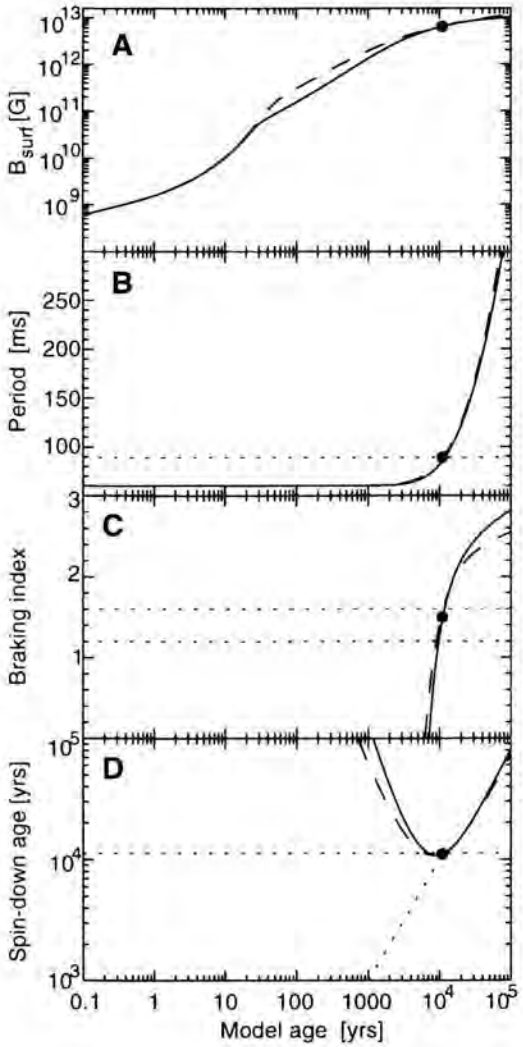

Figure 1. *(A)* Surface field strength, *(B)* pulsar period, *(C)* braking index, and *(D)* spin-down age in our model with two cooling histories which reproduce the observed value of the Vela pulsar temperature: fast cooling with a kaon condensate without *(solid lines)* and with *(dashed lines)* frictional heating in the inner crust (Page 1997). The dots on curves show the values obtained by our modelling, and the horizontal dotted lines point to the observational values. The inclined dotted line in *(D)* corresponds to the spin-down age = model age line.

II Theoretical model and results

We exploit the theoretical model described in MP95, MP96, and we shall not reproduce it here. Our calculations have been performed for a model of 1.4 $M_{\odot}$ NS constructed with the Friedman-Pandharipande equation of state and two different cooling scenarios best fitting the surface temperature measurements for the Vela pulsar (Page 1997). Details of our modelling of the magnetic field evolution will be described in a separate publication. Results are shown in Figure 1. Since the value of the braking index is very sensitive to the depth of submergence of the magnetic field, it is essential that, given the derived value of the braking index, we immediately restrict the range of depths of submergence in our calculations. This allows us to tune the field evolution (especially its latest stage) of a NS. Then, by varying the values of the initial spin period and surface magnetic field, we fit all the observed and derived pulsar parameters. The low value of the braking index necessarily occurs near the very minimum of curve shown in Fig. 1D. It is this fact that puts yet another restriction that the initial spin period of a NS should be very close to its present spin period, and that the historic age of a NS should be comparable to its spin-down age.

III Conclusions

Our main conclusions for the Vela pulsar are:
(1) The anomalously low braking index is, in principle, consistent with the hypothesis that the surface value of the stellar dipole magnetic field grows as the NS ages. It is the diffusion of the initially submerged magnetic field up through the crust (MP95, MP96) that causes the secular growth of surface magnetization.
(2) The initial spin period was $\sim$ 60–70 ms.
(3) The depth of submergence of the magnetic field of the NS at birth may amount to $\sim$ 200 m.
(4) The low braking index inevitably results in that the historic age (according to our calculations $\sim$ 12,000 yr) of the pulsar may only slightly exceed its spin-down age ($\sim$ 11,300 yr).
This may potentially contradict the estimated age (which is still greatly uncertain) of the Vela supernova remnant and result in subsequent revision of the field submergence model for the Vela pulsar.

Acknowledgements

This work is supported under the Senior Research Associateship at the LHEA, NASA/GSFC, and under grants No. IN105495 (DGAPA-UNAM) and 2127P-E9507 (Conacyt) at the University of Mexico.

References

Blandford, R.D. & Romani, R.W. 1988, MNRAS, 234, 57
Lyne, A.G. et al. 1996, Nature, 381, 497 (LPG-SC96)
Manchester, R.N. & Taylor, J.H. 1977, Pulsars (San Francisco: Freeman)
Michel, F.C. 1994, MNRAS, 267, L4
Muslimov, A. & Page, D. 1995, ApJ, 440, L77 (MP95)
Muslimov, A. & Page, D. 1996, ApJ, 458, 347 (MP96)
Page, D. 1997, ApJ, 479, L43

Authors' Addresses

A. Muslimov: Code 661, NASA/GSFC, Greenbelt, MD 20771 U.S.A.; muslimov@lhea1.gsfc.nasa.gov

D. Page: Instituto de Astronomia, UNAM, México, 04510 México; page@astroscu.unam.mx

D. Pines

Pulsar Glitches: To What Extent Do These Probe Crustal Superfluidity, Core-Crust Coupling, and the Equation of State of Dense Neutron Matter?

Abstract

Following a brief introduction to alternative models for pulsar glitches, the discussion by symposium participants concerning the application of these models to the glitch behavior of the Vela and Crab pulsars is summarized.

I Introduction

In this year, the 28^{th} year of pulsar glitch observations, it seems quite appropriate to devote a significant part of a meeting which brings together theorists and observers to a consideration of glitch observations, their physical origin, and the information they provide on the internal structure and dynamics of neutron stars. I was therefore pleased to be invited by Ed van den Heuvel to introduce and chair a discussion on these general topics, and to prepare a brief written summary of the substance of our remarks.

Our subject was born on March 3, 1969, when Radhakrishnan and Richard Manchester, who are in the audience, observing in Australia the newly discovered Vela pulsar, and George Downs and Paul Reichley, carrying out comparable observations in the U.S., discovered a quite extraordinary glitch in the otherwise steady spin down of the Vela pulsar (Radhakrishnan & Manchester 1969; Reichley & Downs 1969). The comparative regularity of such glitches (eleven so far over a twenty-seven year period) should not blind us to the unusual nature of these events, corresponding as they do to a relative jump in pulsar spin of a few parts in a million, with an energy release comparable to an earthquake of magnitude 17 in which the entire surface of the earth shifts by 50 feet! Equally extraordinary was the observation that the relative jump in the spin down rate was several orders of magnitude larger, and that both jumps subsequently decayed over a period of weeks to months.

That summer, in a collaboration at the Aspen Center for Physics, a group of us proposed a simple two-component model for the glitch and post-glitch behavior of the Vela pulsar in which the physical origin of the glitch was a starquake which reduced the strain in the stellar crust brought on by pulsar spin down, while the observed

long decay time (dynamical processes in a neutron star typically take place in times $\sim R/c \sim 3 \times 10^{-5}$ s) reflected the presence of superfluid neutrons in the core which couple slowly to the crust on time scales of order days to months (Baym et al. 1969). The model was consistent with observation, and received additional support with the observation of a glitch in the Crab pulsar which possessed generally similar characteristics, albeit with a glitch magnitude some two orders of magnitude smaller, and a significantly shorter decay time scale (of order days) (Boynton & Groth 1969).

These and subsequent glitch observations, and the theoretical efforts to explain them, opened up the intriguing possibility that by combining theory and observation, one could use pulsar glitches and postglitch behavior to place strong constraints on theories of neutron star structure and internal superfluid dynamics; put another way, that glitching pulsars might be used as a cosmic laboratory for the study of the behavior of hadron matter at high densities and (comparatively) low temperatures.

Although starquakes and core neutron superfluidity play a role in many glitching pulsars, subsequent work called attention to the possibility that it is the pinning of vortices in the crustal neutron superfluid to the nuclei with which they coexist which is responsible for "Vela-size" glitches and post-glitch behavior in the Vela and Crab pulsars (Pines & Alpar 1985), while Ruderman has proposed that the coupling between vortices in the core-neutron superfluid and the core flux lattice can give rise to magnetic field evolution, starquakes, and some aspects of post-glitch behavior (Ruderman 1997).

Earlier at this meeting, Andrew Lyne has reviewed glitch observations, while Ali Alpar, Bennett Link, and Jim Sauls have discussed glitch theories, and their relation to our present understanding of neutron star superfluidity; we shall hear from Mal Ruderman subsequently about the possible connection between glitches and magnetic field evolution. In this session we shall focus on alternative proposals for the physical origin of glitches and the constraints which glitch observations place on descriptions of the stellar crust and core. Observations to consider include glitch size, post-glitch behavior, and the time between glitches in the Vela, Crab, and other pulsars. Among the questions these observations raise are:

- The physical origin of the differences in glitch behavior between the Vela, Crab, and other pulsars.
- The relationship between glitch statistics and glitch origin(s).

Further questions relating to constraints on theories we might discuss include:

- Given the constraints already provided by detailed studies of the Vela and Crab pulsars over the past 25 years, are there alternative scenarios, equally compatible with observation, to the vortex creep description of post-glitch behavior?

- Assuming the vortex creep description is appropriate, are the constraints (on the inertial moment of the pinned neutron superfluid, the existence of multiple time scales for the response of the pinned crustal superfluid to a glitch, and the crust-core coupling time) obtained using it to fit observations on the Vela and Crab pulsars, consistent with microscopic theories of neutron star structure and superfluid dynamics?

- How are glitches triggered? Is there evidence for a different trigger mechanism in the Crab and Vela pulsars?

- Is there observational evidence for a link between glitch and post-glitch behavior and magnetic field or thermal evolution?

II Discussion

Let me now attempt to summarize the discussion which ensued. First, it is important to emphasize that the following view of glitch behavior was generally accepted:

- The pinned crustal superfluid provides an essential ingredient to understanding glitches.

- Glitches involve primarily the catastrophic, and nearly simultaneous unpinning of a quite large number of pinned vortices. Based on his detailed analysis of postglitch behavior, Alpar estimates that number as some 10^{13} for both Crab and Vela pulsar glitches, despite their quite different magnitude.

- Vortex creep theory provides a satisfactory phenomenological description of postglitch behavior. Typically it involves a series of exponential decays with time values of order days to months associated with the response of distinct pinning regions, followed by a slow recovery of the spindown rate, with a constant positive second derivative of the rotation rate associated with the non-linear response of vortex creep.

- The fractional inertial moment $\delta Ip/I$ of the pinned superfluid which participates in glitches and postglitch behavior is $\sim 2\%$ for the Vela pulsar; here I is the inertial moment of that part of the star which couples to the crust on a time scale which is fast compared to the glitch rise time ($\lesssim 100$ s); if, as Alpar and Sauls have calculated, the core crust coupling time is $\lesssim 100$ s, then I is the core inertial moment. The constraint, $(\delta Ip/I) \sim 2\%$ then serves to rule out a soft neutron matter equation of state; put another way, the equation of state must be sufficiently stiff that a 1.4 $M_\odot$ neutron star possesses a radius in excess of 10 km, with an inner crust (in which neutron superfluid and crustal nuclei coexist) which is at least 300 m in radial extent.

- The apparently low braking index recently reported for the Vela pulsar ($n = 1.4$) as well as the earlier reported braking indices in other young pulsars of less than the canonical value of 3 (which Ruderman pointed out should be expected on quite general grounds) may well reflect glitch activity.

On the other hand, the following issues were not resolved.

What triggers a glitch?

- Is it, as Bennett Link has argued at this meeting, a thermal pulse associated with a starquake?

- Is it a starquake brought on by the spin-down induced outward motion of vortices in the core, a motion which Ruderman argues drives core flux lines outwards, thereby inducing crustal stresses which exceed a critical shear angle?

- Is it a spin-down induced unpinning of a given vortex cluster, an unpinning which sets off an avalanche in the course of which the remaining crustal pinned vortices become unpinned, as Alpar and I have proposed?

Note that while the third alternative utilizes a single cluster as the trigger, the starquakes proposed by Link and Ruderman could, in principle, also act initially to unpin a given cluster of pinned vortices which then act to unpin the others, either through changes in the local crust-superfluid velocity differential, or through transmission of thermal pulses or critical strain.

What brings about the reduced value of the braking index measured for the Vela pulsar?

- Graham-Smith points out that it could be caused by either a glitch-induced increase in the effective magnetic moment or a glitch-induced decrease in the effective moment of inertia. He argues that the second alternative poses a problem, since the magnitude of such reductions is such that after some 10^4 yr one would have "used up" the available pinned crustal inertial moment.

- Ruderman favors Graham-Smith's first alternative, which he argues is a natural consequence of his magnetically-induced crustal stress build-up. If both magnetic poles of a young pulsar are in the same rotational hemisphere initially, spindown will make them migrate towards the rotational equator, thereby increasing the effective magnetic moment of the star.

- Alpar and I favor the second alternative. We point out that the creation of vortex traps in Crab-like glitches, a process which provides a natural explanation for the postglitch behavior of that pulsar (see below), reduces the effective pinned crustal inertial moment, and that at least two "Crab-like" small glitches have been observed in the Vela pulsar in the past twenty-seven years. We argue that since vortex trap formation is a property of young pulsars, the "trap creation" era might be expected to come to an end sometime within the next few thousand years, so that this kind of pinned vortex cluster rearrangement need not exhaust the available pinned vortex crustal superfluid inertial moment.

- Here one encounters two significant and, hopefully, observable differences between the predictions of the Ruderman scenario and the Alpar/Pines scenario. In the Ruderman scenario, over time the magnetic field stress-induced glitches become more and more frequent as the pulsar spin down sweeps out the core magnetic field. By the time the pulsar has slowed down to a period of some 0.7 s, the field should have been swept out, so that large glitches are not to be expected for longer period pulsars. Moreover, since in the latter stages of this process, the effective magnetic field acting to spin down the pulsar is proportional to Ω, the braking index, after possibly initially falling below three, should increase until it becomes ~ 5 for a slow pulsar. By contrast, in the Alpar/Pines scenario, once a vortex cluster network is fully established, the braking index should return to three as a long-term value averaged over many glitches. However, as Vela sized glitches are expected to continue, at a rate proportional to $\dot{\Omega}$, so that the time interval between glitches of a typical pulsar is of the order of a hundred years, these pulsars would be observed in interglitch epochs except for an occasional glitch from one pulsar among the hundreds now monitored. The typical interglitch behavior of such pulsars seems to be like that of the Vela pulsar, with a constant and large second derivative due to interglitch recovery. Thus glitches are predicted for all slow pulsars, albeit infrequently, since in this population the spin down time is much longer.

What is responsible for the difference in glitch behavior of the Crab and Vela pulsars?

- On the Link scenario, it is the difference in the thermal time scale for the response to starquakes which release comparable amounts of energy ($\sim 10^{42}$ ergs in the example discussed by Link at this conference), a difference brought about by pulsar cooling. If this scenario continues to be applicable to pulsars older (and cooler) than Vela, one might expect rather different glitch and postglitch signatures to emerge. Now that there is a considerably larger population of glitching pulsars, evidence for signatures of thermal burst triggering should be sought.

- On the Ruderman scenario, crust-core coupling plays a significant role in the Crab glitches; thus the characteristic signature seen by Lyne et al. in the 1989

glitch, an apparent glitch-induced delay in the crustal spin-up occurring during the first few days after the glitch, is attributed to the response of the core superfluid to the glitch; the slower additional spin-up represents the response of the vortex array in the superfluid to changes in the flux tube pull out after the movement of the crustal magnetic field in a glitch. On this scenario, I in the inertial fraction, $\delta Ip/I$, does not represent the full inertial moment of the core; to the extent that it does not, the absolute magnitude of the pinned crustal superfluid inertial moment inferred from post-glitch behavior may be considerably less than the minimum value of the stellar moment of inertia obtained on the assumption that core-crust coupling occurs rapidly.

- On the Alpar/Pines scenario, what Lyne et al. are observing is the creation of a new vortex-free region and pinning cluster, a phenomenon we argue is to be expected during the first few thousand years of a young pulsar's life. On invoking this process we are able to obtain detailed quantitative fits to the observed Crab pulsar glitches for the period 1971–95.

- These rather different interpretations of postglitch behavior might be subject to observational test. One such is the postglitch behavior associated with the June 1996, Crab pulsar glitch, which was seen by both the Backer and Lyne groups; it will be instructive to compare with observation the predictions for its behavior based on the vortex trap creation, thermal pulse initiation, and crust-core coupling scenarios. A second test would be the extent to which evidence for crust-core coupling can be found in fits to the Vela glitch data; if such evidence cannot be found, it would seem reasonable to use the fits to that data to rule out soft equations of state for neutron matter.

Given these multiple scenarios, to what extent can we presently regard pulsars as cosmic hadron physics laboratories? At one level, while not in the same league with the use of binary pulsars as a laboratory for general relativity, it may be argued that the community is off to a promising start, in that it has proved possible to build a consistent model in terms of pinned crustal superfluid, and make a first attempt to "pin down" the relevant pinning parameters. It would be my hope that further theoretical work on these problems, together with a closer examination of the predictions of the various glitch scenarios, will bring us much closer to our goal of regarding pulsars as cosmic hadron physics laboratories, which are capable of providing detailed information about the neutron matter equation of state and the character and extent of the pinned crustal superfluid.

Let me conclude this brief summary with a few comments about some desirable future theoretical studies. First, although the phenomenological vortex creep theory appears to work quite well, it is highly desirable to carry out more realistic estimates of pinning energies, in which account is taken of both the shape of nuclei near the crust-core boundary, discussed by Chris Pethick, and proximity effects, discussed by Jim Sauls. Second, the issue raised by Mal Ruderman, of the extent to which neutron

vortex lines in the core can move through the much denser proton vortex lines, has so many potential observable consequences that it behooves us to examine anew the creation of the core proton vortex lattice in the presence of the already existing core neutron vortices, and how these coevolve as the pulsar spins down.

Acknowledgements

I should like to thank Ali Alpar and Jim Sauls for a stimulating discussion of the issues raised at this conference, Ali Alpar for helpful suggestions concerning the content of this summary, and Bennett Link and Mal Ruderman for a critical reading of this manuscript. This work was supported by the National Science Foundation Grant AST93-15133 and the Los Alamos National Laboratory.

References

Baym G. et al. 1969, Nature 224, 872
Boynton, P. et al. 1969, IAU Circ. 2179
Pines, D. & Alpar, M.A. 1985, Nature, 316, 27
Radhakrishnan, V. & Manchester, R.N. 1969, Nature 222, 228
Reichley, P.E. & Downs, G. S. 1969, Nature, 222, 229
Ruderman, M., these proceedings

Authors' Address

Center for Nonlinear Studies, Los Alamos National Laboratory and University of Illinois at Urbana-Champaign, Department of Physics Loomis Laboratory of Physics, 1110 West Green Street, Urbana, IL 61801-3080, U.S.A.

N.K. Glendenning

Spin-up of Solitary Pulsars: Signal of Phase Transition

Abstract

A phase transition in the nature of matter in the core of a neutron star, such as quark deconfinement or Bose condensation, can cause the spontaneous spin-up of a solitary millisecond pulsar. The spin-up epoch for our model lasts for 2×10^7 years or 1/50 of the spin-down time (Glendenning, Pei and Weber 1997).

I Introduction

Neutron stars have a high enough interior density as to make phase transitions in the nature of nuclear matter a distinct possibility. According to the QCD property of asymptotic freedom, the most plausible is the quark deconfinement transition. According to lattice QCD simulations, this phase transition is expected to occur in very hot ($T \sim 200$ MeV) or cold but dense matter.

Since neutron stars are born with almost the highest density that they will have in their lifetime, being very little deformed by centrifugal forces, they will possess cores of the high density phase essentially from birth if the critical density falls in the range of neutron stars. However the global properties such as mass or size of a slowly rotating neutron star are little affected by whether or not it has a more compressible phase in the core. In principle, cooling rates should depend on interior composition, but cooling calculations are beset by many uncertainties and competing assumptions about composition can yield similar cooling rates depending on other assumptions about superconductivity and the cooling processes. Moreover, for those stars for which a rate has been measured, not a single mass is known. It is unlikely that these measurements will yield conclusive evidence in the present state of uncertainty.

Nevertheless, it may be possible to observe the phase transition in millisecond pulsars by the easiest of measurements—the sign of $\dot{\Omega}$. The sign should be negative corresponding to loss of angular momentum by radiation. However, as we will show, a phase transition, either first or second order, that occurs near or at the limiting mass star, can cause spin-up during a substantial era compared to the spin-down time of millisecond pulsars. We sketch the conventional evolutionary history of

millisecond pulsars with the addition of the supposition that the critical density for quark deconfinement falls in the density range spanned by neutron stars.

As already remarked, with this supposition, the star has a quark core from birth but its properties are so little affected that this fact cannot be discerned in members of the canonical pulsar population. However, by some mechanism, usually assumed to be accretion from a companion during the radio silent epoch following its 10^7 year spin down as a canonical pulsar, the neutron star may be spun up. As it spins up, it becomes increasingly centrifugally deformed and its interior density falls. Consequently, the radius at which the critical phase transition density occurs moves toward the center of the star—quarks recombine to form hadrons. When accretion ceases, and if the neutron star has been spun up to a state in which the combination of reduced field strength and increased frequency turn the dipole radiation on again, the pulsar recommences spin-down as a visible millisecond pulsar.

During spin-down the central density increases with decreasing centrifugal force. First at the center of the star, and then in an expanding region, the highly compressible quark matter will replace the less compressible nuclear matter. The quark core, weighed down by the overlaying layers of nuclear matter is compressed to high density, and the increased central concentration of mass acts on the overlaying nuclear matter, compressing it further. The resulting decrease in the moment of inertia causes the star to spin up to conserve angular momentum not carried off by radiation. The phenomenon is analogous to that of "backbending" predicted for rotating nuclei (Mottelson and Valatin 1960) and discovered in the 1970's (Johnson et.al. 1972, Stephens and Simon 1972) (see Figure 1) In nuclei, it was established that the change in phase is from a particle spin-aligned state at high nuclear angular momentum to a superfluid state at low angular momentum. The phenomenon is also analogous to an ice skater who commences a spin with arms outstretched. Initially spin decreases because of friction and air resistance, but a period of spin-up is achieved by pulling the arms in. Friction then reestablishes spin-down. In all three examples, spin up is a consequence of a decrease in moment of inertia beyond what would occur in response to decreasing angular velocity.

II Calculation

In our calculation, nuclear matter was described in a relativistically covariant theory (Garpman, Glendenning and Karant 1979, Glendenning 1985, Glendenning and Moszkowski 1991) and quark matter in the MIT bag model (Chodos et.al. 1974). The phase transition occurs in a substance of two conserved quantities, electric charge and baryon number, and must be found in the way described in Glendenning (1992). The moment of inertia must incorporate all effects described above—changes in composition of matter, centrifugal stretching—and frame dragging, all within the framework of General Relativity. The expression derived by Hartle is inadequate

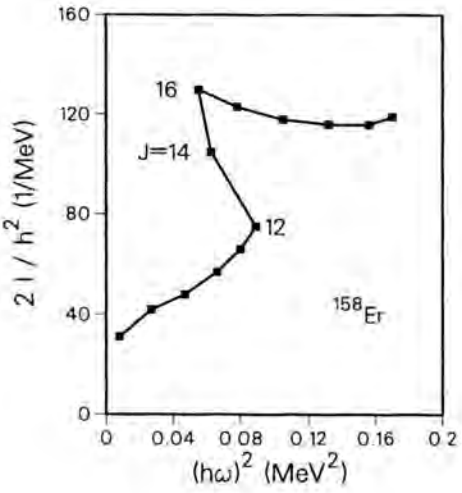

Figure 1. Nuclear moment of inertia as a function of squared frequency for ^{158}Er, showing backbending in the nuclear case.

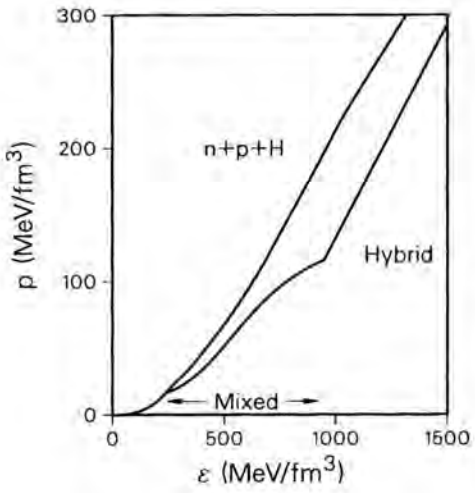

Figure 2. Equation of state for the first order deconfinement phase transition described in the text.

because it neglects these effects (Hartle and Thorne 1968). Rather we must use the expression derived by us (Glendenning and Weber 1992a, 1992b).

For fixed baryon number we solve General Relativity for a star rotating at a sequence of angular momenta corresponding to an equation of state that describes the deconfinement phase transition from charge neutral nuclear matter to quark matter. The equation of state is shown in Figure 2. The moment of inertia as a function of angular momentum does not decrease monotonically as it would for a gravitating fluid of constant composition. Rather, as described above, the epoch over which an enlarging central region of the star enters the more compressible phase is marked by spin-up (Figure 3).

III Spin-up era

To estimate the duration of the spin-up, we solve the deceleration equation for the star with moment of inertia having the behavior shown in Fig. 3.

From the energy loss equation

$$\frac{\mathrm{d}E}{\mathrm{d}t} = \frac{\mathrm{d}}{\mathrm{d}t}\left(\frac{1}{2}I\Omega^2\right) = -C\Omega^4 \qquad (1)$$

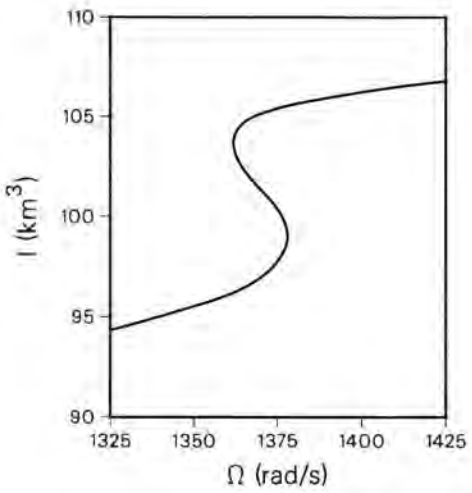

Figure 3. Moment of inertia corresponding to a change of phase. Time flows from large to small I.

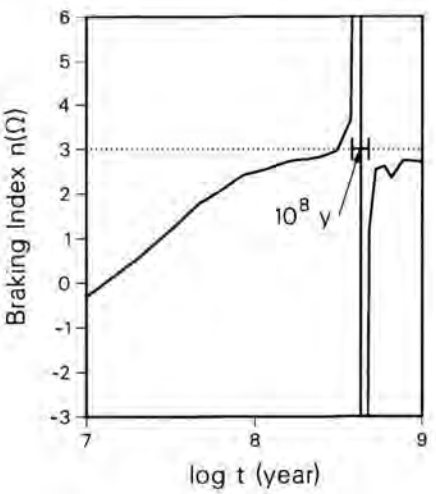

Figure 4. The time evolution of the braking index plotted over one decade that includes the epoch of the phase transition.

for magnetic dipole radiation we find

$$\dot{\Omega} = -\frac{C}{I(\Omega)}\left[1 + \frac{I'(\Omega)\,\Omega}{2I(\Omega)}\right]^{-1}\Omega^3 . \tag{2}$$

This expression reduces to the usual braking equation when the moment of inertia is held fixed. The braking index is not constant but varies with angular velocity and therefore time according to

$$n(\Omega) \equiv \frac{\Omega\ddot{\Omega}}{\dot{\Omega}^2} = 3 - \frac{3I'\Omega + I''\Omega^2}{2I + I'\Omega}, \tag{3}$$

where $I' \equiv \mathrm{d}I/\mathrm{d}\Omega$ and $I'' \equiv \mathrm{d}I^2/\mathrm{d}\Omega^2$. This holds in general even for a star whose internal composition does not change with angular velocity (inconceivable). In particular one can see that for very high frequency, the derivatives will be largest and the braking index for any millisecond pulsar near the Kepler frequency will be less than the dipole value of $n = 3$.

The braking index is shown as a function of time in Figure 4. An anomalous value endures for 10^8 years corresponding to the slow spin down of the pulsar and the corresponding slow envelopment of a growing central region by the new phase. The two points that go to infinity correspond to the infinite derivatives of I at which

according to (2), the deceleration vanishes. They mark the spin-up era. The actual spin-up lasts for 2×10^7 years or 1/50 of the spin-down time for this pulsar. This could be easily observed in a solitary pulsar and would likely signal a phase transition.

IV Summary

We have found the spin-up phenomenon in a pulsar model for which the change in phase occurs in a star near the maximum mass. The phase transition can be first or second order as long as it is accompanied by a sufficient softening of the equation of state. We have not quantified the meaning of "sufficiently soft".

If no pulsar is observed to produce the signal, little is learned. Just as in nuclear collisions, failure to observe a signal does not inform us that the deconfined phase does not or cannot exist.

Acknowledgements

This work was supported by the Director, Office of Energy Research, Office of High Energy and Nuclear Physics, Division of Nuclear Physics, of the U.S. Department of Energy under Contract DE-AC03-76SF00098.

References

Chodos, A. et al. 1974 Phys. Rev. D 9, 3471
Garpman, S.I.A., Glendenning, N.K. & Karant, Y.J. 1979, Nuc. Phys. A322, 382
Glendenning, N.K., 1985, ApJ, 293, 470
Glendenning, N.K. & Moszkowski, S. A., 1991, Phys. Rev. Lett. 67, 2414
Glendenning, N.K., 1992, Phys. Rev. D, 46, 1274
Glendenning N.K. & Weber, F., 1992, ApJ, 400, 647
Glendenning, N.K. & Weber, F., 1994, Phys. Rev. D 50, 3836
Glendenning, N.K., Pei, S. & Weber, F., 1997, Phys. Rev. Lett. 79, 1603
Hartle J.B. & Thorne, S.K., 1968, ApJ, 153, 807
Johnson, A., Ryde, H. & Hjorth, S.A., 1972, Nucl. Phys. A179, 753
Mottelson, B.R. & Valatin, J.G., 1960, Phys. Rev. Lett. 5, 511
Stephens, F.S.& Simon, R.S., 1972, Nucl. Phys. A183, 257

Authors' Address

Nuclear Science Division & Center for Nuclear and Particle Astrophysics, Lawrence Berkeley National Laboratory, Berkeley, California, USA

Part VI:

Evolution and Modeling

F. Verbunt, J.W. Hartman, D. Bhattacharya, R.A.M.J. Wijers and G. Nelemans

Applications of Radio Pulsar Population Synthesis

Abstract

Improved population synthesis of single radio pulsars with $B \geq 10^{11}$ G confirms that the time scale on which the magnetic field of neutron stars decays is 30 Myr or more. Our simulations suggest that a fair number of neutron stars are born with velocities less than ~ 200 km/s. The derived birth rate of neutron stars near the Sun is low enough to be compatible with the assumption that all neutron stars are formed in OB associations from stars with $M > 10\,\mathrm{M}_\odot$. There is no need in our simulations for a second pulsar population (e.g., of mildly recycled pulsars) injected at $B \geq 10^{11}$ G, in addition to the neutron stars formed directly from type II supernovae.

I Population synthesis

For each prescription of the evolution of the pulse period P and its derivative $\dot{P}$ of radio pulsars, we can predict their motion in the P-$\dot{P}$ diagram. Only sufficiently luminous pulsars in an area of the sky that has been observed can be placed in the diagram. Thus, the study of pulsar evolution via population synthesis proceeds as follows (Bhattacharya et al. 1992, updated and improved by Hartman et al. 1997).

First, we assume distributions for the properties of neutron stars at birth, viz. , distributions for initial position $\vec{r}_i$ in the Galaxy, initial velocity $\vec{v}_i$, initial period P_i, and initial magnetic field $B_i \propto \sqrt{P_i \dot{P}_i}$. $\vec{r}$ and $\vec{v}$ evolve in the gravitational potential Φ of the Galaxy. The evolution of P and $\dot{P}$ is determined by $P\dot{P} = 10^{-39}(B_i e^{-t/\tau})^2$ s/G^2, where τ is the time scale on which the magnetic field decays. For $\vec{r}_i$ we choose roughly the galactic distribution of the OB stars. For $\vec{v}_i$ we use the distributions shown in Figure 1. P_i is fixed at 0.1 s. For B_i we assume a Gaussian in $\log B_i$ centered on $\log B_o$ and with width σ_B. For Φ we use the Kuijken & Gilmore (1989) potential.

We use a Monte Carlo method to choose an age $t \in (0, n\tau)$ ($n = 5, 3$ for short, long decay times) and to choose initial values $\vec{r}_i$, $\vec{v}_i$, P_i and B_i, which we then evolve to the values at age t, viz. , $\vec{r}$, $\vec{v}$, P, and B. If the P-B combination lies above the death line, we calculate the pulsar beam width from P and $\dot{P}$ (after Narayan & Vivekanand 1983),

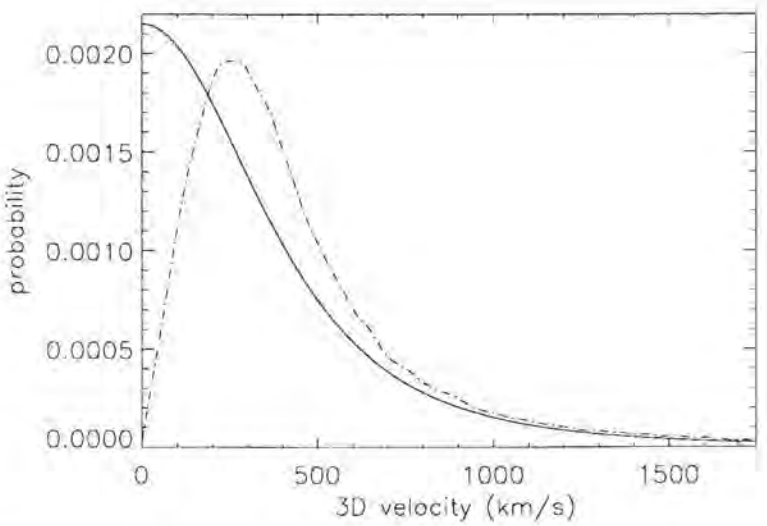

Figure 1. The initial velocity distribution of neutron stars, according to Lyne & Lorimer (1994, dash-dotted line) or to Eq. (1) (Phinney & Hansen, private communication, solid line).

and from this we decide on a probability basis whether the pulsar beam is directed to the Earth. If so, the luminosity L is found from P and B via a model luminosity L_m (according to Prószyński & Przybicień 1984), and a distribution around this with minimum luminosity $\log L_{min} = \log L_m - a$ and a width determined by $1/b$ (after Narayan & Ostriker 1990). From $\vec{r}$ we calculate the position in the sky of the simulated pulsar, and its dispersion measure DM (after Taylor & Cordes 1993), and with L its flux S at Earth, to check whether any of four investigated surveys would have detected the pulsar. We then choose the age of the next pulsar, and repeat the procedure, until we have 2000 simulated detections. Whereas pulsar birth and motion are simulated throughout the Galaxy, we limit the detections to pulsars which have a projected distance $d_{\rm proj}$ on the Galactic plane to the Sun of less than 4 kpc.

II Comparison with observations

We compare the simulated distributions of P, B, L and $\mathrm{DM}\sin b_g$—where b_g is the galactic latitude—with the observed ones, by means of Kolmogorov-Smirnov tests. By varying $\log B_o$, σ_B, a and b we find that good simulations of the observed properties of radio pulsars can be produced only for decay times $\tau \geq 30$ Myr. The best simulations are found for $\tau \simeq 100$ Myr, and have $\log B_o(G) \simeq 12.34$, $\sigma_B \simeq 0.34$, $a \simeq 1.5$,

$b \simeq 3.5$. The problem with the models with short decay times $\tau < 30\,\mathrm{Myr}$ is that they have difficulty producing pulsars with long periods and strong fields. If one tries to solve this by enhancing the detection of long-period pulsars via a change in the luminosity law (specifically, by reducing a), then the simulations show far too many high-luminosity pulsars.

The two assumed velocity distributions both give acceptable results, but there is a hint in our simulations that models with the Lyne-Lorimer velocity distribution produce too many pulsars at large distance from the plane but with short characteristic age. This may suggest that the actual distribution of initial velocities has a fair number of pulsars at low velocities, $v_i < 200\,\mathrm{km/s}$, say, as is the case for the Phinney-Hansen adaptation of the Paczyński (1990) function

$$p(u)du = \frac{4}{\pi}\frac{du}{(1+u^2)^2}, \qquad \text{where} \qquad u \equiv \frac{v_i}{\sigma_v} \tag{1}$$

which has $\sigma_v \simeq 600\,\mathrm{km/s}$.

Hartman (1997) calculates the transverse velocities for young ($< 3\,\mathrm{Myr}$) detected radio pulsars in our population synthesis for both Lyne-Lorimer and Phinney-Hansen initial velocity distributions. Comparing them with those derived from the proper motion measurements of 25 young pulsars from Lyne & Lorimer (1994), and taking into account the errors in the measurements (sometimes comparable to the measured value) he finds that the Phinney-Hansen distribution describes the observations better (Figure 3).

III Progenitor mass

Our simulations show that some 60% of the pulsars detected at $d_{\mathrm{proj}} < 4\,\mathrm{kpc}$ were also born with $d_{\mathrm{proj}} < 4\,\mathrm{kpc}$, i.e., most pulsars detected near the Sun were born near the Sun (see Figure 2). This indicates that our simulations provide better constraints on the local birthrate, $\sim 2\,\mathrm{kpc}^{-2}\,\mathrm{Myr}^{-1}$, than on the Galactic birthrate. Indeed, models with very different pulsar birth rates near the Galactic Center produce very similar results near the Sun. The local birthrate is sufficiently low that all neutron stars can be produced in OB associations from stars with $M \geq 10\,\mathrm{M}_\odot$. Blaauw (1985) argued that the local birthrate of neutron stars was about $20\,\mathrm{kpc}^{-2}\,\mathrm{Myr}^{-1}$, which required all nearby stars with masses down to $5\,\mathrm{M}_\odot$ to turn into neutron stars. The main reason for this different conclusion is that Blaauw assumed a short decay time, $\tau < 5\,\mathrm{Myr}$, and thereby concluded that all detectable pulsars were produced in the last few Myr; in our models with long decay times, the detected pulsars can be produced over a much longer time interval, and the local birth rate is correspondingly lower.

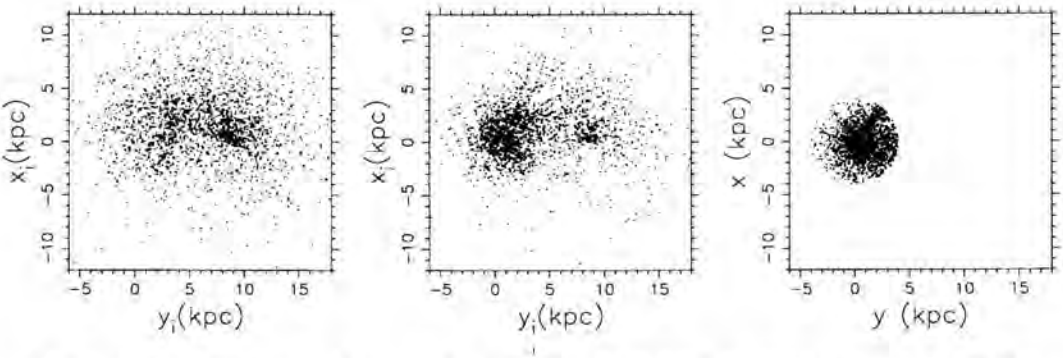

Figure 2. Positions in the Galaxy of neutron stars for a model with $\tau = 100$ Myr. The Sun is at (y,x=0,0), the Galactic Center at (8.5,0). The left frame shows the birth place of neutron stars that now have $d_{\rm proj} < 4$ kpc, the middle frame the birth place of pulsars detected at $d_{\rm proj} < 4$ kpc, and the right frame the current position of these detected pulsars. 1000 pulsars are plotted in each frame.

IV Other arguments against field decay

A kinematic argument for a long time scale for field decay, can be made as follows (Lorimer 1994, 1996, Hartman & Verbunt 1995). Pulsars which started to move away from the Galactic plane between 60 and 100 Myr ago currently are close to the Galactic plane again, having completed about half an oscillation. For $\tau \geq 100$ Myr a large characteristic age $\tau_c \equiv P/(2\dot{P})$ corresponds to a large real age, and one predicts that pulsars with $\tau_c \sim 100$ Myr are detected closer to the Galactic plane than pulsars with $\tau_c \sim 50$ Myr. For shorter decay times $\tau \leq 10$ Myr one would predict that the average distance to the plane is a monotonically increasing function of τ_c. The observations suggest that detected pulsars with $\tau_c \sim 100$ Myr are closer to the Galactic plane than pulsars at shorter τ_c, and thus that the decay time of the magnetic field is long.

The detection of a nearby pulsar with very low luminosity and with characteristic age $\tau_c \simeq 1.6 \times 10^8$ yr also suggests a long decay time (Tauris et al. 1994): if the pulsar were only a few Myr old, the detection of a nearby specimen would be extremely unlikely unless the birthrate of such low-luminosity pulsars were uncomfortably high. A high real age for this pulsar does not lead to such problematic conclusions.

V Variance of DM

Small-scale structure in the galactic electron distribution leads to variance in the dispersion measures. To investigate this, we perform a thought experiment in which we compare a homogeneous, smooth electron distribution with one in which all electrons are enclosed in spheres, all of which have the same size and electron density in them

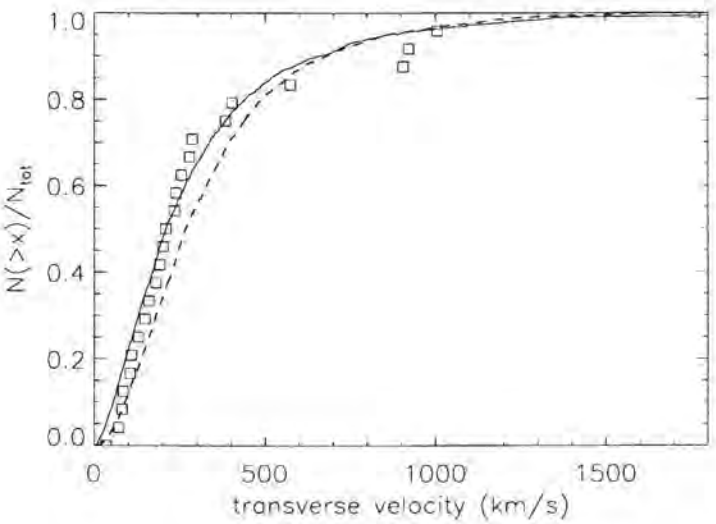

Figure 3. The cumulative transverse velocity distribution of 25 young pulsars from Lyne & Lorimer (1994) (open squares), together with simulated samples for initial distributions according to Eq. (1) (solid line) and to Lyne & Lorimer (1994) (dashed line), where measurement errors have been taken into account.

(Nelemans et al. 1997). In the inhomogeneous model, the average dispersion measure at a given distance d is the same as the dispersion measure for this distance in the smooth model, $\overline{\mathrm{DM}} = \mathrm{DM}_s$, but the dispersion measures are spread around this average with a variance given by $\sigma_{\mathrm{DM}} = (\,\overline{\mathrm{DM}}\frac{9}{8}dm_1\,)^{1/2}$ where dm_1 is the expected dispersion measure for passage through one sphere. This relation is essentially the result of the Poissonian variance in the number n of clouds encountered along the line of sight, for which $\sigma_n = \sqrt{n}$.

We implement this variance in our simulations as follows. From the actual simulated position and the Taylor & Cordes (1993) model we calculate the expected dispersion measure $\mathrm{DM}_s \equiv \mathrm{DM}_{\mathrm{TC}}$. We then choose a simulated dispersion measure from a Gaussian distribution around $\mathrm{DM}_{\mathrm{TC}}$ with width $\propto \sqrt{\mathrm{DM}_{\mathrm{TC}}}$. This new dispersion measure is then combined with the Taylor & Cordes model to get the derived distance and luminosity of the simulated pulsar. A smooth model for the dispersion measures leads to a peak in the simulated distributions at the maximum dispersion measure in each direction, caused by the pulsars above the electron layer. The implementation of the inhomogeneous electron distribution removes this peak, in agreement with observation (Figure 4). However, the new simulations still predict too many pulsars at $|\mathrm{DM}\sin b| \leq 5$; the Kolmogorov-Smirnov tests are not sufficiently sensitive to detect this, but we do consider it as an unsolved problem of our simulations. Many pulsars in

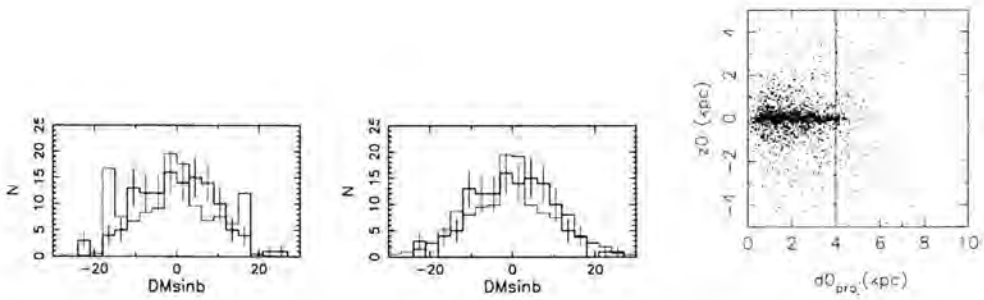

Figure 4. The observed (thick line with error bars) and simulated (thin line) distributions of DM $\sin b$ for simulations that do not and that do include variance in DM (left and middle, respectively). Right: actual distances projected on the plane $d0_{\rm proj}$ as a function of actual distance from the plane $z0$ for pulsars detected in the simulation that includes variance in the dispersion measure. The derived projected distances $d_{\rm proj}$ for all these pulsars is less than 4 kpc.

our simulations with inhomogeneous electron distributions are assigned a $d_{\rm proj} < 4$ kpc even though they have rather large projected distances; this is true especially for simulated pulsars at larger distances from the Galactic plane ($|z| > 1.5$ kpc).

VI Reliability of population synthesis

To put it succinctly: the reliability of a population synthesis is as good as the input assumptions.

The form and period dependence of the pulsar beam is still the subject of debate. The derived birthrate of pulsars is directly proportional to the absolute value of the beaming factor. The relative detection probabilities as a function of P, and thereby the observed P distribution, depend on the period dependence of the beaming factor at $P > 0.1$ s. We have verified that the differences between the different proposed beaming models are not large enough to affect our conclusions.

The luminosity function is highly uncertain, and thus causes appreciable uncertainty in the simulations. It should be noted however that the simulations themselves offer good constraints. For example, if one assumes very large numbers of low-luminosity pulsars one predicts that the detected pulsar population is dominated by very nearby pulsars, contrary to observation. We also have found that the condition that the input model luminosity for detected pulsars should be the same as the output simulated one, in the dependence of L_m on P and $\dot{P}$, puts significant constraints on the form of this dependence. The uncertainties are still large, but in our estimation not large enough to impair our main conclusion that there is no evidence for field decay on short time scales.

The detection algorithms for our simulations are too simple. The sharp lower boundary to the detectable fluxes leads to the prediction that many pulsars will be detected close to the detection limit, contrary to observation. If we arbitrarily impose a minimum flux for detection of 10 mJy, in addition to the ones described for the simulations that we use, the quality of our simulations actually improves, especially with respect to the description of the flux distribution. (This extra limit removes only 6 of the 129 pulsars in the comparison sample of the real pulsars.) Bailes (private communication) stresses that the pulsar surveys are affected by radio interference, which causes pulsars to remain undetected which could have been detected in ideal circumstances. Failure to model this leads to an underestimate of the pulsar birth rate, but does not affect the conclusions about field decay, as long as the interference treats all pulsars equally, i.e., does not bias detection towards pulsars with specific periods or magnetic fields.

The various proposed velocity distributions that are compatible with the observed proper motions of radio pulsars all lead to acceptable simulations; as remarked above, there may be a hint that the number of low-velocity ($v_i < 200$ km/s) pulsars is not small. We do not consider the uncertainty in the dispersion measure to be a problem.

The success of our simulations shows that there is no evidence for the presence in the population of ordinary pulsars (i.e., single pulsars with $P > 0.1$ s) of any second population, such as mildly recycled pulsars. We have investigated how far this absence of evidence can be used as evidence for absence (Hartman, Portegies Zwart & Verbunt, 1997). Binary evolution scenarios and radio pulsar population synthesis both indicate that the fraction of recycled pulsars amongst the observed single radio pulsars is less than 1% at $B \geq 10^{11}$ G.

References

Bhattacharya, D. et al. 1992, A&A, 254, 198
Blaauw, A. 1985, in Birth and Evolution of Massive Stars and Stellar Groups, ed. W. Boland & H. van Woerden (Dordrecht: Reidel), 211
Hartman, J.W. 1997, A&A, 322, 127
Hartman, J.W. et al. 1997, A&A, 322, 477
Hartman, J.W., Portegies Zwart, S. & Verbunt, F. 1997, A&A, 325, 1031
Hartman, J.W. & Verbunt, F. 1995, A&A, 296, 110
Kuijken, K. & Gilmore, G. 1989, MNRAS, 239, 571
Lorimer, D. 1994, Ph.D. Thesis, Univ. of Manchester
Lorimer, D. 1996, in Pulsars: Problems and Progress, IAU Coll. 160, ed. S. Johnston, M.A. Walker & M. Bailes (San Francisco: ASP), 31
Lyne, A. & Lorimer, D. 1994, Nat, 369, 127
Narayan, R. & Ostriker, J. 1990, ApJ, 352, 222
Narayan, R. & Vivekanand, M. 1983, A&A, 122, 45
Nelemans, G. et al. 1997, A&A, 322, 489

Paczyński, B. 1990, ApJ, 348, 485
Prószyński, M. & Przybicień, D. 1984, in Millisecond Pulsars, ed. S. Reynolds & D. Stinebring (Green Bank: NRAO), 151
Tauris, T. et al. 1994, ApJ, 428, L53
Taylor, J. & Cordes, J. 1993, ApJ, 411, 674

Authors' Addresses

F. Verbunt, J.W. Hartman, and G. Nelemans: Astronomical Institute, Utrecht University, Postbox 80.000, 3508 TA Utrecht, the Netherlands

D. Bhattacharya: Raman Research Institute, Bangalore, 560 080, India

R.A.M.J. Wijers: Institute of Astonomy, Madingley Road, Cambridge 0HA CB3, United Kingdom

M. Ruderman and K. Chen

Evolving Magnetic Fields in Neutron Stars

Abstract

The interaction between the spinning superfluid neutrons and the magnetized superconducting protons in the core of a neutron star link stellar spin-down and spin-up to changes in the core magnetic field configurations. These, in turn, can move the stellar crust and alters the star's surface field. Many observed quantities such as spin-down indices of young radio pulsars, reductions in the magnetic dipole moments of relatively older canonical pulsars, the very much weaker magnetic dipole moments of neutron stars spun-up to millisecond periods, the large abundance of orthogonal and nearly aligned rotators among the disk population millisecond pulsars, and the timing "glitch" as observed in more rapidly spinning canonical pulsars can be understood in the context of this model.

I Surface magnetic field evolution in neutron stars

The motion of superfluid neutrons in the core of a spinning neutron star is determined by the positions of quantized vortex lines which form a dense array of area density $\rho_n \sim 10^4/P$ cm^{-2}, where P is the spin period (in seconds). During spin-up (e.g., by accretion from a companion in a low mass X-ray binary) or spin-down, each vortex a distance $\mathbf{r}_\perp$ from the stellar spin axis moves with a velocity

$$\mathbf{V_v} = -\mathbf{r}_\perp \dot{P}/2P. \tag{1}$$

Below the stellar crust the superconducting protons coexist with the superfluid neutrons. The core of each neutron vortex line is surrounded by a solenoidal sheath of superconducting proton current. The solenoid radius (Λ) is about 10^{-11} cm and the magnetic field within it (B_s) is typically 10^{15} G. The total magnetic flux carried by the vortex cores is negligible when averaged over the entire star ($B \sim \rho_n \pi \Lambda^2 B_s \sim 3 \times 10^{-3}/P$ G). However, these solenoids do cause strong magnetic interactions between moving neutron vortex lines and magnetic field inhomogeneities within the proton sea. Such inhomogeneities are abundant because the stellar magnetic field passing through the superconducting protons below the stellar crust is organized

into sub-microscopic regions between which the magnetic field almost vanishes. The expected field structure just below the crust, and possibly extending all the way to the center of the neutron star, is a very dense array of quantized tubes ($n_\Phi \sim 5 \times 10^{18} B_{12}$ cm^{-2}). Each of these flux tubes has the same radius as the solenoid around each neutron vortex line core and carries a magnetic field $\hbar e/\Lambda^2 \sim 10^{15}$ G.

In addition to the magnetic interaction between neutron vortex line solenoids and flux tubes, there is a direct one from the velocity dependence of the nuclear interaction between neutrons in a vortex and protons in a flux tube. The magnetic and direct interactions are of comparable magnitude. Because of both, flux tubes will be pushed (or pulled) by moving with neutron vortices (Sauls 1989; Srinivasan et al. 1990; Ruderman 1991; Ruderman 1991a). A flux tube array will move along the moving neutron superfluid vortices which thread it as long as the forces at vortex-flux tube junctures are not large enough to cause the vortex lines to cut through the flux tubes. Estimates of the maximum force per unit volume on the vortices at which this occurs ($\mathbf{F_M}$) have not included the non-magnetic part of the interaction between a vortex line and a flux tube. The corresponding maximum velocity for flux tubes moving through the stellar electron-positron core plasma is

$$\mathbf{V_\Phi} \sim \frac{\mathbf{F_M} c^2}{\sigma B^2}, \tag{2}$$

where B is the averaged magnetic field in the stellar core ($B \sim 10^{12}$ G in canonical pulsars) and σ is the effective conductivity in the densely flux threaded electron-superconducting proton sea. (Because this conductivity is so large, the velocity from Eq. (2) dominated by the inductive forces which link distant flux tubes, is far less than that found in the literature which calculates only the drag on the moving flux tubes as if they were completely isolated from each other.) If $|\mathbf{V_V}| > |\mathbf{V_\Phi}|$, some flux tube cutting through by neutron vortices must occur: plasma regions of the stellar interior with large B may tend to be carried with the moving vortices, while plasma backflow with flux tube cutting could be mainly in low field regions. In most neutron star core flux tube geometries, the dissipation required to allow flux tube motion through the plasma in which they are imbedded comes mainly from electron-flux tube scattering. It has been estimated that this effect gives a conductivity $\sigma_e \sim 10^{26}\ B_{12}^{-1}$ s^{-1} (Zhu 1997; Zhu & Ruderman 1997). The corresponding maximum velocity for flux tubes pushed (or pulled) through the neutron star by the moving neutron superfluid array of a spinning-up neutron star is then, very approximately,

$$|\mathbf{V_\Phi}(\max)| \sim \frac{10^{-7}}{B_{12} P} \text{cm s}^{-1}. \tag{3}$$

For a young Crab-like radio pulsar, $\mathbf{V_V} \geq 10^{-5}$ cm s^{-1}. Therefore, the flux tube arrays in the core of these pulsars would be expected to expand more slowly than their vortex arrays. In older pulsars with spin-down ages $\geq 10^4$ yrs, the core magnetic

field flux array can move at the same velocity as the expanding neutron superfluid vortex array. A crucial question is how the surface magnetic field of the star changes in response to this core flux tube movement. In young pulsars, where there is a high density of both vortex lines and flux tubes, stress on the crust will first exceed the crustal yield strength where the crust is penetrated by the largest B from the core. The surface field there would then reflect the changing flux tube distribution of the core just below the crust. In much older pulsars with much longer periods (and weaker core magnetic field because of considering core flux expulsion), the crust can be strong enough to freeze the remaining field through the crust.

A schematic model curve of external magnetic dipole field changes in the early stages of core field evolution is plotted in Figure 1. There are four expected stages which reflect the different ways in which the stellar magnetic dipole moment μ varies with changing spin angular frequency Ω. We define a parameter α to describe such change by

$$\frac{\dot{\mu}}{\mu} = \alpha \frac{\dot{\Omega}}{\Omega}. \tag{4}$$

Stage (a). Young Crab-like pulsars with $|\mathbf{V_V}| > |\mathbf{V_\Phi}|$, and an assumed "sunspot geometry" with magnetic flux from each spin hemisphere mainly returning to the same spin hemisphere, have $-1 < \alpha \leq 0$. This gives a "spin-down index", $n = \ddot{\Omega}\Omega/\dot{\Omega}^2$, somewhat less than 3, as observed for the Crab pulsar and its siblings.

Stage (b). In Vela-like pulsars where $|\mathbf{V_V}| \sim |\mathbf{V_\Phi}|$, but before much flux expulsion from the core into the crust has been achieved, $\alpha \sim -1$. This is in rough agreement with the observed spin-down index of Vela (Lyne et al. 1996).

Stage (c). Continual magnetic reconnection after core flux expulsion gives $\alpha \sim +1$ for canonical pulsars much older than Vela.

Stage (d). In substantially spun-down pulsars the remaining stress can no longer break the crust, then crustal flux freezing is effective and $\alpha = 0$.

This a-b-c-d crustal magnetic field evolution scenario is not in conflict with observations. We note that nine young radio pulsars found in SNRs (age $\sim 10^4$ yrs) seem to have magnetic dipole moments higher than that of relatively older radio pulsars around 10^{6-7} yrs old. Unless there is strong subsequent μ reduction, there will be a paradox in trying to account for the descendents of the young radio pulsars found in SNRs. This discrepancy is even more dramatic, after magnetic field evolution, implied by the observed $n \sim 1.4$ for Vela. However, in the model presented above, the magnetic dipole moments for old canonical pulsars will subsequently become proportional to $1/P$ (corresponding to $\alpha = 1$ and $n = +5$).

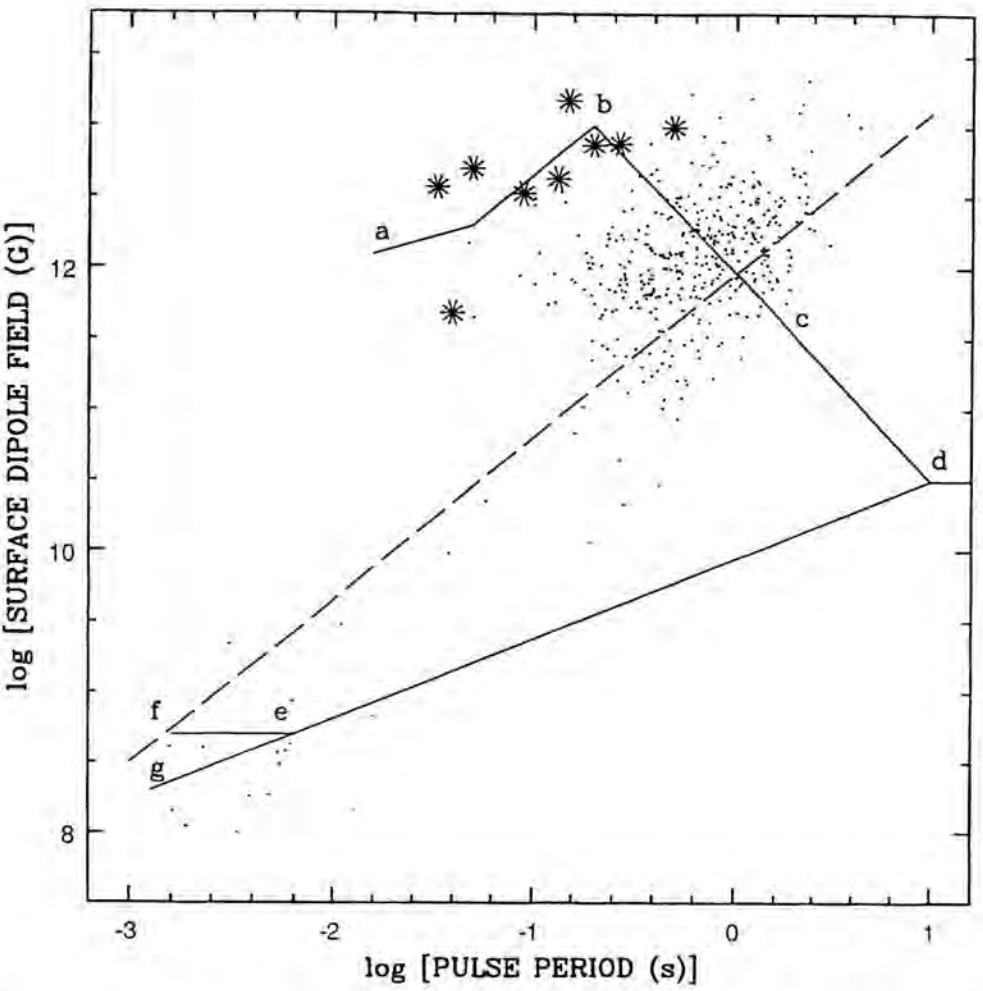

Figure 1. Model evolution of magnetic dipole fields of radio pulsars. Starlike designations correspond to radio pulsars found in SNRs. Solitary spinning-down radio pulsars would follow the path *(a-b-c)*. The path *(a-b)* corresponds to the first and second stages discussed in the text. Spin-down follows the path *(b-c-d)* when field-pulled crust moves toward the equator where reconnection takes place after core flux expulsion. The region *d* may not be reached by a solitary pulsar but may be by a neutron star in a binary. Further spin-down beyond *d* will not be effective in reducing B because the crust will no longer be stressed above its yield strength. Subsequent accretion induced spin-up could return the neutron star to *c*, depending upon the magnetic field configuration. Segment *(d-e-g)* is that for a sunspot-like geometry of Figure 3a. Figure 3b would give the path *(d-e-f)*. The dashed line is the spin-up line.

II Spun-up pulsars

The limit of Eq. (3) is very much greater than the superfluid vortex velocities within neutron stars being spun-up to millisecond periods in LMXBs where

$$|\mathbf{V_V}| \sim 10^{-9} \text{ cm s}^{-1}. \tag{5}$$

Therefore, superfluid-superconductor microphysics supports the model in which the flux tubes below the crust of such stars are progressively squeezed toward the stellar spin-axis (Chen & Ruderman 1993) together with the core's neutron vortex lines. The strongly conducting crust's yield strength would then ultimately be exceeded by the pull on it of the flux tubes (Ruderman 1991; Ruderman 1991a), which merge as they pass through it. In addition, for an accreting neutron star within a LMXB, nuclear pinning of the vortex lines of the intranuclear superfluid neutrons within the stellar crust also causes a motion of the crust lattice (and the field through it) toward the star's spin axis (Zhu 1997; Zhu & Ruderman 1997). (Because of the steady mass accretion during spin-up, the crust is continually pushed downward and replaced, so that crust stratification does not entirely prevent crustal movement toward the spin axis in response to spin-up induced forces by crustal pinned neutron superfluid vortices.) The effect on the surface magnetic field coincides with and reinforces that from flux tube motion below the crust. Such strongly spun-up neutron stars may have exceptionally thin crusts: crust thickness is diminished inversely to the increased surface gravity. (In order to spin-up neutron stars such as PSRs B1937+21 and B1957+20 to a period of 1.6 ms, of order one $M_\odot$ may have been accreted.) This also reduces considerably the possibility for the crust, in any way, keeping the surface field configuration from reflecting that of the flux tubes at the crust's base. Finally, accreted H and He must ultimately fuse, often by explosive burning, to much heavier nuclei. In so far as the resulting crust consists of a mixture of heavy nuclei, impurity scattering may greatly reduce the new crustal electrical conductivity and thereby speed up the surface field response to the changes of core magnetic field.

The above considerations of core flux and crustal movements lead to the model (Chen & Ruderman 1993) for the evolution of the surface magnetic field of a slowly spun-up neutron star sketched in Figure 2 and 3. The corresponding evolutionary tracks in the B_{dipole}-P diagram are those in Fig. 1.

Three kinds of final configurations for surface magnetic field and open field line bundles are thus expected.

Case (a). If the field configuration before spin-up begins as one in which magnetic flux from one spin-hemisphere largely returns to the other, spin-up moves the pulsar back along path (d-c) of Fig. 1 until the accretion spin-up line is reached.

Case (b). If, before spin-up, the surface magnetic field can be approximated by a sunspot-like configuration idealized in Fig. 3a, a very much smaller final dipole

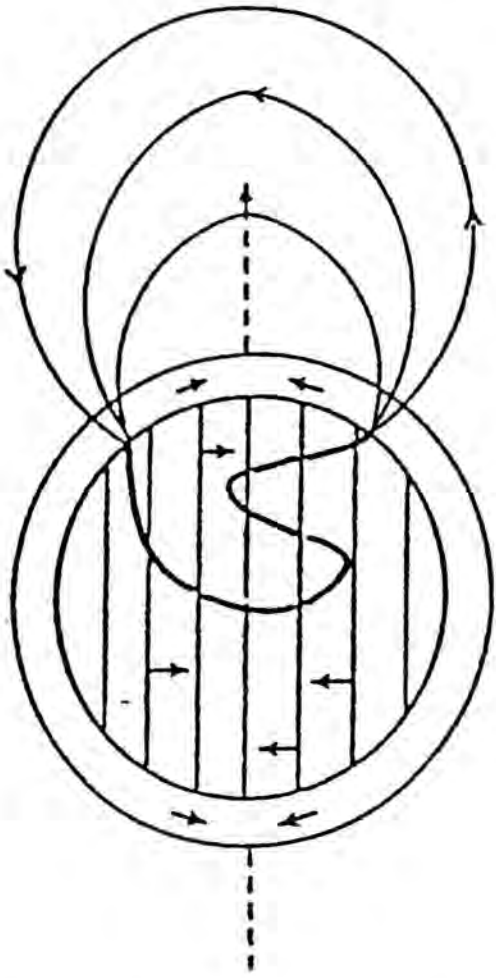

Figure 2. Direction of motion of vortex lines, crust and flux tubes in a spinning-up neutron star.

field like that of Figure 4a will be reached. In this case P continues to grow smaller until it approaches the smallest possible spin period of a neutron star.

Case (c). If in the pre-spun-up state, enough magnetic flux from one spin-hemisphere returns to the opposite one, prolonged spin-up would compress the component of μ perpendicular to the spin axis and put the main magnetic dipole component along the spin-axis as in Figure 4b. (While the perpendicular component is continually diminished by the spin-up the parallel one is modestly increased by it.)

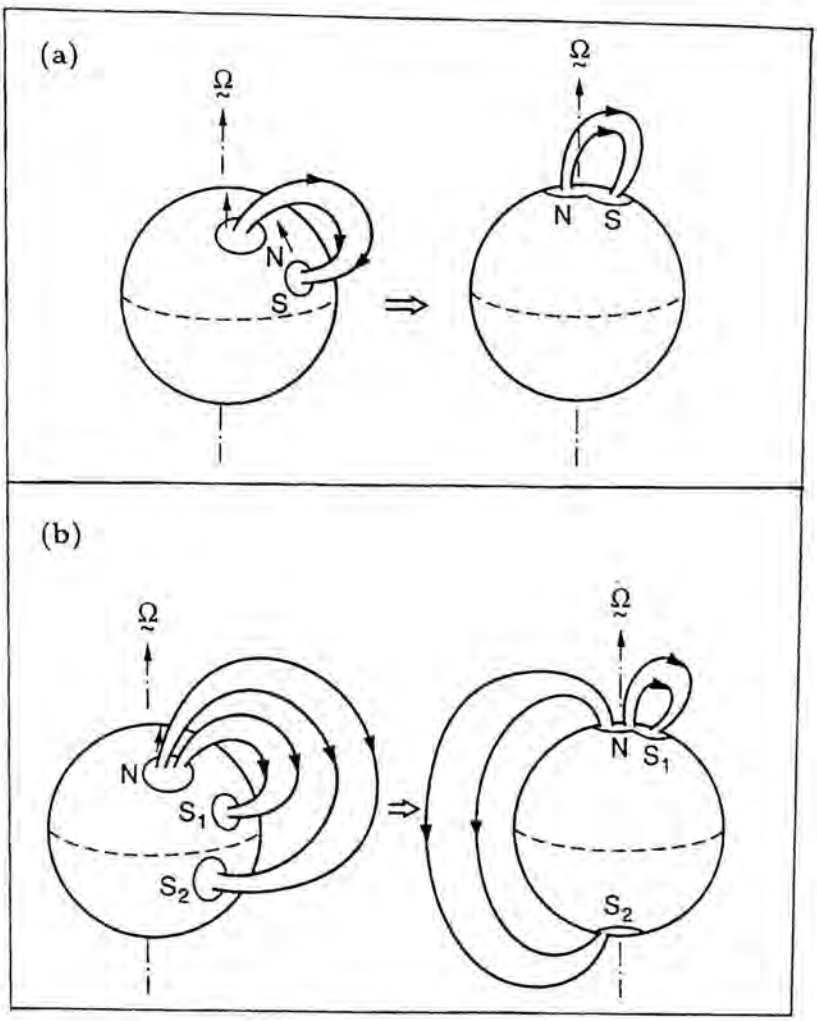

Figure 3. Evolution of surface magnetic field structure in a spun-up neutron star when *a)* all of the magnetic flux returns to the same (spin) hemisphere as that from which it leaves the stellar surface and *b)* some flux returns in the opposite hemisphere.

Thus, the extremely rapid spinning low-dipole field tail of the millisecond pulsar population should have a high fraction which are either: 1) orthogonal rotators as in case (b), characterized by two radio-subpulses separated by approximately half a period; or 2) nearly aligned rotators as in case (c), with rotating radio emission beams which make relatively small angles (θ) with the neutron star spin axis. The observed pulse width of such nearly aligned rotators should be anomalously broadened typically by a factor $\sin^{-1}\theta$.

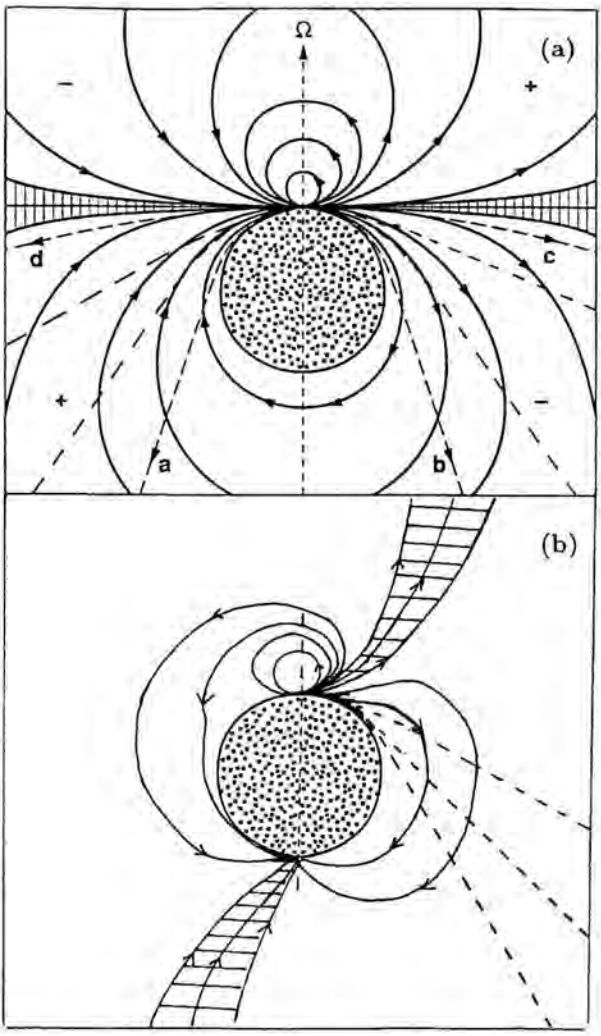

Figure 4. Magnetic field configuration achieved by spin-up for *a)* the initial field of Fig. 3a and *b)* of Fig. 3b. The open field line bundles are shaded. The fan beams are those discussed in the text.

In the recent catalogue of 558 pulsars (Taylor, Manchester & Lyne 1993), only 5 among the 526 disk-population radio pulsars with $P \geq 6$ ms have strong interpulses separated by frequency independent intervals of around $P/2$. By comparison, at least 4 among the 11 radio pulsars in the disk with $P \leq 6$ ms have such strong interpulses (cf. Figure 5). Jayawardhana & Grindlay (1996) identify 6 of the 20 reported disk millisecond pulsars as orthogonal rotators. It has been suggested that

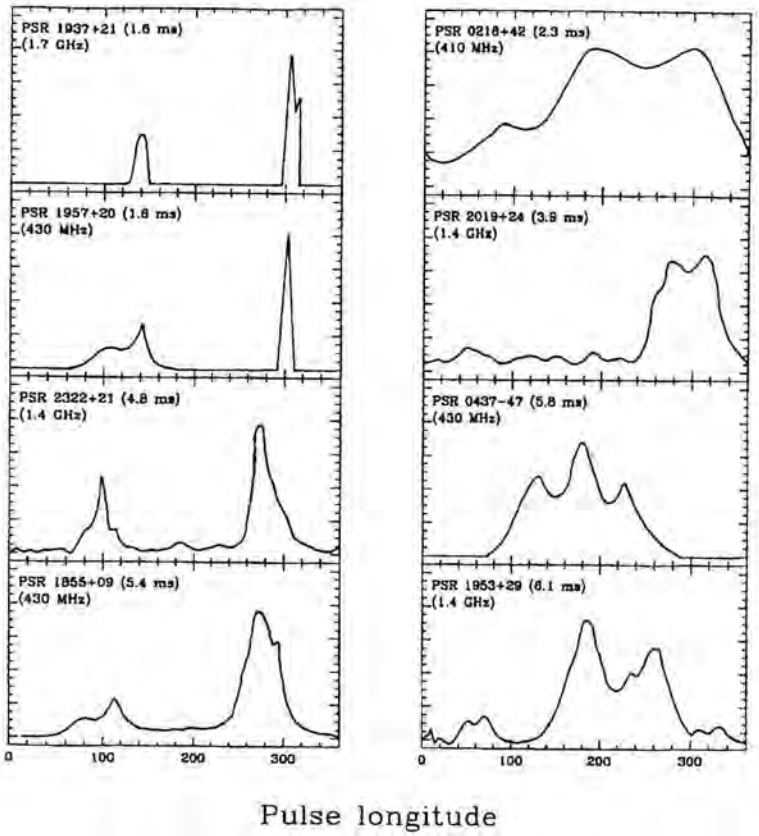

Figure 5. Radio pulse profiles of millisecond pulsars most simply interpreted as *a)* four orthogonal rotators and *b)* four nearly aligned rotators.

this common pulse-interpulse structure of millisecond pulsars is attributable to the double observation of a single conal beam: the wide opening angle expected for millisecond pulsars (width $\propto \Omega^{1/2}$) is then proposed as the reason for the large pulse-interpulse separation. This alternative interpretation has great problems with at least two questions. Why doesn't the separation phase between the two pulses vary with the observed radio frequency as is usually the case for double pulsed cone beam observation of a canonical pulsar? Why are the pulse-interpulse separations so close to 180°?

Remarkably, although 1/3 of the millisecond pulsars seem to be orthogonal rotators, another 1/3 are most easily interpreted as nearly aligned ones (Fig. 5). Four of the millisecond pulsars with $P \leq 6$ ms have extraordinarily large pulse widths. Even if broad pulses are expected from millisecond pulsars just because they spin so rapidly, the exceptionally large observed widths, e.g., 360° for J0218+4232 (Navarro et al.

Table 1: Field strength and area of central dipole and squeezed field polar caps.

	Field strength (G)	Area (cm^2)
Central dipole	$\leq 10^9$	4×10^{11}
Squeezed field	10^{11}–10^{12}	4×10^8–4×10^9

1995) and 270° for J0437−4715, seem to put pressure on such an explanation. The analysis of Gil & Krawczyk (1997), which incorporates polarization data, gives $\theta \sim 20°$ for PSR J0437−4715.

The local surface magnetic fields of "squeezed" polar caps are quite different from those inferred from canonical central dipole models (Table 1). We note in the "squeezed field" model the polar cap magnetic field and characteristic Goldreich-Julian charge density ($\sim \Omega B/2\pi c$) do not differ much from those of canonical pulsars even though the millisecond pulsars' dipole moments inferred from spin-down rates are 3 to 4 orders of magnitude smaller. Quantitative properties, including the formation of structures which lead to coherent radio emission with frequency of order a GHz, may have the same explanation in both. It is often argued (e.g., Rankin 1990) that the narrow core emission beam observed from many younger canonical radio pulsars originates at the polar cap itself. If so, one might also expect such core emission beams (e.g., a beam with properties similar to those for the "precursor" in the Crab pulsar) to be common from the polar caps of a spun-up millisecond pulsar. The narrow widths of such beams suggest that not only are they formed at or very near the stellar surface but also that they have a component whose propagation direction is thereafter no longer determined by the diverging open field line bundle. If so, such beams when they are initially formed with a propagation direction tangential to the stellar surface as in Fig. 4a or formed at the upper polar cap in Fig. 4b, may be gravitationally bent into fan beams which extend them greatly in latitude while preserving their narrow longitudinal width. It has been argued (Chen & Ruderman 1993) that the polarization properties of the two observed radio beams from PSR B1937+21 do indeed seem to be those of a pair of narrow fan beams which have passed through the closed field line part of that pulsar's corotating magnetosphere (Fig. 4a). (The model also explains the small shoulder notch in one of the beams at higher frequencies, just where a second polarization model enters.) PSR B1957+20, on the other hand, is probably viewed from a direction nearly orthogonal to the spin axis since it is eclipsed by its light companion. This would allow observation of the cone emission expected from its open field bundle and then 180° later with either its narrow core fan beam or part of the other broad cone beam from the other side. The detailed pulse structure and polarization suggests the former.

The aligned rotator model with "squeezed" polar caps should give an explanation of the strongly modulated X-ray light curve of PSR J0437. PSR J0437 was observed

to be a modest soft X-ray source, most likely a heated polar cap (Becker & Trumper 1993). Its X-ray light curve is characterized by a single broad peak which is strongly modulated with spin period. But if, as discussed above, the extraordinary broad radio pulse width indicates that this neutron star is indeed nearly an aligned rotator and that it is viewed from a direction not too far away from the pulsar spin-axis, why should its spinning X-ray hot polar cap give such strong X-ray modulation? If it has the canonical 10^9 G polar cap field (for which $\hbar eB/m_e c \sim 30$ eV), this low field should have essentially no effect on X-ray emission. However, the $10^{11} - 10^{12}$ G local polar cap field from the "squeezed flux" model could greatly modulate observed X-rays in several ways as its aspect to the observer rotates. One possibility for strong modulation depends upon cyclotron-resonant scattering of X-rays by e^- very near the polar cap (Becker & Trumper 1993), only possible for a magnetic field similar to that of a squeezed polar cap of Table 1. The area (A) of a squeezed polar cap should also be much smaller than the $A_0 \sim 10$ km^2 from the conventional central dipole model with $P = 5.75 \times 10^{-3}$ s. Indeed, Becker & Trumper (1993) reported $A \sim 0.05$ km^2, comparable to what is expected from the "squeezed flux" model ($A \sim 10^{-2} A_0 \sim 0.1$ km^2). However, the new analysis of Halpern et al. (1996) admits both the canonical A_0 and small squeezed flux $10^{-2} A_0$ as possible.

III Spinning-down pulsars and glitches

The arguments for core and crust magnetic field evolution during neutron star spin changes is, at present, somewhat less compelling for spinning-down canonical young pulsars because of their large $|\mathbf{V_v}|$. However, the expected core magnetic field changes should certainly stress the crust of such a star to near or above its yield strength. If the growing crustal strains are suddenly relaxed by a crust cracking event, various features observed or observable in such glitches would result. These include

a) a sudden jump in Ω from the movement (probably because of vortex unpinning) of crustal superfluid neutron vortices;

b) a sudden unhealed jump in $\dot{\Omega}$ because the sudden surface magnetic field changes because of crustal movement in a cracking event and alter the spin-down torque on the star;

c) readjustment of the core neutron superfluid vortex array when the flux tube array in which it is imbedded changes because of the sudden crust cracking;

d) cessation of glitching after the core field is completely expelled.

While feature a) is common to most glitch theories (Alpar et al. 1984), the others are not and may lead to ways of discriminating among models.

Acknowledgements

This work is supported in part by the NASA grants NAG5-2841 and NAG5-3229.

References

Alpar, M.A., Langer, S.A. & Sauls, J.A. 1984, ApJ, 276, 325
Alpar, M.A. et al. 1984 ApJ, 278, 791
Becker, W. & Trumper, J. 1993, Nature, 365, 528
Chen, K. & Ruderman, M. 1993, ApJ, 408, 179
Gil, J. & Krawczyk, A. 1997, MNRAS, 285, 561
Halpern, J.P., Martin, C. & Marshall, H. 1996, ApJ, 462, 908
Jayawardhana, R. & Grindlay, J.E. 1996, preprint
Lyne, A.G. et al. 1996, Nature, 381, 497
Navarro, J. et al. 1995, ApJ, 455, L55
Rankin, J. 1990, ApJ, 352, 247
Ruderman, M. 1991, ApJ, 366, 261
Ruderman, M. 1991a, ApJ, 382, 576
Sauls, J. 1989, in Timing Neutron Stars (NATO ASI Series), ed. H. Ögelman & E.P.J. van den Heuvel (Dordrecht: Kluwer), 457
Srinivasan, G. et al. 1990, Curr. Sci., 59, 31
Taylor, J., Manchester, R. & Lyne, A.G. 1993, ApJSS, 88, 529
Zhu, T. 1997, Ph.D. Thesis, Columbia Univ.
Zhu, T. & Ruderman, M. 1997, ApJ, 478, 701
Zhu, T. & Ruderman, M. 1997, in preparation

Authors' Addresses

Physics Department and Columbia Astrophysics Laboratory, Columbia University, New York NY 10027, U.S.A.

D. Bhattacharya

Models for the Evolution of Neutron Star Magnetic Fields

Abstract

Recent observations indicate that the magnetic field of a neutron star decays significantly only when the neutron star is in an interacting binary. This paper reviews the theoretical attempts to model such evolution. Three main possibilities are discussed: the expulsion of the magnetic flux from superconducting core during propeller spin-down in companion's wind, screening of the magnetic field by accreted matter and rapid ohmic decay of crustal magnetic field as a result of heating during accretion. It is found that the screening is unlikely to be effective because of strong Rayleigh-Taylor instabilities. The spindown-induced flux expulsion as well as the crustal heating models remain promising.

I Introduction

The earliest model for the evolution of the magnetic fields of neutron stars was due to Gunn and Ostriker (1970), who suggested a simple exponential ohmic decay of the field strength with a time scale of a few million years. This was the accepted picture of field evolution for nearly two decades, despite theoretical objections raised quite early on (e.g., Baym, Pethick & Pines 1969). Of late, however, there is a growing consensus that the decay of the magnetic field of a neutron star is associated with the interaction of the neutron star with a companion star in a binary system, and in isolated neutron stars there is little evidence of field decay (see contribution by F. Verbunt et al. in this volume).

Building a physical model for the reduction of the magnetic field strength of a neutron star primarily because of interaction with a companion poses a theoretical challenge. The last few years has seen a large number of models being proposed. These models have been explored to different degrees of detail, but it would be fair to say at present that no single model has been fully developed, and no single model is consistent with all observed data. I have been asked to give an overview of these models, but in view of the limited length of this contribution I would like to confine my description to a few models which in my opinion are, or have been considered, most promising.

One of the major uncertainties surrounding the picture of the field evolution is the location of the magnetic field in the interior of the star. This issue is not unrelated to the origin of neutron star magnetic fields. If the magnetic field is a fossil remnant from the progenitor stage, the field is likely to penetrate the whole star. The major fraction of the magnetic flux in such a case would pass through the superconducting interior of the neutron star. On the other hand, if the magnetic field is generated via thermomagnetic instabilities after the birth of the neutron star (e.g., Blandford, Applegate & Hernquist 1983), then the resulting field is likely to be confined to the outer crust of the neutron star. Physical processes affecting the core field and the crustal field are different, and one therefore needs to investigate different classes of models for these two cases.

II Magnetic field in a normal n-p-e core

Some attention has been devoted in the last few years to the evolution of the magnetic field permeating the neutron star core, assuming that the matter there is in a normal (i.e., non-superfluid) state. Although this may not be the situation in a real neutron star, the results obtained from this exercise are instructive, and a number of concepts have applications also in the case of a superfluid interior.

The evolution of the magnetic field in the normal n-p-e core is governed by a generalized form of Ohm's law (Shalybkov & Urpin 1995):

$$\mathbf{E} + \frac{\mathbf{v}}{c} \times \mathbf{B} = \frac{\mathbf{G}}{2en_{\rm e}} - \frac{\mathbf{u}_{\rm n}}{c} \times \mathbf{B} + \mathbf{R} \cdot \mathbf{j}, \tag{1}$$

where $\mathbf{G}$ is a force term including pressure and partial pressure gradients. If this term has a non-zero curl, then magnetic field can be spontaneously generated via battery effect (Biermann 1950). However, in a neutron star this effect is unimportant (Shalybkov and Urpin 1995). $\mathbf{u}_{\rm n}$ is the drift velocity of neutrons, and $\mathbf{R} \cdot \mathbf{j}$ stands for

$$\mathbf{R} \cdot \mathbf{j} = R_{\parallel} j_{\parallel} + R_{\perp} j_{\perp} + \frac{R_{\rm H}}{B} \mathbf{j} \times \mathbf{B}, \tag{2}$$

where the parallel and perpendicular components are in reference to the direction of the magnetic field $\mathbf{B}$, and $R_{\rm H}$ is the Hall resistance. $\mathbf{R} \cdot \mathbf{j}$ includes the effects of Ohmic diffusion, Ambipolar diffusionand Hall effect (Goldreich and Reisenegger 1992; Shalybkov & Urpin 1995). Other symbols in equation (1) have their usual meaning.

A number of important evolutionary time scales can be isolated in this context (Goldreich & Reisenegger 1992):

$$t_{\rm ohmic} \sim 2 \times 10^{13} \frac{L_6^2}{T_8^2} \left(\frac{\rho}{\rho_{\rm nuc}} \right)^3 \ {\rm yr}$$

$$t_{\rm ambip}^{\rm s} \sim 3 \times 10^{11} \frac{T_8^2 L_6^2}{B_{12}^2} \ {\rm yr}$$

$$t^{\rm ir}_{\rm ambip} \sim \frac{5\times10^{15}}{T_8^6 B_{12}^2}(1+5\times10^{-5}T_8^8 L_6^2) \ {\rm yr}$$

$$t_{\rm Hall} \sim 5\times10^{10}\frac{L_6^2}{B_{12}}\left(\frac{\rho}{\rho_{\rm nuc}}\right) \ {\rm yr}$$

where L_6 is the scale length of the field distribution in units of 10^6 cm, T_8 is the temperature in units of 10^8 K and B_{12} is the field strength in units of 10^{12} G. These time scales are for ohmic diffusion, solenoidal ambipolar diffusion irrotational ambipolar diffusion and Hall drift respectively. In ambipolar diffusion, compared to the solenoidal component of field movement, the time scale is much longer for the irrotational component, because the attendant drift of charged particles is suppressed by chemical imbalance. This drift can therefore take place only in the time scale over which chemical balance can be restored. The estimate of $t^{\rm ir}_{\rm ambip}$ above assumes restoration of chemical equilibrium via the modified URCA process. Ohmic diffusion and ambipolar iffusion cause dissipation of magnetic energy, while Hall drift only rearranges the magnetic field configuration. Goldreich & Reisenegger (1992) conjectured that Hall drift may work like a turbulent cascade, creating very small current loops which would eventually undergo quick Ohmic decay. Hall-cascade-assisted ohmic dissipation may indeed be a very important process operating in the inner crusts of neutron stars.

III Magnetic field in the superconducting interior

The interior of the neutron star is believed to contain a mixture of superfluid neutrons and superconducting protons. The proton superconductor is estimated to have a coherence length much smaller than the London penetration depth, causing it to exhibit a type II behavior. Magnetic flux passing through the core must therefore be carried by quantized Abrikosov fluxoids in the proton superconductor (see reviews by Srinivasan, this volume, Bhattacharya & Srinivasan 1995 and Sauls 1989). The total number of such fluxoids in the neutron star interior would be $\sim 10^{31}(B/10^{12}$ G). The angular momentum of the core neutron superfluid, on the other hand, is carried by Onsager-Feynman vortices, the number density of which is proportional to the angular speed of the superfluid. The number of neutron superfluid vortices in the core is $\sim 2\times10^{16}(P/1\ {\rm s})^{-1}$. As the neutron star spins down, these vortices migrate outward, and are shed upon reaching the boundary of the superfluid.

Muslimov and Tsygan (1985) first recognized that there is likely to be a strong interpinning between the proton fluxoids and the neutron vortices. The physical nature of this pinning was elaborated upon, and its magnitude was estimated by Sauls (1989). Srinivasan et al (1990) suggested that this may be the main mechanism for the expulsion of flux from the superconducting interior—as the star spins down, the neutron vortices migrate outward, carrying with them the fluxoids. The magnetic flux is then deposited in the crust, where it can decay due to ohmic processes. In an isolated

neutron star spinning down by dipole torque, the net spindown is small, and only a modest amount of flux is expelled. A neutron star in a binary can spin down to a very long period in the phase of interaction with the stellar wind of the companion, and hence a large amount of field decay can occur.

Jahan Miri and Bhattacharya (1994) explored in detail the spindown process and the consequent field decay in wide low-mass X-ray binaries, systems that appear to have produced neutron stars with the lowest known magnetic fields (millisecond pulsars). They found that the field strengths, their correlation with the orbital periods, and the apparent lower limit to the field at $\sim 10^8$ G, can be explained if the ohmic decay time of the magnetic field after expulsion to the crust is around 10^8–10^9 yr. If the field decays too quickly, then the spindown torque due to the companion's wind diminishes too early to achieve enough flux expulsion. If it decays too slowly, then eventual spin-up to millisecond periods becomes impossible.

Bhattacharya and Datta (1996) investigated the ohmic evolution of the expelled field in the crust, and found that in a cold neutron star with the temperature of the inner crust of $\sim 10^6$ K, the ohmic evolution of the field is decided mainly by the resistivity arising out of impurity scattering. Ohmic time scale in the range 10^8–10^9 can be obtained with a fairly modest impurity concentration, the parameter

$$Q = \sum_i n_i (Z_i - Z_0)^2 / n_0$$

being in the range 0.01–0.1 depending on the equation of state of neutron star matter; here n_i and Z_i are the density and the charge number of the i-th species of impurity atoms, and n_0 and Z_0 that of atoms of pure matter. If the crust is heated to a temperature $\sim 10^8$ K, say by accretion, then phonon scattering makes a significant contribution to the resistivity, and field decay is hastened.

It is, however, the massive binary systems that seem to place stronger constraints on this scenario (Jahan Miri 1996). Many X-ray pulsars with long spin periods still appear to have quite strong fields $\sim 10^{12}$ G (see White, Nagase & Parmar 1995), while by the time the spin-up in heavy accretion finishes, the field has already decayed by some two orders of magnitude (e.g., pulsars B1913+16, B1534+12, J1518+4904). This constrains the required Ohmic time scale after flux expulsion very strongly, and is barely consistent at $10^{7.5}$ yr.

How is one to reconcile this constraint with that for low-mass binaries? One possibility is to attribute most of the ohmic decay of the expelled flux to the phase of heavy accretion by Roche-lobe overflow, when the crust is heated to a high temperature. A low mass binary takes a long time to evolve to this stage, before which a slow but steady propeller phase removes angular momentum from the neutron star. This is also an ideal situation for flux expulsion; if the spin-down is too quick then flux expulsion efficiency is reduced because of the drag on flux lines, as well as possible back-reaction from flux accumulated at the bottom of the crust (Jones 1988;

Ding, Cheng & Chau 1993; Jahan Miri & Bhattacharya 1994). Massive binaries may well suffer from this inefficient expulsion, being thereby unable to produce neutron stars with as low magnetic fields as in low-mass binaries. The other possibility is a progressive lengthening of effective decay time as, for example, is expected in case of a Hall cascade-mediated decay.

While this remains an attractive model for the field decay in neutron stars, a number of unsolved problems still shroud the fluxoid dynamics. Foremost of these is the collective effects on their motion. The drag on fluxoids, for example, is strongly dependent on collective effects. If large groups of fluxoids act as macroscopic, collective entities then an important restriction applies on their motion: they cannot move faster than the rate allowed by Ohmic diffusion (see Ruderman, this volume on how to turn this into an effective drag coefficient). If they do, then they must carry the charged component with them, causing a chemical imbalance which would suppress the irrotational part of the flow, akin to ambipolar diffusionGoldreich & Reisenegger 1992). On the scale of the width of a single fluxoid, however, the Ohmic diffusion time is too small to be important for dynamics. It is therefore very important to understand the collective effects, to which end not much progress has been made so far. Another important question is whether the proton superconductor does exhibit Type II properties. Some recent calculations have revised the estimate of the proton energy gap downwards (e.g., Wambach, Ainsworth and Pines 1991) almost into the Type-I regime. If the superconductor does happen to be of Type I, then quantized fluxoids no longer exist, and the field may be trapped into macroscopic regions of normal matter sandwiched between superconducting layers. There is no clear picture of how the magnetic flux would behave under such condition, and whether accretion can have any effect on its evolution.

In the category of spin-magnetic field coupling falls another set of models by Ruderman (1991a,b,c). In this picture crustal plate tectonics causes the magnetic poles to migrate to the (rotational) equator as the star spins down. At the equator the poles may come very near each other due to flux-line tension, and thereby annihilate a part of the dipole moment. On spin-up, the poles are pushed to the rotational poles of the star. The magnetic moment increases if the magnetic poles migrate to opposite rotational poles, and decreases further if they migrate to the same rotational pole.

IV Screening of the magnetic field by accreted matter

Suggestions that the accreted matter on the neutron star surface can reduce its externally visible magnetic moment by diamagnetic screening have been in the literature for a long time (e.g., Bisnovatyi-Kogan and Komberg 1974), and has been developed beyond a mere suggestion more recently (Romani 1990,1993). The basic idea is that the accreted matter arrives at the magnetic poles, guided by the magnetic field. At the pole an accretion column builds up till the pressure at the bottom of the column exceeds the

confining magnetic pressure. At this point matter begins to flow sideways, dragging the field lines with it. Upon reaching the equator from both poles field reconnections occur, causing an eventual burial of the original field under the newly acquired layer of accreted matter. Once the screening is accomplished, the buried field can be driven deeper by further accretion. This mechanism, if it works in practice, would not care if the original magnetic field resides in the core of the star or in the crust.

However, whether this mechanism works at all is in serious doubt, mainly because of the matter flow being strongly susceptible to Rayleigh-Taylor instability. To stretch the vertical field lines in the horizontal direction, the flow must create a horizontal component of the magnetic field of magnitude similar to the original vertical field. The pressure of this horizontal magnetic field therefore nearly equals the hydrostatic pressure of the accretion column. Under this condition, the Rayleigh-Taylor instability grows very rapidly: at the burial depths estimated by Romani (1993) (density at burial depth $\rho \sim 10^6 B_{12}^{-1.5}$ g cm^{-3}) the overturn time works out to be a few microseconds, much shorter than the "flow time" (time needed for the accretion column to be replenished with accreted matter). The accreted matter is therefore likely to just move through the magnetic field, continuously creating horizontal extensions which overturn, reconnect and disappear, leaving the original vertical field essentially undisturbed in the end (Konar 1996).

V Magnetic fields confined to the outer crust

Over the last few years, a number of papers have investigated the ohmic decay of magnetic field initially confined only to the outer crust (Sang & Chanmugam 1987; Urpin and Muslimov 1992; Urpin & van Riper 1993; Geppert and Urpin 1994; Urpin & Geppert 1995,1996). Initial magnetic field configuration such as this may be expected if the field is generated after the birth of the neutron star via thermomagnetic instabilities (Blandford, Applegate and Hernquist 1983). The evolution of this field is determined by two major parameters: (i) electrical conductivity σ which is a function of the density, temperature and impurity strength Q in the crust, and (ii) the scale length of the field distribution. The smaller the scale length, the faster the Ohmic diffusion. An initially tightly confined field distribution near the surface diffuses to larger scales, into regions of higher density in the interior. This phase results in a power-law decay of the field strength at the surface (see Bhattacharya 1995 for a review). In practice, in an isolated neutron star the crustal temperature is high enough for some field decay (by $\lesssim$ an order of magnitude, depending on the initial penetration depth of the field configuration) to occur in the first $\lesssim 10^6$ yr or so, beyond which the decay proceeds very slowly. This early phase of decay might be responsible for the field strengths of very young pulsars associated with supernova remnants being somewhat larger than the average field strength of the majority of isolated pulsars which are a little older.

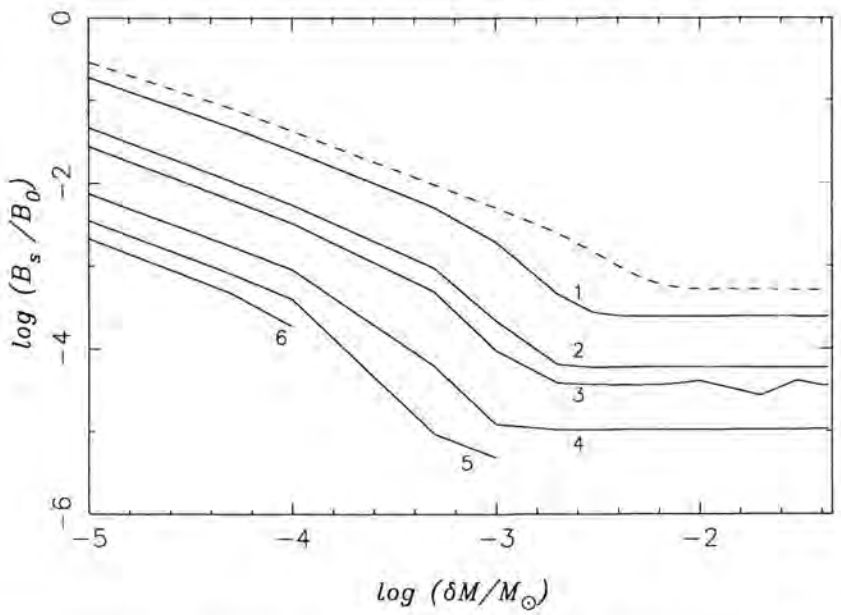

Figure 1. Evolution of the magnetic field of a neutron star undergoing accretion. The initial field is assumed to be confined to the outer crust. Accretion causes heating, enhancing ohmic diffusion rate, and also pushes current-carrying layers to higher densities (and hence higher conductivities), thereby slowing down the decay. The net result is an initial rapid decay followed by freezing. The figure plots the surface field strength versus the amount of mass accreted. Curves 1 to 6 correspond to accretion rates of 10^{-9}, 2×10^{-10}, 10^{-10}, 10^{-11}, 10^{-12} and 10^{-13} $M_\odot$/yr. The crustal temperatures as a function of accretion rate were obtained from a fit to the results of Zdunik et al. (1992). The dashed curve corresponds to 10^{-9} $M_\odot$/yr, but for a factor-of-two lower temperature of $10^{8.5}$ K. The evolution is shown for a maximum of 10^9 yr. Taken from Konar & Bhattacharya (1997).

A substantial decay of the magnetic field would, however, take place once the crust is heated by accretion. The work of Urpin and Geppert (1995,1996) showed that the decay due to even mild accretion could be quite substantial. Konar and Bhattacharya (1997) developed this further and included the effect of the inward convection of current-carrying layers due to accreted overburden: all of the original crustal matter is pushed into the core if the total accreted mass exceeds $\sim 10^{-2}$ $M_\odot$. The effect of accretion is therefore found to be to first hasten the field decay, and then to *freeze* it at a residual value as most of the flux enters the core. The higher the accretion rate, the stronger is the residual field. Figure 1 shows an example of such evolution. As can be seen, the field strength depends not only on the net accreted mass, but also on the accretion rate.

VI Summary

To sum up, the present situation on modeling neutron star magnetic field evolution appears to be as follows.

If the magnetic field is trapped in the superconducting interior of the neutron star, expulsion is a must for field decay to take place. Spindown-induced flux expulsion remains the most promising mechanism for this. Many uncertainties still remain in the dynamics of magnetic flux under this condition, and reliable quantitative predictions cannot be made unless some of these are settled.

In the crust, Hall-cascade assisted ohmic decay appears very promising. Detailed investigation of this would be very useful.

Burying of the magnetic field by accreted matter has serious difficulties. This picture is unlikely to explain the low fields of recycled pulsars.

If the field is entirely in the crust to start with, it is expected to show $\sim$ 1 order of magnitude decay in the early life of isolated neutron stars. On accretion, heating hastens decay while migration of currents to higher densities stabilizes the field.

It has been popular in recent literature to parametrize the amount of field reduction as a simple function of the total mass accreted. There is no physical model which can accomplish this. The closest is the scenario where the field is originally confined to the crust and the decay happens due to heating on accretion. Even in this scenario, however, the final field has a major dependence on the accretion rate itself, in addition to the net accreted mass.

Acknowledgements

I thank the Royal Netherlands Academy of Arts and Sciences for a travel grant, and hospitality during the conference. Discussions with many colleagues, in particular B. Datta, S. Konar, M. Jahan Miri, A. Reisenegger, M. Ruderman, J. Sauls, G. Srinivasan and V. Urpin are gratefully acknowledged.

References

Baym, G., Pethick, C. & Pines, D. 1969, Nature, 224, 673
Bhattacharya, D. 1995, J. Astrophys. Astron., 16, 227
Bhattacharya, D. & Datta, B. 1996, MNRAS, 282, 1059
Bhattacharya, D. & Srinivasan, G. 1995, in X-Ray Binaries, ed. W.H.G. Lewin, J.A. van Paradijs & E.P.J. van den Heuvel (Cambridge: Cambridge University Press), 495
Biermann, L. 1950, Zs. f. Naturforsch., 5a, 65

Bisnovatyi-Kogan, G.S. & Komberg, B.V. 1974, Soviet Ast., 18, 217
Blandford, R.D., Applegate, J.H. & Hernquist, L. 1983, MNRAS, 204, 1025
Ding, K.Y., Cheng, K.S. & Chau, H.F. 1993, ApJ, 408, 167
Geppert, U., & Urpin V.A. 1994, MNRAS, 271, 490
Goldreich, P. & Reisenegger, A. 1992, ApJ, 395, 250
Gunn, J.E. & Ostriker, J.P. 1970, ApJ, 160, 979
Jahan Miri, M. 1996, Ph. D. Thesis, Indian Institute of Science
Jahan Miri, M. & Bhattacharya, D. 1994, MNRAS, 269, 455
Jones, P.B. 1988, MNRAS, 233, 875
Konar, S. 1996, Ph. D. Thesis, Indian Institute of Science
Konar, S. & Bhattacharya, D. 1997, MNRAS, 284, 311
Muslimov, A.G. & Tsygan, A.I. 1985, Soviet Ast. Lett., 11, 80
Romani, R.W. 1990, Nature, 347, 741
Romani, R.W. 1993, in Isolated Pulsars, ed. K.A. Van Riper, R. Epstein & C. Ho (Cambridge: Cambridge University Press), 75
Ruderman, M. 1991a, ApJ, 366, 261
Ruderman, M. 1991b, ApJ, 382, 576
Ruderman, M. 1991c, ApJ, 382, 587
Sang, Y., & Chanmugam, G. 1987, ApJ, 323, L61
Sauls, J. 1989, in Timing Neutron Stars, ed. H. Ögelman & E.P.J. van den Heuvel (Dordrecht: Kluwer), 457
Shalybkov, D.A. & Urpin, V.A. 1995, MNRAS, 273, 643
Srinivasan, G. et al. 1990, Curr. Sci., 59, 31
Urpin, V.A. & Geppert, U. 1995, MNRAS, 275, 1117
Urpin, V.A. & Geppert, U. 1996, MNRAS, 278, 471
Urpin, V.A. & Muslimov, A.G. 1992, MNRAS, 256, 261
Urpin, V.A. & Van Riper, K. 1993, ApJ, 411, L87
Wambach, J., Ainsworth, T.L. & Pines, D. 1991, in Neutron Stars: Theory and Observation, ed. J. Ventura & D. Pines, (Dordrecht: Kluwer), 37
White, N.E., Nagase, F. & Parmar, A.N. 1995, in X-Ray Binaries, ed. W.H.G. Lewin, J.A. van Paradijs & E.P.J. van den Heuvel, (Cambridge: Cambridge University Press), 1
Zdunik, J.L. et al. 1992, ApJ, 384, 129

Authors' Address

Raman Research Institute, Bangalore 560080, India

A. Muslimov and E.P.J. van den Heuvel

Novel Mechanism of Field Reduction in Accreting Neutron Stars in Binaries

Abstract

We suggest that in a rapidly rotating accreting neutron star the tangential material stresses produced by the pinned superfluid vortices on the crustal lattice (discussed by Ruderman) may result in continual shearing of the segments of the magnetic field lines that traverse the inner crust where they are embedded into a charged component. The magnetic field that is initially anchored into the highly-conducting stellar core becomes separated (owing to continual shearing and weakening of the regular poloidal magnetic field in the inner crust) into a long-lived core component and a short-lived crustal component. The combined effects of the shearing of an initial poloidal magnetic field and subsequent ohmic decay and diffusion of a crustal component may self-consistently explain the available data on the spin and magnetic characteristics of binary pulsars.

I Introduction

We assume that (cf. Bhattacharya & van den Heuvel 1991) a neutron star (NS) in a binary system initially (before the onset of accretion phase) possesses the poloidal magnetic field of strength $\sim 10^{12}$ G anchored into a highly conducting core, and that the ohmic decay time for the lowest order (dipole) component of the field is comparable to a Hubble time.

We introduce a hitherto ignored effect, the radial shearing of the poloidal magnetic field in the inner crust of a spinning-up accreting NS. The shearing results from the stresses which the superfluid (s/f) neutron vortices (that are subject to the collective displacements caused by the differential rotation between them and the s/f) produce on the crustal lattice to which they are pinned (Ruderman 1991a). We discuss the way in which the radial shearing modifies the subsequent evolution of the poloidal magnetic field of a NS, and we find that the resulting modification is fundamental for the field evolution in rapidly rotating NSs in binaries.

II Shearing of the magnetic field in the inner crust of a rapidly spinning accreting neutron star

In our model we exploit the possibility of occurrence of a neutron superfluidity in the inner crust of a NS and incorporate very interesting concept introduced by Ruderman (1991a; see also 1991b,c) that in rapidly spinning NSs the material stresses from the pinned s/f neutron vortices in the crustal lattice may be sufficiently strong to move the crust. We suggest that the slow meridional motions ("plate tectonic" motions, discussed by Ruderman), caused by these stresses, will result in an irreversible shearing of the segments of the magnetic field lines located in the inner crust. As an inevitable consequence of this shearing the whole pattern of the magnetic field within a star transforms into two differently evolving poloidal structures: (the details of this process will be discussed in a separate publication) one is confined to the crust; the other is mostly confined to the core. In an accreting NS the "crustal" component becomes short-lived ($\sim 10^5$–10^6 yr), while the "core" component remains essentially long-lived ($\sim$ Hubble time). We suggest the following sequence of the main physical events that may eventually determine the resulting surface magnetization of a NS in a binary:

1. An initially high-magnetic-field NS is heated up by accretion. As a result, the electric resistivity of the crustal matter substantially increases, causing redistribution of the electric currents sustaining large-scale magnetic configuration of a NS. This redistribution results in a decrease (by a factor of $\lesssim 10$) in the surface value of the magnetic field strength. The latter then allows a NS to spin-up during acccretion phase to the critical spin period at which the shearing of the poloidal magnetic field in the inner crust will begin ($P \lesssim 0.1$ s).

2. The shearing of the poloidal magnetic field in the inner crust of a rapidly spinning accreting NS separates the crustal component of the field and results in its accelerated decay (owing to the enhanced ohmic dissipation).

3. In a post-accretion NS the core component of the poloidal magnetic flux subsequently diffuses up through the crust and emerges from the stellar surface.

As a result of the spin and magnetic evolutions in a binary, depending on the duration of the accretion phase and on the total accreted mass and angular momentum, three types of NSs in binaries are expected to occur: the NSs with a rather strong ($\sim 10^{11}$–10^{12} G) long-lived surface magnetic field, NSs "without" ($< 10^8$ G) magnetic field, and NSs with a considerably reduced ($\sim 10^8$–10^{10} G) long-lived surface magnetic field.

In a spinning-up NS the crustal s/f rotates slightly slower than the rest of a star owing to the weak coupling of the neutron s/f with a charged component in the inner crust. In the picture envisaged by Ruderman (1991a), before the vortex unpinning occurs, the lattice-s/f angular velocity difference ω reaches the maximum value, $\omega_{\rm B}$, above

which the growing material stresses caused by vortex lines pinned to lattice nuclei will break and move the crust. This occurs at the pulsar spin period (see Ruderman 1991a, formula [30] and relevant discussion) $P < 0.1(10^{-3}/\theta_{\rm m})s$, where $\theta_{\rm m}$ is the maximum value of the dimensionless strain θ (fractional change in length) which matter deep in the crust can bear before yielding.

These stresses result in the slow radial shearing of the crust lattice with embedded into it parts of the field lines that traverse the inner crust.

The shearing of the magnetic field lines in the inner crust of a NS results in that the regular component of a poloidal magnetic field in this region decreases. The formation of such a predominantly tangential magnetic structure in the inner crust should be facilitated by accretion-produced compression of a crustal matter. The shearing produces a dip in a radial profile of the poloidal magnetic flux (through the hemisphere) in the inner crust. This dip continually maintained by the shearing in the inner crust effectively traps the crustal currents, thus making their inward diffusion very inefficient and preventing them from restoring the initial distribution of currents. After the currents trapped in the crust are died off the large-scale magnetic field confined to the stellar interiors and having closed configuration gets dominated.

The initial poloidal magnetic field of a NS is expected to be transformed into the final configuration over timescale $t_{\rm sh} \sim \omega_{\rm B}\,\dot{\Omega}^{-1}$. Using the expression for the rate of change of the angular velocity of a standard NS (see e.g., Ghosh & Lamb 1979) and the value of $\omega_{\rm B}$ derived by Ruderman (1991a, see equation [18b]), we obtain $t_{\rm sh} \sim 10^5\ (P/1\ s)(\theta_{\rm m}/10^{-3})(\rho/4\times10^{13}\ {\rm g\ cm^{-3}})^{-1}\mu_{30}\,\mathcal{M}_{30}^{-2/7}\,L_{\rm X37}^{-1}$ yr, where ρ is the density of matter, $\mu_{30} \equiv \mu/10^{30}$ dyn cm^{-2}, μ is the shear modulus, $\mathcal{M}_{30} \equiv \mathcal{M}/10^{30}$ G cm^3, $\mathcal{M}$ is the magnetic dipole moment of a NS, and $L_{\rm X37} \equiv L_{\rm X}/10^{37}$ erg s^{-1}, $L_{\rm X}$ is the accretion-driven X-ray luminosity.

If during the accretion phase the spin period of a NS does not decrease down to the critical value of $\sim 0.1(10^{-3}/\theta_{\rm m})$ s introduced by Ruderman (1991a), then the shearing of the magnetic field in the inner crust is unlikely to occur. Instead, the magnetic field partially diffuses into the core, so that the strength of the surface magnetic field decreases only by a small factor of $\lesssim 10$. In the regime where an accreting NS spins up to the period less than $\sim 0.1\ (\theta_{\rm m}/10^{-3})$ s and reaches the equilibrium period $P_{\rm eq} \sim 0.1\ B_{\rm s11}^{6/7}\,L_{\rm X37}^{-3/7}$ s (where $B_{\rm s11} = B_{\rm s}/10^{11}$ G; $B_{\rm s}$ is the surface value of the magnetic field strength), we obtain $t_{\rm sh} \sim 3\times10^4(\theta_{\rm m}/10^{-3})(\rho/4\times10^{13}\ {\rm g\ cm^{-3}})^{-1}B_{\rm s11}^{4/7}\mu_{30}\,L_{\rm X37}^{-10/7}$ yr, which implies a positive feedback between the shearing and reduction of the magnetic field if the latter occurs during accretion at an approximately steady rate. Note that in the shear region the radius of curvature of a field line should be limited by some minimum value $l_{\rm min} \sim 0.4\ (R/10\ {\rm km})(10^{-3}/\theta_{\rm m})B_{\rm s11}^2\mu_{30}^{-1}$ cm ($\lesssim 1$ cm) so that arising magnetic stresses do not exceed the maximum stress the crust could bear before breaking. For the magnetic field configuration resulted from shearing the radius of curvature of the field lines is well above this limit.

The shearing of the magnetic field in the inner crust results therefore in the effective separation of crustal electric currents from the core currents thus making them evolve differently. If $t_{\rm sh}$ is less than ohmic decay timescale of the crustal currents, then the currents trapped in the crust continuously decay until they practically die off. In this case we come up with the situation where the magnetic flux of the poloidal magnetic field (through the hemisphere) is maximum in the outer core–inner crust region and vanishes within the crust (cf. Muslimov 1995). An immediate consequence of this is that a post-accreting NS that has undergone a prolonged phase of heavy accretion and spin-up, should not reveal any detectable surface magnetic field until the component of the magnetic field trapped in the core has diffused up through the crust. This is likely to occur on a Hubble timescale, but vanishingly small component of the magnetic field partially penetrated the inner crust may diffuse on a timescale of $\sim 10^7$–10^8 yr. We suggest that what is usually referred to as the *asymptotic* (*residual*) value ($B_\infty \sim 10^8$–10^9 G) of the magnetic field strength at the surface of a NS in low-field binary pulsars may well be the small fraction of the core component of the magnetic field that has diffused up through the stellar surface. We predict that the more matter a NS accreted the lower the asymptotic value of the magnetic field should be. This is due to the fact that the accretion tends to significantly reduce the value of the field strength in the outer core–inner crust region (as a result of accretion-induced compression of stellar matter and compactification of the internal structure of a NS) from which it can diffuse up through the surface during the post-accretion cooling phase of a NS.

The characteristic time for ohmic decay of the magnetic field trapped in the crust may be estimated as $\tau_{\rm d} \sim 10^5\ \rho_{13}^{7/6}(2 \times 10^8\ {\rm K}/T)^2(x/0.1)^{5/3}(h/300\ {\rm m})^2$ yr, where $\rho_{13} \equiv \rho/10^{13}\ {\rm g\ cm^{-3}}$ Thus, for a NS accreting at a rate of $\gtrsim 3 \times 10^{-10}{\rm M}_\odot\ {\rm yr}^{-1}$, one can expect that the crustal component of the magnetic field virtually disappears on a timescale of $\sim 10^5$–10^6 yr. The crustal component (that has been effectively "detached" from the core component by the radial shearing in the inner crust region) can apparently survive only a very short and relatively low-rate accretion phase.

In the scenario we suggest the radial distribution of the magnetic flux (through the stellar hemisphere) corresponding to the lowest order poloidal component of the magnetic field in the core of a post-accretion NS is such that it increases with the radial distance from the center and reaches some maximum value in the outer core, then it gradually decreases and penetrates the inner crust. Such a radial profile of the internal poloidal magnetic flux is a result of the transformation of the initial monotonic profile caused by the radial shearing of the initial poloidal magnetic field in the inner crust. It is the value of the relatively weak poloidal magnetic flux in the inner crust that may subsequently diffuse up through the crust and appear at the stellar surface. The value of a magnetic flux through the hemisphere in the inner crust depends on the amount of matter accreted by a NS: in a heavily accreting NS the maximum of the radial profile of the magnetic flux will occur at higher densities (owing to substantial compression of the surrounding matter caused by accretion), and the poloidal magnetic flux in the inner crust will level off at a much lower value.

III Magnetic field evolution in accreting neutron stars in binaries

The recent examination (van den Heuvel & Bitzaraki 1995) of 24 Low-Mass Binary Pulsars (LMBPs) with known orbital periods has revealed a remarkable correlation between the derived surface value of the magnetic field strength B_s of a NS and orbital period P_{orb} of a system. Since for systems with a donor star with a degenerate helium core the orbital period determines the amount of mass accreted by a NS, the correlation between B_s and P_{orb} is well consistent with the hypothesis that the efficiency of field reduction increases with increasing the amount of accreted matter. We suggest — in terms of the field reduction mechanism presented here — the following scenario for these systems. Before the beginning of the accretion phase a NS has a long-lived magnetic field with the canonical value ($\sim 10^{12}$ G) at the surface. The accretion heats up the stellar interiors and reduces the conductive properties throughout most of the crust. In less than $\sim 10^6$–10^7 yr the magnetic flux within the star will be slightly redistributed due mostly to the enhanced inward ohmic diffusion, so that the surface value of a magnetic field strength will decline by a factor of not more than 10. If in the course of spinning up the accreting NS does not reach the critical period of ~ 0.1 s, then a NS with $B_s \sim 10^{11}$ G may be left behind after the accretion is ceased. If, however, the NS is spun-up during the accretion phase to a rather short period ($\lesssim 0.1$ s), then the poloidal magnetic flux within the star breaks up into a core and a crustal component, owing to the radial shearing of the magnetic field in the inner crust. The crustal component decays very rapidly (over a timescale of $\lesssim 10^5$–10^6 yr). Then, after the accretion has ceased, it takes $\sim 10^7$–10^8 yr for the field component penetrated the inner crust from the core to diffuse up through the crust, which eventually results in the phenomenon of a weakly-magnetized, very old millisecond pulsar. This scenario is consistent with the available data (see, e.g., van den Heuvel & Bitzaraki 1995) on the spin periods, derived values of the magnetic field strength, and estimated efficiencies of accretion phase for LMBPs.

We also suggest that, as a consequence of our scenario, the NSs associated with the so-called atoll X-ray sources (van der Klis 1995) may well represent the abnormally weakly-magnetized NSs with $B_s < 10^8$ G.

The variety of possible (B_s, P) outcomes for a NS in a binary system that may be produced by the mechanism under discussion potentially covers all available data on the derived values of the surface magnetic field strength and measured spin periods observed in binary pulsars. For each binary system the evolution of the magnetic field of the NS is determined by its spin evolution, duration of the accretion phase, and total mass accreted by a NS.

IV Conclusions

We summarize that: (1) In LMBPs the shearing of the magnetic field in the inner crust of the NS likely has occurred. The crustal component died off rapidly, and the core component partially diffused up through the crust over time $\sim 10^8$–10^9 yr and now "shows up" at the stellar surface as the residual (asymptotic) magnetic field of strength $B_\infty \sim 10^8$–10^9 G. (2) In Intermediate-Mass Binary Pulsars (IMBPs) and High-Mass Binary Pulsars (HMBPs) the effect of the shearing should be less pronounced because the stage of accretion for these pulsars is typically much shorter than that for LMBPs. Also the rotational evolution of NSs in I(H)MBPs was apparently more diverse than in LMBPs. Our tentative analysis shows that the resulting range of values of the surface field strength and spin period of an associated NS for each particular group of BPs can be consistently explained within the framework of our scenario, provided that the generally accepted evolutionary scenarios for these systems are adequate. Finally, the main distinctive consequences of our scenario that may be (in future) tested observationally are: (a) the existence of anomalously weakly magnetized NSs ($B_s \lesssim 10^8$ G, age $\lesssim 10^7$–10^8 yr) in binaries (atoll X-Ray sources ?); (b) the possibility that magnetic field of strength $\gtrsim 10^{12}$–10^{13} G can survive even long-lasting phases of heavy accretion onto a NS; and (c) slowly rotating NSs in binaries should not necessarily have weak fields, even if they have accreted a lot of matter.

It must be pointed out that the existing scenarios of "field decay by accretion" predict that a heavily accreted NS should always have a weak field, no matter what was its spin history. The only theory that also predicts that a heavily accreted NS may keep a strong magnetic field is Ruderman's theory of "neutron star plate tectonics:" if a star is born with the magnetic poles in opposite rotational hemispheres, then the field will never weaken, no matter how much accretion took place. In this aspect our scenario cannot be distinguished from the Ruderman's scenario. Moreover, we think that at some points these two scenarios may well supplement rather than exclude each other.

Acknowledgements

This work is supported under the Senior Research Associateship at the LHEA, NASA/GSFC. The authors thank Mal Ruderman for useful conversations.

References

Bhattacharya, D. & van den Heuvel, E.P.J. 1991, Phys. Rep. 203, 124
Ghosh, P. & Lamb, F.K. 1979, ApJ, 234, 296
Muslimov, A. 1995, A&A, 295, L27
Ruderman, M.A. 1991a, ApJ, 366, 261
Ruderman, M.A. 1991b, ApJ, 382, 576

Ruderman, M.A. 1991c, ApJ, 382, 587
van den Heuvel, E.P.J. & Bitzaraki, O. 1995, A&A, 297, L41
Van der Klis, M. 1995, in X-Ray Binaries, ed. W.H.G. Lewin, J. van Paradijs & E.P.J. van den Heuvel (Cambridge: Cambridge Univ. Press), 274

Authors' Addresses

A. Muslimov: Code 661, NASA/GSFC, Greenbelt, MD 20771 USA

E.P.J. van den Heuvel: Astronomical Institute, "Anton Pannekoek," University of Amsterdam, Kruislaan 403, 1098 SJ Amsterdam, The Netherlands

E. Ergma

Evolution of Millisecond Binary Pulsars with Short Orbital Periods

Abstract

We discuss a white dwarf mass versus orbital period relation for binary millisecond pulsars with short orbital periods (less than 20 days). Due to effects of angular momentum losses the $P_{\rm orb}$-$M_{\rm WD}$ relation is more complex than relations based on "conservative" binary evolution so far used in literature. Effects of angular momentum losses (possibly in combination with the absence of a unique core mass-radius relation for star $M_{\rm He} < 0.15$ M$_\odot$) leads to systematically larger $M_{\rm WD}$ at the same final binary period.

I Introduction

The evolutionary history of low-mass X-ray binaries (LMXB) which leads to a binary millisecond pulsar system (BMSP) depends on two main timescales: 1) hydrogen burning timescale $t_{\rm nuc}$, 2) angular momentum loss timescale $t_{\rm am}$. The latter includes angular momentum losses by magnetic braking and by mass loss from the system. For systems with initial orbital periods longer than 10 days, $t_{\rm nuc}$ is much shorter than $t_{\rm am}$ and the angular momentum losses by magnetic braking can be neglected. In this case the relation between final orbital period and $M_{\rm WD}$ may be described by rather simple approximation formula (see latest revised form in Rappaport et al. 1995).

However if $t_{\rm nuc} \simeq t_{\rm am}$ the angular momentum losses begin to play a crucial role. If the initial periods are near the so called bifurcation point (Tutukov et al. 1985; Pylyser & Savonije 1988) then the binary evolution may become quite complicated. Small changes in the initial period (P_i) may lead to three possibilities for the final periods (P_f): 1) $P_f < P_i$, 2) $P_f \simeq P_i$, 3) $P_f > P_i$. Here I should like to show how the effects of the angular momentum losses in combination with making a full binary evolutionary calculations modify the relation between $M_{\rm WD}$-$P_{\rm orb}$ (final).

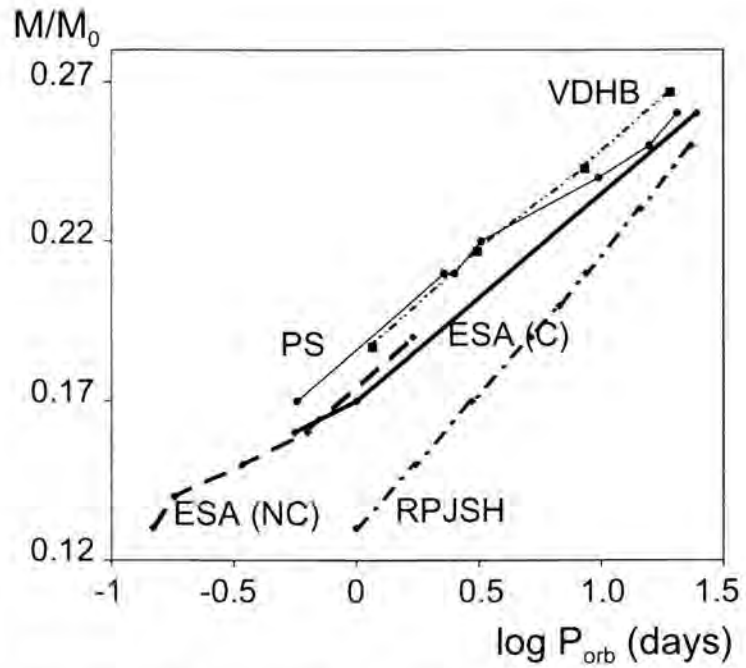

Figure 1. The relation between final $M_{\rm WD}$ and $P_{\rm orb}$. Thick line, c models (ESA); dot line, $n-c$ models (ESA). $n-c$ case where besides the orbital angular momentum loss by magnetic braking, mass and angular momentum losses from the system have been taken into account. c case where only orbital angular momentum loss by magnetic braking has been used. Dash-dot-dot line, van den Heuvel & Bitzaraki (1994) models; thin line, Pylyser & Savonije (1988) models; and dash-dot line, semi-empirical relation RPJSH.

II Evolutionary calculations

To investigate the binary evolution when $t_{\rm nuc} \simeq t_{\rm am}$ it is necessary to use full binary evolutionary computations which include both the nuclear evolution of the secondary as well as the orbital evolution of the binary. In our analysis we have used for the following combinations of donor mass and accretor mass ($M_d/{\rm M}_\odot, M_{acc}/{\rm M}_\odot$): Pylyser & Savonije (1988) (1,1) (1.5,1) $Z = 0.02$; van den Heuvel & Bitzaraki (1994) (1,1.4) $Z = 0.02$; Ergma, Sarna & Antipova (1996; hereafter ESA) (1,1.4) $Z = 0.03$; results of the ESA calculations have been obtained using the program described by Muslimov & Sarna (1993), and Sarna & De Greve (1994) has been used.

In Figure 1 we have drawn the $M_{\rm WD}$-$P_{\rm orb}$ dependence obtained in various calculations where $M_{\rm WD}$ is the mass of the remaining white dwarf core of the donor star. Also we have used the period-mass relation obtained by Rappaport et al. (1995; hereafter RPJSH)

$$P_{\rm orb} \approx 0.374[R_0 M_{\rm WD}^{4.5}/(1+4M_{\rm WD}^4)+0.5]^{1.5} \cdot M_{\rm WD}^{-0.5}$$

where $M_{\rm WD}$ is in solar units, $P_{\rm orb}$ is in days, and the quantity in square brackets is expressed in units of solar radii ($R_0 = 4850$ R$_\odot$).

From this figure the influence of making a full evolutionary calculations, including the angular momentum losses is clearly seen. If we compare the $M_{\rm WD}$-$P_{\rm orb}$ dependence resulting from full binary evolution calculations with realistic angular momentum losses with those computed using the above semi-empirical relation then we see that this relation gives systematically lower white dwarf mass values, the differences increasing from ~ 0.02 M$_\odot$ at $P_{\rm orb} \sim 20$ days, to more than 0.05 M$_\odot$ for $P_{\rm orb} \sim 1.5$ day. Futhermore, for a fixed white dwarf mass the estimated orbital period value is much longer ($\Delta \log P_{\rm orb}$(days) $\approx$ ranges from 0.7 to 0.4). One clearly notices the convergence of all tracks when the orbital period increases.

III Discussion

As to the reasons for the systematically enlarged core masses at the same final orbital periods, which result from the full evolutionary, we can think of two possibilities (or a combination of these): 1) as pointed out by Rappaport et al. (1995) for stars with small helium core mass ($\leq 0.15 - 0.2$ M$_\odot$) there probably is no longer a unique core-mass radius relation, i.e. the value of the outer radius will also depend on the mass of the hydrogen-rich envelope. Using full evolutionary computations such an effect will automatically be taken into account and will yield a systematic difference relative to the outcomes in which a unique core-mass. 2) The fact that for short initial orbital periods and low donor masses, the mass transfer may cause the donor to no longer be completely in thermal equilibrium as the mass transfer timescale differs by less than an order of magnitude from the thermal timescale of the donor. In this case the radius of the donor will no longer be its thermal equilibrium radius, such that a standard core-mass radius relation does not longer apply.

IV Conclusion

It was shown that for BMSP with orbital period less than 20 days, the relation between $M_{\rm WD}$ and $P_{\rm orb}$ is more complicated than relation based on "conservative" binary evolution so far used in literature. Due to the effects of angular momentum losses the orbital periods increase less during the evolution, which, possibly in combination with the other effects mentioned in section 3, leads to systematically longer white dwarf masses at the same final binary period. At the shortest orbital periods (near one day) the difference may be as large as over 30%. For orbital period longer than 20 days the difference becomes negligible.

References

Ergma, E., Sarna, M. & Antipova, J. 1996, MNRAS, 280, 1000 (ESA)
Muslimov, A. & Sarna, M.J. 1993, MNRAS, 262, 164
Pylyser, E. & Savonije, G.J. 1988, A&A, 191, 57
Rappaport, S. et al. 1995, MNRAS, 273, 731 (RPJSH)
Sarna, M.J. & De Greve, J.P. 1994, A&A, 281, 433
Tutukov, A.V. et al. 1985, SVA, 11, 123
van den Heuvel, E.P.J. & Bitzaraki, O. 1994, in Evolutionary Links in the Zoo of Interacting Binaries, Mem. Soc. Astron. Ital. Vol. 65, ed. F. D'Antona (Florence: Soc. Astron. Ital.), 237

Authors' Address

Physics Department Tartu University, Ülikooli 18, EE2400 Tartu, Estonia

Part VII:

Timing and Evolution of X-ray Binaries

M. van der Klis

Kilohertz Quasi-Periodic Oscillations in Low-Mass X-Ray Binaries

Abstract

In early 1996 a series of discoveries began with NASA's Rossi X-ray Timing Explorer of a new, up to then unknown astrophysical phenomenon. It turned out that accreting low magnetic-field neutron stars show quasi-periodic oscillations in their X-ray flux at rates of up to more than a kilohertz. These kHz QPO, now reported from eleven different systems, are among the fastest phenomena in the sky and can provide us with new information about the fundamental properties of neutron stars and help testing general relativity in the strong-field regime. If, for example, their frequencies can be identified with the Keplerian frequencies of matter in orbit around a 1.4 $M_\odot$ neutron star, then the radius of the star would have to be less than 15 km, which directly constrains the equation of state of bulk nuclear-density matter, and for an only slightly tighter orbit or slightly more massive neutron star the orbital radius would equal the Schwarzschild-geometry general-relativistic marginally stable orbit (12.5 km for a 1.4 $M_\odot$ object). So far all models that have been put forward for explaining the new phenomenon have encountered problems. In this paper I review the relatively simple and highly suggestive phenomenology as it has emerged from the data up to now, and discuss some of the proposed models.

I Introduction

There are two places in the universe where we can study neutron stars. In radio pulsars, which form the main theme of this meeting, nature performs for us the experiment of spinning a magnetized neutron star, and this allows us to derive interesting conclusions about the fundamental properties of these objects by making it possible to measure their spin rates with very high precision. In X-ray binaries a completely different experiment is performed: take a neutron star (or a black hole) and throw large amounts of matter at it. Analysis of the results of this experiment provides information about the nature of neutron stars and the properties of the space-time around them that can not be obtained from radio pulsars. So, in my view the main motivation for studying X-ray binaries is not that they exhibit a wide range of complex phenomenology, which they do, but that they contain neutron stars (and black holes), objects of fundamental physical interest,

and allow to derive information about the equation of state of high-density matter and perform tests of general relativity in the strong-field regime. In this talk, I shall be discussing low-mass X-ray binaries (LMXBs) containing neutron stars exclusively, as it is in the understanding of the physics of these systems that great progress has recently become possible by the discovery, with NASA's Rossi X-ray Timing Explorer (RXTE), of a new phenomenon, kilohertz quasi-periodic oscillations (kHz QPO).

In these X-ray binary systems matter is transferred from a low-mass ($\lesssim M_\odot$) star to a neutron star by way of an accretion disk. The X-rays originate from the hot ($\sim 10^7$ K) plasma comprising the inner few 10^1 kilometers of the flow. This is very close to the neutron star, which itself has a radius, R, of order 10 km, so that by studying the properties of this flow one expects to be able to derive information about the star.

The high temperatures in the inner flow are caused by the release of large amounts of gravitational energy when the matter descends into the neutron star's very deep gravitational potential well ($GM/R \sim 0.2c^2$; here and below I assume $M = 1.4\ M_\odot$ for the neutron star's mass). The characteristic velocities near the star are of order $(GM/R)^{1/2} \sim 0.5c$. Therefore the dynamical time scale, the time scale for motion of matter through the emitting region, is short; $\tau_{\rm dyn} \equiv (r^3/GM)^{1/2} \sim 0.1$ ms for $r = 10$ km, and $\sim$2 ms for $r = 100$ km.

Up to less than a year ago, no direct information existed about the properties of these flows at these time scales. In this paper I report on how, since February 1996, we are for the first time actually observing time variability from accretion flows onto neutron stars at the expected millisecond time scales. A new rapid-variability phenomenon has been discovered, namely quasi-periodic oscillations in the X-ray flux with amplitudes of up to several 10% of the total flux, quality factors $Q \equiv \Delta\nu/\nu$ (see §II) of up to several 100, and frequencies of up to $\sim$1200 Hz. I shall call this phenomenon "kHz QPO" (kilohertz quasi-periodic oscillations) throughout the rest of this paper.

A great deal of information is available about the properties of LMXBs and the physics of accretion onto a neutron star. The last pre-kHz-QPO overview of rapid X-ray variability in X-ray binaries can be found in the Lewin et al. book *X-Ray Binaries* (Van der Klis 1995; look here if you wish to find out about atoll sources, Z sources and the latters' 16–60 Hz horizontal-branch oscillations and the 6–20 Hz normal-flaring branch oscillations). For understanding what follows, it is useful to remind the reader of the usual terminology with respect to the subclasses of LMXBs (Hasinger & Van der Klis 1989): Z sources are near-Eddington accretors and probably have somewhat stronger (1–5 10^9 G) magnetic fields, atoll sources are often X-ray burst sources, have luminosities between $10^{-3}\ L_{\rm Edd}$ and a few $10^{-1}\ L_{\rm Edd}$, and are thought to have somewhat weaker magnetic fields (10^8–10^9 G).

X-ray astronomers are presently scrambling to try and make sense of the phenomenology of kHz QPO, which turn out to be at the same time highly suggestive of interpretation and very restrictive of possible models, and theorists have already begun working out sophisticated models. None of this has reached an equilibrium

state yet, and what I report in this paper will necessarily be of a "snapshot" nature. What is clear at this point is that for the first time we are seeing a rapid X-ray variability phenomenon that is directly linked with a neutron star's most distinguishing characteristic (only shared among macroscopic objects with stellar-mass black holes): its compactness. This is particularly evident if the phenomena are in some way related to orbital motion. After all, a Keplerian orbital frequency $\nu_K = P_{\rm orb}^{-1} = (GM/4\pi^2 r_K^3)^{1/2}$ of 1200 Hz around a 1.4 $M_\odot$ neutron star as seen from infinity corresponds to an orbital radius $r_K = (GM/4\pi^2\nu_K^2)^{1/3}$ of 15 km, directly constraining the equation of state of the bulk nuclear-density matter, and only just outside the general-relativistic marginally stable orbit. Whatever the model, for the first time we have to seriously worry about general-relativistic effects in describing the observable dynamics of the physical system.

II Observations and interpretation

Kilohertz QPO have now[1] been reported from 11 LMXBs, 3 of which are Z sources and 8 of which are atoll sources and probable atoll sources (see Van der Klis 1995; hereafter I shall use "atoll source" for LMXBs that probably fall in this class as well as for those that definitely do so), together covering nearly three orders of magnitude in X-ray luminosity ($\sim 10^{-3}$ to ~ 1 $L_{\rm Edd}$). Table 1 summarizes some of these results, and provides an overview of the literature that is approximately complete as of this writing. Rather than getting into an exhaustive description of the phenomenology or following the historical line, I shall concentrate on what I consider at this point to be the main clues. I refer to the table for all kHz QPO observational references in the remainder of this section.

A clear pattern of systematic behavior has emerged. In most sources (8 out of 11) two simultaneous kHz peaks (hereafter: twin peaks) are observed in the power spectra of the X-ray count rate variations (Figure 1). The lower-frequency peak (hereafter the *lower peak*) has been observed at frequencies between 325 and 920 Hz, the higher-frequency peak (hereafter the *upper peak*) has been observed at frequencies between 500 and 1207 Hz. When the accretion rate $\dot{M}$ increases, both peaks move to higher frequency. In atoll sources $\dot{M}$ is inferred to correlate with X-ray count rate, and kHz QPO frequency increases with count rate. In Z sources in their so-called "normal branch" (NB), $\dot{M}$ is inferred to *anticorrelate* to count rate, and indeed in Z sources in the NB kHz QPO frequency increases when the count rate drops.

[1] March 21, 1997

Table 1: Observed frequencies of kilohertz QPO.

Source (in order of RA)	Lower peak freq. (Hz)	Upper peak freq. (Hz)	Peak separation (Hz)	"Third" freq. (Hz)	References
4U 0614+091		520 ↓			Ford et al. 1996, 1997 Van der Klis et al. 1996d
	480 ↓ 800	750 ↓ 1150	327±4	328	Méndez et al. 1997 Vaughan et al. 1997
4U 1608−52	691 830 ↓ 890				Van Paradijs et al. 1996 Berger et al. 1996 Vaughan et al. 1997
Sco X-1	570 ↓ 800 ↓ 830	870 ↓ 1050 ↓ 1080 ↓ 1130	292±2 ↓ 247±3		Van der Klis et al. 1996a,b,c, 1997b
4U 1636−53	898 ↓ 920 835 ↓ 897	1147 ↓ 1183 ↓ 1193	249±13	581	Zhang et al. 1996, 1997 Van der Klis et al. 1996d Wijnands et al. 1997 Vaughan et al. 1997
4U 1728−34	640 ↓ 790	500 ↓ 990 ↓ 1100	355±5	363	Strohmayer et al. 1996a,b,c
KS 1731−260	898	1159 ↓ 1207	260±10	524	Morgan & Smith 1996 Smith et al. 1997 Wijnands & Van der Klis 1997
4U 1735−44	1150				Wijnands et al. 1996

In three atoll sources (4U 1728−34, 4U 1636−53 and KS 1731−260), "third peak" oscillations have been seen during X-ray bursts whose frequencies (360–580 Hz) are consistent with being equal to the frequency *differences* between the twin peaks (in 4U 1728−34), or twice that (in the other two sources). In a fourth atoll source

Table 1: *(cont.)*

Source (in order of RA)	Lower peak freq. (Hz)	Upper peak freq. (Hz)	Peak separation (Hz)	"Third" freq. (Hz)	References
X 1743−29?				589	Strohmayer et al. 1996d
GX 5−1		567 ↓			Van der Klis et al. 1996e
	325 ↓ 448	652 ↓ 746 ↓ 895	327±11		
GX 17+2	682 ↓ 880	988	306±5		Van der Klis et al. 1997a
4U 1820−30	546 ↓ 796	1065	275±8		Smale et al. 1996, 1997

Arrows indicate observed frequency variations.
Frequencies in the same row were observed simultaneously, except "third" frequencies.
Entries straddling the upper and lower peak columns are of single, unidentified peaks.

(4U 0614+09) there is marginal evidence for a third peak at the twin-peak separation frequency which corresponds to an oscillation in the persistent emission rather than in X-ray bursts.

These cases of three commensurate frequencies very strongly suggest that some kind of beat-frequency model is at work, with the "third peaks" at the neutron star spin frequencies (or twice that), the upper kHz peak at the Kepler frequency corresponding to some preferred orbital radius around the neutron star, and the lower kHz peak at the difference frequency between these two. Strohmayer et al. (1996c) suggested that this preferred radius is the magnetospheric radius. Miller, Lamb & Psaltis (1996) proposed it is the sonic radius. In models of this kind, which involve the neutron-star spin as one of the frequencies participating in the beat-frequency process, the twin-peak separation is predicted to be constant. However, in Sco X-1 the peak separation varies systematically with inferred $\dot{M}$, from ~310 Hz when the upper peak is near 870 Hz to ~230 Hz when it is near 1075 Hz: the peaks move closer together by ~80 Hz while they both move up in frequency as $\dot{M}$ increases. This is in strong contradiction to straightforward beat-frequency models (see §III).

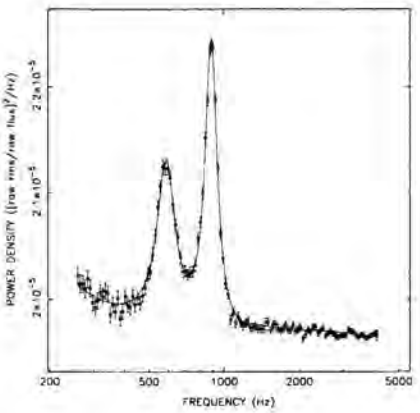

Figure 1. Power spectrum of Sco X-1 showing double kHz QPO peaks (Van der Klis et al. 1997). The sloping continuum above 1 kHz is instrumental.

In the Z sources Sco X-1, GX 5−1 and GX 17+2 twin kHz QPO peaks and the so-called horizontal-branch oscillations (HBO; Van der Klis et al. 1985) are seen simultaneously (Figure 2). HBO are thought to be a product of the magnetospheric beat-frequency mechanism (Alpar and Shaham 1985, Lamb et al. 1985). If this is correct, then this model can *not* explain the kHz QPO in these sources. It is possible in principle that the kHz QPO in the Z sources is a different phenomenon from that in the atoll sources (e.g., Strohmayer et al. 1996c), but this seems unlikely: the frequencies, their dependence on $\dot{M}$, the coherencies, the peak separations and the fact that there are *two* peaks, one of which sometimes becomes undetectable at extreme $\dot{M}$, are too similar to attribute to just coincidence. If this is correct, then the variable twin-peak separation seen in Sco X-1, the simultaneous presence of kHz QPO and HBO in Z sources, *and* the direct indications for a beat frequency in the atoll sources must all be explained within the same model, a formidable challenge.

One of the distinguishing characteristics of kHz QPO is that they often show a relatively large coherence. The quality factor Q, defined as the QPO peak's centroid frequency ν divided by its full width at half maximum $\Delta\nu$ regularly reaches values of more than 100 in one or both of the twin peaks (although much lower Q's are also common). This provides a strong constraint on "orbiting clump" type models, as lifetime broadening considerations show that the clumps must persist over hundreds of cycles. The oscillations in bursts have shown even larger coherence. They attained a record-level Q of ~900 in a burst in KS 1731−260 (Smith, Morgan & Bradt 1997). This high Q value supports models where these oscillations are caused by the neutron-star spin. In 4U 1728−34 (Strohmayer et al. 1996c), drifts by ~1 Hz have been observed in the ~363 Hz frequency of the QPO in bursts that are suggestive of the bursting layer slightly expanding and then recontracting, changing its rotation rate to conserve angular momentum and thus modulating the QPO frequency.

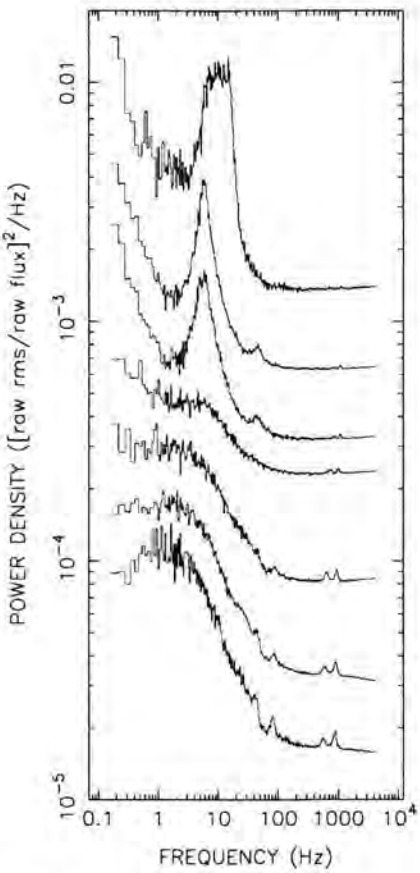

Figure 2. Power spectra of Sco X-1, with inferred $\dot{M}$ increasing upwards. Notice the decrease in strength and increase in frequency of the kHz peaks as a function of $\dot{M}$. The peaks near 45 and 90 Hz are identified as horizontal branch oscillations (HBO), that between 6 and 20 Hz as normal/flaring branch oscillations (N/FBO). The large width of the N/FBO peak in the top trace is due to peak motion. The sloping continua in the kHz range are instrumental.

The amplitudes of kHz QPO have, in all cases where a check was possible, shown a strong positive dependence on photon energy (e.g., Berger et al. 1996, Zhang et al. 1996). Their amplitudes when measured in a broad photon-energy band can therefore be expected to depend strongly on details of the low-energy part of the spectrum, which contributes many photons and little kHz QPO amplitude: detector cutoff and interstellar absorption will affect the overall fractional amplitude. Reported fractional amplitudes vary between 0.5 and a few percent in Z sources and 3 and 15% (rms) in atoll sources when measured over a 2–20 keV band; for higher energies amplitudes up to 40% (rms) have been observed.

A final strong model constraint is provided by the small magnitude of any time lags between the kHz QPO signal as observed in different energy bands (Vaughan et al. 1997). Time-lag measurements require very high signal-to-noise ratios, and have so far only been made in certain single, apparently count-rate independent peaks in 4U 1608−52 and 4U 1636−53 near 850 Hz, and in a 730 Hz peak in 4U 0614+09 which was probably an upper peak. Finite lags of 10–60 μsec were discovered in 4U 1608−52; the hard photons lag the soft ones by increasing amounts as the photon energy increases. Upper limits of 30μsec and 45μsec were set in 4U 1636−53 and 4U 0614+09, respectively. These are by far the smallest lags ever measured; they correspond to light-travel distances of 3–20 km. For rather general assumptions about the spectral formation mechanism, this limits the scale of any Compton scattering regions dominating the spectral shape to between a few and a few tens of km.

The great enigma in the phenomenology right now is, in my opinion, the peculiar lack of correlation between kHz QPO frequency and average source luminosity, whereas *in each individual source* a strong correlation between frequency and $\dot{M}$ is observed. In 4U 0614+09, at a luminosity of a few times 10^{-3} $L_{\rm Edd}$, similar QPO frequencies have been observed as in 4U 1820−30, which is near 10^{-1} $L_{\rm Edd}$, and in Sco X-1, which is inferred to be a near-Eddington accretor, yet in each of these sources the frequency changes by several 10^2 Hz in correlation with $\dot{M}$. In at least 6 sources, spread over this entire range of average X-ray luminosity, the upper peak has been observed to disappear below the detection limit when its frequency is somewhere between 1100 and 1200 Hz as the flux exceeds a certain limit, but this flux limit is widely different between sources. This must mean that another, compensating, parameter than just accretion rate is affecting the properties of the kHz QPO, most likely by directly affecting the frequency, although some kind of selection effect that leads to suppression of any QPO outside the 300–1200 Hz range is also a possibility. This latter possibility of course requires that in sources that go through a large decrease in accretion rate (transients) several "new" QPO peaks would successively appear near 1200 Hz, move down in frequency and disappear near 300 Hz. This has not been seen and seems somewhat unlikely, but can not be excluded at this point.

An obvious candidate for a compensating parameter is the neutron-star magnetic-field strength, but neutron-star mass or spin, either by their effects on the surrounding space-time or directly, might play a role as well. What would be required, specifically, is that there exists a correlation or an anti-correlation between, say, the magnetic field strength B of the neutron star and its mean accretion rate $\langle\dot{M}\rangle$, and that the QPO frequency depends on B in such a way as to approximately compensate the $\dot{M}$ effect. Interestingly, it has been suggested previously (Hasinger and Van der Klis 1989, see Van der Klis 1995) on the basis of comparing Z and atoll source phenomenology that $\langle\dot{M}\rangle$ and B are correlated among LMXBs, and recently spectral modeling (Psaltis et al. 1997) has tended to confirm this. The magnetospheric beat-frequency model (Alpar & Shaham 1985), when combined with this inferred correlation, qualitatively fits the requirements sketched above, but the results on the Z sources make this model

unattractive for the kHz QPO. Perhaps the magnetic field strength affects the inner accretion flows in other ways than by just terminating the disk at the magnetospheric radius. If magnetic stresses could somehow slow down the (for example, orbital) motion responsible for the kHz QPO, that would do it. Of course, radiative stresses diminish the effective gravity and are expected to slow down orbital motion (Miller & Lamb 1993). However, the luminosity is not independent from $\dot{M}$, but instead is expected to vary proportionally to it, so that radiative stresses cannot fulfill this role: we know already that when in a given source $\dot{M}$ goes up so does the luminosity, but this does not prevent the QPO frequency from going up as well.

There is a lively discussion about the nature of the observed frequencies and their potential to constrain neutron-star masses and radii and to test general relativity. Kaaret, Ford & Chen (1997) have proposed that the behavior of the single, count-rate independent QPO peaks in 4U 1608−52 and 4U 1636−53 described above is related to orbital motion near the marginally stable orbit, and from this derive neutron star masses of $\sim$2 $M_\odot$. Zhang, Strohmayer & Swank (1997) have proposed that the narrow range of maximal frequencies (1100–1200 Hz) also mentioned above must be identified with the general relativistic marginally stable frequencies, which leads them to the conclusion that the neutron stars' masses are near 2 $M_\odot$ as well. An alternative possibility is of course that the maximal frequencies are set by the Keplerian frequency at the neutron star surface. This requires the star to be larger than the marginally stable orbit and for $\sim$1.4 $M_\odot$ neutron stars would favor the stiffest equations of state.

Just the assumption that the upper peak corresponds to Keplerian motion around the neutron star allows to set useful limits on neutron star parameters, a point made by Miller, Lamb & Psaltis (1996) in their paper on a model that interprets the upper peak in this way (see §III). Different from the proposals just mentioned, these limits do *not* rely on identifying any of the observed frequencies with the marginally stable orbital frequency. There are two direct constraints on the neutron-star mass and radius from the simple assertion that there is stable Keplerian motion at the frequency ν_u of the upper peak: (1) the radius of the star R must be smaller than the radius of this Keplerian orbit, in a Schwarzschild geometry $R < (GM/4\pi^2\nu_u^2)^{1/3}$, and (2) the radius of the marginally stable orbit must *also* be smaller than this: $6GM/c^2 < (GM/4\pi^2\nu_u^2)^{1/3}$, as no stable orbit is possible within this radius. Condition (1) is a mass-dependent upper limit on the radius of the star, and condition (2) provides an upper limit on the mass: $M < c^3/(2\pi 6^{3/2} G\nu_u)$. For $\nu_u = 1193$ Hz (Wijnands et al. 1997), $M < 1.9$ $M_\odot$ and $R_{NS} < 16.3$ km. Putting in the corrections for the frame dragging due to the neutron star spin requires knowledge of the spin rate (which in the sonic point model is equal to the twin peak separation, or half that; §III). The correction also depends somewhat on the neutron star model, which determines the relation between spin rate and angular momentum, so that the limits become slightly different for each EOS. Putting in these Kerr corrections (for a spin rate of 275 Hz) changes the limits quoted above only slightly, to $M < 2.1$ $M_\odot$ and $R_{NS} < 16.5$ km for a wide range of equations of state (Wijnands et al. 1997).

III Models

Space is lacking to provide a full description of the physical models that have been proposed for kHz QPO. Of course, the phenomenology as described in the previous section very strongly suggests that a beat-frequency model of some kind is at work. Neutron-star spin and disk Keplerian motion are periodic phenomena known to be present in the system and are therefore natural candidates for providing the basic frequencies. However, it is too early to declare any proposed implementation of a beat-frequency model for kHz QPO an unqualified success. Let me briefly mention other models that have been put forward.

(1) Remarkably short shrift has been given so far to *neutron star vibration models*. The short time scale variations in kHz QPO frequency and the lack of higher-frequency peaks have been cited as reasons for rejecting these models. (2) A model based on numerical radiation hydrodynamics calculations has been proposed by Klein et al. (1996) for the case of the kHz QPO in Sco X-1 and is currently being further explored. (3) The dependence between the QPO frequencies observed in Sco X-1 can be nicely explained with a model where each of the two QPO signals comes from one of two diametrically opposed *relativistic jets* emanating from the central source (Van der Klis et al. 1997b), but this model can not explain the atoll sources' kHz QPO properties.

Now let's turn to beat-frequency models. The two versions of the model that have been discussed both identify the upper peak's frequency with the Keplerian frequency of the accretion disk at some preferred radius, and the lower peak with the beat between this Keplerian frequency and the neutron star spin frequency. The magnetospheric beat-frequency model uses the magnetospheric radius r_M as this preferred radius. As HBO and kHz QPO have been seen *simultaneously* in all three Z sources where kHz QPO have so far been observed, at least *one* additional model is required. According to Miller, Lamb & Psaltis (1996), applying the magnetospheric beat-frequency model to the kHz QPO leads to several other difficulties. They propose the *sonic-point model* instead, where the preferred radius is the sonic radius r_S where the radial inflow velocity becomes supersonic.

In Z sources, applying the sonic point model for the kHz QPO, and the magnetospheric beat-frequency model for the HBO indicates $r_S < r_M$ and therefore requires a Keplerian disk flow well within the magnetosphere. The upper peak is caused in the sonic point model by a modulation of the direction into which this luminosity is emitted ("beaming"). This is similar to what is expected of an X-ray pulsar. It may require some fine-tuning of the scattering process that is thought to be smearing the pulsations to allow it to transmit the upper peak oscillations. Miller, Lamb & Psaltis (1996) suggest that as the sonic radius approaches the general-relativistic marginally stable orbit the frequency of the upper peak will hit a "ceiling" and remain stable for further increases in accretion rate. There are so far no data that have shown this. Instead it has been observed that the QPO disappear above some level of inferred accretion rate at frequencies that are mostly in the range 1100–1200 Hz (see §II). Perhaps this is

what *really* happens when R_{MSO} is reached, however, the fact that the accretion rate at which the peaks disappear is very different between sources (much higher in sources with a higher average luminosity), is yet to be explained.

Obviously, a large amount of effort is still required to make any of the models so far proposed stick. Fortunately, as it looks now the theoretical efforts that are underway at this point will be guided by a very constraining body of RXTE data. Eventually, most LMXBs will likely exhibit the new phenomenon, and many of its properties can be measured with RXTE with great precision.

Acknowledgements

This work was supported in part by the Netherlands Organization for Scientific Research (NWO) under grant PGS 78-277 and by the Netherlands Foundation for Research in Astronomy (ASTRON) under grant 781-76-017.

References

Alpar, M.A. & Shaham, J. 1985, Nature, 316, 239
Berger, M. et al. 1996, ApJ, 469, L13
Ford, E. et al. 1996, IAU Circ. 6426
Ford, E. et al. 1997, ApJ, 475, L123
Cook, G.B., Shapiro, S.L. & Teukolsky, S.A. 1994, ApJ, 424, 823
Hasinger, G. & Van der Klis, M. 1989, A&A, 225, 79
Jongert, H.C. & Van der Klis, M. 1996, A&A, 310, 474
Kaaret, P., Ford, E. & Chen, K. 1997, ApJ, 480, L27
Klein, R.L. et al. 1996, ApJ, 469, L119
Kluźniak, W. & Wagoner, R.V. 1985, ApJ, 297, 548
Kluźniak, W., Michelson, P. & Wagoner, R.V. 1990, ApJ, 358, 538
Lamb, F.K. et al. 1985, Nature, 317, 681
Méndez, M. et al. 1997, ApJ, 485, L35
Miller, M.C. & Lamb, F.K. 1993, ApJ, 413, L43
Miller, M.C., Lamb, F.K. & Psaltis, D., 1996, ApJ, submitted; astro-ph/9609157
Morgan, E.H. & Smith, D.A. 1996, IAU Circ. 6437
Patterson, J. 1979, ApJ, 234, 978
Psaltis, D. & Lamb, F. K. 1997, ApJ, 488, 881
Smale, A.P., Zhang, W. & White, N.E. 1996, IAU Circ. 6507
Smale, A.P., Zhang, W. & White, N.E. 1997, ApJ, 483, L119
Smith, D. A., Morgan, E.H. & Bradt, H. 1997, ApJ, 479, L137
Strohmayer, T., Zhang, W. & Swank, J. 1996a, IAU Circ. 6320
Strohmayer, T. et al. 1996b, IAU Circ. 6387
Strohmayer, T. et al. 1996c, ApJ, 469, L9
Strohmayer, T., Lee, U. & Jahoda, K. 1996d, IAU Circ. 6484

Van Paradijs, J. et al. 1996, IAU Circ. 6336
Van der Klis, M. 1989, in Timing Neutron Stars, NATO ASI C262, ed. H. Ögelman & E.P.J. van den Heuvel (Dordrecht: Kluwer), 27
Van der Klis, M. 1995, in X-Ray Binaries, ed. W.H.G. Lewin, J. van Paradijs & E.P.J. van den Heuvel (Cambridge: Cambridge University Press), 252
Van der Klis, M. et al. 1985, Nature, 316, 225
Van der Klis, M. et al. 1996a, IAU Circ. 6319
Van der Klis, M. et al. 1996b, IAU Circ. 6424
Van der Klis, M. et al. 1996c, ApJ, 469, L1
Van der Klis, M. et al. 1996d, IAU Circ. 6428
Van der Klis, M. et al. 1996e, IAU Circ. 6511
Van der Klis, M. et al. 1997a, IAU Circ. 6565
Van der Klis, M. et al. 1997b, ApJ, 481, L97
Vaughan, B.A. et al. 1997, ApJ, 483, L115
Wijnands, R.A.D. et al. 1996, IAU Circ. 6447
Wijnands, R.A.D. et al. 1997, ApJ, 479, L141
Wijnands, R.A.D. & Van der Klis, M. 1997, ApJ, 482, L65
Zhang, W. et al. 1996, ApJ, 469, L17
Zhang, W. et al. 1997, IAU Circ. 6541
Zhang, W., Strohmayer, T. E. & Swank, J. H. 1997, ApJ, 482, L167

Authors' Address

Astronomical Institute "Anton Pannekoek", University of Amsterdam, Kruislaan 403, 1098 SJ Amsterdam, The Netherlands

J. van Paradijs

Masses of Neutron Stars and Black Holes

Abstract

In this paper I give a brief review of the various methods that have been proposed and used to determine masses of neutron stars and black holes in binary stars. I summarize the results obtained from analyses of relativistic effects observed in binary radio pulsars, and from analyses of the orbital parameters of X-ray binaries, supplemented by additional constraints on the orbital inclination and the mass ratio.

I Neutron stars and black holes in X-ray binaries

The first X-ray source which was shown to be a member of a binary star, Cyg X-1, was a strong black-hole candidate as well. In the words of the discoverers: "The mass of the companion probably being larger than about 2 $M_{\odot}$, it is inevitable that we should also speculate that it might be a black hole." (Webster & Murdin 1972); "This raises the distinct possibility that the secondary is a black hole." (Bolton 1972).

Following the discovery of the binary X-ray pulsar Cen X-3 (Schreier et al. 1972) and many other similar systems, and of X-ray bursters (Grindlay et al. 1976; Belian et al. 1976), research in X-ray binaries in the 1970's was dominated by systems in which the accreting compact object is a neutron star. But research in black holes did not disappear altogether. The discovery of strong rapid variability of the X-ray flux of Cyg X-1 (Oda et al. 1971; see also Oda 1976, for a review of early work on Cyg X-1) led to the idea that such variability is a telltale sign of an accreting black hole, which might be used to distinguish them from accreting neutron stars. On the basis of this idea Cir X-1 was long considered a black-hole candidate. However, neutron star X-ray binaries can also show rapid variability, as was strikingly illustrated by the transient V 0332+53, which was initially suggested as a possible black-hole system, but later shown to be an X-ray pulsar (Stella et al. 1985), whose pulse amplitude happened to be relatively weak compared to that of the red-noise component in the PDS. Also Cir X-1 was shown to be a neutron star when it emitted type I X-ray bursts (Tennant et al. 1986).

Ostriker (1977) suggested that black-hole X-ray binaries (BHXB) might be distinguished by the shape of their X-ray spectra. This idea was put on a firm footing

by White & Marshall (1984) who showed that in an X-ray color-color diagram, derived from the HEAO-1 A-2 sky survey the two sources, then known to contain black holes (Cyg X-1, in its soft state, and LMC X-3) were located in the extreme upper-left corner, i.e., their spectra were extremely soft. A few years later, McClintock & Remillard (1986) measured the mass function of the transient source A 0620–00 (which also had a very soft X-ray spectrum during its outburst in 1975) after it had returned to quiescence, to be $3.18 \pm 0.16\ M_\odot$. This immediately (see below) showed that the compact star in this system is too massive to be a neutron star, and gave some confidence in the idea that X-ray spectra may be an efficient way to select BHXBs.

In spite of the fact that some X-ray spectral characteristics of black holes, and rapid variability are also seen in some neutron stars, their combined presence, in particular in X-ray transients, has remained strikingly effective in singling out black holes.

As implied in the above discussion, the main argument that the compact object in a particular X-ray binary is a black hole, is that neutron star masses cannot exceed a certain maximum value. This assumption rests on very general considerations, e.g., that sound cannot travel faster than light, on the basis of which Nauenberg & Chapline (1973) and Rhoades & Ruffini (1974) concluded that any neutron star, independent of the equation of state (EOS) of high-density matter, must have a mass $\lesssim 3.4\,M_\odot$. Rotation of the neutron star (ignored in the above analyses) does not increase the mass limit by more than 20% (Shapiro & Teukolsky 1983). Detailed modeling of neutron stars, for a wide range of equations of state, leads (see Figure 1) to upper mass limits between $\sim 1.5\ M_\odot$ (very soft EOS) and $\sim 2.5\ M_\odot$ (very stiff EOS) (see, e.g., Arnett & Bowers 1977; Datta 1988; Cheng et al. 1993; Cook et al. 1994; Engvik et al. 1996; Glendenning 1998).

The fact that compact objects with dynamical mass estimates exceeding $\sim 3\ M_\odot$ cannot be neutron stars, is not equivalent to their being black holes, as defined by the particular space-time structure described by Schwarzschild and Kerr metrics, which are characterized, in particular, by the absence of a hard surface. This has led to the extensive use of the term "black-hole candidate" for these objects. Of course, detection of X-ray pulsations or X-ray bursts immediately disqualifies a compact star as a black hole, but positive evidence for the absence of a hard surface has been very hard to obtain. This should not come as a surprise, since a nominal ($M = 1.4\,M_\odot$, $R = 10$ km) neutron star is just 2.5 times larger than its Schwarzschild radius, and one may expect the accretion flow to be very similar to that of a black hole of comparable mass. The energy release at the neutron star surface, which is absent for a black hole, might lead to observable differences in spectra and variability, but unless the origin of the spectra and variability of X-ray binaries is much better understood than it is nowadays, the conclusion that a black hole has been found on the basis of such phenomena must be considered weak at best. This difficulty is illustrated by the fact that the spectral and variability characteristics of atoll sources are very similar to those of black holes in their low state (see Van der Klis 1995).

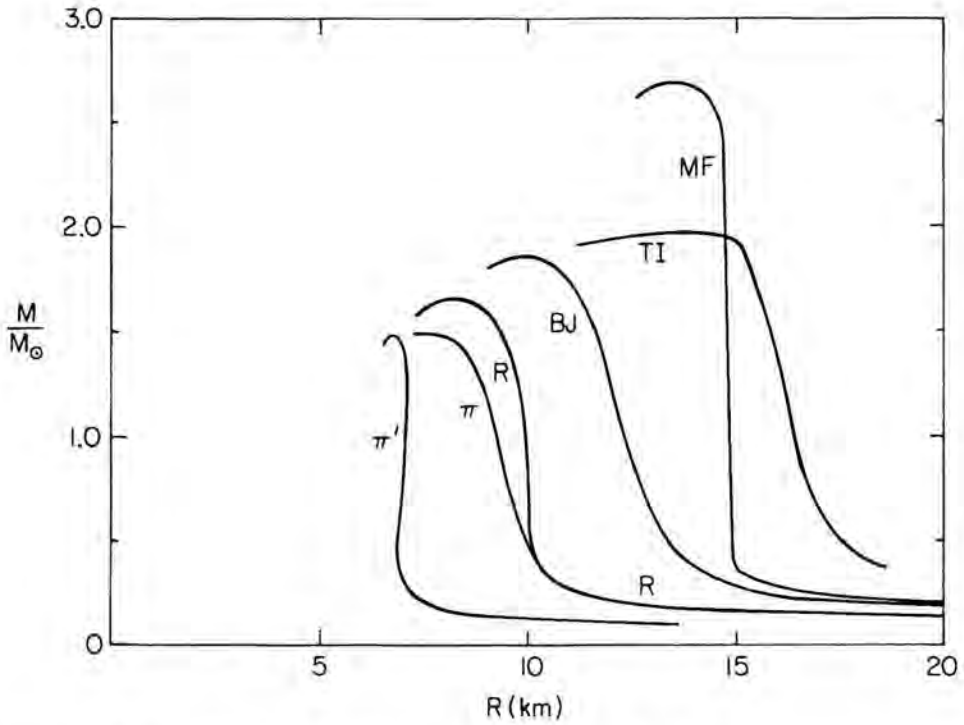

Figure 1. A selection of theoretical mass-radius relations for neutron stars, for several assumed equations of state (from Baym & Pethick 1979).

One way to infer the absence of a hard surface would be to show that at some distance from the compact object matter flows inward which does not give rise, by a large margin, to the emission of X rays from the compact object at the expected rate. Such evidence for the absence of a hard surface has recently been presented by Narayan et al. (1996, 1997) from a comparative study of the X-ray properties of quiescent SXTs with black holes and neutron stars, respectively.

Currently, ten X-ray binaries are known to contain black holes on the basis of a dynamical mass determination; seven of these are transient low-mass X-ray binaries (see Table 3). Another 17 systems are suspected to be BHXB on the basis of their X-ray spectra (White & Van Paradijs 1996). The total number of transient BHXB in the Galaxy is estimated to be of order 10^3 (Tanaka & Lewin 1995; White & Van Paradijs 1996).

II Neutron star masses

Apart from their crucial role in distinguishing black holes from neutron stars, the importance of measuring the masses of compact stars in X-ray binaries is that they may provide constraints on the properties of the high-density matter in the interior of neutron stars.

These properties are described by an equation of state (EOS), which together with the Oppenheimer-Volkov equations allows one to calculate models of the interior structure of neutron stars (see, e.g., Shapiro & Teukolsky 1983). Since neutron stars can be considered to be zero-temperature objects these models form a one-parameter sequence in which mass, M, and radius, R, depend only on the central density. For a given equation of state one thus has a unique mass-radius relation.

As will be discussed in more detail below, most neutron star masses are consistent with a value close to $1.4\,M_\odot$. From Fig. 1 it appears that at this value masses do not allow one to draw conclusions about the stiffness of the EOS of neutron star matter. For that, one would need observed masses in excess of $1.6\,M_\odot$, which would exclude the softest EOS (note that stiff equations of state are not excluded by low neutron star masses). Similarly, measurements of the gravitational redshift, z, at the neutron star surface alone are not a sensitive EOS discriminant, since both stiff and soft equations of state allow M/R ratios up to $\sim 0.2\,M_\odot\ \mathrm{km}^{-1}$ (see Fig. 1), corresponding to redshifts up to ~ 0.6.

Very accurate neutron star masses have been determined from a variety of general-relativistic effects on the radio pulse arrival times of double neutron star systems. These results will be briefly summarized in §III. Neutron star masses have been determined for six HMXB pulsars from pulse arrival time measurements, in combination with radial-velocity observations of their massive companions (see §IV). Masses have also been estimated for the low-mass binary radio pulsar PSR J1012+5307, whose companion is a white dwarf, and for the neutron stars in the LMXBs Cyg X-2 (a Z source), Cen X-4 (an SXT) and 4U 1626–67 (an X-ray pulsar).

In addition to direct measurements of mass and radius, a variety of other ways to obtain observational constraints on the EOS of neutron stars have been proposed. I will limit myself here to just mentioning them.

(i) Measurement of the limiting spin period of neutron stars (Friedman et al. 1986; Glendenning 1998).

(ii) The cooling history of neutron stars (Becker & Trümper 1998).

(iii) Measurement of the neutron star magnetic field from the energy of a cyclotron line in the spectrum of an X-ray pulsar, combined with an interpretation of its spin behavior in terms of an accretion torque model (Wassermann & Shapiro 1983).

(iv) Glitches in the spin period, and its derivative, of radio pulsars (Alpar 1998).

(v) The neutrino light curve during a supernova explosion (Loredo & Lamb 1989).

(vi) Measurements of kHz quasi-periodic oscillations in the X-ray intensity of LMXB, interpreted as Keplerian frequencies of orbits around neutron stars may provide constraints on the mass-radius relation of neutron stars by requiring that the neutron star and the innermost stable orbit around it, must fit inside the Kepler orbit (Kluzniak & Wagoner 1985; Miller, Psaltis & Lamb 1996; Kaaret & Ford 1997; Zhang et al. 1997). A detailed discussion of these kHz QPO is given by Van der Klis (1998).

(vii) Gravitational bending of X rays, as inferred from the X-ray pulse profile for a radio pulsar for which the emission geometry is determined from the radio pulse properties (Yancopoulos et al. 1994).

(viii) Measurement of the gravitational redshift of γ-ray lines emitted as a result of spallation processes on the surface of an accreting neutron star (Bildsten, Salpeter & Wasserman 1993).

(ix) Time-resolved spectroscopy of X-ray bursts, in principle, allows the derivation of constraints on the mass-radius relation of neutron stars (see Lewin, Van Paradijs & Taam 1993, for a detailed discussion). The practical value of this method is limited by the systematic uncertainty in the interpretation of the burst spectra (Van Paradijs et al. 1991) and the possibility that the burst emission is not uniformly distributed across the neutron star surface (Bildsten 1995, 1998).

III Mass determinations for binary radio pulsars

Relativistic effects

Radio pulse arrival times can be measured with exquisite accuracy (to several tens of ns), and at this level of accuracy several relativistic effects become strongly detectable. These have been conveniently described by Taylor & Weisberg (1989), based on a theoretical formalism developed by Damour & Deruelle (1986), for the case that general relativity is explicitly assumed to be valid. I refer the reader to these two papers for details, and limit myself here to a brief listing of the effects, as they have been applied so far to several binary radio pulsars.

By far the largest part of the pulse arrival time variations is the light travel time across the orbit, which Taylor & Weisberg describe by the "Roemer delay" parameter $a_{\rm R}$ (close to the classical semi-major axis of the orbit), which is related to the masses $m_{\rm p}$ and $m_{\rm c}$ of the pulsar and its companion, respectively, their sum M, and the orbital period P, by:

$$\frac{a_{\rm R}^3}{P^2} = \frac{GM}{4\pi^2}\left[1 + \left(\frac{m_{\rm p} m_{\rm c}}{M^2} - 9\right)\frac{GM}{2a_{\rm R}c^2}\right]^2. \qquad \text{(I)}$$

The orbit precesses, at a rate measured by the quantity k, defined by $\dot{\omega} = 2\pi k/P$, where k is given by:

$$k = \frac{3GM}{c^2 a_R (1 - e^2)}. \tag{2}$$

Here ω is the angle between the line of nodes and the direction toward periastron (as measured in the orbital plane), and e is the orbital eccentricity.

The variation along the orbit of the gravitational redshift and time dilation (Einstein delay) is given by the quantity γ, related to the system parameters by:

$$\gamma = \frac{eP G m_c (m_p + 2m_c)}{2\pi c^2 a_R M}. \tag{3}$$

Due to the emission of gravitational radiation the orbit decays; the rate of decrease of the period is given by

$$\dot{P} = -\frac{192\pi}{5c^5} (2\pi G/P)^{5/3} f(e) m_p m_c M^{-1/3}, \tag{4}$$

where

$$f(e) = \left[1 + \frac{73}{24} e^2 + \frac{37}{96} e^4\right] (1 - e^2)^{-7/2}. \tag{5}$$

Finally, the pulses may show a measurable Shapiro delay, which reflects that near the pulsar companion the path along which the pulsar signal travels is curved. The shape of the orbital phase dependence of this delay is characterized by two quantities s and r, given by

$$s = \sin i, \quad r = G m_c / c^3. \tag{6}$$

In the case of the Hulse-Taylor pulsar, PSR B1913+16, all above effects have been measured, each of which provides a different constraint on m_p and m_c. As shown by Taylor & Weisberg (1989), this overdetermined set of constraints leads to one consistent solution ($m_p = 1.442 \pm 0.003\,M_\odot$, $m_c = 1.386 \pm 0.003\,M_\odot$), showing that to the accuracy at which the test can be performed, general relativity provides a consistent description of this system.

For PSR B2127+11C in the globular cluster M15 Deich & Kulkarni (1996) measured the orbital precession, the Einstein delay and the orbital decay rate, from which they derived $m_p = 1.350 \pm 0.040\,M_\odot$, and $m_c = 1.363 \pm 0.040\,M_\odot$.

Table 1: Neutron star masses from relativistic effects on binary pulsar timing

Name	Method[a]	m_p ($M_\odot$)	m_c ($M_\odot$)	Ref.
J1518+4904	R,$\dot{\omega}$	1.54 ± 0.22	1.09 ± 0.19	[1]
B1534+12	R,$\dot{\omega}$,E	1.32 ± 0.03	1.36 ± 0.03	[2]
B1802–07	R,$\dot{\omega}$	$1.4\,(+0.4, -0.3)$	$0.33\,(+0.13, -0.10)$	[3]
B1855+09	R,S	$1.27\,(+0.23, -0.15)$	$0.233\,(+0.026, -0.017)$	[4]
B1913+16	R,$\dot{\omega}$,E,G,S	1.442 ± 0.003	1.386 ± 0.003	[5]
B2127+11C	R,$\dot{\omega}$,E,G	1.350 ± 0.040	1.363 ± 0.060	[6]
B2303+46	R,$\dot{\omega}$	1.16 ± 0.28	1.37 ± 0.24	[3]

[a] R = Roemer delay; $\dot{\omega}$ = periastron advance; E = Einstein delay; G = orbital decay by gravitational radiation; S = Shapiro delay. References: [1] Nice et al. (1996); [2] Wolszczan (1991); [3] Thorsett et al. (1993); [4] Ryba & Taylor (1991); [5] Taylor & Weisberg (1989); [6] Deich & Kulkarni (1996).

Wolszczan (1991) measured the periastron advance and the Einstein delay for the double neutron star system PSR B1534+12; adding the constraint $\sin i \leq 1$ he derived $m_p = 1.32 \pm 0.03\ M_\odot$, and $m_c = 1.36 \pm 0.03\ M_\odot$. Arzoumanian (1995) detected also orbital decay and Shapiro delay, and derived substantially improved masses for PSR B1534+12.

For PSR B1855+09, which is seen almost edge-on, Ryba & Taylor (1991) could measure the Shapiro delay, which directly gives the orbital inclination and the companion mass ($m_c = 0.233^{+0.026}_{-0.017}\ M_\odot$); together with the mass function this gives $m_p = 1.27^{+0.23}_{-0.15}\ M_\odot$. The companion is a low-mass white dwarf; theoretical estimates for its mass (based on evolutionary scenarios for the formation of systems like PSR B1855+09) agree with the measured value (Joss et al. 1987; Savonije 1987).

Thorsett et al. (1993) measured the rate of periastron advance for PSR B1802–07 and PSR B2303+46, from which they derive total system masses M of $1.7 \pm 0.4\ M_\odot$ and $2.53 \pm 0.08\ M_\odot$, respectively. Combining this with the observed mass functions, and assuming a probable inclination range, they derive $m_p = 1.4^{+0.4}_{-0.3}\ M_\odot$, $m_c = 0.33^{+0.13}_{-0.10}\ M_\odot$, for PSR B1802–07, and $m_p = 1.16 \pm 0.28\ M_\odot$, $m_c = 1.37 \pm 0.24\ M_\odot$, for PSR B2303+46. Improved values for the masses of these two systems have been derived by Arzoumanian (1995).

Nice et al. (1996) measured the rate of periastron advance and the mass function for PSR J1518+4904. Following the same argument as Thorsett et al. (1993) one finds for this system $m_p = 1.54 \pm 0.22\ M_\odot$, $m_c = 1.09 \pm 0.19\ M_\odot$.

Non-relativistic mass determinations

Van Kerkwijk et al. (1996) combined the pulse delay curves of the millisecond pulsar PSR J1012+5307 with the radial-velocity curve of its white-dwarf companion. This led to an accurately determined mass ratio $m_{\rm p}/m_{\rm c} = 13.3 \pm 0.7$. For a given white-dwarf composition the surface gravity acceleration, as inferred from model atmosphere fits to the profiles of the Balmer absorption lines in the white-dwarf spectrum, uniquely determine the white-dwarf mass, for which Van Kerkwijk et al. derive a value of $0.16 \pm 0.02\,(1\sigma)\,{\rm M}_\odot$. Combining this with the mass ratio and the mass function they find that the pulsar mass is in the range 1.5 to 3.2 $\rm M_\odot$ (95% confidence).

IV Mass determinations for neutron stars and black holes in X-ray binaries

Mass function

In determining the mass of an X-ray source, using Newtonian effects only, the fundamental quantity is the mass function $f_{\rm opt}(M)$ which is determined from the orbital period, $P_{\rm orb}$, and the amplitude, $K_{\rm opt}$, of the radial-velocity variations of the mass donor by

$$f_{\rm opt}(M) \equiv M_{\rm X}^3 \sin^3 i/(M_{\rm X} + M_2)^2 = \frac{K_{\rm opt}^3\, P_{\rm orb}}{2\pi {\rm G}}. \tag{7}$$

The corresponding quantity $f_{\rm X}(M)$ can be determined for binary X-ray pulsars:

$$f_{\rm X}(M) \equiv M_2^3 \sin^3 i/(M_{\rm X} + M_2)^2 = \frac{4\pi^2\,(a_{\rm X} \sin i)^3}{{\rm G}P_{\rm orb}^2}. \tag{8}$$

(The connection to observational parameters is written differently, since in the case of X-ray pulsars the observed quantities are usually pulse arrival times, whereas from optical spectra one measures radial velocities.)

Incomplete but occasionally extremely useful information may be obtained from a measurement of only one mass function, since it gives a lower limit to the mass of the companion of the star whose orbital motion is measured. As emphasized by McClintock & Remillard (1986) this is of great importance in distinguishing black holes from neutron stars in X-ray binaries.

If both mass functions can be measured, their ratio immediately gives the mass ratio $q \equiv M_{\rm X}/M_2 = f_{\rm opt}(M)/f_{\rm X}(M)$, and both masses are then determined separately, up to a factor $\sin^3 i$.

$$M_{\rm X} \sin^3 i = f_{\rm opt}(M)\,(1+q^{-1})^2 \tag{9}$$

$$M_{\rm opt} \sin^3 i = f_{\rm X}(M)\,(1+q)^2 \tag{10}$$

Inclination angle

To complete the mass determination one needs the orbital inclination i, for whose determination several methods are available, at least in principle: (i) X-ray eclipse durations, (ii) optical light curves, and (iii) polarization variations.

For a spherical companion star with radius R and a circular orbit (separation a, period P) the duration of the eclipse of a point-like X-ray source is related to i by the expression:

$$(R/a)^2 = \cos^2 i + \sin^2 i \sin^2 \theta_{\rm e}. \tag{11}$$

Here $\theta_{\rm e} = 2\pi t_{\rm e}/P$, with $t_{\rm e}$ half the duration of the eclipse. If the relative size of the companion is known, i is a function of $\theta_{\rm e}$ only. Direct estimates of R from the spectrum and luminosity class are not accurate enough to be useful. In general, the companion will not be spherical, due to the gravitational perturbation of the compact star. The relative size of the primary can be expressed as a function of the mass ratio q and a dimensionless potential parameter Ω, which is a measure of the extent to which the companion fills its Roche lobe. An observed eclipse duration then determines a relation between q, Ω, and i. The eclipse duration may be affected by absorbing effects on the X-rays by a stellar wind from the companion (see, e.g., Woo et al. 1995).

Electron scattering of originally unpolarized light in close-binary stars may yield a net polarization which varies with orbital phase, due to the deformation from spherical symmetry of the system (e.g., deformation of the companion star, presence of an accretion disk). Under rather general conditions the fundamental and first harmonic (in orbital frequency) of the variations of the Stokes parameters Q and U (see Tinbergen 1996) describe ellipses in the (Q,U) plane, whose eccentricity e is related to the orbital inclination by $e = \sin i$ for the fundamental, and $e = \sin^2 i/(1+\cos^2 i)$ for the first harmonic (Brown et al. 1978; Rudy & Kemp 1978 ; Milgrom 1979). Polarization variations may therefore provide a measurement of i. The method has been applied to several HMXB, e.g., Cyg X-1 (Dolan & Tapia 1989); for references to early work, see Van Paradijs (1983).

Many HMXB with an evolved companion show moderate (up to $\sim 10\,\%$) optical brightness variations, with two approximately equal maxima, and two different minima, which occur at the quadratures and conjunctions, respectively. These so-called "ellipsoidal" light curves are caused by the rotational and tidal distortion of the companion star, and a non-uniform surface brightness distribution ("gravity

darkening"). The double-waved shape of the light curve reflects the pear-like shape of the companion: near conjunctions the projected stellar disk is smallest, near quadratures largest. For assumed co-rotation of the companion star, its distortion is determined by the mass ratio q, and by the dimensionless potential parameter Ω (see above); Roche lobe filling of the companion corresponds to a (q dependent) critical value of Ω. The distortion, and therefore the shape and amplitude of the ellipsoidal light curve, are determined by q and Ω, and furthermore by i. Thus, in principle, the optical light curve can provide a relation between q, Ω and i. Together with other constraints on these parameters (eclipse duration, q from two observed mass functions) this may lead to a solution for the masses of both components of the binary (see Van Paradijs 1983, for extensive references to early work on light curve modeling of HMXB).

The analysis by Tjemkes et al. (1986) showed that for well-studied HMXB with evolved companions the optical light curves may be reproduced if the best-known system parameters are used. Conversely, however, X-ray heating of the companion, the presence of an accretion disk, and intrinsic variability of the companion have a significant effect on the light curve, to the extent that it is difficult to derive significant constraints on these systems from an analysis of their light curves. For Be/X-ray binaries, irregular brightness variations related to equatorial mass shedding in general dominate any orbital brightness variations.

Ellipsoidal light curves have been observed for several soft X-ray transients in quiescence, whose optical light is then dominated by the companion star. Since these companions fill their Roche lobes, the potential parameter Ω is determined by q, and therefore the light curve depends on q and i only. If needed, the generally small contribution from the quiescent accretion disk may be estimated from a study of the broad-band energy distribution, and corrected for. The contribution of the disk diminishes with increasing wavelength, and recent orbital light curve studies are therefore preferentially carried out in the infra-red (Casares et al. 1993; Beekman et al. 1996; Shahbaz et al. 1997). The ellipsoidal light curves of SXT in quiescence have played an important role in the mass estimates of black holes. However, one should not ignore Haswell's (1995) emphasis that also for quiescent SXT the ellipsoidal light curves may be affected by systematic effects, possibly caused by variable contributions from an accretion disk, analogous to the superhumps in the SU UMa subgroup of the cataclysmic variables.

Additional Constraints

In addition to the above standard ingredients of a mass determination for X-ray binaries two additional pieces of information may be used. The first applies when the source distance is known. Since the apparent magnitude of the companion star (corrected for interstellar extinction) and its spectral type together determine its angular radius, for these sources one can estimate the radius, R_2, of the companion star, and this constrains the relation between M_X and M_2. This was used by Gies & Bolton

Table 2: Neutron Star Masses: X-ray Binaries and Binary Radio Pulsars

Name	i (°)	M_X ($M_\odot$)	M_{comp} ($M_\odot$)	Ref.
HMXB				
Vela X-1	> 74	1.88(+0.69,–0.47)	23.5(+2.2,–1.5)	[1]
4U 1538–52	68(+9,–8)	1.06(+0.41,–0.34)	16.4(+5.2,–4.0)	[1]
SMC X-1	70(+11,–7)	1.6 ± 0.1	17.2 ± 0.6	[2]
LMC X-4	65(+7,–6)	1.47(+0.44,–0.39)	15.8(+2.3,–2.0)	[1]
Cen X-3	> 66	1.09(+0.57,–0.52)	18.4(+4.0,–1.8)	[1]
Her X-1[a]	> 79	1.47(+0.23,–0.37)	2.32(+0.16,–0.29)	[1]
Her X-1	> 79	1.5 ± 0.3	2.3 ± 0.3	[3]
LMXB				
Cen X-4	30-37	1.1-1.9	< 0.2	[4,5]
4U 1626–67[a]	9-36	1.8(+2.8,–1.3)	< 0.5	[6]
Cyg X-2	< 73	$> 1.42(\pm 0.08)$	$> 0.47(\pm 0.03)$	[7]
LMBP				
J1012+5307		1.5-3.2	0.16 ± 0.02	[8]

[a] From Doppler shifted optical pulsations.
References: [1] Van Kerkwijk, Van Paradijs & Zuiderwijk (1995); [2] Reynolds et al. (1993); [3] Reynolds et al. (1997); [4] Chevalier et al. (1989) [5] McClintock & Remillard (1990); [6] Middleditch et al. (1981); [7] Casares, Charles & Kuulkers (1997); [8] Van Kerkwijk, Bergeron & Kulkarni (1996).

(1986) in their analysis of Cyg X-1. In case the companion star fills its Roche lobe, the constraint is simple: for such stars the density is determined by the orbital period alone (see, e.g., Frank et al. 1992), and M_2 follows immediately from R_2. In the case of the SXT Cen X-4 (whose compact star is a neutron star) this served to show that the companion mass is extremely low, less than $0.2\,M_\odot$ (Chevalier et al. 1989; McClintock & Remillard 1990).

If the orbital angular momentum is parallel to that of the companion star (and therefore of the matter flowing through the accretion disk), both K_{opt} and the observed rotational velocity $V_{rot} \sin i$ of the secondary have been decreased by the same projection factor $\sin i$. Therefore, their ratio is not affected. As shown by Gies & Bolton (1986) this constrains the relation between M_X and M_2. In case the companion star co-rotates at the same angular velocity as the orbit, this constraint is an estimate of the mass ratio. Using the expressions for the radius of the Roche lobe by Paczynski (1971), one obtains (Kuiper et al. 1988; Wade & Horne 1988):

$$\left(V_{rot} \sin i / K_{opt}\right) = 0.462\, q^{-1/3}\,(1+q)^{2/3}. \qquad (12)$$

Table 3: Black-Hole Binary Candidates from Radial-Velocity Measurements

Name	Nova	$P_{\rm orb}$ (days)	$f(M)$ ($M_\odot$)	i ($^\circ$)	$M_{\rm X}$ ($M_\odot$)	Ref.
HMXB						
Cyg X-1	No	5.6	0.25	28–38	16 ± 5	[1-3]
LMC X-3	No	1.7	2.3	64–70	3.5–10	[4,5]
LMC X-1	No	4.2	0.144	40–63	4–10	[6]
LMXB						
A 0620–00	Yes	0.32	2.70	66.5–73.5	3.3–4.2	[7,8]
				31–54	14 ± 7	[9]
GS 2023+338	Yes	6.47	6.08	52–60	10–15	[10-12]
GS/GRS 1124–68	Yes	0.43	3.1	55–65	4.5–7.5	[13]
GRO J0422+32	Yes	0.21	1.2	45–51	3.2–3.9	[14,15]
				13–31	> 9	[16]
GRO J1655–40	Yes	2.60	3.16	63–71	7 ± 0.7	[17-19]
GS 2000+25	Yes	0.35	5.0	43–85	4.8–14.4	[20-23]
H 1705–25	Yes	0.52	4.0	60–80	3.5–8.5	[24]

[1] Webster & Murdin (1972); [2] Bolton (1972); [3] Gies & Bolton (1986) [4] Cowley et al. (1983); [5] Kuiper et al. (1988) [6] Hutchings et al. (1987); [7] McClintock & Remillard (1986); [8] Marsh et al. (1994); [9] Shahbaz et al. (1994a); [10] Casares et al. (1992); [11] Casares & Charles (1994); [12] Shahbaz et al. (1994b); [13] Remillard, McClintock & Bailyn (1992); [14] Filippenko, Matheson & Ho (1995); [15] Casares et. al. (1995a); [16] Beekman et al. 1997; [17] Bailyn et al. (1995); [18] Van der Hooft et al. (1998); [19] Orosz & Bailyn (1997); [20] Casares, Charles & Marsh (1995b); [21] Filippenko, Matheson & Barth (1995); [22] Beekman et al. (1996); [23] Callanan et al. (1996); [24] Remillard et al. (1996).

The cancellation of the $\sin i$ factor has also been applied to the rotational velocity at some radial distance in the accretion disk, as inferred from emission line profiles. Warner (1976) applied this to cataclysmic variables, and Johnston et al. (1990) to the SXT A0620–00. Since relatively little is known about the emission line structure of accretion disks, the interpretation of the q values inferred from this method is somewhat uncertain.

Optical pulsations

Optical pulsations have been detected from Her X-1 and 4U 1626–67. These pulsations arise from the reprocessing of pulsed X rays in the companion star and the accretion disk, and can be used to study the orbital parameters of these systems.

A detailed analysis of the optical pulsations of Her X-1 was made by Middleditch & Nelson (1976). The orbital motion of the neutron star is known from the Doppler

shifts of the X-ray pulse arrival times. Optical pulsations in phase with the X-ray pulsations are present, but also optical pulsations with a slightly different frequency. The former arise from reprocessing in the accretion disk, the latter from the surface of the companion; their frequency difference is just the orbital frequency (beat frequency relation). The pronounced variation with orbital phase of the amplitude of the optical pulsations indicates that the companion is non-spherical and fills its Roche lobe. By assuming that across the surface of the Roche lobe filling companion the X-ray reprocessing time is constant Middleditch & Nelson used the Doppler shift information of these optical pulsations to estimate the mass ratio, which together with the eclipse duration and the X-ray mass function leads to $M_X = 1.30 \pm 0.14\,M_\odot$ and $M_{opt} = 2.18 \pm 0.11\,M_\odot$. These values are consistent with those obtained from the radial-velocity curve of the late A-type companion star (Reynolds et al. 1997).

Doppler shifts of the 7.7 s X-ray pulsations of 4U 1626–67 have not been detected so far: $a_X \sin i < 10$ ms (Levine et al. 1988). Optical pulsations, arising from reprocessing of X rays in the disk and in the companion star were detected by Middleditch et al. (1981; see also Chakrabarty 1998). From a detailed modeling of these pulsations, similar to that for Her X-1, they derived $M_X = 1.8^{+2.9}_{-1.3}\,M_\odot$ and $M_2 < 0.5\,M_\odot$.

V Summary of mass determinations of neutron stars and black holes

The results of the mass estimates, described in §§III and IV, are summarized in Table 1 (relativistic effects in binary radio pulsars), Table 2 (neutron stars in X-ray binaries, and non-relativistic orbital analyses of binary radio pulsars), and in Table 3 (black holes in X-ray binaries). From these tables one may draw the conclusion that with few exceptions neutron star masses are consistent with a relatively narrow mass range near the "canonical" value of $1.4\,M_\odot$. Vela X-1 and Cyg X-2 present interesting examples of substantially higher neutron star masses, but the possible presence of systematic effects on these mass determinations has to be investigated before the consequence, i.e., that very soft equations of state are excluded, can be accepted.

References

Alpar, M.A. 1998, in The Many Faces of Neutron Stars, ed. R. Buccheri, J. van Paradijs & M.A. Alpar (Dordrecht: Kluwer), 59
Arnett, W.D. & Bowers, R.L. 1977, ApJS, 33, 415
Arzoumanian, Z. 1995, Ph.D. Thesis, Princeton University
Bailyn, C. et al. 1995, Nature, 378, 157
Baym, G. & Pethick, C. 1979, ARA&A, 17, 415
Becker, W. & Trümper, J. 1998, in The Many Faces of Neutron Stars, ed. R. Buccheri, J. van Paradijs & M.A. Alpar (Dordrecht: Kluwer), 525
Beekman, G. et al. 1996, MNRAS, 281, L1
Beekman, G. et al. 1997, MNRAS, 290, 303
Belian, R.D., Conner, J.P. & Evans, W.D. 1976, ApJ, 206, L135
Bildsten, L. 1995, ApJ, 438, 852
Bildsten, L. 1998, in The Many Faces of Neutron Stars, ed. R. Buccheri, J. van Paradijs & M.A. Alpar (Dordrecht: Kluwer), 419
Bildsten, L., Salpeter, E.E. & Wasserman, I. 1993, ApJ, 408, 615
Bolton, C.T. 1972, Nature, 235, 271
Brown, J.C., McLean, I.S. & Emslie, A.G. 1978, A&A, 68, 415
Callanan, P.J. et al. 1996, ApJ, 470, L57
Casares, J., Charles, P.A. & Naylor, T. 1992, Nature 355, 614
Casares, J. et al. 1993, MNRAS, 265, 834
Casares, J. & Charles, P.A. 1994, MNRAS, 271, L5
Casares, J. et al. 1995a, MNRAS, 276, L35
Casares, J., Charles, P.A. & Marsh, T. 1995b, MNRAS, 277, L45
Casares, J., Charles, P.A., & Kuulkers, E. 1997, ApJ, 493, L39
Chakrabarty, D. 1998, ApJ, 492, 342
Cheng, K.S., Dai, Z.G. & Yao, C.C. 1996, ApJ, 464, 348
Chevalier, C. et al. 1989, A&A, 210, 114
Cook, G.B., Shapiro, S.L. & Teukolsky, S.A. 1994, ApJ, 424, 823
Cowley, A.P. et al. 1983, ApJ, 272, 118
Damour, T. & Duruelle, N. 1986, Ann. Inst. H. Poincaré (Phys. Theorique), 43, 107
Datta, B. 1988, Fund. Cosmic Phys., 12, 151
Deich, W.T.S. & Kulkarni, S. R. 1996, in Compact Stars in Binaries, IAU Symposium 165, ed. J. van Paradijs, E.P.J. van den Heuvel & E. Kuulkers, (Dordrecht: Kluwer), 279
Dolan, J.F. & Tapia, S. 1989, ApJ, 344, 830
Engvik, L. et al. 1996, ApJ, 469, 794
Filippenko, A.V., Matheson, T. & Barth, S. 1995, ApJ, 455, L139
Filippenko, A.V., Matheson, T. & Ho, L. C. 1995, ApJ, 455, 614
Frank, J., King, A.R. & Raine, D.J. 1992, Accretion Power in Astrophysics, 2nd Edition (Cambridge: Cambridge University Press)
Gies, D.R. & Bolton, C.T. 1986, ApJ, 304, 371
Glendenning, N. 1998, in The Many Faces of Neutron Stars, ed. R. Buccheri, J. van

Paradijs & M.A. Alpar (Dordrecht: Kluwer), 15
Grindlay, J.E. et al. 1976, ApJ, 205, L127
Haswell, C.A. 1996, in Compact Stars in Binaries, IAU Symposium 165, ed. J. van Paradijs, E.P.J. van den Heuvel & E. Kuulkers (Dordrecht: Kluwer), 351
Hutchings, J.B. et al. 1987, AJ, 94, 340
Johnston, H.M.., Kulkarni, S.R., & Oke, J.B. 1990, ApJ, 345, 492
Joss, P.C., Rappaport, S.A. & Lewis, W. 1987, ApJ, 319, 180
Kaaret, P. & Ford, E.C. 1997, Science, 276, 1386
Kluzniak, W. & Wagoner, R.V. 1985, ApJ, 297, 548
Kuiper, L., Van Paradijs, J. & Van der Klis, M. 1988, A&A, 203, 79
Levine, A.M. et al. 1988, ApJ, 327, 732
Lewin, W.H.G. & Van den Heuvel, E. P. J. (ed) 1983, Accretion Driven Stellar X-ray Sources (Cambridge: Cambridge University Press)
Lewin, W.H.G., Van Paradijs, J. & Taam, R.E. 1993, SSR, 62, 223
Lewin, W.H.G., Van Paradijs, J. & Van den Heuvel, E.P.J. (ed) 1995, X-ray Binaries (Cambridge: Cambridge University Press) [*XRB*]
Loredo, T. & Lamb, D.Q. 1989, Ann. N.Y. Ac. Sci., 571, 601
Marsh, T.R., Robinson, E.L. & Woods, J.H. 1994, MNRAS, 266, 137
McClintock. J.E. & Remillard, R.A. 1986, ApJ, 308, 110
McClintock, J.E. & Remillard, R.A. 1990, ApJ, 350, 386
Middleditch, J. & Nelson, J. 1976, ApJ, 208, 567
Middleditch. J. et al. 1981, ApJ, 244, 1001
Milgrom, M. 1979, A&A, 76, 338
Miller, C., Psaltis, D. & Lamb, F.K. 1996, ApJ, submitted
Narayan, R. 1996, ApJ, 462, 136
Narayan, R. et al. 1997, ApJ, 478, L79
Nauenberg, M. & Chapline, G. 1973, ApJ, 179, 277
Nice, D.J., Sawyer, R.W. & Taylor, J.H. 1996, ApJ, 466, L87
Oda, M. 1976 SSR, 20, 757
Oda, M. et al. 1971, ApJ, 166, L1
Orosz, J. & Bailyn, C. 1997, ApJ, 477, 876
Ostriker, J.E. 1977, Ann. N.Y. Ac. Sci., 302, 229
Paczynski, B. 1971, ARA&A, 9, 183
Remillard, R.A. et al. 1996, ApJ, 459, 226
Remillard, R.A. McClintock, J.E. & Bailyn, C. 1992, ApJ, 399, L145
Reynolds, A.P. et al. 1993, MNRAS, 261, 337
Reynolds, A.P. et al. 1997, MNRAS, 288, 43
Rhoades, C.E. & Ruffini, R. 1974, Phys. Rev. Lett., 32, 324
Rudy, R.J. & Kemp, J.C. 1978, ApJ, 221, 200
Ryba, M.F. & Taylor, J.H. 1991, ApJ, 371, 739
Savonije, G.J. 1987, Nature, 325, 416
Schreier, E. et al. 1972, ApJ, 172, L112
Shahbaz, T., Naylor, T. & Charles, P.A. 1994a, MNRAS, 268, 756
Shahbaz, T. et al. 1994b, MNRAS, 271, L10

Shahbaz, T. et al. 1997, MNRAS, 285, 607
Shapiro, S.L. & Teukolsky, S.A. 1983, Black Holes, White Dwarfs and Neutron Stars (New York: John Wiley and Sons)
Stella, L. et al. 1985, ApJ, 288, L45
Tanaka, Y. & Lewin, W.H.G. 1995, in *XRB*, 126
Taylor, J.H. & Weisberg, J. 1989, ApJ, 345, 434
Tennant, A., et al. 1986, MNRAS, 221, 27P
Thorsett, S.E. et al. 1993, ApJ, 405, L29
Tinbergen, J. 1997, Astronomical Polarimetry (Cambridge: Cambridge University Press)
Tjemkes, S.A., Van Paradijs, J. & Zuiderwijk, E.J. 1986, A&A, 154, 77
Van der Hooft, F. et al. 1998, A&A, 329, 538
Van der Klis, M. 1998, in The Many Faces of Neutron Stars, ed. R. Buccheri, J. van Paradijs & M.A. Alpar (Dordrecht: Kluwer), 337
Van Kerkwijk, M.H., Bergeron, P. & Kulkarni, S.R. 1996, ApJ, 467, L89
Van Kerkwijk, M.H., Van Paradijs, J. & Zuiderwijk, E.J. 1995, A&A, 303, 497
Van Paradijs, J. 1983, in Accretion Driven Stellar X-ray Sources, ed. W.H.G. Lewin & E.P.J. Van den Heuvel (Cambridge: Cambridge University Press), 189
Van Paradijs, J. et al. 1991, PASJ, 42, 633
Wade, R.,& Horne, K. 1988, ApJ, 324, 411
Warner, B. 1976, in Structure and Evolution of Close Binary Systems, ed. P. Eggleton, S. Mitton & J. Whelan (Reidel), 85
Wassermann, I. & Shapiro, S.L. 1982, ApJ, 265, 1036
Webster, B.L. & Murdin, P. 1971, Nature, 235, 37
White, N.E. & Marshall, F.E. 1984, ApJ, 281, 354
White, N.E. & Van Paradijs, J. 1996, ApJ, 473, L25
Wolszczan, A. 1991, Nature, 350, 688
Woo, J. W. et al. 1995, ApJ, 445, 896
Yancopoulos, S., Hamilton, T.T. & Helfand, D.J. 1994, ApJ, 429, 832
Zhang, W., Strohmayer, T.S. & Swank, J.H. 1997, ApJ, 482, L167

Authors' Address

Astronomical Institute 'Anton Pannekoek', University of Amsterdam & Center for High Energy Astrophysics, Kruislaan 403, 1098 SJ Amsterdam, The Netherlands

Department of Physics, University of Alabama in Huntsville, Huntsville AL 35899, USA

B. Datta

Disk Luminosity for Accreting, Weak Magnetic Field Neutron Stars in the "Slow" Rotation Approximation

Abstract

For accretion onto neutron stars possessing weak surface magnetic fields and substantial rotation rates (corresponding to the secular instability limit), we calculate the disk and surface layer luminosities general relativistically using the Hartle & Thorne formalism, and illustrate these quantities for a set of representative neutron star equations of state.

I Introduction

Disk accretion onto a neutron star possessing a weak surface magnetic field provides interesting X-ray emission scenarios, and is relevant for understanding X-ray bursters and low-mass X-ray binaries (e.g., van Paradijs 1991). An important aspect of this scenario is that the neutron star will get spun up to very short rotation periods ($\lesssim$ millisecond) over a time of the order of hundreds of millions of years. For such rapid rates of rotation, the relativistic effect of dragging of inertial frames in the vicinity of the neutron star is expected to be important. This will alter the trajectories of infalling particles as compared to the non-rotational case. We address this question and calculate the disk and surface layer luminosities incorporating the rotational effects in a general relativistic framework. We take the spun up neutron star to be rotating at a particular value, namely, the secular instability limit so as to illustrate the maximal reasonable effects of rotation. This corresponds to the late stages of accretion. We use the Hartle & Thorne (1968; hereafter HT) formalism, to describe the rotational space-time. This is valid for strong gravitational fields but in the limit of uniform rotation with a rate that is "slow" compared to the critical speed for centrifugal break-up. Neutron star models rotating at the secular instability limit (assuming the star to be homogeneous), relevant in the context of accretion induced spun up neutron stars, are within this limit (Datta & Ray 1983).

II Disk and boundary layer luminosities

Let x and x^* denote $r/2M'$ and $R'/2M'$ respectively (we take c = G = 1), where M' and R' are the mass and radius of the rotating star. Further let $x_{\rm orb}$ denote the radius of the innermost stable orbit corresponding to the rotating space time (in dimensionless units). The following two cases are possible:

Case (a): Radius of the star is greater than the innermost stable orbit radius

If an accretion disk were to form around a relatively large neutron star (i.e., $x^* > x_{\rm orb}$), the ingress of a particle of rest mass m_B from infinity to the inner disk boundary will release an amount of energy given by

$$E'_D = m_B\{1 - \tilde{E}_k(x^*)\}\,, \tag{1}$$

where $\tilde{E}_k(x^*)$ stands for the specific energy of the particle in the stable orbit just above the surface. The energy loss in the boundary layer will be

$$E'_S = m_B\{\tilde{E}_k(x^*) - \tilde{E}_o(x^*)\}\,, \tag{2}$$

where $\tilde{E}_o(x^*)$ is the energy of the particle at rest on the surface of the neutron star.

Case (b): Radius of the star is smaller than innermost stable orbit radius

In this case, $x^* < x_{\rm orb}$ and the accretion disk will extend inward to a radius corresponding to $x = x_{\rm orb}$. Now the energy released in the disk as the particle comes in from infinity to the innermost stable orbit will be

$$E'_D = m_B\{1 - \tilde{E}_{\rm orb}\}\,, \tag{3}$$

and the energy released in the boundary layer will be

$$E'_S = m_B\{\tilde{E}_{\rm orb} - \tilde{E}_o(x^*)\}\,. \tag{4}$$

Here, $\tilde{E}_{\rm orb}$ is the specific energy of the infalling particle in the innermost stable orbit. The quantities $\tilde{E}_k$ and $\tilde{E}_o$ and $\tilde{E}_{\rm orb}$, as a function of x, can be evaluated by numerically solving the condition for the turning point of the motion, the extremum of the energy and the minimum of the energy, corresponding to the Hartle-Thorne rotational space-time (see Datta, Thampan & Wiita 1995 for the details).

III Results and discussions

Our calculations are performed for the following equations of state of high density matter in neutron star interior: (A) Pandharipande (1971), (B) Wiringa UV14 + UVII model (Wiringa, Fiks & Fabrocini 1988), (C) Sahu, Basu & Datta (1993). Of these, models (A) and (C) are respectively very soft and very stiff equations of state and model (B) is intermediate in stiffness.

We consider neutron stars rotating with $\Omega = \Omega_s$, the secular rotational instability limit, given by

$$\frac{\Omega_s^2}{2\pi G\overline{\rho}} = 0.18\ , \tag{5}$$

($\overline{\rho}$ is the average density of the star), so as to illustrate the maximal reasonable effects of rotation. The rotating neutron star's mass (M') and radius (R') are calculated by numerically evaluating the rotational deformations corresponding to the HT metric (Datta & Ray 1983; Datta 1988).

Table 1 summarizes the results. In the second and third columns of this table, we give values of the non-rotating mass M and the rotationally enhanced mass M' for a maximal reasonable rotation rate ($\Omega = \Omega_s$). Columns (4) and (7) show the disk and boundary layer luminosities for non-rotating configurations (E_D and E_S respectively). The values of E'_D and E'_S, including rotational effects treated consistently within the HT framework, are given in columns (5) and (8). All values of luminosity listed in the table are in units of the baryonic rest mass. The boundary layer luminosity values listed in Table 2 do not include corrections for the energy that goes into spinning up the neutron star. We have made estimate of this correction following the prescription of Popham & Narayan (1995) for the case of 1.4 $M_\odot$ neutron star corresponding to the EOS model by Wiringa et al. 1988), and find this correction to be unimportant for $\Omega = \Omega_s$ (Datta, Thampan & Wiita 1995).

In our notation, the total luminosity is: $L = (E'_D + E'_S)\dot{M}c^2$, with $\dot{M}$ the mass accretion rate. According to our calculations, typical values for $(E'_D + E'_S)$ are of the order of 0.2. A typical value of L equal to 10^{37} ergs s^{-1} would then correspond to $\dot{M} \sim 5.6 \times 10^{16}$ g s^{-1}. Such accretion rates are close to the ones estimated in X-ray binaries (Ghosh & Lamb 1991), so that our computations are relevant for systems with significant accretion onto old neutron stars whose surface magnetic fields have undergone substantial decay (to about 10^8 G). Under these circumstances of weak neutron star magnetic fields, we have shown that an incorporation of general relativistic rotational effects always increases the disk luminosity, and usually decreases the boundary layer luminosity. For accretion spun-up neutron star, these effects can be substantial to merit their consideration in analyses of observations of low-mass X-ray

Table 1: Disk and Boundary Layer Luminosities

EOS (1)	$M/M_\odot$ (2)	$M'/M_\odot$ (3)	E_D (m_0c^2) (4)	E'_D (m_0c^2) (5)	$\Delta E_D/E_D$ (6)	E_S (m_0c^2) (7)	E'_S (m_0c^2) (8)	$\Delta E_S/E_S$ (9)
A	1.045	1.121	0.057	0.071	0.2379	0.138	0.130	−0.0534
	1.289	1.371	0.057	0.074	0.2926	0.215	0.206	−0.0431
	1.319	1.400	0.057	0.074	0.2957	0.228	0.218	−0.0423
	1.400	1.476	0.057	0.075	0.3099	0.276	0.266	−0.0395
	1.414	1.485	0.057	0.075	0.3176	0.298	0.285	−0.0409
B	1.053	1.153	0.055	0.063	0.1541	0.097	0.096	−0.0114
	1.282	1.400	0.057	0.071	0.2430	0.131	0.126	−0.0384
	1.400	1.526	0.057	0.074	0.2896	0.150	0.144	−0.0439
	1.680	1.817	0.057	0.075	0.3148	0.201	0.194	−0.0359
	2.188	2.305	0.057	0.078	0.3653	0.355	0.342	−0.0369
C	1.017	1.128	0.045	0.051	0.1140	0.066	0.067	0.0189
	1.261	1.400	0.052	0.059	0.1455	0.085	0.085	0.0075
	1.400	1.553	0.055	0.064	0.1686	0.097	0.097	−0.0010
	1.644	1.817	0.057	0.070	0.2260	0.120	0.118	−0.0224
	2.592	2.771	0.057	0.076	0.3274	0.263	0.255	−0.0324

binaries. An extension of this study for rapidly rotating neutron stars, going beyond the HT approximation, has been done (Datta & Thampan 1997), which will be reported in a future publication.

Acknowledgements

The work presented in this paper was done in collaboration with A. V. Thampan and P. J. Wiita.

References

Datta, B. & Ray, A. 1983, MNRAS, 204, 75
Datta, B., 1988, Fund. Cosmic Phys., 12, 151
Datta, B., Thampan, A.V. & Wiita, P.J. 1995, J. Astrophys. Astr., 16, 357
Datta, B. & Thampan, A.V. 1997, preprint
Ghosh, P. & Lamb, F.K. 1991, in Neutron Stars: Theory and Observations, ed. J.

Ventura & D. Pines (Dordrecht: Kluwer), 363
Hartle, J.B. & Thorne, K.S. 1968, ApJ, 153, 807 (HT)
Pandharipande, V.R. 1971, Nucl. Phys., A178, 123
Popham, R. & Narayan, R. 1995, ApJ, 442, 337
Sahu, P.K., Basu, R. & Datta, B. 1993, ApJ, 416, 267
van Paradijs, J. 1991, in Neutron Stars: Theory and Observations, ed. J. Ventura & D. Pines (Dordrecht: Kluwer), 245
Wiringa, R.B., Fiks, V. & Fabrocini, A. 1988, Phys. Rev. C, 38, 1010

Authors' Address

Indian Institute of Astrophysics, Bangalore 560 034, India

Raman Research Institute, Bangalore 560 080, India

R.A.M.J. Wijers

On the Correlation Between Neutron Star Magnetic Field and Accreted Mass

Abstract

The correlation between accreted mass and field which appears to hold for a class of binary millisecond pulsars is tested for wider applicability. When all known constraints from X-ray binaries and recycled pulsars are combined, no universal relation between amount of field decay and amount of accreted mass remains viable; other factors in the state or evolution of a system must be at least as important in determining the magnetic field.

I Introduction

It has been suggested that fields of recycled pulsars decay simply in proportion to the amount of mass accreted (Taam & Van den Heuvel 1986; Shibazaki et al. 1989; Van den Heuvel & Bitzaraki 1995). Here I investigate a general power-law type dependence of field on accreted mass:

$$B/B_0 = (1 + \Delta M/M_c)^{-\beta} \tag{1}$$

(B and B_0 are the current and initial fields, ΔM is the amount of accreted mass, and M_c a parameter that regulates the onset of decay.) The standard form has $\beta = 1$ and $M_c \sim 10^{-4}$ $M_\odot$, and the extension to an arbitrary exponent is to cover a wider range of possibilities in the investigation. Evolutionary tracks have been calculated for accreting neutron stars, including their spin history. Space does not suffice here to give all details, but in some circumstances the requirement that a pulsar be spun up to a period under 2 ms provides significant constraints on the model (Wijers 1997). Here I shall focus on the constraints provided by accreted mass alone.

II Systems with known amounts of accreted mass

To get as good constraints as possible, we need to find systems with a wide range of estimated amounts of accreted mass. For high and intermediate amounts of accreted

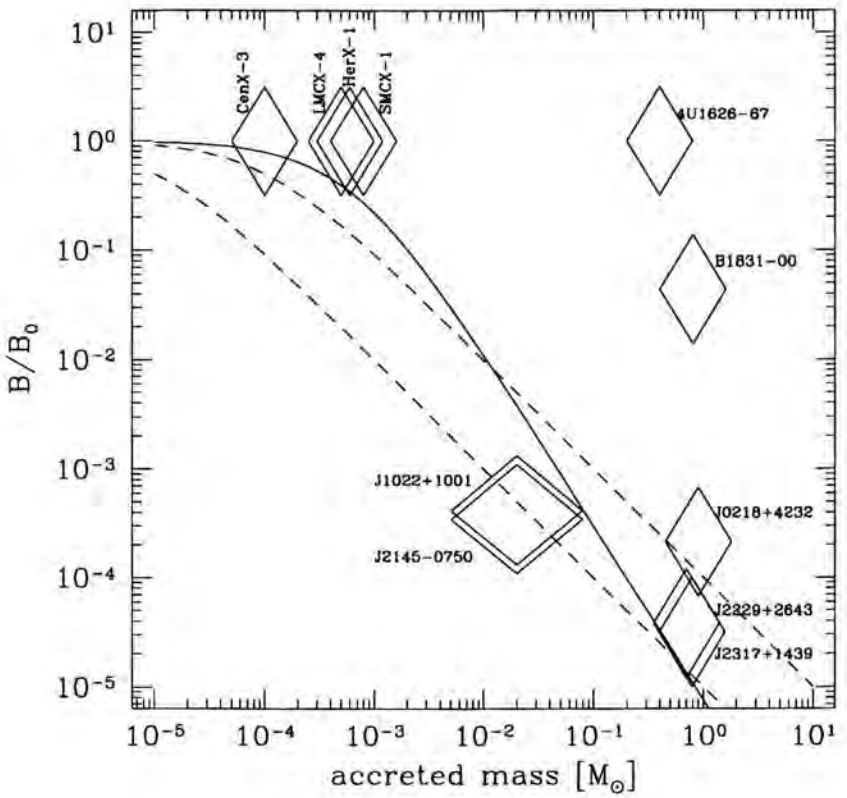

Figure 1. The relation between the ratio of initial to final magnetic field and the amount of accreted mass for systems where both can be estimated. The dashed curves are for $\beta = 1$, with $\log \Delta M = -4$ (top) and -5 (bottom). The solid curve ($\beta = 1.6$, $\log \Delta M = -3.2$) comes closest to fitting the systems along the diagonal.

mass I use recycled pulsars, with the accreted mass estimates taken from Van den Heuvel & Bitzaraki (1995) and Van den Heuvel (1994). For small amounts of accreted mass I use bright high-mass X-ray binaries, with amounts of accreted mass as estimated elsewhere (Wijers 1997). The ratios of initial to final magnetic field and amounts of accreted mass are plotted in Figure 1 (each system is identified next to its symbol). The sizes of the diamonds represent uncertainties in the quantities. For the magnetic field, the current value is mostly well known, and the main uncertainty stems from the value of the initial field. I assume $\log B_0 = 12.3$ for all systems, and the vertical size of the diamonds indicates the consequence of changing this by a factor of 3 either way. (This range will nominally cover 87% of all initial fields according to the population study of Hartman et al. 1997.) The uncertainties in the amounts of accreted mass are taken to be a factor 2, except in PSR J2145−0750 and PSR J1022+1001, where the theoretical uncertainty is greater and a factor of 4 total uncertainty was adopted.

III Conclusion

The fact that high-field objects exist over the full range of ΔM values in Fig. 1 and that at the highest ΔM all field values are represented bodes ill for any model of a causal relation between the two quantities. A few curves of the type of Eq. (1) are also shown, indicating that even for all the objects that do roughly lie in a band from top left to bottom right the model has difficulties.

It has been argued (e.g., Van den Heuvel & Bitzaraki 1995) that 4U 1626−67 and PSR B1831−00 should not be at the locations shown here because they have been formed by accretion-induced collapse of a white dwarf. This, however, does not solve their problematic location and creates other problems (Wijers 1997; Verbunt et al. 1990). Consequently, the conclusion that no mass-induced decay model fits the data has to be faced: there must be other quantities than accreted mass that play at least as important a role in determining pulsar field decay.

References

Hartman, J.W. et al. 1997, A&A, 322, 477
Shibazaki, N. et al. 1989, Nature, 342, 656
Taam, R.E. & van den Heuvel, E.P.J. 1986, ApJ, 305, 235
van den Heuvel, E.P.J. 1994, A&A 291, L39
van den Heuvel, E.P.J. & Bitzaraki, O. 1995, A&A, 297, L41
Verbunt, F., Wijers, R.A.M.J. & Burm, H.M.F. 1990, A&A 234, 195
Wijers, R.A.M.J. 1997, MNRAS, 287, 607

Authors' Address

Institute of Astronomy, University of Cambridge, Madingley Road, Cambridge CB3 0HA, United Kingdom

Part VIII:

Pulsar Velocities and Merger Rates

M. Bailes

The Merger Rate of Neutron Star Binaries in the Galaxy

Abstract

The major uncertainties in the merger rates of neutron star binaries are discussed, as well as a method of placing an upper limit on the binary neutron star population using simple ratios. We find that the merger rate is most unlikely to be greater than 10^{-5} yr^{-1} in our Galaxy, but is almost certainly greater than 10^{-7} yr^{-1}. The prospects for hardening the merger rate in the near future are relatively bleak, with recent deep surveys failing to discover any systems capable of merging within a Hubble time. Other possible mergers involving black holes are briefly discussed.

I Introduction

Observations of the 8-hour binary pulsar PSR B1913+16 have given strong experimental support for Einstein's General Theory of Relativity. In this fascinating system, the orbital period has been shown to decrease at the rate predicted by Einstein's theory if the neutron star binary is emitting gravitational waves (Weisberg & Taylor 1984, Taylor & Weisberg 1989). Thus, although we have not "seen" gravitational waves, we have good evidence that they exist. There is another exciting implication of the decay of PSR B1913+16's orbit. In roughly 300 million years from now the system will completely coalesce. In the last few seconds before coalescence the orbital period will only be a few milliseconds and the system will emit a large fraction of its remaining orbital energy in the form of gravitational waves. The Galactic population of relativistic neutron star binaries is therefore of great interest to physicists hoping to detect gravitational waves (Abramovici et al. 1992). The advanced LIGO detector is capable of detecting these merger events out to at least a few 100 Mpc, and so the Galactic population of neutron star binaries is of great importance.

The first reasonable attempts to estimate the merger rate of relativistic binaries (from here on the term "relativistic binary" will refer to neutron star binaries where the companion is thought to be another neutron star and will coalesce in less than a Hubble time) in our Galaxy were made by Phinney (1991) and Narayan, Piran and Shemi (1991; hereafter, P91 and NPS91 respectively). They obtained lower limits on

the merger rate of neutron stars in our Galaxy of around 10^{-6} yr^{-1}, but hinted that these estimates were extremely conservative, and that the event rate was much higher than the lower limit and probably greater than 10^{-5} yr^{-1}. Curran and Lorimer (1995; hereafter, CL95) repeated these calculations taking into account the revised pulsar distance scale and the results of more recent surveys and concluded that a lower limit on the merger rate was more like 10^{-7} yr^{-1}.

II The limitations of merger rate calculations

The same recipe for calculating the merger rate was followed by all of the authors mentioned above. For each binary pulsar known that will coalesce in a Hubble time, they computed a "scale factor" indicative of the number of similar pulsars that exist in the Galaxy but which are unobserved due to the finite sensitivity and sky coverage of pulsar surveys. These scale factors were based upon relatively straight-forward computations involving the observed physical parameters of the pulsar, the sensitivity of pulsar surveys, and the assumed distribution of the parent population of relativistic binary pulsars. This gives an estimate of the number of potentially observable binary pulsars with similar luminosities and periods to those we already know about. These estimates are considered a lower limit because it seems reasonable to assume that there exist binary pulsars which are fainter than those we know about due to some combination of beaming and/or intrinsically lower luminosity.

While the computation of the scale factors and modeling of the pulsar surveys is straightforward, some of the assumptions that need to be made are not, and there are a number of limitations that we should remain aware of.

The first of these is small-number statistics. Unfortunately, there are only three binary neutron star systems known that will coalesce in a Hubble time, and one of these, PSR B2127+11C, was discovered in a targeted search of the globular cluster M15, and is thought not to greatly influence the merger rate (P91). The major computations were thus primarily concerned with just two systems, PSR B1913+16 and PSR B1534+12. The coalescence rate for our Galaxy was dominated by the low-luminosity object PSR B1534+12 in the studies of P91 and NPS91. In fact its merger rate was roughly 10 times that of the PSR B1913+16 system. The minimum merger rate computed by CL95 is much lower, primarily because of the reduced importance of PSR B1534+12 in the merger rate calculations for reasons we discuss below. We should note however, that even if the three binary pulsars we know of were the only ones in the entire Galaxy, the merger rate would still be of order 10^{-8} yr^{-1}. This could be viewed as an extremely conservative lower limit.

The second major uncertainty involves the luminosities of the objects in question. The scale factors are crucially dependent upon d the assumed distance to the source, with the number of implied sources in the Galaxy scaling as d^{-3} for very low-luminosity objects, and d^{-2} for higher luminosity objects. Since the initial scale

factor calculations were made the pulsar distance scale has been extensively revised (Taylor and Cordes 1993), moving PSR B1534+12 from its initial estimate of 400 pc to 680 pc from the Sun. This has had the effect of decreasing its scale factor by a factor of a few. PSR B1913+16 has also had its distance increased from 5.2 to 7.1 kpc, again lowering the implied number of similar systems in the Galaxy. Unfortunately the distances to individual objects cannot be trusted to better than a factor of ~ 2.

The third major uncertainty is the underlying distribution of relativistic binaries in the Galaxy, with the total population scaling in rough proportion to the assumed scale height (see NPS91). The scale height depends upon the assumed velocities of the parent population, which can be estimated from the effects of mass loss and kick velocities on the pre-supernova system (Cordes & Wasserman 1984). Given that we only know of two relativistic binaries thought to be formed from massive binaries, we cannot realistically constrain their scale height. This leads to a factor of at least two uncertainty in the merger rate.

The final and perhaps most severe limitation is the question of how many relativistic binary pulsars are fainter than those we observe—and thus unseen but still potential mergers. One can imagine that we only ever see the brighter members of the pulsar population and therefore the Galaxy contains a huge population of incredibly low-luminosity binary pulsars. Whilst this is a tantalizing prospect, until we find one it remains conjecture. One can also postulate the existence of all kinds of other potentially observable (with gravitational wave detectors) systems, such as black hole-black hole binaries, or black hole-neutron star binaries, or neutron star binaries so relativistic at birth that their merger time is significantly shorter than a typical pulsar's lifetime. These will all increase the event rate for gravitational wave detectors but by how much is difficult to gauge.

Rather than repeat in detail the calculations of scale factors by previous authors, or speculate about potential populations of ultra-low luminosity neutron stars, I will restrict the immediate discussion to a lower limit on the merger rate. Curran and Lorimer claimed a lower limit to the merger rate one tenth of that of the previous authors. There were two major reasons for this. The first was the adoption of the new pulsar distance model. The distance to PSR B1534+12 has changed, leading to a factor of few *decrease* in the merger rate. This seems entirely reasonable. Whilst the 1993 Taylor and Cordes distance model is probably not the final word in pulsar distance models, there were good reasons for its adoption, especially for nearby pulsars such as PSR B1534+12, the distances of which were systematically underestimated.

The second major cause for Curran and Lorimer's lower merger rate was the increased volume of the Galaxy that had been searched for relativistic binaries without success. They claimed that this leads to a lowering of the scale factor by a further factor of six for PSR B1534+12. Perhaps a quick way to assess the increase in Galactic volume surveyed for these pulsars is to look at the increase in the number of millisecond pulsars known between the time of the computations. When PSR B1534+12 was

discovered, there were only 6 other millisecond pulsars known in the disk. At the time of CL95's calculations the number was closer to 25, which implies a factor of 4 increase in the volume of sky effectively surveyed, near the factor 6 that they claimed. However, since then, the number of millisecond pulsars known has steadily increased to $\sim$ 35–40 (depending upon your definition of "millisecond pulsar") with still no new detections of relativistic binaries. We therefore conclude that a factor of ten decrease in the lower limit for mergers is reasonable, and that this lower limit is indeed near $10^{-7}\mathrm{yr}^{-1}$.

A different approach relies on the simple fact that at least one of the neutron stars in a "disk" relativistic binary must be just a normal pulsar, and we know of about 700 "normal" pulsars in the disk of the Galaxy but no "normal" pulsars in relativistic binaries (Bailes 1996). The first-born neutron star in a relativistic binary has the opportunity to be spun-up to a period of a few tens of milliseconds, and its magnetic field reduced, probably by mass accretion (Bhattacharya & van den Heuvel 1991). In both of the neutron star binaries in the disk, we see the first-born or recycled neutron star. A limit to the binary neutron star birthrate can therefore be obtained by comparing the relative birthrate of normal (unrecycled) pulsars in neutron star binaries to that of normal single pulsars. The only assumption here is that the second-born pulsars in relativistic binaries possess similar luminosities to normal pulsars in the disk. Since there are no normal pulsars observed in "relativistic" neutron star binaries (this excludes PSR B2303+46 since it is irrelevant in merger rate calculations) we conclude that their birthrate is at most 1/700th that of the general pulsar population. Taking Lorimer et al. 's (1993) estimate of the pulsar birthrate of 1 per $\sim$ 150 years, we find a maximum birthrate of $\sim 10^{-5}$ for relativistic binaries (we note in passing that most of the other recent computations of the single pulsar birthrate would yield similar values if the new distance model is adopted). The advantage of this limit over the scale-factor estimates is that it is based on the properties of 700 objects, not two.

NPS91 discussed the relative populations of neutron star binaries to single pulsars, but concluded that the observable binary neutron star population should be of order a few percent of the single pulsar population. This is clearly not the case, 3% would imply an observed population of relativistic neutron stars of about 20, where we see none. The upper limit discussed above is the most assumption-free method of limiting the merger rate, and similar to the "conservative" merger rates of most authors. It is ten times the best estimate of Lipunov et al. (1995) which was based on binary evolution codes! Whilst the use of these so-called "scenario machines" can be an interesting way of gaining insights into the relative importance of different phases of binary evolution, I feel they have no value in computing accurate merger rates. There are simply too many highly uncertain assumptions required. To obtain some idea of the uncertainties involved, an independent analysis by Portegies Zwart and Spreeuw (1997) obtained a merger rate of $\sim 10^{-5}$ yr^{-1}, one tenth that of Lipunov et al.

The same argument used to restrict the birthrate of relativistic binaries with neutron star companions can be used to limit the birthrate of neutron star-black hole binaries. None of the 700 pulsars we know of are orbiting a black hole. We therefore conclude the formation rate of black hole-pulsar binaries is less than 10^{-5} yr^{-1}. Through simulations, it is probably possible to gain an order of magnitude estimate of the relative formation rates of black hole-black hole binaries to black hole-neutron star binaries. This is probably the most effective method of limiting the merger rate of all classes of mergers that would give rise to detectable gravitational wave emission.

III Conclusions

The merger rate of neutron star binaries in our Galaxy is probably between 10^{-7} and 10^{-5} yr^{-1}. Without the discovery of large numbers of relativistic binaries in the near future, it is unlikely that this number will firm significantly. Perhaps the best estimate of the merger rate will ultimately come from gravitational wave detectors.

Acknowledgements

I would like to thank the ARC for financial support and Annie Hughes for the scale factors used in the oral presentation.

References

Abramovici, A., et al. 1992, Science, 256, 325
Bailes, M. 1996, in Compact Stars in Binaries, IAU Symp. 165, ed. J. van Paradijs, E.P.J. van den Heuvel & E. Kuulkers (Dordrecht: Kluwer), 213
Bhattacharya, D. & van den Heuvel, E.P.J. 1991, Phys. Rep., 203, 1
Cordes, J.M. & Wasserman, I. 1984, ApJ, 279, 798
Curran, S.J. & Lorimer, D.R. 1995, MNRAS, 276, 347 (CL95)
Lipunov, V.M. et al. 1995, A&A, 298, 677
Lorimer, D.R. et al. 1993, MNRAS, 263, 403
Narayan, R., Piran, T. & Shemi, A. 1991, ApJ, 397, L17 (NPS91)
Phinney, E.S. 1991, ApJ, 380, L17 (P91)
Portegies Zwart, S.F. & Spreeuw, H.N. 1997, A&A, 312, 670
Taylor, J.H. & Cordes, J.M. 1993, ApJ, 411, 674
Taylor, J.H. & Weisberg, J.M. 1989, ApJ, 345, 434
Weisberg, J.M. & Taylor, J.H. 1984, Phys. Rev. Letters, 52, 1348

Authors' Address

Physics Department, The University of Melbourne, Parkville, Vic, 3052, Australia

Australia Telescope National Facility, P.O. Box 76, Epping, NSW 2121, Australia

N. Itoh and T. Kotouda

Velocity-Magnetic Field Correlation of Pulsars

Abstract

Monte Carlo simulations of the evolution of pulsars are carried out in order to compare with the recent measurement of the pulsar transverse velocity by Lyne & Lorimer (1994). The new electron density distribution model of Taylor & Cordes (1993) is adopted in the simulation. Accurate pulsar orbits in the Galactic gravitational field are calculated. It is found that the constant magnetic field model of pulsars can account for the new measurement of the pulsar transverse velocity, and the apparent correlation between the strength of the magnetic field and the transverse velocity of the pulsars. The present finding confirms the validity of the constant magnetic field model of pulsars, and consolidates the idea that the apparent correlation between the strength of the magnetic field and the transverse velocity of the pulsars is caused by observational selection effects.

I Introduction

We have recently shown, through the method of Monte Carlo simulations of the evolution of pulsars, that the constant magnetic field model of pulsars can account for the apparent correlation between the strength of the magnetic field and the transverse velocity of the pulsars (Itoh & Hiraki 1994). Their Monte Carlo simulation method is an extension of the one of Wakatsuki et al. (1992). Bhattacharya et al. (1992) also carried out Monte Carlo simulations of the evolution of pulsars and showed that the decay timescale of the pulsar magnetic field is longer than 10^8 yr.

As discussed by Itoh & Hiraki (1994), the problem of the observed correlation between the strength of the magnetic field and the transverse velocity of the pulsars is a long-standing problem discussed by many authors (Harrison & Tademaru 1975; Helfand & Tademaru 1977; Lyne, Anderson, & Salter 1982; Anderson & Lyne 1983; Radhakrishnan 1984; Cordes 1986; Stollman & van den Heuvel 1986; Bailes 1989; Narayan & Ostriker 1990).

Itoh & Hiraki (1994) used the observational data compiled by Harrison, Lyne, & Anderson (1993). Their work was a major addition to the previous radio interferometry

measurements of the proper motions of pulsars carried out by Anderson, Lyne & Peckham (1975), Lyne et al. (1982), Backer & Sramek (1982), Gwinn et al. (1986), Bailes et al. (1990), and Fomalont et al. (1992). Itoh & Hiraki (1994) succeeded in accounting for the observed correlation between the strength of the magnetic field and the transverse velocity of the pulsars. The reason for the apparent correlation has been due to the fact that old high-velocity pulsars escape observation because they are generally located far from the Galactic plane; thus, observed high-velocity pulsars tend to be young ones. On the other hand, there exists an apparent negative correlation between the characteristic age and the strength of the magnetic field, which is mainly due to the fact that the range of the observed pulsar periods is narrower than that of the observed pulsar period derivatives. Owing to these two apparent correlations, high-velocity pulsars appear to have strong magnetic fields.

Recently, Lyne & Lorimer (1994) reassessed the velocities of radio pulsars using the Galactic electron density distribution model of Taylor & Cordes (1993). They obtained significantly higher values for the pulsar velocity than reported by Harrison et al. (1993) on which Itoh & Hiraki's (1994) analysis has been based.

It is the purpose of the present paper to carry out new Monte Carlo simulations of the evolution of pulsars using Taylor & Cordes's (1993) electron density distribution model. We also calculate the pulsar orbits in the Galactic gravitational field accurately. We shall compare the Monte Carlo simulation results with the pulsar velocity data compiled by Lyne & Lorimer (1994).

II Observational data

In Figure 1, we show the observational data of the velocity-magnetic field correlation of pulsars. The data have been published in Lyne & Lorimer (1994) in a graphical form. The data have been provided to us by D.R. Lorimer in tabular form. The original data consist of 99 pulsars. We have excluded one millisecond pulsar and two binary pulsars, because these pulsars are considered to have experienced mass accretion from the companion star which might have significantly affected the magnetic field of the pulsars. Therefore, the remaining 96 pulsars have been taken into our analysis. Of these 96 pulsars, eight pulsars have only upper limits to their transverse velocities. Following Lyne & Lorimer (1994), we have assumed that these eight pulsars have half the values of the upper limits as the values of the transverse velocities.

The observed data of the 96 pulsars give the Spearman rank order correlation coefficient between the transverse velocity V_t and the strength of the magnetic field B

$$r_s = 0.171. \tag{1}$$

The strength of the magnetic field B is defined by

$$B = 3.2 \times 10^{19} (P\dot{P})^{1/2}\,\mathrm{G}, \tag{2}$$

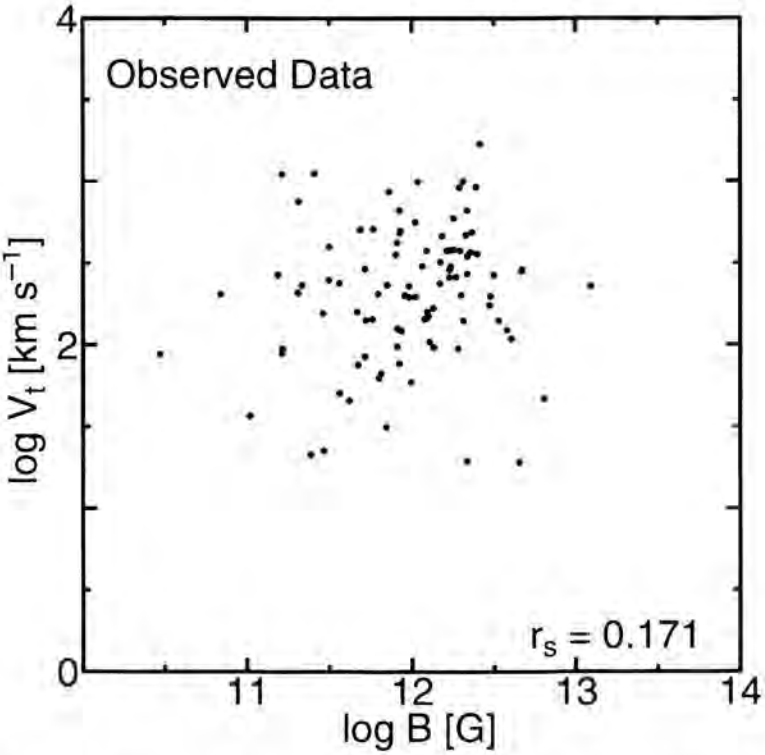

Figure 1. Observed data of 96 pulsars for the transverse velocity and the strength of the magnetic field. The data are based on the tabular version of the paper of Lyne & Lorimer (1994).

corresponding to the pulsar radius $R = 1.0 \times 10^6$ cm and the pulsar moment of inertia $I = 1.0 \times 10^{45}$ g cm^2. In Eq. (2), the period P is measured in seconds, and the period derivative $\dot{P}$ is measured in seconds per second. This correlation is significant at the 91% level.

In Figure 2, we show the correlation diagram for the transverse velocity V_t and the characteristic age $P/2\dot{P}$. This diagram is essentially the same as Fig. 1 of Lyne & Lorimer (1994), except that we have excluded one millisecond pulsar and two binary pulsars. In Figure 3, we show the correlation diagram for the strength of the magnetic field B and the characteristic age $P/2\dot{P}$.

III Simulation results

The procedure of the Monte Carlo simulation is described in Itoh et al. (1995). As is done by Wakatsuki et al. (1992) and Itoh & Hiraki (1994), we optimize the adjustable

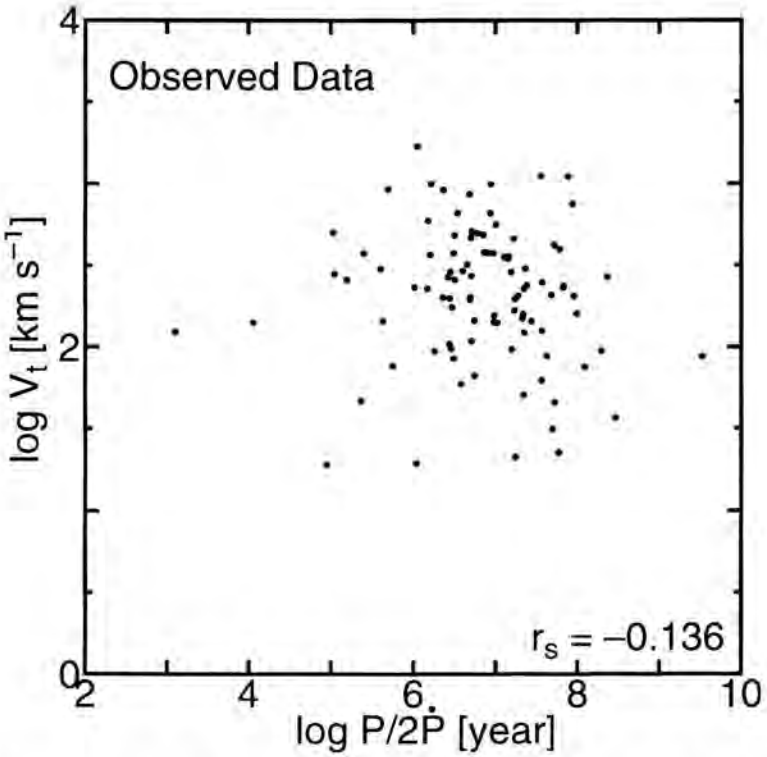

Figure 2. Observed data of 96 pulsars for the transverse velocity and the characteristic age.

parameters so that the simulation results produce the best fit for the distributions of P, $\dot{P}$, L_r, and V_t. The age of the pulsar is chosen randomly as $t \in (0, 5 \times 10^8$ yr). In each simulation, we generate pulsars until we have detected 2000 pulsars. This is about 12 times the number of the observed pulsars with which we compare our simulation results. We adopt this method in order to minimize the Monte Carlo noise which is caused by the choice of different series of random numbers. We have confirmed by our Monte Carlo simulation that this number (2000 observed pulsars by simulation) is sufficiently large to stabilize the simulation results. This method was first adopted by Bhattacharya et al. (1992). Thus, the birthrate of the pulsars in the Galaxy r_b is defined as

$$r_b = \frac{164N/2000}{5 \times 10^8 \text{ yr}} \tag{3}$$

where N is the number of the generated pulsars.

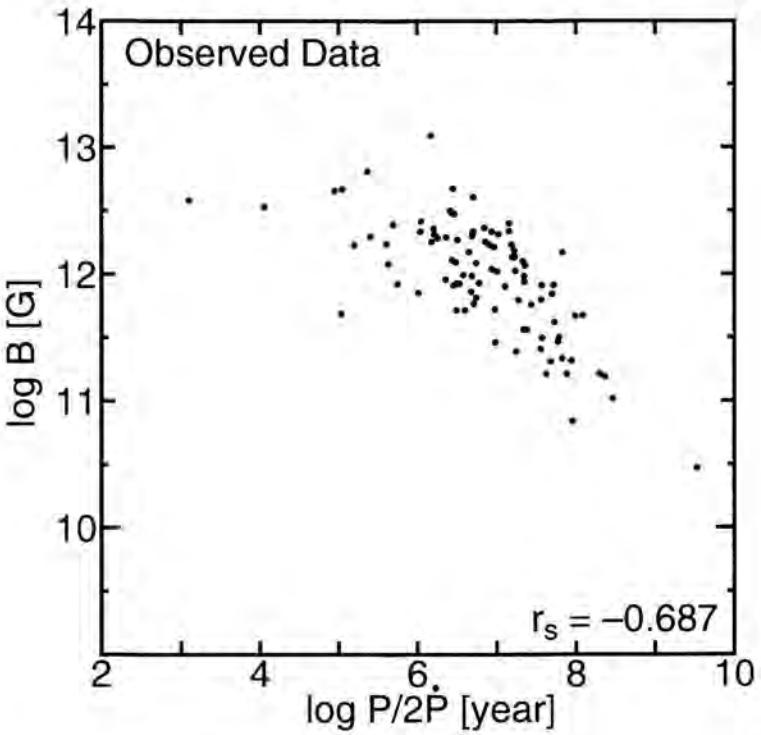

Figure 3. Observed data of 96 pulsars for the strength of the magnetic field and the characteristic age.

In the following, we show an example of the simulation. First, we search for the best set of parameters that reproduce the observed distributions of periods, period derivatives, and radio luminosities as closely as possible. We adopt the following parameters: $\bar{P}_0 = 0.1$ s, $\sigma_u = 0.18$, $\bar{Q}_0 = 10^{-6.84}$ s$^{1/2}$, $\sigma_w = 0.45$, $\alpha_i = -2.28$, $\beta_i = 2.28/3$, $\gamma_i = 11.64$, $\sigma_\lambda = 0.8$, $\bar{s} = 2.60$, $\sigma_s = 0.45$, $r_b = 7.92 \times 10^{-3}$ yr^{-1}. The value of $\bar{Q}_0$ corresponds to $B = 3.3 \times 10^{12}$ G.

Next, we choose the pulsars which are located within 3 kpc from the Earth, and have the radio flux density at 408 MHz higher than 10 mJy, out of the simulated 2000 pulsars as the pulsars whose proper motion we wish to compare with the observation. In order to simulate the detectability of the proper motion of the pulsars, we employ the following method. If the proper motion of the simulated pulsar is greater than 7 mas-yr^{-1}, we take its velocity as the observed velocity. If the proper motion is smaller than 7 mas-yr^{-1}, we take 7 mas-yr^{-1} as the upper limit of the proper motion and deduce the corresponding upper limit for the velocity. Then we take half of these upper limit values as the velocities of the simulated pulsars. This procedure simulates the real proper-motion measurement (Harrison et al. 1993), 7 mas-yr^{-1} being the typical error.

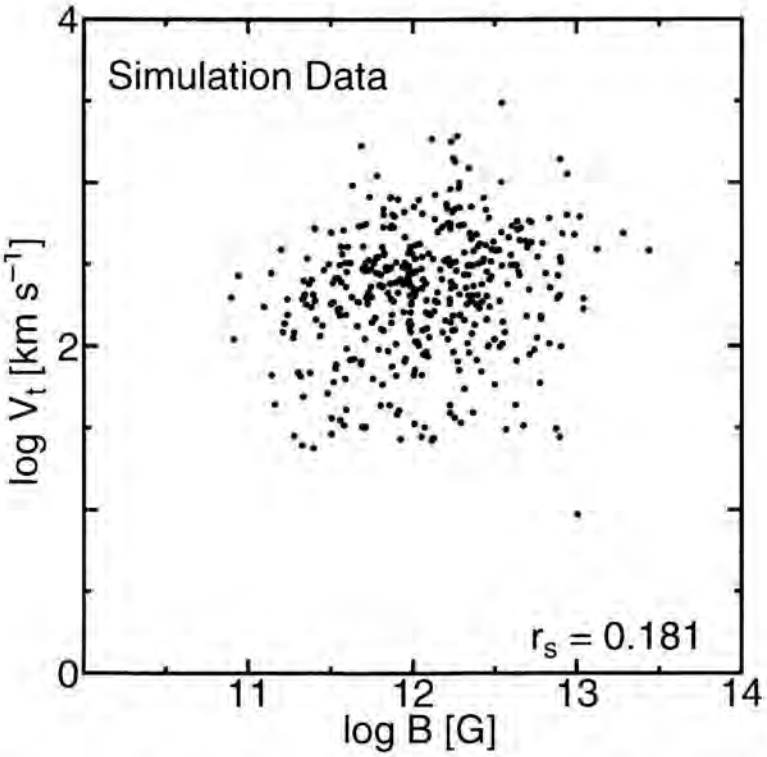

Figure 4. Correlation diagram of the strength of the magnetic fields and the transverse velocity of the simulated pulsars.

In Figure 4, we show the correlation diagram of these 411 pulsars. The Spearman rank order correlation coefficient between the transverse velocity and the strength of the magnetic field is $r_s = 0.181$. This result is in essential accord with the observational data presented in Section 2. Therefore, we reach the conclusion that the observed correlation between the transverse velocity and the strength of the magnetic field can be accounted for by the ordinary pulsar model of constant magnetic field.

The apparent correlation is caused by the selection effects. Old high-velocity pulsars escape observation because they are generally located far from the Galactic plane; thus, observed high-velocity pulsars tend to be young ones. On the other hand, there exists an apparent negative correlation between the strength of the magnetic field and the characteristic age, which is mainly due to the fact that the range of the observed pulsar periods is very much narrower than that of the observed pulsar period derivatives. In Figure 5, we show the apparent negative correlation between the transverse velocity and the characteristic age for the simulated pulsars. In Figure 6, we show the apparent negative correlation between the strength of the magnetic field and the characteristic age for the simulated pulsars. The observational data for the 96 pulsars of these

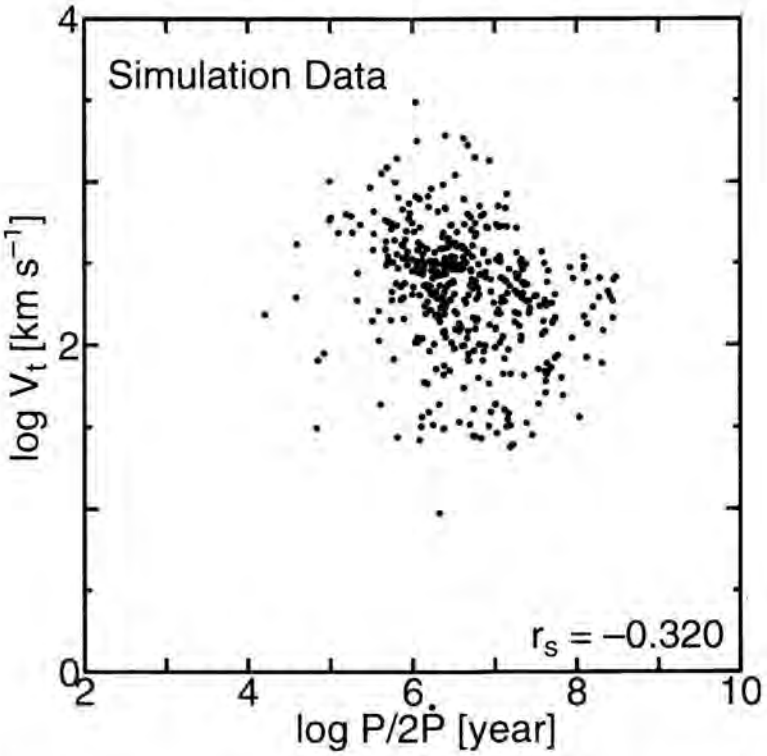

Figure 5. Characteristic age and transverse velocity of the simulated pulsars.

correlations are shown in Figs. 2 and 3. Owing to these two apparent correlations, high-velocity pulsars appear to have strong magnetic fields.

Stollman & van den Heuvel (1986) were the first to attempt to examine whether the velocity-magnetic field strength correlation of pulsars may arise due to selection effects. They concluded that the observed correlation at that time cannot be explained by selection effects. Their Monte Carlo simulation method differs from the present one in various ways, such as a different temporal behavior of the magnetic field strength, a different functional dependence of the pulsar radio luminosity on the period and period derivative, and a different treatment of the pulsar proper motion. However, the most important difference appears to be the observational data of the pulsar transverse velocity. Stollman & van den Heuvel (1986) used the data of Anderson & Lyne (1983) which included 26 pulsars. The correlation coefficient between the transverse velocity and the magnetic field strength of those 26 pulsars is 0.63. This high correlation coefficient no longer exists in the most recent data of Lyne & Lorimer (1994) with which we have compared our Monte Carlo simulation results.

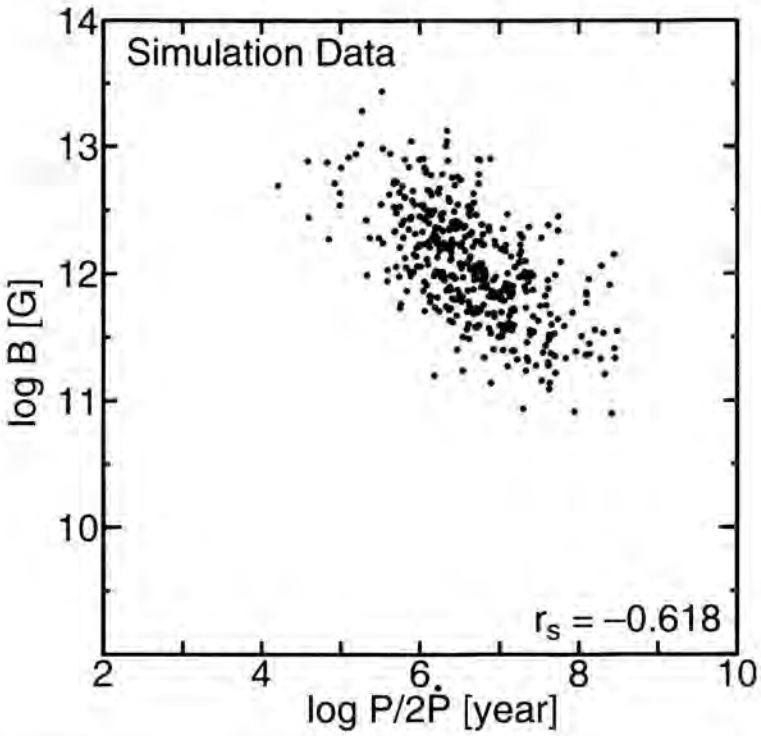

Figure 6. Characteristic age and strength of the magnetic field of the simulated pulsars.

Stollman & van den Heuvel (1986) have, however, pointed out that the correlation coefficient of order 0.2 can be reproduced by their Monte Carlo simulations.

IV Concluding remarks

We have carried out Monte Carlo simulations of the evolution of pulsars based on the constant magnetic field model in order to investigate the apparent correlation between the strength of the magnetic field and the transverse velocity of the pulsars. There exist three important improvements made upon our previous work (Itoh & Hiraki 1994). First, we have used the observational data of the pulsar transverse velocities of Lyne & Lorimer (1994), which are significantly more accurate than the previous data of Harrison et al. (1993), which have been used by Itoh & Hiraki (1994). Second, we have used the Galactic electron density distribution model of Taylor & Cordes (1993), which is remarkably more detailed than the electron density distribution model of Manchester used by Itoh & Hiraki (1994). Third, we have calculated the pulsar orbits in the Galactic gravitational field accurately using the potential of Hartmann et al. (1990).

In this paper, we have confirmed the conclusion reached by Itoh & Hiraki (1994) that the apparent correlation between the strength of the magnetic field and the transverse velocity of the pulsars is caused by observational selection effects. Old high-velocity pulsars are biased against the observation because they are generally located far from the Galactic plane. The lack of the sample of the old high-velocity pulsars causes the apparent correlation in the observed data of the strength of the magnetic field and the transverse velocity of the pulsars, because old pulsars appear to have weak magnetic fields.

References

Anderson, B. & Lyne, A.G. 1983, Nature, 303, 597
Anderson, B., Lyne, A.G. & Peckham, R.J. 1975, Nature, 258, 215
Backer, D.C. & Sramek, R.A. 1982, ApJ, 260, 512
Bailes, M. 1989, ApJ, 342, 917
Bailes, M. et al. 1990, MNRAS, 247, 322
Bhattacharya, D. et al. 1992, A&A, 254. 198
Cordes, J.M. 1986, ApJ, 311, 183
Fomalont, E.B. et al. 1992, MNRAS, 258, 497
Gwinn, C.R. et al. 1986, AJ, 91, 338
Harrison, P.A., Lyne, A.G. & Anderson, B. 1993, MNRAS, 261, 113
Harrison, E.R. & Tademaru, E. 1975, ApJ, 201, 447
Hartmann, D., Epstein, R.I. & Woosley, S.E. 1990, ApJ, 348, 625
Helfand, D.J. & Tademaru, E. 1977, ApJ, 216, 842
Itoh, N. & Hiraki, K. 1994, ApJ, 435, 784
Itoh, N., Kotouda, T. & Hiraki, K. 1995, ApJ, 455, 244
Lorimer, D.R. 1994, Ph.D. Thesis, Univ. of Manchester
Lyne, A.G., Anderson, B. & Salter, M.J. 1982, MNRAS, 201, 503
Lyne, A.G. & Lorimer, D.R. 1994, Nature, 369, 127
Narayan, R. & Ostriker, J. P. 1990, ApJ, 352, 222
Radhakrishnan, V. 1984, in Millisecond Pulsars, ed. S.P. Reynolds & D.R. Stinebring (Green Bank: NRAO), 130
Stollman, G.M. & van den Heuvel, E.P.J. 1986, A&A, 162, 87
Taylor, J.H. & Cordes, J.M. 1993, ApJ, 411, 674
Wakatsuki, S. et al. 1992, ApJ, 392, 628

Authors' Address

Department of Physics, Sophia University, 7-1 Kioi-cho, Chiyoda-ku, Tokyo, 102, Japan

T.M. Tauris

Pulsar Velocities

I Introduction

Observations of proper motions of single radio pulsars enable the determination of transverse velocities and hence provide a tool for measuring the amount of asymmetry (i.e., the magnitude of the kick velocity $\vec{\mathbf{w}}$) in supernovae (SNe). However, single pulsars are thought to originate from both isolated early type stars which explode in a type II SN and from the collapse of He-stars in a SN of type Ib/c in massive binaries which are disrupted as a result of the explosion. Other, more exotic, formation mechanisms of isolated neutron stars (NS) include the possibility of accretion-induced collapse (AIC) of a white dwarf (WD) and a merging event of two white dwarfs in a very tight binary system (possibly resulting in a type Ia SN). It is therefore complicated to get a direct measure of the magnitude of kick velocities imparted to neutron stars at birth.

II Discussion

The possible evolutionary paths which lead to the formation of single pulsars are illustrated in the flow chart in Figure 1. The space velocity distribution (e.g., Lyne & Lorimer 1994) is not an actual measurement of the kick velocity distribution since it is "polluted" by escape velocities $\vec{\mathbf{v}}_{\rm esc}$ of disrupted binaries as well as systemic velocities $\vec{\mathbf{v}}_{\rm sys}$ imparted to binary systems as a result of the recoil effect due to a sudden mass loss. Furthermore, the magnitude of the kick velocity is possibly related to the type of SN (II, Ib/c or AIC) which creates a given NS.

In order to evaluate the expected velocity distribution of single pulsars which have their origin in a binary system, the aim is to use the evolutionary code of Tauris & Bailes (1996) to keep track of the binary parameters. This will enable us to use realistic input distributions of masses and separations prior to the SNe. The calculations of the runaway velocities of stellar components originating from disrupted binaries due to asymmetric SNe, can be performed using the analytic formulae of Tauris & Takens (1998).

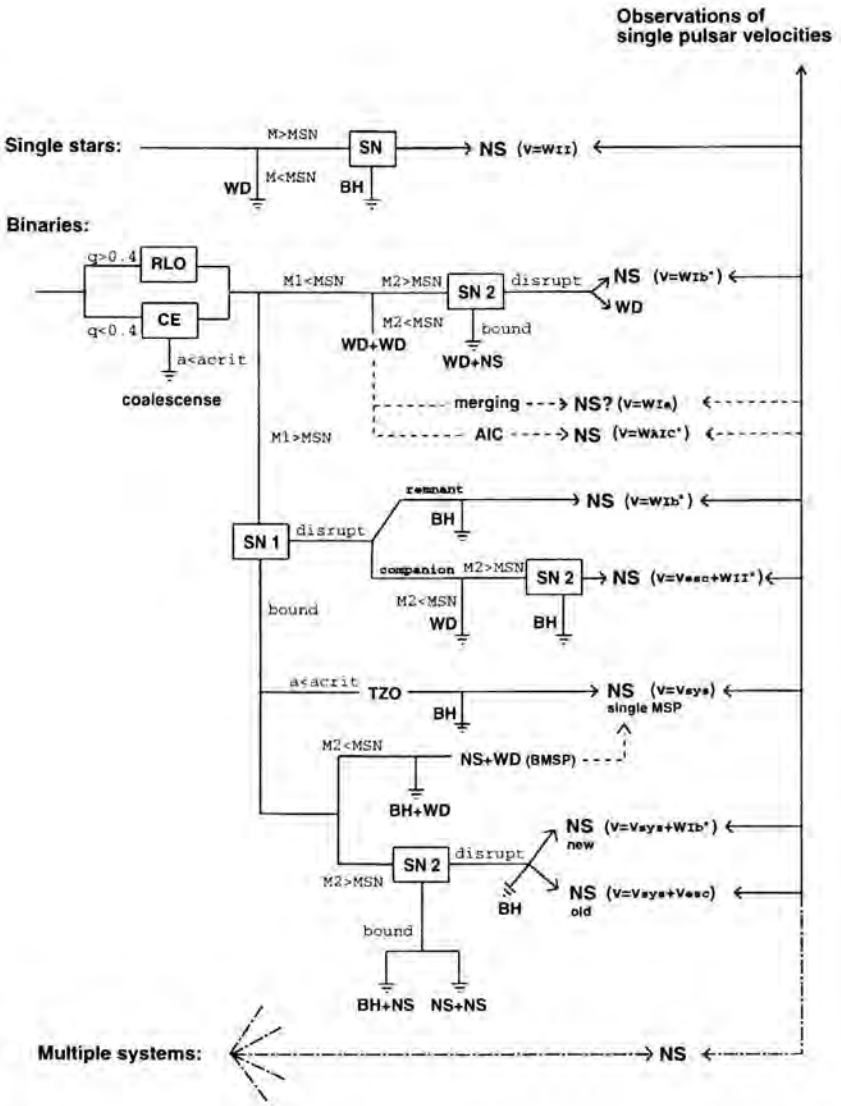

Figure 1. Possible formations of single pulsars. "NS"=neutron star; "WD"=white dwarf; "BH"=black hole; "SN"=supernova; "RLO"=Roche-lobe overflow; "CE"=common envelope; "TZO"=Thorne-Żytkow object; "M_1"=mass of primary star; "M_2"=mass of secondary star; "$M_{\rm SN}$"=threshold mass for SN; "q"=M_2/M_1; "a"=binary separation; "v"=velocity of single NS; "w"=kick velocity (index refer to type of SN, * indicates the effective velocity taken into account the energy loss due to escape); "$v_{\rm sys}$"=systemic velocity of binary due to a sudden mass loss; "$v_{\rm esc}$"=velocity of NS escaping a binary.

From the observed transverse velocity distribution of Lyne & Lorimer (1994) we have obtained a 3-D space velocity distribution assuming isotropy in velocity space:

$$P(v_{3d}) = \frac{(v_{3d}/200\ \mathrm{km\,s^{-1}})^{1.3}}{1 + (v_{3d}/200\ \mathrm{km\,s^{-1}})^{3.2}} \quad (1)$$

We have calculated the expected velocities of single (and binary) millisecond pulsars using this velocity distribution as the input kick distribution of type Ib/c SNe. The result of this analysis should match that of the observed velocities of millisecond pulsars *if* the Lyne-Lorimer distribution is a good representative of the kick velocities associated with type Ib/c SNe. Early indications are that Eq. (1) slightly overestimates the pulsar velocities. However, beware of selection effects at work here against observations of high velocity pulsars.

We plan to calculate velocity distributions for all the formations routes which lead to single NS.

Acknowledgement

I thank Roelf Takens for many helpful discussions.

References

Lyne A.G. & Lorimer, D.R. 1994, Nature, 369, 127
Tauris T.M. & Bailes, M. 1996, A&A, 315, 453
Tauris T.M. & Takens, R. 1998, A&A, 330, 1047

Authors' Address

Institute of Physics & Astronomy, Aarhus University, DK-8000 Aarhus C., Denmark

Part IX:

Observations Giant Pulses

S. Sallmen, D.C. Backer, T. Hankins, D. Moffett, and S. Lundgren

Simultaneous Dual Frequency Observations of Giant Pulses

Abstract

Simultaneous data of Giant Pulses in the Crab Pulsar were taken at two widely spaced frequencies, using the detection of a giant pulse at 1.4 GHz at the VLA to trigger the observation of that same pulse period at 0.610 GHz at Green Bank. About 70% of these pulses are seen at both 1.4 and 0.6 GHz, implying they have a bandwidth of *at least* 0.8 GHz at 1 GHz. At both frequencies, the pulses are characterized by a fast rise and an exponential decay, consistent with scattering in the nebular filament zone only at 0.610 GHz.

I Introduction

The Crab pulsar was first discovered by detection of its extremely strong giant pulses. These giant pulses occur only in the main pulse and interpulse, and never in the radio precursor. They are seen at all radio frequencies. Giant pulses contribute $\sim$ 5–7% of the pulse energy at 0.430 GHz. Essentially all the energy at 1.4 GHz comes from $< 1\%$ of the pulses.

II Experiment

The data shown here were all taken on 1996 May 21. The 1.4 GHz data were taken at the VLA, while the 0.610 GHz data were taken using the 85-3 telescope at Green Bank, West Virginia. The VLA resolves out the emission of the Crab Nebula, hence the exquisite signal to noise.

Using the phased array mode of the VLA, observers there were able to detect giant pulses in real time at 1.4 GHz and generate a trigger, the UTC time of which was sent over the internet, with a socket link between programs. A program written by Lundgren received the trigger, calculated the transit time of the trigger, and compared that to the difference in arrival time between 1.435 GHz and 0.618 GHz (the top of our 0.610 GHz band) due to interstellar dispersion. In this case, this time is $\delta t = 0.503$ s. In addition

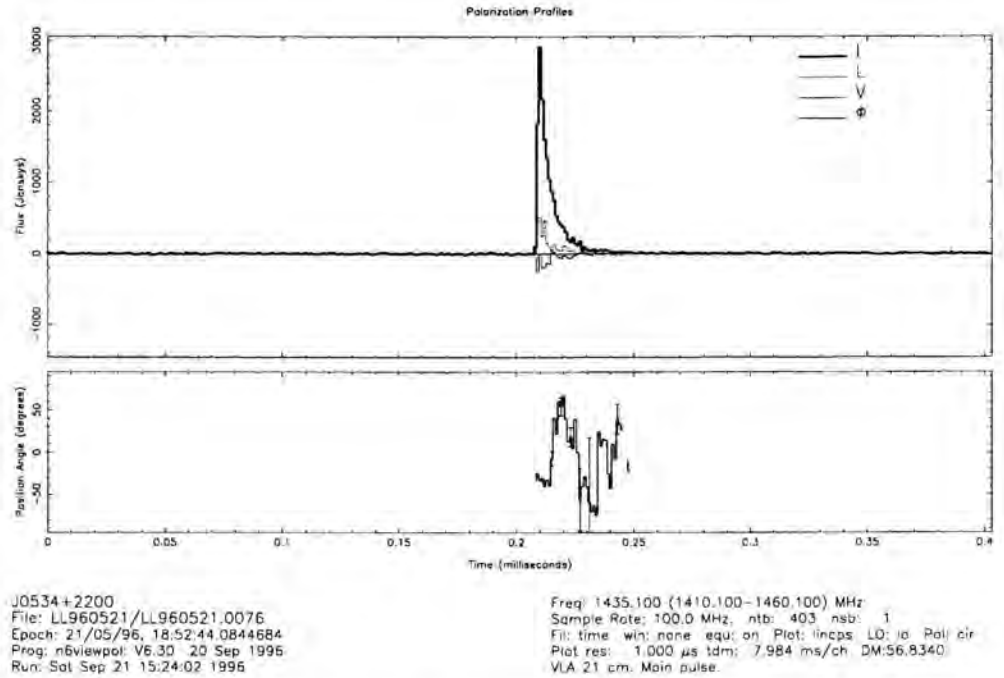

Figure 1. Displays the data for a single giant pulse at 1.4 GHz. The top panel displays the total intensity I, along with linear and circular polarizations L and V. The vertical scale indicates that this pulse reached a peak flux of 3000 Janskys. The lower panel indicates the position angle of the linear polarization across the pulse.

to this delay, we included other factors such as the difference in arrival due to the separation between observing sites on the earth, and the latency in the GBPP (Green Bank Berkeley Pulsar Processor) hardware, which were of similar orders. If the trigger arrived in time for us to detect the pulse at 0.610 GHz, we signalled the GBPP to take data. Due to the slow rate of data dumped from the GBPP, it could only accept such a command approximately every 12 seconds. Some triggers were therefore missed.

III Discussion

A total of 77 triggers sent by the VLA observers reached Green Bank within the required time, and were accepted by the GBPP. For a variety of reasons, including a drifting clock used to identify the time at which the trigger was sent, we are currently only certain that we observed the correct period with the GBPP for 42 pulses. Of these, 29 were definitely detected at 0.610 GHz as well as at 1.4 GHz. Thus about 70% of the pulses must have a bandwidth of *at least* 0.8 GHz at 1 GHz. The emission is clearly

wide band for these cases, as expected for models wherein the fundamental radiating unit has a scale of about a meter and emits a pulse of nanosecond width. The remaining pulses may be too weak to be seen with the 85′ telescope at Green Bank or they simply may not be present at this second frequency.

At 0.610 GHz, these pulses have profiles displaying a fast rise, and exponential decay. The decay time scale is about 90 μs and is consistent with that expected due to scattering in the nebular filament zone at the time of the observation. The fast rise indicates that the intrinsic time scale of the pulse is unresolved, $\lesssim 10$ μs. At 1.4 GHz, the pulse shown (Figure 1) has a fast rise, $\lesssim 3$ μs, and an exponential decay time scale of approximately 5 μs. Assuming $\tau_{\rm ISS} \sim \nu^{-4}$, we would expect 3 μs based on the 0.610 GHz measurement. Additionally, the position angle of the linear polarization does not remain constant during the decay at 1.4 GHz, so it is likely that the profile shape is not simply due to scattering by the nebular material.

The pulse displayed in Fig. 1 is also clearly polarized at 0.610 GHz, although some of the giant pulses are not polarized at the lower frequency. The relative arrival times of the detected pulses at the two frequencies are, however, highly correlated, and there is a weak amplitude correlation between the two frequencies as well.

Authors' Addresses

S. Sallmen and D.C. Backer: Department of Astronomy, Campbell Hall, University of California, Berkeley, CA, USA 54720-3411

T. Hankins and D. Moffett: Physics Dept., New Mexico Tech., Campus Station, Socorro, NM, USA 87801

S. Lundgren: Radio Astronomy Dept., NRL, Code 7210, Washington, D.C., USA 20375

T.J. Galama, J. van Paradijs, A.G. de Bruyn, L. Hanlon and K. Bennett

Unusual Increase in the 325 MHz Flux Density of PSR B0655+64

Abstract

We detected a large amplification of the flux density of PSR B0655+64 at 325 MHz (a factor of ~ 43) lasting about one hour and restricted to a very narrow bandwidth (3.6 ± 0.4 MHz). The decorrelation bandwidth and duration are in agreement with the values expected for diffractive interstellar scintillation. However, the observed amplification of the flux density of PSR B0655+64 is too large. The extreme flux density amplification of PSR B0655+64 might be explained in terms of caustics.

I Introduction

Irregular plasma refraction by the interstellar medium between the source and the observer cause scintillation of the source. The scintillation occurs on two distinct scales. Variations on time scales of minutes to hours are caused by the familiar diffractive interstellar scintillation (DISS). Variations on time scales of days to months are produced by refractive interstellar scintillation (RISS). Apart from "ordinary" scintillation strongly non-Gaussian "spikes" have been reported in long-term pulsar flux monitoring (e.g., Cole et al. 1970; Helfand et al. 1977). Goodman et al. (1987) argued that these might be due to strong focusing events or caustics. Another type of strong refractive focusing, so-called Fiedler events, have been observed in radio quasars (Fiedler et al. 1987). In the most dramatic event Fiedler et al. observed intensity increases of roughly threefold on refractive time scales.

In this paper we report on the discovery of a very large amplification of the flux density of PSR B0655+64 at 325 MHz. A more extensive treatment can be found in Galama et al. (1997).

II Observations and data reduction

The event was discovered serendipitously in data taken in a GRB follow-up project with the Westerbork Synthesis Radio Telescope. The data cover a period of three

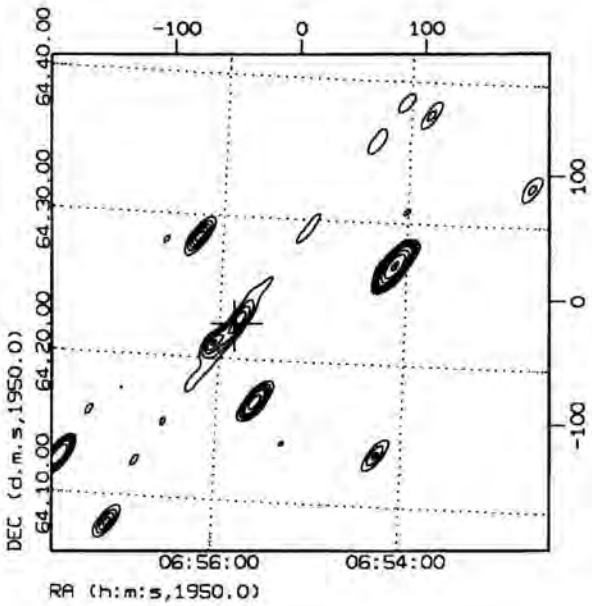

Figure 1. Contour plot of a WSRT image at 325 MHz. The position of PSR B0655+64 is indicated by the cross. The plot shows the elongated structure of PSR B0655+64 in the image of June 25. Contour levels are 15, 30, 45, 60, 75, 120, 240, 480, 960, and 1075 mJy. Map noise is 3.6 mJy (1σ).

months (April–June 1994; additional observations January 15 and 16, 1996). The WSRT is an East-West array consisting of 14 parabolic dishes, each 25 m in diameter. The data were reduced using the Netherlands East-West Synthesis Telescope Array Reduction package (NEWSTAR).[1]

III Results

In a map obtained from data of June 25, 1994, we noticed a faint straight elongated structure, repeating itself at the grating response distances (see Figure 1). The feature was detected with all interferometers. The elongated image response is that of an object that flared for only a short period of time. The feature and the binary pulsar PSR B0655+64 coincide to within $1\farcs3$ in the direction perpendicular to the elongation. Smoothed light curves of PSR B0655+64 are shown in Figure 2. The phenomenon

[1] See URL `http://www.nfra.nl:80/newstar/`.

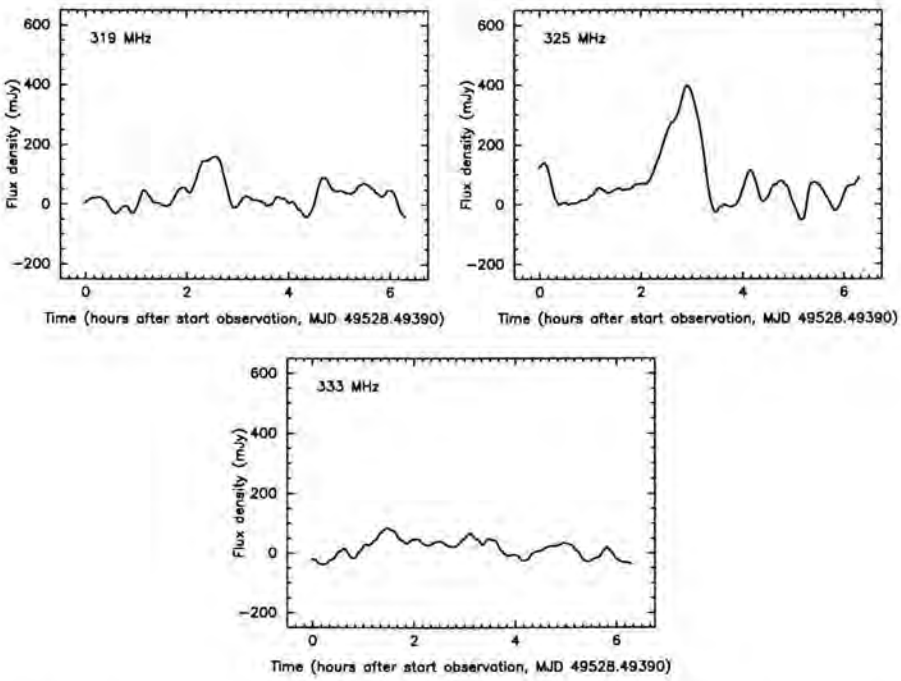

Figure 2. Light curves of the source at the position of PSR B0655+64 from the 92 cm observations of June 25, smoothed with a triangular function of 14 min. full-width at half maximum. From upper-left to lower-right corner: 319.3, 325, and 333 MHz. R.M.S. noises are 40, 55 and 35 mJy (1σ), respectively.

is restricted to a very narrow bandwidth (see Fig. 2). The decorrelation bandwidth was derived to be 3.6 ± 0.4 MHz (see Galama et al. 1997). A non-smoothed (1 min. integration) 325 MHz light curve of PSR B0655+64 shows a peak of 580 mJy (5.8σ), and a duration of about one hour. This yields an amplification of a factor 43 ± 9 (compared to an average derived from the data, excluding the observation of June 25; compared to Lorimer et al.'s 1995 flux density values we have a factor of 69 ± 23).

IV Discussion

The decorrelation bandwidth and characteristic time scale of the variation are in good agreement with the values expected for diffractive interstellar scintillation (compared with Lyne's 1984 values, assuming a Kolmogorov spectrum of the interstellar turbulence). However, the observed amplification of the flux density of PSR B0655+64 is too large to be explained by this mechanism. Perhaps the observed flux density amplification can be explained in terms of a caustic (strong focusing event; Goodman

et al. 1987). Caustics can explain a larger amplification (a factor < 40). Caustics are rare events, lasting about a refractive time scale ($\sim$ 3 days for PSR B0655+64). This explains the lack of similar events on other days. However, even caustics, as produced by a "normal" interstellar medium (e.g., the model of Goodman et al. 1987) can not satisfactorily explain the huge increase we observed.

Acknowledgements

We thank Prof. Narayan for a fruitful discussion on caustics and Dr. Ramachandran for comments. We are grateful for the assistance of the WSRT telescope operators T. Spoelstra and R. de Haan.

References

Cole, T.W., Hesse, H.K. & Page, C.G. 1970, Nature, 225, 712
Fiedler, R.L. et al. 1987, Nature, 326, 675
Galama, T.J. et al. 1997, A&A, 325, 631
Goodman, J.J. et al. 1987, MNRAS, 229, 73
Helfand, D.J., Fowler, L.A. & Kuhlman, J.V. 1977, AJ, 82, 701
Lorimer, D.R. et al. 1995, MNRAS, 273, 411
Lyne, A.G. 1984, Nature, 310, 300

Authors' Addresses

T.J. Galama & J. van Paradijs: Astronomical Institute 'Anton Pannekoek'. Kruislaan 403, 1098 SJ, Amsterdam, the Netherlands

A.G. de Bruyn: NFRA. Postbus 2, 7990 AA, Dwingeloo, the Netherlands

L. Hanlon & K. Bennett: Astrophysics Division, ESTEC. Noordwijk, the Netherlands

V. Radhakrishnan

Summary

As will be evident from looking at the contents of this volume, the Academy Colloquium was an excellent meeting with the majority of the talks given over three and a half days of a very high standard. In the following summary of my impressions I shall attempt to do more justice to the many valuable presentations than was possible in the allotted 15 minutes at the end of the last day.

Well over a year before the meeting, the motivation for its topic was communicated by the chairman to the other members of the scientific organizing committee; and much closer to the meeting he defined the focus of the Colloquium as on the questions of: What can we learn from pulsar timing about:

1. General and Special Relativity. How can we use relativity to study neutron stars (masses, density distribution, parallaxes, etc.)?
2. The internal structure of neutron stars.

These few questions governed the choice of both topics and speakers for the review talks and I take as my task here to assess how far the meeting succeeded in its aims. The first area touched upon was Relativity, and what we have learnt from timing binary and millisecond pulsars.

I Relativistic phenomena

The nature of the theories of Relativity, both Special and General are such that neither terrestrial experiments nor astronomical observations have ever *taught* us anything (new) about them. What they have done is to provide *tests* of the predictions of these theories to higher and higher levels of accuracy. Among the various predictions verified in earlier days may be listed time dilation, the bending and retardation of radiation when passing close to massive bodies, the gravitational redshift, and of course the precession of the perihelion of Mercury which was known even before but not understood in Newtonian theory. And as everyone here knows, it was the discovery of the Hulse-Taylor binary pulsar B1913+16 with its special combination of spin and orbital characteristics that ushered in a new era of testing of relativistic gravity. A few

more binary systems suitable for similar tests have been found since then, and the accuracies achieved in timing measurements have become so high that proper motion and galactic acceleration must also be taken careful account of, not to mention the cluster potential in the case of systems in globular clusters.

Testing different theories of gravity means comparing observations with predictions in a way that can discriminate between them. And it is here, as we learnt from various speakers on this subject, that Damour's work with Deruelle, and with Taylor and others later, has made a profound contribution as a user interface between theoreticians and observers. The particular approach used has made it possible to isolate a number of independent, potentially measurable "post-Keplerian" parameters which are not inter-related by built-in theoretical constraints. They take different values in different theories of gravity, and Gilles Esposito-Farèse explained how some tensor-scalar theories of gravity which were strictly equivalent to GR in weak field conditions (solar-system experiments) are nevertheless ruled out by binary pulsar tests. Jon Bell talked about the PPN formalism (the weak field, slow-motion, predecessor to PPK) and said that three of its ten parameters related to Lorentz invariance and conservation laws have already had severe limits put on them using pulsar data, one of them being as accurate as any null measurement in physics to date. The clearer and clearer message from all the results so far is that GR has been vindicated to amazing precision and alternative theories of gravity are falling by the wayside.

Including the recent discovery of J1518+4904 reported by Nice at this meeting, there appear to be five certain double neutron star binaries known to date. The similarities and differences in the values of their spin rates, and their orbital periods and eccentricities, provide important clues to the evolutionary histories of these systems. As testers of theories of gravity however, the proper motion, distance and even the orbit inclination to the line of sight affect the performance of any given system. For example, the orbit of B1534+12 lying nearly in the line of sight amplifies the Shapiro delay within the orbit, and this enabled the first purely strong-field test. The larger inclination of the orbit of B1913+16 allowed only a mixed test of the strong-field and radiation aspects of gravity. On the other hand, the proper motion of B1534+12 makes a substantial (20%) contribution (*à la* Shklovskii) to the observed orbital period derivative; and as pointed out by Bell and Bailes this limits the verification of gravitational wave emission to a precision of 7% of the predicted value or so unless the distance estimate to the system can be improved. Also as suggested by them, this effect looked at the other way, provides a new method of determining binary pulsar distances. Turning to orbital eccentricity, the 10% or so increase in this parameter for B2127+11C over that of B1913+16 is expected according to Taylor to make it a much better system for tests of gravitational radiation.

Next to the spectacular confirmation of the precise amount of gravitational radiation to be expected from neutron star binaries, the most impressive GR results in my view are the mass determinations of all six stars in three of the five systems, four of which are incredibly accurate values. In the other two systems, which are wide binaries, the large

orbital periods (days instead of hours) reduce the amount of gravitational radiation expected, thus precluding or making very difficult the detection of the relativistic decay of their orbits. But precessions of periastrons yield total masses of systems and these have been determined to an accuracy of a few percent. Two more binaries, with low mass companions, have also yielded mass estimates. They were included in a plot of measured neutron star masses shown by Taylor at the meeting.

The remarkable closeness of all the values in Taylor's plot suggests very strongly that as the errors in these and other methods of determination are reduced, all neutron star masses will end up in the neighborhood of the Chandrasekhar mass minus the binding energy, as is not unreasonable to expect. If this happens, there will be little or no information to be gained from the mass determinations about the equation of state of neutron matter, as was also noted by van Paradijs in his talk later in the Colloquium. Some indication of the spread of masses at birth, as distinct from changes due to accretion, is however already evident from an intercomparison of the six accurate values, three of which relate to spun-up pulsars.

Matthew Bailes talked about the dearth of such double neutron star binaries in the galaxy—only about 5 in 700 or more known pulsars—saying that this indicated a very high disruption rate, which in turn would require substantial kicks in 25 to 50% of all SN explosions. A consequence of this related to GR was that the estimated number of Galactic ns-ns mergers (of interest to LIGO say) was definitely below 10^{-5} per year and probably only around 10^{-6} per year. Another consequence is that the spin axes are likely to be tilted with respect to the orbit normals and should cause a change in shape and/or polarisation structure of the pulse with time due to geodetic precession.

Arzoumanian reported on observations of B1534+12 and said that although the pulse shape variation expected from orbital-phase dependent aberration was not detected, a significant long term change was seen and has been interpreted as due to the expected precession. Although not discussed at this meeting, strong evidence has been accumulating that the pulse of B1913+16 is also changing slowly with time at a rate roughly consistent with the expected precession. But the difficulties of interpretation of the observed changes have so far precluded any quantification of the tilt angles. So much for testing General Relativity and using it to find out things.

II Newtonian phenomena

Still staying with binaries, there were several very interesting presentations dealing with observations of what we might call purely Newtonian phenomena. Simon Johnston discussed the results of continued observations of 1259−63, the remarkable binary pulsar with a Be star companion of ten solar masses and six solar radii. The new development was that the fit for the first observed orbit does not work for the second one. Neither tidal or frictional drag, nor GR effects, can explain the observations which are now interpreted in terms of classical spin-orbit interaction.

Another neutron star binary with a B star companion of similar mass is J0045−7319 in the Small Magellanic Cloud. Vicky Kaspi reported on the significant deviations from a simple Keplerian orbit which indicate an advance of the pulsar's periastron as well as spin-orbit coupling. Both effects are believed to arise out of a rotationally induced equatorial bulge in the companion coupled with a substantial tilt of its spin axis with respect to the orbit normal. There are several more very nice results which have come out from timing this particular pulsar. The B star's rotation must be retrograde to enable enough coupling to the tidal potential to decrease the orbital decay time scale to a mere half million years. As this is only a fraction of the characteristic age of the pulsar, its spin rate at birth must have been close to its present period of around a second! Although other lines of evidence have suggested for years that most pulsars will not have a very short period at birth, this is perhaps the first time that there is direct observational evidence of a long initial period. Finally, both the inclination of the spin axis of the B star with respect to the orbit, as well as its being retrograde provide compelling evidence for a birth kick of at least 100 km/s if not much greater.

The evidence provided by this system for a substantial kick at birth is perhaps considered the most important result from the timing of this pulsar. I would like to add that an equally if not more important result may be the circumstantial evidence that the long period at birth was also a result of the kick. See later.

Very interesting timing results on the binary system J0437−4715 containing the nearest and brightest millisecond pulsar were reported by Manchester. The secular acceleration associated with its enormous proper motion of 140 mas/yr accounts for most of its period derivative and affects the field estimation. What is more, it causes a clearly measurable change in the orbit inclination with time.

If pulsar binaries are rare, multiple systems should be even rarer, as in fact they are. Wolszczan discussed observations on B1257+12, the first such system found several years ago. In addition to the three confirmed inner planets whose orbital perturbations have been seen, a fourth possible outer one is suspected from the residuals. Evidence for planets around other pulsars he said was not convincing. An interesting point he made was that timing noise observed in various pulsars could be due to "junk" in orbit around them. Steve Thorsett described continued observations of the only other multiple system known that is associated with a pulsar and which is in the globular cluster M4. No less than four derivatives of the spin frequency have been measured, the second being too large to be due to timing noise, and of such a value that the first derivative will change sign in 2001! The data are inconsistent with acceleration in the cluster field and indicate the presence of a third object with a mass $< 0.015\ M_{\odot}$—a brown dwarf?—in a wide orbit only a part of which has been sampled so far. It was estimated that two more years of data should tell us for sure.

III Timing accuracy

All of the interesting results mentioned so far depended for their success on the steadiness of the spin and slow-down rates of pulsars and the accuracy of the clocks used for timing them. The present state of the art of timekeeping was covered by Petit who also compared the stability of atomic clocks with that of millisecond pulsars. As of now, the relative superiority depends on the time scale involved, atomic clocks being better for periods of months or shorter, and millisecond pulsars winning over years. The most recent progress has resulted from the use of "Cesium fountains" which have enabled reaching a stability of 3×10^{-15}; and a goal believed to be achievable in the not too distant future has been set at 10^{-16}.

Even if pulsars are stable rotators, their signals get mauled in passage through the interstellar medium as very nicely explained by Don Backer in his Primer on Interstellar Weather. The movement of inhomogeneities in the electron density distribution gives rise to both diffractive and refractive scintillations including some long term changes such as the DM for Vela which has a linear gradient with time. Multiple frequency observations do not solve all problems because different frequencies sample different volumes of the ISM resulting in scattering making DM a function of frequency! Disturbances close to the pulsar can also play havoc as in the case of the Crab where the movements of filaments in the Nebula cause wild variations in DM and also changes in the scattering and flux density. Lestrade describing timing observations carried out at Nancay noted that refractive interstellar scintillation can cause long term flux variations and that dispersion delay variations dominate the time of arrival analyses as seen by an anticorrelation with flux variations.

Unconnected with problems associated with propagation, there is an unpredictable aspect of pulsar timing behavior due to internal causes, namely glitches and timing noise. These were discussed by Lyne who presented an impressive amount of data obtained over the years. About 50 glitches have been observed so far, three quarters of them in the last ten years, and three young pulsars out of 21 accounting for half the total number of glitches. The largest and most recent glitch was observed in the pulsar B1930+22 in June 1996 and has a value for $\delta\nu/\nu$ of 4.5×10^{-6}. These sudden increases in rotation rates are followed by relaxations which have both a short term and a long term behavior, but which tend to leave a small permanent change in frequency derivative. Glitch "activity" (defined as the total frequency change in glitches divided by total observation time) is greatest for pulsars with ages 10,000 to 30,000 years and for greater ages falls off roughly as the frequency derivative.

Timing noise, or irregularities in pulse arrival times, while present to some extent in all normal pulsars, is greatest in young pulsars with large slow-down rates. Both positive and negative period second derivatives are found but a comparison with glitch activity suggests that in younger pulsars timing noise could be mostly recovery from glitches seen or unseen. Both glitches and timing noise are attributed to the loose coupling of the neutron superfluid to the crust. Sudden unpinning of the superfluid in

the crust appears the most likely cause of glitches, with the post glitch relaxation giving information on the amount of fluid in the star and the transfer of angular momentum from the core.

IV Neutron superfluid

Following an overall review of neutron star interiors by Srinivasan, Ali Alpar discussed superfluid dynamics in neutron stars. While starquakes could work for smaller glitches such as seen in the Crab, they cannot explain the larger and more frequent glitches typical of Vela. He elaborated on his work with others on the superfluid vortex unpinning model which suggests that the Crab would evolve to becoming like Vela with the growth of the region of trapped vortices. An interestingly different scenario was put forward by Link who used both quakes and vortices. Sudden heating in the neutron star interior leads to angular momentum transfer from the core superfluid to the crust causing the spin jump. The difference between the Crab and Vela type glitches is attributed to temperature effects with the spacing depending on the quake frequency.

The last of the presentations in this group was by Sauls who talked about proximity effects on neutron superfluidity in the inner crust. Instead of being one continuous entity the neutron sea is separated into pieces interspersed by np matter. The scattering of the Cooper pairs at the interfaces and subsequent loss of a fraction of them reduces drastically the number available for superfluidity in the n region. As a result both gap and pinning energies are reduced greatly. Following this was a discussion session with several contributors and led by David Pines. The aim was to understand "to what extent do pulsar glitches probe crustal superfluidity, core-crust coupling and the EOS of dense matter". My own impression at the end of considerable discussion was that it was highly inconclusive. There was no clear consensus, and I for one was not much wiser after than before.

V Internal structure & EOS

An excellent tutorial by Chris Pethick dealt with neutron rich matter at subnuclear densities and its implication for neutron star crusts. The bulk and surface properties of such matter were discussed and non-spherical shapes predicted for the nuclei in the crust (... spaghetti, lasagna...). The main points were that at low density, the nuclear attributes of neutron star crusts are determined directly by properties of nuclei, like their masses, that can be obtained in the laboratory. But at increasing density, a greater degree of theory is required to deduce these attributes. On the matter of experimental data, Gerry Brown discussed the most recent conclusions from the interpretation of heavy-ion collision experiments at CERN and GSI Darmstadt which indicate a softening of the EOS at 2 to 3 times nuclear matter density. He made a case for negative kaon condensation which would lead to a soft EOS and give a maximum neutron star mass of 1.5 $M_{\odot}$ and a corresponding radius of 7 km.

On the matter of constraining the EOS several presentations touched on possible observational probes. Jan van Paradijs discussed the masses and radii of neutron stars, and as already mentioned concluded that masses do not tell us anything definite. On the other hand, the radius relates to the red shift and hence to the luminosity, and thus X-ray bursts could be used to constrain radii. A different form of X-ray emission also leading to constraints are the newly discovered "kiloHertz" quasi periodic oscillations in low mass X-ray binaries. Michiel van der Klis described remarkable observations with NASA's RXTE satellite of six sources (now ten) which displayed oscillations in the range 500 to 1200 Hz. Most of the sources showed double peaks separated by a few hundred Hz, and which move up and down in frequency together. In an exceptionally interesting presentation, Fred Lamb described a new model aimed at explaining these observations. In this Sonic Point model, the higher frequency is the Keplerian one at the sonic point at the inner edge of the accretion disk, and the lower is the beat between this and the 150 to 500 Hz spin frequency of a weakly magnetic (10^7 to 10^9 Gauss) neutron star, a millisecond pulsar in the making! A relativistic treatment of the problem shows that if the kiloHertz QPOs are indeed Keplerian frequencies, their measurement will provide new bounds on masses and radii of neutron stars, in turn constraining the EOS at high densities.

One more very fine contribution connecting X-rays and the EOS by Bhaskar Datta illustrated GR effects (frame dragging) of rotation on disk and boundary layer luminosities for disk accretion on to low magnetic field neutron stars. The X-ray emission will depend on the thinness of the boundary layer which in turn depends on the EOS. Finally on the topic of X-rays, a very important all sky monitoring programme using BATSE was reported on by Tom Prince. Half of the 43 known X-ray pulsars were detected and an impressive data base on their timing and spectral behavior has been accumulated, which is available to the public.

VI Magnetic field

I come now to the last—but far from least important—topic, namely the magnetic fields of neutron stars on which there were seven presentations all devoted to aspects of their evolution. Dipankar Bhattacharya set the scene by reviewing the current models for the evolution of the field subsequent to its creation at or soon after the birth of the neutron star when it attains its canonical value of 10^{12} G. The present belief is that this value remains constant for the rest of the life of the star unless it is a member of a binary system, when interaction with the companion appears to result in the decay of the dipole field strength. Among the mechanisms for this decay, in roughly decreasing order of credibility (mine), are the outward transport of magnetic fluxoids to the crust during spin down followed by ohmic decay due to impurities in the inner crust, and movement of crustal plates towards the equator where poles come together and reconnect. A second class of models where the initial magnetic field is all in the crust, invokes enhanced resistivity due to heating during accretion, or the screening of the

field by the accreted diamagnetic plasma burying it, the latter scheme being unlikely to succeed because of Rayleigh-Taylor instabilities with microsecond time scales.

The movement of neutron star crustal plates was the brainchild of Mal Ruderman who has pursued the consequences of such readjustments for many years now. Apart from the diminution of the dipole field strength mentioned above, there are numerous other consequences (e.g., shape change of the pulsar beam) which Mal has been investigating and which he discussed in a presentation following Dipankar's. A pitch for much higher field strengths at birth than generally believed was made by Shri Kulkarni who suggested that many pulsars may be born with 10 to 1000 times the canonical value of 10^{12} Gauss. As supporting evidence for this hypothesis were cited weak plerions in most SN remnants, break frequencies $< 10^{11}$ Hz, and soft gamma ray repeaters, the last of which were to be explained as neutron stars with fields around 10^{15} G which have evolved to periods of 8 seconds or so in times of the order of 10^4 years.

Among the contributed papers on this topic was one by Muslimov on the field evolution in millisecond pulsars, and another by Itoh on a Monte Carlo simulation to investigate the claimed velocity-field correlation, which it failed to find support for, like several previous investigations. Frank Verbunt reported on an improved population synthesis of single radio pulsars with $B > 10^{11}$ G, which confirmed that the time scale for field decay was > 30 Myr, and that a fair number of neutron stars are born with velocities less than 200 km/s. The derived birth rate is compatible with formation in OB associations from progenitors with $M > 10$ $M_\odot$, and with no need for a second population in addition to those formed directly from Type II supernovae.

The more difficult question of how the neutron star field was created in the first place was tackled by Sterl Phinney in his characteristically original style. That he also provided an explanation of the spin of the neutron star in the bargain made this easily the star (unavoidable) contribution to the Colloquium. Also the one most difficult to follow in real time because of the large number of complicated physical phenomena in stellar evolution which were dealt with in typical rapid fire sequence. The message that I was left with at the end was that in the course of the evolution most of the angular momentum ends up in the envelope and the core of the progenitor is left with very little. The resulting huge differential rotation drives something known as the Balbus-Hawley instability to create the magnetic field. On collapse, the field will have a value of less than 10^{12} G going up to 10^{13} G, if the progenitor goes through a bare He star phase, and it is conjectured that if there is convection in young neutron stars, the field could go up to 10^{14}–10^{15} G.

But as far as the spin is concerned, it is unlikely to be less than 1 second and probably very much slower if due only to angular momentum conservation. An alternative mechanism is needed to explain short periods and it was pointed out that the asymmetric kicks now recognized as being essential to explain pulsar velocities, are surely likely to also impart angular momentum to the star and spin it up. The physical

model is uneven removal of neutrino momentum by convection cells, and a correlation of short periods with high kick velocities is predicted by the model. But it seems to me that if the spin due to angular momentum conservation happens to be non-negligible, then the impulse could either add to or subtract from the rate depending on the kick direction. We saw earlier that in the case of pulsar J0045−7319 it was deduced that the direction of the kick must have been such as to change the direction of the orbit. Perhaps it was also such as to counter the "conserved" spin of the neutron star making it as slow at birth as deduced from the considerations described earlier.

One final thought is regarding the developments that have taken place since the Bonn Pulsar Symposium in 1980. I came away from that meeting after listening to Ed's and Joe's talks there, convinced that even if the relative number of binaries was very small, their study would teach us a great deal even about single pulsars. The discussions at this meeting seem to have amply justified that expectation. And that brings to an end my summary of the scientific part but not of the whole programme.

VII Good times

At the end of the second day, a delightful boat trip along the beautiful canals of Amsterdam was laid on and followed by a magnificent conference dinner in arguably the very best restaurant in the city. Ed, our host, took this opportunity to entertain us with the history of Anton Pannekoek, who 75 years ago founded the Institute now named after him. It was a fascinating story about a very independent and colorful character which most of us participants were quite unaware of, and so glad to hear. I would also like to mention here Matthew Bailes' impromptu post-prandial contribution in which he expressed so well what all visitors to the Pannekoek Institute have felt, namely the warm, friendly and scientifically stimulating atmosphere that Ed has engendered there. And the same is true for meetings organized by Ed, of which the present one was an excellent example. I am sure I speak on behalf of all the participants and guests in expressing our appreciation and thanks for a rewarding and enjoyable Colloquium.

Authors' Address

Raman Research Institute; University of Amsterdam

Keyword Index

Object Index

Name Index